DONDERS
INSTITUTE

ISBN 978-94-6284-053-9

Radboud University Radboudumc

EMERGING BRAIN CIRCUITS *IN SILICO* AND *IN VITRO*

Marijn B Martens

DONDERS SERIES

229

Emerging brain circuits *in silico* and *in vitro*

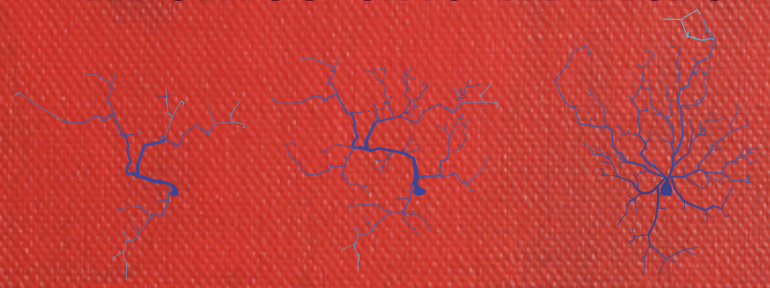

Marijn B Martens

DONDERS SERIES

Emerging brain circuits
in silico and *in vitro*

Proefschrift

ter verkrijging van de graad van doctor
aan de Radboud Universiteit Nijmegen
op gezag van de rector magnificus,
volgens besluit van het college van decanen
in het openbaar te verdedigen op donderdag 26 mei 2016
om 12:30 uur precies
door

Marijn Bart Martens

geboren op 11 april 1986
te Nijmegen

Promotor:
Prof. dr. P.H.E. Tiesinga

Copromotoren:
Dr. D. Schubert
Dr. N. Nadif Kasri

Manuscriptcommissie:
Prof. dr. A.J. van Opstal
Prof. dr. H.D. Mansvelder (Vrije Universiteit Amsterdam)
Dr. B. Englitz

Nederlandse Organisatie voor Wetenschappelijk Onderzoek

Dit onderzoek is gefinancieerd door de Nederlandse Organisatie voor Wetenschappelijk Onderzoek (NWO), TOPTalent projectnummer 62001113 (MB Martens)

ISBN 978-94-6284-053-9

Omslag: Marijn Martens en Anneke Kersten, geïnspireerd door werk van Mark Rothko (1903-1970)

Contents

Chapter 1

General introduction

"What mysterious forces precede the appearance of these processes... promote their growth and ramification... and finally establish those protoplasmic kisses... which seem to constitute the final ecstasy of an epic love story?" - Santiago Ramón y Cajal [1882-1934]

We can learn from and adapt to our environment, an astonishing feat that is enabled by the patterns of electrical activity produced by our brain [1]. Today, more than a century after Ramón y Cajal discovered that the discrete building blocks of our brain are neurons, and that they connect to each other by synapses, we have gained a wealth of knowledge about the rules by which cells produce their intrinsic activity patterns and synapses change their strengths [1–4]. The experimentally determined learning rules assume already established and interconnected brain circuits, starting from which the neuronal spiking activity can store information by adjusting the connections accordingly. A fundamental question is, what is needed to build interconnected and stable brain circuits to begin with?

The development of technologies and infrastructure to investigate brain circuits at an incredibly detailed level are the focus of current, large-scale initiatives in brain research [5, 6]. How can we use the resulting tools to unravel the brain's blueprint? In this thesis, we consider neuronal circuits *in silico* to generate novel hypotheses regarding the emergence of functional brain circuits and measure from developing cultured neurons *in vitro* to monitor their development over prolonged periods of time during development. In this introductory section, we first briefly review the development of brain circuits and discuss mechanisms to regulate the level of neuronal activity. We then review in detail the physical and chemical processes that characterize Multi-Electrode Array (MEA) technology, an experimental technique that we extensively use to perform our experiments. Finally, we provide an outline of the various chapters in the thesis.

1.1 Development of brain circuits

Neurodevelopment is a complex process involving a precisely orchestrated sequence of genetic, environmental, biochemical and physical events [7]. In this section, we will briefly review three stages that are important for the formation of brain circuits: neurogenesis, synaptogenesis and synaptic selection. These three stages relate primarily to synaptic maintenance and selection studied in Chapter 2, and the network formation studied in Chapter 3.

Neurogenesis and synaptogenesis

Neurogenesis involves the generation, proliferation, migration and differentiation of neural progenitor cells [8]. Neural progenitor cells originate from the ventricular zone of the developing brain and migrate along radial glial cells to the cortical plate. These processes are guided by extracellular signals, e.g. the Notch and fibroblast growth factor (FGF) signaling pathways, and regulated by internal (epi)genetic programs (for reviews, see [8, 9]). Neurogenesis is most active during the human prenatal developmental period and provides the cortex with the appropriate neuronal cell types at the appropriate time [10].

Synaptogenesis involves the formation of synaptic contacts between neurons. The synaptic contacts, or synapses, consist of an axonal terminal at the presynaptic neuron and a dendritic spine at the postsynaptic neuron. Several growth rules for synaptogenesis have been proposed, addressing the relation between spinogenesis (the formation of dendritic spines) and synaptogenesis (the formation of synaptic contacts) [11, 12]. According to the Sotelo rule, spinogenesis occurs independently of the presence of an axonal terminal [13]. The Miller/Peters rule states that the axonal terminal induces spinogenesis [14], while the filopodial rule describes synaptogenesis as the capturing of axonal terminals by dendritic filopodia to form spines and subsequently synapses [15]. The contribution of each of these rules to synaptogenesis is thought to depend on the developmental stage [16, 17]. This notion is supported by confocal imaging in rat hippocampal slices that show that although the turnover rate of dendritic protrusions are different between young and adult animals, the process of stabilization of new spines, in terms of time course and low level of efficacy, remained comparable throughout development [18]. In this thesis, to connect the recurrent neural networks that we use in our simulations, we use a Bernoulli process to generate the synaptic connections between pre- and postsynaptic neurons. This process of synaptogenesis is in line with the random generation of synaptic connections proposed by the three models above that use proximity of the pre- and postsynaptic areas as a criteria for synaptogenesis.

In humans, synaptogenesis is most active around the time of birth, where synapse formation occurs in bursts at different ages that depend on the cortical regions [19]. For example, in the human visual cortex synapse formation is accelerated between 3 and 4 months and the maximum density is reached between

4 and 12 months, while synaptogenesis in the prefrontal cortex reaches its peak well after the first year [19]. The peak of synaptic density is about 150% of the adult levels [19, 20]. In general, the sequence of developmental patterns is highly conserved throughout many species [21].

An important aspect of synaptogenesis is the formation of functional synapses such that the information that an action potential occurred in the presynaptic neuron is reliably and with temporal precision transmitted to the postsynaptic neuron. Experimental observations have shown that early in development pre- and postsynaptic structures are co-localized, even in the absence of any action potential activity [22], while functional connectivity emerges later in development [22]. Several developmental mechanisms contribute to the formation of functional synapses. For example, newly generated synapses often lack functional α-amino-3-hydroxy-5-methyl-4-isoxazolepropionic acid (AMPA) receptor-mediated transmission [23]. These 'AMPA-silent' synapses can be selected for AMPA unsilencing by correlated pre- and postsynaptic activity, thereby establishing a functional synaptic connection (for review see [23]). Furthermore, during early development newly generated synapses have predominately neurotransmitter release that is not correlated with the occurrence of a presynaptic action potential [24], whereas later in development the neurotransmitter release becomes temporally locked to presynaptic action potentials (for review of the neurotransmitter release modes, see [25]). This developmental switch in neurotransmitter release mode is another mechanism to form functional synapses, by changing the properties of the presynaptic neuron [26], in contrast with the AMPA unsilencing discussed above, in which the properties of the postsynaptic neuron are changed.

Synaptic selection

Synaptic selection involves the activity-dependent pruning (removal) of some contacts and strengthening of others. Synaptic selection through Hebbian plasticity guides the refinement of brain circuits [27]. A popular and simple definition of Hebbian plasticity is "cells who fire together, wire together". More specifically, an often observed mechanism for Hebbian plasticity is spike timing-dependent plasticity (STDP) [4]. The STDP rule states that synaptic contacts are strengthened when presynaptic neurons fire an action potential just before the postsynaptic neuron spikes, whereas synaptic contacts are weakened when presynaptic neurons fire an action potential just after the postsynaptic neuron. For repetitive and persistent spike patterns some synapses strengthen and stabilize whereas others weaken and are eventually pruned.

The postsynaptic pathways involved in the developmental stages of Hebbian plasticity are well characterized [28, 29]. In Chapter 2, we computationally study a novel presynaptic mechanism that can be used to switch on Hebbian plasticity during development.

The growth rules for synaptogenesis that were described above do not include any additional rules for establishing connectivity based on, for instance,

the number of afferent (in-degree) and efferent (out-degree) connections, quantities which may impact metabolism and firing rate in the neurons. Thus, networks that form according to these rules will not necessarily have a correlation in the in- and out-degree distribution. In Chapter 3, we show that synaptic selection by Hebbian plasticity in networks with an uncorrelated degree distribution leads to anti-correlation in the degree distribution. We found that brain circuits with anti-correlations in the degree distribution simultaneously increase stability in maintaining sparse action potential activity, and make stimulus detection more effective by lowering the rate of false positives in the case of high neuronal noise.

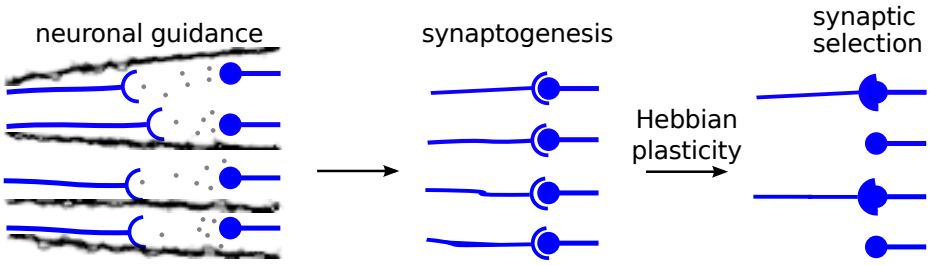

Figure 1.1: Neuronal growth guidance, synaptogenesis and synaptic selection are important processes in brain circuit development. Axonal and dendritic growth processes bring pre- and postsynaptic parts closer together, after which (too) many synapses form, of which the relevant ones are strenghtened and the irrelevant ones are weakened and pruned. For details, see main text.

Network growth and synaptic selection are thus involved in establishing functional brain circuits (**Figure 1.1**, [27, 30]). Premature activation or delays in these processes have been implicated in neurodevelopmental disorders (for review see [23]).

Action potential activity is necessary for the appropriate development of brain circuits. In the following section, we describe the regulation of action potential activity that can occur at a diverse range of time scales.

1.2 Activity regulation in brain circuits

Excitatory activity in recurrent brain circuits that activates other excitatory neurons can lead to a runaway process in neuronal activity. To remain in a stable state, neuronal networks therefore need regulation of action potential activity. In Chapter 3, we investigate how the graph theoretical structure of brain circuits can contribute to stability in neuronal activity. In this section, we review different mechanisms that regulate brain activity, which each operate at a different time scale (**Figure 1.2**).

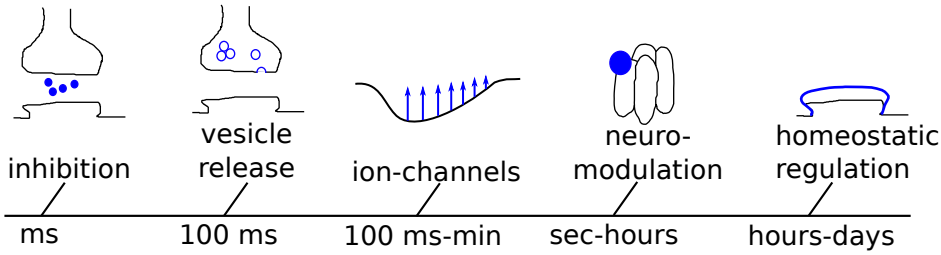

Figure 1.2: Action potential activity can be adjusted through several synaptic and cellular mechanisms, which each operate at a different time scale (ms is short for milliseconds, sec for seconds and min for minutes). For details, see main text.

Inhibition

About 20% of the cortical neurons are inhibitory [31]. Most interneurons release γ-aminobutyric acid (GABA), the main inhibitory neurotransmitter in the mature brain. Binding of GABA to the ionotropic $GABA_A$ receptor opens a chloride ion-selective pore. The increased chloride conductance drives the membrane potential towards its reversal potential, typically around -75 mV for mature neurons.

Interneurons can be divided into many functionally and morphologically distinct classes which can be partially identified by molecular markers [32–34]. Interneurons have a strong local connectivity and project to most nearby pyramidal neurons [33, 35, 36]. Thus, interneurons can regulate action-potential activity by providing a transient and local reduction in neuronal excitability at time scales in the order of tens of milliseconds (ms).

Vesicle release

Short-term plasticity (STP) refers to the changes in synaptic efficacy of vesicle release due to the recent history of presynaptic activity. Action potentials that arrive in the axonal terminal open calcium channels, and the resulting calcium influx triggers the merging of vesicles, which are filled with neurotransmitters, with the cell membrane. STP can refer to an enhancement (facilitation) of synaptic efficacy, where residual calcium, which entered the axonal terminal as a result of recent action potentials, facilitates vesicle release. STP can also refer to a reduction (depression) in synaptic efficacy, whereby the depletion of available vesicles due to recent release lowers the release probability [37–39]. The degree of facilitation and depression depends on the protein composition at the axonal terminal and can be regulated in a cell and synapse-type specific way (for reviews see [25, 40]). STP affects synaptic transmission at time scales on the order of hundreds of ms, and thereby provides a mechanism to regulate the action potential activity at functionally relevant time scales.

Ion channels

Intracellular and extracellular ligands can activate ion channels that either de- or hyperpolarize the neuron. The ion channels are often activated indirectly by G-protein-coupled receptors; other common intracellular ligands include calcium ions, ATP, cyclic AMP and GMP, and phosphatidylinositol (PI) [41]. Furthermore, hyperpolarization of the membrane potential below -50 to -70 mV can activate cyclic nucleotide-gated (HCN) channels, which in turn depolarize the membrane potential towards its resting potential [42–44]. The opening and closing of these ion channels can thus affect neuronal excitability on time scales on the order of hundreds of ms to minutes, and experiments suggest that they are involved in subthreshold oscillations and generation of spike clusters [45, 46].

Neuromodulation

Neuromodulators are a class of chemical compounds that alter the physiological function of neurons by binding to specific receptors in the cell membrane. Major neuromodulators include dopamine, serotonin, acetylcholine, histamine and epinephrine/norepinephrine [47]. Volume transmission of neuromodulators can alter the excitability of those neurons that express the relevant receptors, in a large region of the brain [48]. Neuromodulation is involved in e.g. sleep-wake control, and has important roles in the regulation of arousal and attention (for review see [49]). Typically, neuromodulators remain in the extracellular space for a prolonged period of time; time scales for the clearance, degradation or re-uptake of neuromodulators are on the order of minutes [50, 51]. Recent findings have shown that cholinergic activity can also be modulated at a time scale of seconds [52]. Taken together, neuromodulation can thus regulate neuronal excitability in a cell-type specific manner, at time scales ranging from seconds to hours [49, 52].

Homeostatic regulation

Homeostatic regulation comprises a diverse set of cellular mechanisms to change neuronal excitability. Action potential activity that deviates from the physiologically preferred range can trigger a calcium-induced transcriptional cascade [53, 54]. For instance, the most well-known compensatory mechanism is adjustment of the synaptic strengths, which involves the removal or incorporation of post-synaptic AMPA receptors, the main receptor for excitatory neurotransmission in the brain [53]. Other mechanisms include adjustment of ion channel expression, neurotransmitter receptor abundance or modulation of presynaptic release [3, 54, 55]. Homeostatic restoration of action potential activity, when it was blocked by pharmacological compounds, occurred over days, with some reports showing homeostatic recovery as fast as 12 hours [56, 57].

The (dis)advantages of the various regulatory repertoires

The above-discussed repertoire of regulatory mechanisms provides neurons the ability to maintain their action potential activity in a stable, physiologically relevant regime. Each regulatory mechanism has unique benefits, which sometimes come at a price. For example, STP and ion channel dynamics are fast and have a large dynamic range (ms to minutes), but neurotransmitter release and maintaining transmembrane potentials are energetically expensive to perform for neurons [58, 59]. Therefore, these regulatory mechanisms are well-suited to return activity to baseline levels at short time scales, but not for long-term recovery of action potential activity. In the case of neuromodulators, the passive volume transmission is energy efficient, but this type of regulation is nonspecific due to the large volume that is affected. Homeostatic regulation can act at the resolution of single cells and provides long-lasting changes, but requires transcription and therefore can only operate at time scales longer than hours. The interactions between different forms of regulation, and whether there is cooperation or competition, are currently not well understood [57].

Previously, regulatory mechanisms, such as inhibition [60] and neuromodulation [50], have been suggested as candidates to switch on Hebbian plasticity and initiate a critical learning period by making the circuits sensitive to external input. We computationally show that a developmental transition in the vesicle release mode can switch on Hebbian plasticity [26].

Regulation of action potential activity is thus a delicate process and requires appropriate genetic regulation [54]. Recently, an emerging landscape of epigenetic regulators was linked to misregulation of neuronal function in disease [61, 62]. In Chapter 6, we study EHMT1, an epigenetic regulator that is important in early development [63, 64]. We found that EHMT1 deficiency in neuronal cultures resulted in reduced action potential activity early in development, which led to more disorganized (irregular) patterns of action potential bursting later in development. These results are in line with the view that action potential activity plays an important role in brain circuit rewiring during development (for review see [3, 65]); altered wiring during early development has previously been proposed to underlie several phenotypes associated with neurodevelopmental disorders, including ID and autism [66–68].

To record action potential activity we used the MEA technology in Chapters 5 to 7. In the next section, we provide a description of how MEAs work.

1.3 MEAs

Neuronal *in vitro* cell cultures can be monitored during development using electrophysiological techniques, such as MEAs to record extracellularly and the whole-cell patch clamp technique for intracellular recording (**Figure 1.3**, [69, 70]).

In this thesis, we have extensively used the MEA technique: in Chapter 5 we propose and test a novel pre-processing method for MEA data to improve the

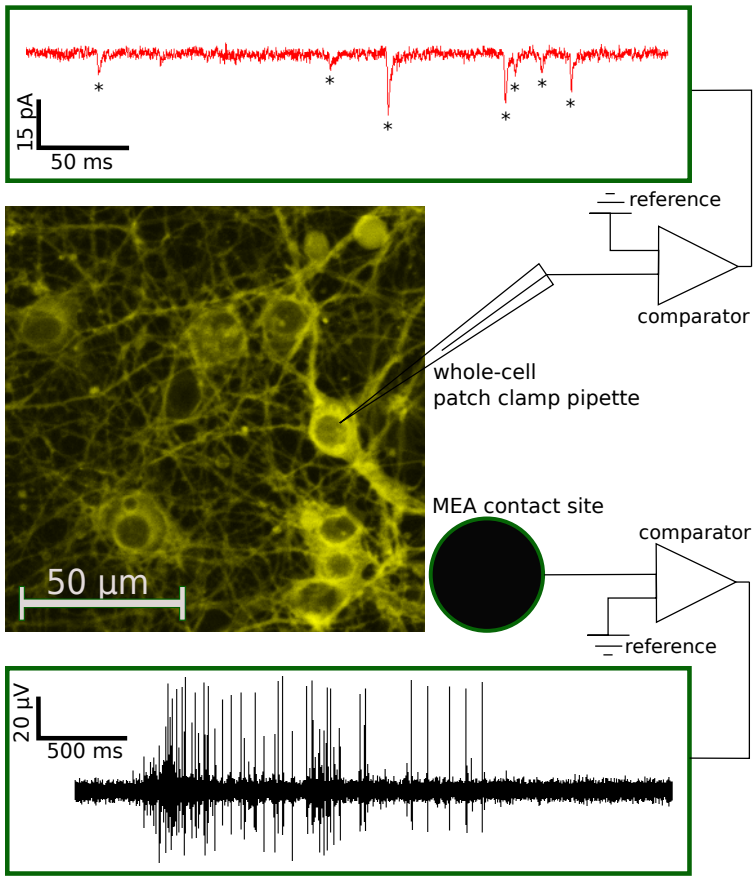

*Figure 1.3: Intra- (top) and extracellular (bottom) techniques to record neuronal networks in culture during development. Top trace: whole-cell patch clamp can be used to record synaptic inputs: EPSCs, indicated by a *. Here, the sodium channels were pharmacologically blocked in order to prevent action potentials; the recorded synaptic inputs originate from spontaneously exocytosed vesicles. Bottom trace: MEAs show a deflection in the extracellular potential when a nearby neuron fires an action potential. Spontaneous activity can erupt into a network-wide, synchronous activation of the neurons. Each MEA electrode records the activity of one or a few neurons.*

quality of burst detection; in Chapter 6 we study the effect of EHMT1 deficiency on action potential activity during development using MEAs and in Chapter 7 we investigate spontaneous and stimulated activity in structured small neuronal networks on MEAs.

In this section, we review the physics and chemistry involved in MEA fabrication, recording and stimulation with the aim to better understand the use of MEAs for neuronal recordings.

Neuro-silico interface

Given the typical signal strength of an action potential in relation to the voltage noise of the device, MEAs can typically record the electrical activity from the somas (<30 μm) or axons (<5 μm) in proximity of the electrodes [71]. Neuronal cell cultures can be densily plated on MEAs, such that neurons are often in proximity of the planar electrodes, which allows to stimulate and record from the neurons [72, 73].

Electrode-liquid boundary

When no external electrical potential is applied between electrode and ground, the metal electrode and the liquid neuronal culture medium are in electrochemical equilibrium, during which no irreversible reactions are expected. However, the performance of electrodes in physiological solution, especially for use of chronic stimulation, is critical for the success of functional electrical devices [74]. Two strategies to perform electrical stimulation, faradaic and capacitive stimulation, are discussed below.

Faradaic current stimulation

Faraday's law of electrolysis states that the mass of a substance altered at an electrode during electrolysis is directly proportional to the quantity of electric charge transferred:

$$i_f = \frac{dQ}{dt} = zF\frac{dN}{dt} \tag{1.1}$$

With i_f being the faradaic current, Q the total electric charge passed through the substance, N the amount of atoms removed from the electrode, z the valency of the ions entering the solution and F Faraday's constant equal to 96485 C·mol^{-1}. Thus, monophasic charge injection would slowly dissolve the electrode. Neurons can also be stimulated using rapid, charged-balanced (biphasic) current injections, improving the life-time of electrodes [74].

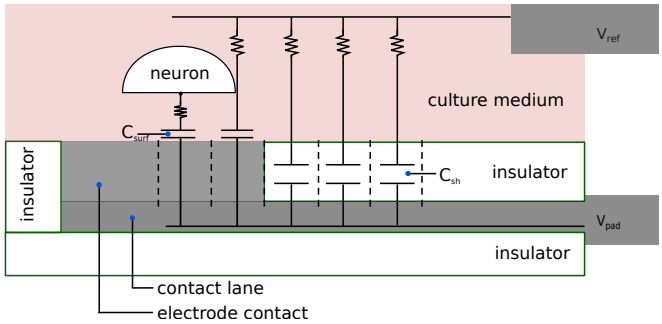

Figure 1.4: The activity of a neuron, represented by in- and outward currents through its cell membrane, causes modulations in the extracellular potential that change the potential of a nearby MEA electrode relative to the distant reference electrode in the medium. Likewise, the MEA electrode can be used for stimulation. For symbols, see main text. Image modified from [75].

Capacitive stimulation

A voltage step (V) between a stimulation electrode (V_{pad}, **Figure 1.4**) and the reference electrode (V_{ref}) applied across a capacitor induces a capacitive current i_C according to:

$$i_C = \frac{dq}{dt} \tag{1.2}$$

With q being the charge stored in the capacitor:

$$q = C \cdot \Delta V \tag{1.3}$$

The capacitance (C) of a parallel plate capacitor is given by:

$$C = \frac{\epsilon_0 \epsilon_r}{d_{layer}} \cdot A \tag{1.4}$$

Where ϵ_0 is the vacuum permittivity ($8.85{\cdot}10^{-12}$ F/m), ϵ_r the relative permittivity, d_{layer} the distance between the plates and A the surface area of the capacitor.

The capacitors around the MEA contact lane, such as the insulation layer (C_{sh} in **Figure 1.4**) are in a parallel configuration. The equivalent capacitance (C_{eq}) for capacitors placed in parallel is given by:

$$C_{eq} = C_1 + C_2 + ...C_n \tag{1.5}$$

For parallel capacitors, the materials with a large relative permittivity, contribute most to the equivalent capacitance. Furthermore, capacitive effects of layers between the electrode and the neuron, such as the Helmholtz double layer (C_{surf} in **Figure 1.4**), are set in series. The equivalent capacitance is then given by:

$$\frac{1}{C_{eq}} = \frac{1}{C_1} + \frac{1}{C_2} + ... \frac{1}{C_n} \tag{1.6}$$

For capacitors in series, the materials with a small relative permittivity, such as the insulation layer around the contact lane ($\epsilon_r = 7.5$ in Equation 1.4 for silicon nitride, the insulation material of the MEAs used in our experiments), contribute most the equivalent capacitance.

Thus, for capacitive stimulation using an applied voltage difference, the electrode material needs to be of large capacitance in comparison to the insulation around the electrode shaft (set in parallel), and for charge transfer from the electrode into the neurons, the number of capacitive effects between the electrode and neuron needs to be minimized.

For the surface area of the electrode we can distinguish the geometric surface area (GSA), which is the 2D spatial extent of the electrode, and the real surface area (RSA), which is determined by the atomic organization. The MEAs that we used in our experiments have a large RSA to GSA ratio to increase the capacitive stimulation capabilities [76]. Furthermore, we applied glow discharge plasma treatment to the MEAs to thoroughly clean the electrode surface to increase the capacitance of the electrode [77]. The appropriate intensities and durations have to be used to avoid formation of a thin oxide layer on the electrode surface [78]. An insulating oxide layer acts as a capacitor in series with the electrode and will likely decrease the capacitance of the electrode.

Furthermore, the amplitude of the recorded signal depends linearly on the ratio of the electrode area covered by the neuron to the entire electrode area. The relation between the voltage at the contact pad (V_{pad}) and the neuro-silico cleft (V_J) can be given by the frequency-independent relation [75]:

$$\frac{V_{pad}}{V_J} = \frac{C_{JE}}{C_E + C_{sh}} \approx \frac{\alpha_{JE}}{\alpha_E}$$

Where C_{JE} is the capacity of the area (α_{JE}) of the electrode that is covered by a neuron, C_E is the capacity of the entire electrode area (α_E), and C_{sh} is the shunt capacity of the contact lane. Given that $C_{sh} \ll C_E$, the amplitude of the recorded signal depends linearly on the ratio of the covered electrode area and the entire electrode area [75].

1.3.1 MEA fabrication methods

To deploy planar MEAs for recording of neuronal activity and stimulate at high spatial resolution, different materials that can be used for the electrode surface have been explored (see **Figure 1.5**). Generally, an ideal MEA electrode can deliver enough charge to activate nearby neurons, without damaging the electrode (e.g. it has a high charge injection capacity (CIC)), can record with high signal-to-noise ratio (low impedance) and record a small subset of neurons (small GSA). The CIC is the effective charge that can be injected with a single short stimulus

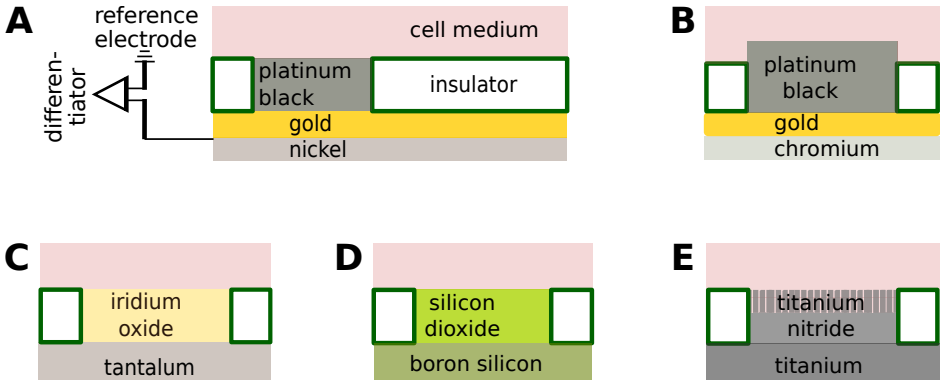

Figure 1.5: MEA designs and fabrication methods. Each device typically is comprised of an electrically conducting contact site (dark gray) with the electrophysiological medium (pink), connected via a good conductor (yellow) to the MEA output, shielded from other lanes and the environment by an insulator (white). Performance can be tuned by changing the electrode and insulator properties: ***A****: Using platinum black as the electrode contact, the first planar MEA was capable of recording the group contraction of chick heart cells [79].* ***B****: Improvements in the insulation layer and electrode surface allowed for recording of action potentials and stimulation of single neurons [70].* ***C****: Activated (oxidized) iridium allows high charge injections [80].* ***D****: A thin dielectric layer (SiO_2) between the electrode and the medium prevents faradaic ionic charge transfer [73]. This electrode can be used for stimulation, but not recording of neuronal activity.* ***E****: The surface structure of sputtered titanium nitride provides a relative high real surface area for capacitive charge transfer [76].*

pulse, generally within 200 μs. Because MEA are in contact with tissue for extended periods of time, electrode stability is important. Below we list several important electrode surface materials with their properties.

The first MEA substrate with embedded planar electrodes was a 30-element microelectrode array of platinum electrodes ([79], **Figure 1.5A**). The production process involves vacuum metal deposition of nickel and gold patterns on glass coverslips [79]. When electrochemical deposition was used to add a platinum black layer onto the electrode, the impedance was lowered [79, 81]. The MEA surface was covered with an insulating coating, and etching was used for removal of the coating parts that covered the electrodes. Using this MEA, charge injections for 100 μs at 100 μA (20 mC/cm^2) were reported to pass without effecting the electrode impedance. High electrode impedance and leakage through the electrode shank across the insulator resulted in low signal-to-noise ratio, but was sufficiently high to be able to record potentials from embryonic chick myocytes [79].

Subsequent developments reduced leakage through the insulation layer and increased the RSA to GSA ratio by use of a rough electrode surface, such that, for the first time, individual action potentials from neurons in culture could be recorded ([70], **Figure 1.5B**). This study shows the correlation between intracellularly recorded action potentials and action potentials detected by nearby MEA electrodes, providing validation for the use of MEAs to record action potentials.

Iridium oxide has also become popular in neuronal charge delivery and recording. Iridium is a rare earth metal and resistant against electrochemical corrosion. The CIC of iridium sharp electrodes was found to increase by a 100-fold if the iridium was electrochemically activated to form an oxide layer [82]. Iridium electrodes can be produced using electrochemical activation [80, 82] (**Figure 1.5C**), thermal decomposition [83] and reactive sputtering [84]. The density and roughness of the iridium oxide layer differed between production methods, with sputtered iridium oxide electrodes achieving the highest CIC (1-3 mC/cm^2) [74].

Although iridium oxide transfers charge mainly by faradaic reactions, the reactions are reversible. During charge delivery iridium changes valence (mainly between Ir(III) and Ir(IV)) and the oxide layer undergoes hydrolysis. The faradaic charge transfer during the reversible IrO reactions are the result from a valence (oxidation) state transition between Ir(V) and Ir(IV) (reaction 1.7) or between Ir(IV) and Ir(III) (reaction 1.8).

$$Ir(OH)_3 \rightleftharpoons IrO(OH)_2 + H^+ + e^- \tag{1.7}$$

$$IrO(OH)_2 \rightleftharpoons IrO_2(OH) + H^+ + e^- \tag{1.8}$$

Alternative MEA production methods were developed with the aim to completely eliminate faradaic ionic charge transfer in order to use capacitive stimulation and recording. In 1995, Fromherz and Stett introduced the conducting electrode, which is separated from the medium by a thin dielectric layer ([73], **Figure 1.5D**). This electrode can be used for stimulation, but the strong insulation from the dielectric layer however prevents recording of any neuronal activity [73].

In more recent years, titanium nitride (TiN) has been increasingly adapted as an electrode material. Reactively sputtered titanium has a rough, columnar surface ([76], **Figure 1.5E**). This columnar surface results in a high real to GSA to RSA ratio and allows for a high capacitive CIC, initially reported to be as high as 23 mC/cm^2. Subsequent papers report safe CIC limits ranging from 0.2 μC/cm^2 to 3 μC/cm^2, but the pulse duration and waveform differ between these studies. The studies report a safe voltage range between -1V to +1V [77]. A typical pulse duration of 200 μs on a 30x30 μm surface applied at the recommended maximum settings of 750 μA translates into a safe CIC of 21 μC/cm^2.

In this section, we reviewed the different methods for stimulation and recording using MEAs, and discussed various MEA fabrication methods. For the experiments in this thesis we used planar TiN electrodes that provide a high real to geometric surface area for capacitive stimulation. We were able to use these MEAs to record cultures up to 17 days in vitro, with typical recording sessions of 20 minutes and re-used MEAs multiple times without noticable damage as a result of recording and/or stimulation.

1.4 Outline of the thesis

A graphical overview of the thesis is shown in **Figure 1.6**. Chapters 2 to 4 represent computational work; in Chapter 5 we present a novel data analysis method; Chapters 6 and 7 report on experimental findings.

More specifically, in Chapter 2 we show for the first time that a molecularly regulated switch in the mode of neurotransmitter release turns on Hebbian plasticity and initiates a period of rapid learning. This developmental switch makes neural circuits sensitive to external stimuli. However, at the same time these circuits have to be stable against intrinsic noise.

In Chapter 3, we consider whether structural organization of the brain circuits can improve the stability against noise and simultaneously increase sensitivity to external stimuli. We show that this can be achieved by anti-correlations in the number of afferent and efferent connections within neurons, also referred to as correlation in the degree distribution. As we show, a Hebbian plasticity rule can reshape networks with no correlation to networks with anti-correlations in degree distribution.

We next wondered whether the brain can use temporal structure in the spike train to increase sensitivity to external stimulation. Therefore, in Chapter 4 we study the effect of spike train regularity on detectability in recurrent neural circuits. We find that irregular spike trains are easier to detect because cells are more sensitive to small interspike intervals, and analyze several ways by which the cells can tune this sensitivity to irregular spike trains.

Computational predictions on neural circuits can be tested in cortical cultures, which are monitored using intra- and extracellular recording techniques. However, in particular extracellular recordings yield noisy data. To accurately analyze these experimental data, we develop in Chapter 5 a method to separate burst from background spikes.

We use this separation method to study how bursting emerges in recurrent networks grown from embryonic cortical rat neurons. In Chapter 6, we investigate the development of these networks and find that interference with epigenetic regulator EHMT1 delays the formation of bursting neural networks. As we show in our computational work, neuronal activity is important for many developmental processes. Disruption of the activity patterns early in development can thus have important consequences for the wiring of the brain.

Currently, experimental studies in cortical cultures are often limited to single networks. In Chapter 7, we develop a device that can be used to grow separated neural networks, which connect by forming axonal projections through microtunnels. We show that spontaneous and stimulated activity propagates through these networks at short delays.

Finally, we present the general discussion and conclusions of our research efforts in Chapter 8.

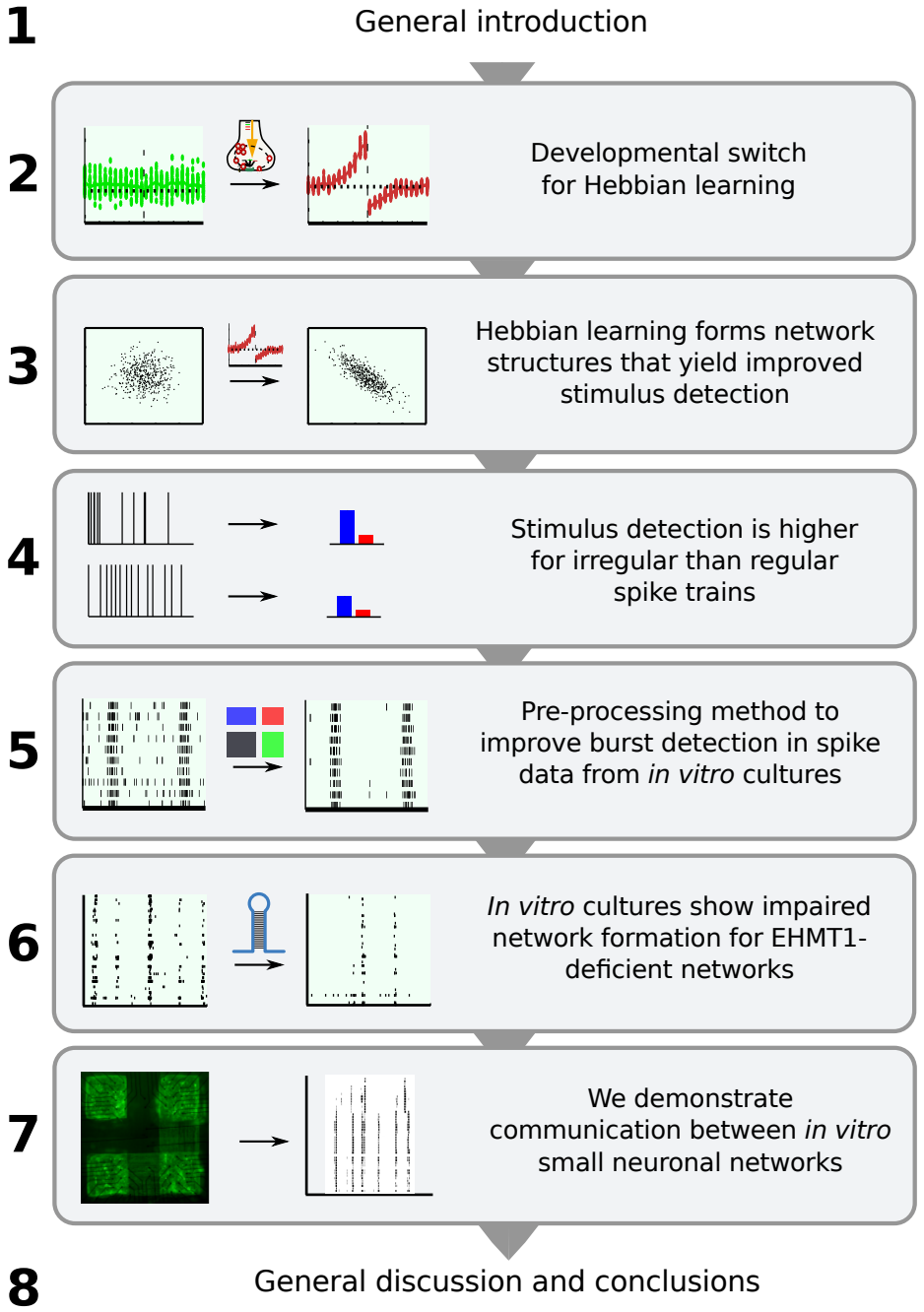

Figure 1.6: Graphical overview of the chapters in this thesis.

References

[1] A Pascual-Leone, A Amedi, F Fregni, and LB Merabet. "The plastic human brain cortex". In: *Annual Review of Neuroscience* 28.1 (2005), pp. 377–401.

[2] G Turrigiano. "Homeostatic synaptic plasticity: local and global mechanisms for stabilizing neuronal function". In: *Cold Spring Harbor perspectives in biology* 4.1 (2012), a005736.

[3] GW Davis. "Homeostatic Signaling and the Stabilization of Neural Function". In: *Neuron* 80.3 (2013), pp. 718–728.

[4] N Caporale and Y Dan. "Spike Timing-Dependent Plasticity: A Hebbian Learning Rule". In: *Annual Review of Neuroscience* 31.1 (2008), pp. 25–46.

[5] A Abbott. "Brain-simulation and graphene projects win billion-euro competition". In: *Nature* (2013).

[6] H Shen. "Neurotechnology: BRAIN storm". In: *Nature* 503 (2013), pp. 26–28.

[7] S Budday, P Steinmann, and E Kuhl. "Physical biology of human brain development". In: *Frontiers in Cellular Neuroscience* 9.257 (2015).

[8] MK Lehtinen and CA Walsh. "Neurogenesis at the Brain: Cerebrospinal Fluid Interface". In: *Annual Review of Cell and Developmental Biology* 27.1 (2011), pp. 653–679.

[9] T Lilja, N Heldring, and O Hermanson. "Like a rolling histone: Epigenetic regulation of neural stem cells and brain development by factors controlling histone acetylation and methylation". In: *Biochimica et Biophysica Acta (BBA) - General Subjects* 1830.2 (2013), pp. 2354–2360.

[10] J Stiles and TL Jernigan. "The Basics of Brain Development". In: *Neuropsychology Review* 20.4 (2010), pp. 327–348.

[11] DH Bhatt, S Zhang, and W Gan. "Dendritic Spine Dynamics". In: *Annual Review of Physiology* 71.1 (2009), pp. 261–282.

[12] R Yuste and T Bonhoeffer. "Genesis of dendritic spines: insights from ultrastructural and imaging studies". In: *Nat Rev Neurosci* 5.1 (2004), pp. 24–34.

[13] C Sotelo. "Purkinje Cell Ontogeny: Formation and Maintenance of Spines". In: *Maturation of the Nervous System*. Ed. by MA Corner, RE Baker, NE Vandepoll, DF Swaab, and HBM Uylings. Vol. 48. Progress in Brain Research. Elsevier, 1978, pp. 149–170.

[14] M Miller and A Peters. "Maturation of rat visual cortex. II. A combined Golgi-electron microscope study of pyramidal neurons". In: *The Journal of Comparative Neurology* 203.4 (1981), pp. 555–573.

[15] JE Vaughn. "Fine structure of synaptogenesis in the vertebrate central nervous system". In: *Synapse* 3 (1989), pp. 255–285.

[16] Y Yoshihara, M De Roo, and D Muller. "Dendritic spine formation and stabilization". In: *Current Opinion in Neurobiology* 19.2 (2009), pp. 146–153.

[17] P García-López, V García-Marín, and M Freire. "Dendritic Spines and Development: Towards a Unifying Model of Spinogenesis". In: *Neural Plasticity* 2010 (2010), pp. 1–29.

[18] M De Roo, P Klauser, P Mendez, L Poglia, and D Muller. "Activity-Dependent PSD Formation and Stabilization of Newly Formed Spines in Hippocampal Slice Cultures". In: *Cerebral Cortex* 18.1 (2008), pp. 151–161.

[19] MH Johnson. "Functional brain development in humans". In: *Nat Rev Neurosci* 2.7 (2001), pp. 475–483.

[20] EI Knudsen. "Sensitive Periods in the Development of the Brain and Behavior". In: *Journal of Cognitive Neuroscience* 16.8 (2004), pp. 1412–1425.

[21] AD Workman, CJ Charvet, B Clancy, RB Darlington, and BL Finlay. "Modeling Transformations of Neurodevelopmental Sequences across Mammalian Species". In: *The Journal of Neuroscience* 33.17 (2013), pp. 7368–7383.

[22] L Kay, L Humphreys, BJ Eickholt, and J Burrone. "Neuronal activity drives matching of pre- and postsynaptic function during synapse maturation". In: *Nature Neuroscience* 14.6 (2011), pp. 688–690.

[23] E Hanse, H Seth, and I Riebe. "AMPA-silent synapses in brain development and pathology". In: *Nat Rev Neurosci* 14.12 (2013), pp. 839–850.

[24] LC Andreae, NB Fredj, and J Burrone. "Independent Vesicle Pools Underlie Different Modes of Release during Neuronal Development". In: *Journal of Neuroscience* 32.5 (2012), pp. 1867–1874.

[25] PS Kaeser and WG Regehr. "Molecular Mechanisms for Synchronous, Asynchronous, and Spontaneous Neurotransmitter Release". In: *Annual Review of Physiology* 76.1 (2014), pp. 333–363.

[26] MB Martens, T Celikel, and PHE Tiesinga. "A developmental switch for Hebbian plasticity". In: *PLoS Computational Biology* 11.7 (2015), e1004386.

[27] H Ko et al. "The emergence of functional microcircuits in visual cortex". In: *Nature* 496.7443 (2013), pp. 96–100.

[28] C Lohmann and HW Kessels. "The developmental stages of synaptic plasticity". In: *The Journal of Physiology* 592.1 (2014), pp. 13–31.

[29] P Caroni, F Donato, and D Muller. "Structural plasticity upon learning: regulation and functions". In: *Nat Rev Neurosci* 13.7 (2012), pp. 478–490.

[30] JR Sanes and M Yamagata. "Many Paths to Synaptic Specificity". In: *Annual Review of Cell and Developmental Biology* 25.1 (2009), pp. 161–195.

[31] T Ma et al. "Subcortical origins of human and monkey neocortical interneurons". In: *Nat Neurosci* 16.11 (2013), pp. 1588–1597.

[32] The Petilla interneuron nomenclature Group. "Petilla terminology: nomenclature of features of GABAergic interneurons of the cerebral cortex". In: *Nat Rev Neurosci* 9.7 (2008), pp. 557–568.

[33] CK Pfeffer, M Xue, M He, ZJ Huang, and M Scanziani. "Inhibition of inhibition in visual cortex: the logic of connections between molecularly distinct interneurons". In: *Nat Neurosci* 16.8 (2013), pp. 1068–1076.

[34] J DeFelipe et al. “New insights into the classification and nomenclature of cortical GABAergic interneurons”. In: *Nat Rev Neurosci* 14.3 (2013), pp. 202–216.

[35] C Holmgren, T Harkany, B Svennenfors, and Y Zilberter. “Pyramidal cell communication within local networks in layer 2/3 of rat neocortex”. In: *The Journal of Physiology* 551.1 (2003), pp. 139–153.

[36] AM Packer and R Yuste. “Dense, Unspecific Connectivity of Neocortical Parvalbumin-Positive Interneurons: A Canonical Microcircuit for Inhibition?” In: *The Journal of Neuroscience* 31.37 (2011), pp. 13260–13271.

[37] CF Stevens and Y Wang. “Facilitation and depression at single central synapses”. In: *Neuron* 14.4 (1995), pp. 795–802.

[38] H Markram and M Tsodyks. “Redistribution of synaptic efficacy between neocortical pyramidal neurons”. In: *Nature* 382.6594 (1996), pp. 807–810.

[39] M Tsodyks, A Uziel, and H Markram. “Synchrony Generation in Recurrent Networks with Frequency-Dependent Synapses”. In: *The Journal of Neuroscience* 20.RC50 (2000), pp. 1–5.

[40] R Jahn and D Fasshauer. “Molecular machines governing exocytosis of synaptic vesicles”. In: *Nature* 490.7419 (2012), pp. 201–207.

[41] T Pussa. *Principles of Food Toxicology*. Boca Raton, FL, USA: CRC Press, 2013.

[42] A Lüthi and DA McCormick. “H-Current: Properties of a Neuronal and Network Pacemaker”. In: *Neuron* 21.1 (1998), pp. 9–12.

[43] I van Welie, JA van Hooft, and WJ Wadman. “Homeostatic scaling of neuronal excitability by synaptic modulation of somatic hyperpolarization-activated Ih channels”. In: *Proceedings of the National Academy of Sciences of the United States of America* 101.14 (2004), pp. 5123–5128.

[44] LM Giocomo and ME Hasselmo. “Time Constants of h Current in Layer II Stellate Cells Differ along the Dorsal to Ventral Axis of Medial Entorhinal Cortex”. In: *The Journal of Neuroscience* 28.38 (2008), pp. 9414–9425.

[45] CT Dickson et al. “Properties and Role of I h in the Pacing of Subthreshold Oscillations in Entorhinal Cortex Layer II Neurons”. In: *Journal of Neurophysiology* 83.5 (2000), pp. 2562–2579.

[46] E Fransén, AA Alonso, CT Dickson, J Magistretti, and ME Hasselmo. “Ionic mechanisms in the generation of subthreshold oscillations and action potential clustering in entorhinal layer II stellate neurons”. In: *Hippocampus* 14.3 (2004), pp. 368–384.

[47] J Smythies. “Some Aspects of the Normal Role of Neuromodulators in the Immune System”. In: *Neuroscience & Medicine* 2.3 (2011), pp. 275–281.

[48] M Sarter, V Parikh, and WM Howe. “Phasic acetylcholine release and the volume transmission hypothesis: time to move on”. In: *Nat Rev Neuroscience* 10.5 (2009), pp. 383–390.

[49] SH Lee and Y Dan. “Neuromodulation of Brain States”. In: *Neuron* 76.1 (2012), pp. 209–222.

[50] V Pawlak, JR Wickens, A Kirkwood, and JND Kerr. "Timing is not Everything: Neuromodulation Opens the STDP Gate". In: *Frontiers in Synaptic Neuroscience* 2.146 (2010).

[51] AC Michael and LM Borland. *Chapter 7: Determining Serotonin and Dopamine Uptake Rates in Synaptosomes Using High-Speed Chronoamperometry*. CRC Press/Taylor & Francis, 2008.

[52] V Parikh, R Kozak, V Martinez, and M Sarter. "Prefrontal acetylcholine release controls cue detection on multiple time scales". In: *Neuron* 56.1 (2007), pp. 141–154.

[53] GG Turrigiano. "The Self-Tuning Neuron: Synaptic Scaling of Excitatory Synapses". In: *Cell* 135.3 (2008), pp. 422–435.

[54] T OLeary, AH Williams, A Franci, and E Marder. "Cell Types, Network Homeostasis, and Pathological Compensation from a Biologically Plausible Ion Channel Expression Model". In: *Neuron* 82.4 (2014), pp. 809–821.

[55] S Bergquist, DK Dickman, and GW Davis. "A Hierarchy of Cell Intrinsic and Target-Derived Homeostatic Signaling". In: *Neuron* 66.2 (2010), pp. 220–234.

[56] HS Bateup, CL Denefrio, CA Johnson, JL Saulnier, and BL Sabatini. "Temporal dynamics of a homeostatic pathway controlling neural network activity". In: *Frontiers in Molecular Neuroscience* 6.28 (2013).

[57] G Turrigiano. "Too Many Cooks? Intrinsic and Synaptic Homeostatic Mechanisms in Cortical Circuit Refinement". In: *Annual Review of Neuroscience* 34.1 (2011), pp. 89–103.

[58] D Attwell and SB Laughlin. "An Energy Budget for Signaling in the Grey Matter of the Brain". In: *J Cereb Blood Flow Metab* 21.10 (2001), pp. 1133–1145.

[59] JJ Harris, R Jolivet, and D Attwell. "Synaptic Energy Use and Supply". In: *Neuron* 75.5 (2012), pp. 762–777.

[60] T Toyoizumi et al. "A Theory of the Transition to Critical Period Plasticity: Inhibition Selectively Suppresses Spontaneous Activity". In: *Neuron* 80.1 (2013), pp. 51–63.

[61] H van Bokhoven. "Genetic and Epigenetic Networks in Intellectual Disabilities". In: *Annual Review of Genetics* 45.1 (2011), pp. 81–104.

[62] C Mozzetta et al. "The Histone H3 Lysine 9 Methyltransferases G9a and GLP Regulate Polycomb Repressive Complex 2-Mediated Gene Silencing". In: *Molecular Cell* 53.2 (2014), pp. 277–289.

[63] MCM Balemans et al. "Reduced exploration, increased anxiety, and altered social behavior: Autistic-like features of euchromatin histone methyltransferase 1 heterozygous knockout mice". In: *Behavioural Brain Research* 208.1 (2010), pp. 47–55.

[64] MCM Balemans et al. "Hippocampal dysfunction in the Euchromatin histone methyltransferase 1 heterozygous knockout mouse model for Kleefstra syndrome". In: *Human Molecular Genetics* 22.5 (2013), pp. 852–866.

[65] LC Andreae and J Burrone. “The role of neuronal activity and transmitter release on synapse formation”. In: *Current Opinion in Neurobiology* 27 (2014), pp. 47–52.

[66] Dh Geschwind and P Levitt. “Autism spectrum disorders: developmental disconnection syndromes”. In: *Current Opinion in Neurobiology* 17.1 (2007), pp. 103–111.

[67] JLR Rubenstein and MM Merzenich. “Model of autism: increased ratio of excitation/inhibition in key neural systems”. In: *Genes, Brain and Behavior* 2.5 (2003), pp. 255–267.

[68] G Testa-Silva et al. “Hyperconnectivity and Slow Synapses during Early Development of Medial Prefrontal Cortex in a Mouse Model for Mental Retardation and Autism”. In: *Cerebral Cortex* 22.6 (2012), pp. 1333–1342.

[69] B Sakmann and E Neher. “Patch Clamp Techniques for Studying Ionic Channels in Excitable Membranes”. In: *Annual Review of Physiology* 46.1 (1984), pp. 455–472.

[70] J Pine. “Recording action potentials from cultured neurons with extracellular microcircuit electrodes”. In: *Journal of Neuroscience Methods* 2.1 (1980), pp. 19–31.

[71] JP Meeks, X Jiang, and S Mennerick. “Action potential fidelity during normal and epileptiform activity in paired soma-axon recordings from rat hippocampus”. In: *The Journal of Physiology* 566.2 (2005), pp. 425–441.

[72] D Wagenaar, J Pine, and S Potter. “An extremely rich repertoire of bursting patterns during the development of cortical cultures”. In: *BMC Neuroscience* 7.1 (2006), p. 11.

[73] P Fromherz and A Stett. “Silicon-Neuron Junction: Capacitive Stimulation of an Individual Neuron on a Silicon Chip”. In: *Phys. Rev. Lett.* 75 (1995), pp. 1670–1673.

[74] S Negi, R Bhandari, L Rieth, R Wagenen, and F Solzbacher. “Neural electrode degradation from continuous electrical stimulation: Comparison of sputtered and activated iridium oxide”. In: *Journal of Neuroscience Methods* 186.1 (2010), pp. 8–17.

[75] M Fejtl, A Stett, W Nisch, K Boven, and A Möller. *On Micro-Electrode Array Revival: Its Development, Sophistication of Recording, and Stimulation.* Springer US, 2006, pp. 24–37.

[76] M Janders, U Egert, M Stelzle, and W Nisch. “Novel thin film titanium nitride micro-electrodes with excellent charge transfer capability for cell stimulation and sensing applications”. In: *Engineering in Medicine and Biology Society, 1996. Bridging Disciplines for Biomedicine. Proceedings of the 18th Annual International Conference of the IEEE.* Vol. 1. 1996, pp. 245–247.

[77] MultiChannelSystems. “Safe Charge Injection Limits”. In: *Microelectrode Array (MEA) Manual*. www.multichannelsystems.com, 2012.

[78] BO Aronsson, J Lausmaa, and B Kasemo. “Glow discharge plasma treatment for surface cleaning and modification of metallic biomaterials”. In: *Journal of Biomedical Materials Research* 35.1 (1997), pp. 49–73.

[79] CA Thomas, PA Springer, GE Loeb, Y Berwald-Netter, and LM Okun. “A miniature microelectrode array to monitor the bioelectric activity of cultured cells”. In: *Experimental Cell Research* 74.1 (1972), pp. 61–66.

[80] SJ Tanghe, K Najafi, and KD Wise. “A planar IrO multichannel stimulating electrode for use in neural prostheses”. In: *Sensors and Actuators B: Chemical* 1.1-6 (1990), pp. 464–467.

[81] RC Gesteland, B Howland, JY Lettvin, and WH Pitts. “Comments on micro-electrodes”. In: *Proc. IRE* 47 (1959), pp. 1856–1862.

[82] LS Robblee, J Leftko, and SB Brummer. “Activated iridium: an electrode suitable for reversible charge injection into saline solutions”. In: *Journal of the Electrochemical Society* 130 (1983), pp. 731–733.

[83] LS Robblee, MM Mangaudis, ED Lasinsky, AG Kimball, and SB Brummer. “Charge Injection Properties of Thermally-Prepared Iridium Oxide Films”. In: *MRS Proceedings* 55.5 (1985), pp. 303–310.

[84] JD Klein, SL Clauson, and SF Cogan. “Morphology and charge capacity of sputtered iridium oxide films”. In: *Journal of Vacuum Science Technology A: Vacuum, Surfaces, and Films* 7.5 (1989), pp. 3043–3047.

Chapter 2

A developmental switch for Hebbian plasticity

This chapter was published as:

M.B. Martens, T. Celikel, P.H.E. Tiesinga (2015). *A developmental switch for Hebbian plasticity.* PLoS Computational Biology; 11(07):e1004386

2.1 Abstract

Hebbian forms of synaptic plasticity are required for the orderly development of sensory circuits in the brain and are powerful modulators of learning and memory in adulthood. During development, emergence of Hebbian plasticity leads to formation of functional circuits. By modeling the dynamics of neurotransmitter release during early postnatal cortical development we show that a developmentally regulated switch in vesicle exocytosis mode triggers associative (i.e. Hebbian) plasticity. Early in development spontaneous vesicle exocytosis (SVE), often considered as 'synaptic noise', is important for homogenization of synaptic weights and maintenance of synaptic weights in the appropriate dynamic range. Our results demonstrate that SVE has a permissive, whereas subsequent evoked vesicle exocytosis (EVE) has an instructive role in the expression of Hebbian plasticity. A timed onset for Hebbian plasticity can be achieved by switching from SVE to EVE and the balance between SVE and EVE can control the effective rate of Hebbian plasticity. We further show that this developmental switch in neurotransmitter release mode enables maturation of spike-timing dependent plasticity. A mis-timed or inadequate SVE to EVE switch may lead to malformation of brain networks thereby contributing to the etiology of neurodevelopmental disorders.

2.2 Introduction

Functional circuits in the brain are rapidly established during early development and are fine-tuned by experience throughout life. In the rodent neocortex, for example, cortical columns form in the first three weeks after birth [1, 2]. During this period, thalamo-cortical input is essential for columnar formation [3] and stimulus-evoked activity patterns further refine cortical connectivity [4]. Activity-dependent forms of synaptic plasticity, in particular Hebbian plasticity, guide the cortical refinement and are required for functional maturation of cortical circuits [5]. Although the postsynaptic pathways involved in the developmental stages of synaptic plasticity are well characterized (e.g. [6, 7]), the cellular mechanism on the presynaptic side that triggers the onset of Hebbian plasticity is still unclear [7].

Early in development pre- and postsynaptic structures are co-localized, even in the absence of any action potential activity [8], while functional connectivity emerges later in development [8]. Initially, synapses are thus established, but functional communication between neurons is lacking. During this initial phase, spontaneous vesicle exocytosis can help to maintain synapses [9, 10]. Reduced vesicle release during development reduces the rate of synapse formation (for review see [11]). Here we studied the role of vesicle exocytosis for maturation of associative plasticity. We propose that a switch in vesicular exocytosis mode ensures a discrete onset for Hebbian plasticity and triggers the activity-dependent

neural circuit formation during neurodevelopment.

The mode of vesicular exocytosis changes rapidly during early development [12]. In immature synapses, neurotransmitter vesicles spontaneously fuse with the membrane whether or not there was a preceding action potential (spontaneous vesicle exocytosis, SVE), whereas in mature synapses evoked vesicle exocytosis (EVE) dominates synaptic communication [12]. EVE can occur within an interval of several milliseconds (synchronously evoked vesicle exocytosis (sEVE)) or delayed by up to several hundred milliseconds (asynchronous evoked vesicle exocytosis (aEVE)) after the action potential (**Figure 2.1A**). Each mode of vesicle exocytosis has the ability to coordinate activity across a synapse, potentially leading to associative plasticity in neural networks. Immature neurons, due to their high input resistance, small size, slow membrane time constant and prolonged decay constant of the excitatory postsynaptic potential (EPSP) [13, 14], have a relatively high probability to generate an action potential resulting from postsynaptic integration of uncorrelated synaptic inputs (SVE). The impact of vesicle exocytosis on synaptic communication changes with development. With reduced input resistance and a faster decay of EPSP [13, 14] the postsynaptic window of opportunity for coincidence detection is shortened such that only temporally correlated presynaptic activity (EVE) can be efficiently integrated by the postsynaptic neuron.

While the molecular mechanisms for the three principal modes of vesicle exocytosis (SVE, aEVE, sEVE) have been characterized [15], the functional role of SVE and aEVE is currently not clear [15–17]. Here, by modeling the developmental changes in exocytosis mode, we show that SVE optimally prepares neural circuits for learning by maintaining synaptic weights in the appropriate dynamic range and homogenizing the synaptic weights into a tight homogeneous distribution. A switch to EVE initiates a period of rapid synaptic plasticity where synaptic input can be efficiently stored in the network. The SVE-EVE balance regulates the rate of Hebbian plasticity in the synapse and learning in neuronal networks. Besides the role of asynchronous exocytosis in gain modulation [18], we show that increased locking of vesicle exocytosis to the action potential causes maturation of the STDP rule [19]. These results argue that SVE, often considered as 'synaptic noise', plays an important role in synaptic plasticity during neurodevelopment and predict that a developmentally regulated switch in the mode of vesicular exocytosis contributes to the activity dependent organization of the developing circuits.

2.3 Results

Effective communication across a chemical synapse starts with vesicular exocytosis and subsequent diffusion of neurotransmitters to the postsynaptic terminal. We studied the effect of the three primary modes of vesicular exocytosis (SVE, aEVE and sEVE) on synaptic competition between synapses using a vesicle-

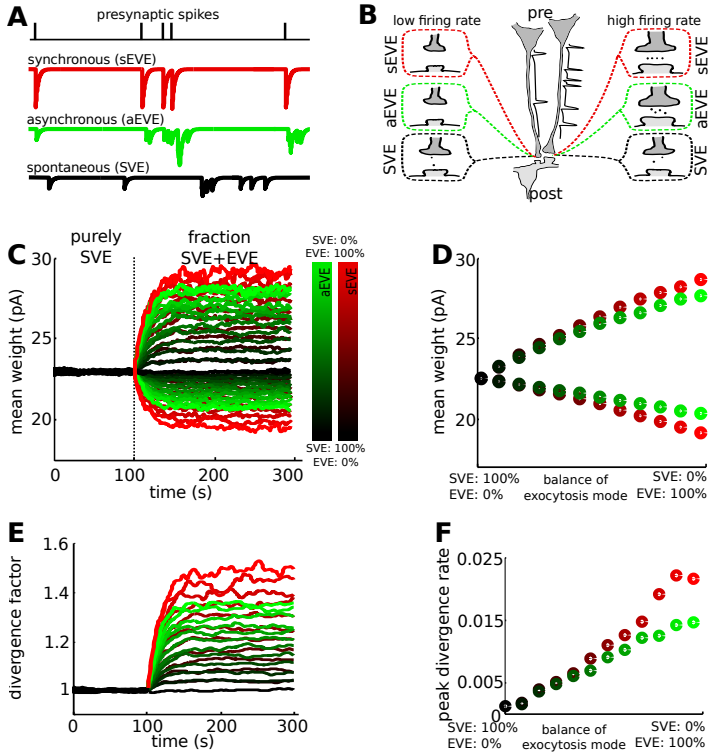

Figure 2.1: The balance between spontaneous and evoked vesicle exocytosis provides control for the rate of Hebbian plasticity. We used the VTDP model represented by Equations 2.1 to 2.8. ***A****: Vesicle exocytosis can occur directly following a presynaptic spike (sEVE), with a high probability after a presynaptic spike (aEVE) or randomly, independent of a presynaptic spike (SVE).* ***B****: Each exocytosis mode can coordinate activity across the synapse. When the EVE mode dominates the release process, there will be competition between synapses of neurons that have low (left presynaptic neuron) and high (right presynaptic neuron) firing rates, with the former decreasing in strength and the latter increasing in strength (top and middle synapses). There is no such competition for SVE-dominated synapses (bottom synapses).* ***C****: Following a switch from SVE to EVE, the synapses at which many action potentials arrive (upper traces) are potentiated at the expense of synapses emanating from the lower firing rate neurons (lower traces). The (partial) switch to EVE occurs at the dotted line and is either to aEVE or sEVE. The colorbar denotes the SVE-aEVE (green) and SVE-sEVE (red) balance.* ***D****: The final difference in weight for the synapses of the low- and high firing rate neurons depends on the SVE-EVE balance. Dots are the mean of the last 100 seconds for the upper (top) and lower (bottom) traces in panel C. Colors represent the same degree of balance as in panel C.* ***E****: The divergence factor between the synapses of the high and low firing rate neurons (upper and lower traces in panel C, respectively) increases after the SVE to EVE switch.* ***F****: The divergence rate is calculated as the change in divergence factor (panel E) per time unit. The maximal rate of divergence depends on the SVE-EVE balance.*

timing dependent plasticity model. For Hebbian plasticity it was necessary that the presynaptic neurotransmitter release correlated with postsynaptic activity. We subsequently used a rate model to characterize the differential effects of the vesicle exocytosis modes on the ability of a neural network to represent a particular pattern of action potentials in matching synaptic weights.

2.3.1 Vesicle-timing dependent plasticity (VTDP) – modeling framework

Most computational studies of synaptic plasticity with spiking neurons use a spike-timing dependent plasticity (STDP) rule [20, 21], implicitly assuming that a presynaptic action potential leads to correlated vesicle exocytosis within a short interval. We focus on the timing of vesicular exocytosis, irrespective of whether it is preceded by presynaptic action potentials, leading to vesicle-timing dependent plasticity (VTDP model). Vesicles that are exocytosed within a canonical STDP time window contribute to time-dependent weight changes as described by the STDP model (Equation 2.7).

Vesicle exocytosis can occur in three different modes (**Figure 2.1A-B**). For SVE, exocytosis is independent of the arrival of an action potential at the presynaptic terminal [15]. For aEVE, exocytosis depends on the calcium concentration and the timing of exocytosis is therefore only loosely coupled to an action potential; each action potential induces a presynaptic calcium influx, whose intracellular concentration exponentially decays. For sEVE, exocytosis immediately follows an action potential.

To study synaptic competition using the VTDP model, we simulated a network model comprised of feed-forward connections from 500 presynaptic neurons to 10 postsynaptic neurons. A subset of the presynaptic neurons (20%) had a higher firing rate (8 Hz) compared to the rest (4 Hz). We used a Poisson process to generate action potentials at these rates. In turn, vesicle exocytosis from the presynaptic terminal was modeled as Poisson processes for SVE, aEVE and sEVE. In the model the probability of exocytosis depended on proteins that are available to support each of the different exocytosis modes. The switch from SVE to EVE is implemented by reducing the fraction of vesicles that are available for SVE and increasing the fraction of vesicles that are available for aEVE or sEVE such that the sum of the fractions remains constant. The probability for vesicle exocytosis also depended on the fraction of available vesicles at the synapse (Equation 2.3).

The rate of vesicle release for sEVE was directly related to the firing rate of each neuron. The release rate of SVE was scaled with the mean firing rate of all presynaptic neurons to obtain the same mean release rate as EVE. The rate of asynchronous release depended on the amount of residual Ca^{2+}, which decays exponentially (Equation 2.4). The total amount of Ca^{2+} entering the presynaptic terminal in response to a single action potential was also scaled to yield the same mean release rate as the other exocytosis modes. Thus, to effectively titrate the

differential contribution of the release rate to synaptic plasticity, the cumulative release was normalized such that the mean and total vesicle release rates were equal for the three modes of neurotransmission.

An exocytosed vesicle was moved from the active pool to the recycling pool. Recovery from the recycling pool to the active pool was modeled as an exponential process (Equation 2.5). The neurotransmitters released from each vesicle induced an excitatory postsynaptic current that decayed within several ms. We used leaky integrate-and-fire neurons with an adaptive spike threshold for the postsynaptic neurons. A homeostatic rule kept the firing rate of the postsynaptic neurons at the desired dynamic range (∼5 Hz) by scaling the synaptic weights accordingly (Equation 2.8).

Thus, for SVE, vesicle exocytosis was spatially (across synapses belonging to the same neuron) and temporally (across time within individual synapses) random and was not coupled to the onset of presynaptic action potentials (**Figure 2.1B**). For aEVE, vesicle exocytosis was spatially biased to synapses belonging to presynaptic neurons with higher firing rates, but it was temporally diffuse (**Figure 2.1B**). For sEVE the vesicle exocytosis was both temporally and spatially linked to the spiking activity of the neurons (**Figure 2.1B**).

2.3.2 Spontaneous exocytosis has a permissive and evoked exocytosis has an instructive role in Hebbian plasticity

Synaptic plasticity leads to competition between synapses when presynaptic cells are active at different rates [20]. In the VTDP model, synapses that were active prior to a postsynaptic action potential were strengthened whereas the others were weakened. We used the VTDP model to study how the three vesicle exocytosis modes contribute to synaptic competition. When synaptic communication was mediated by SVE alone, the chemical neurotransmission did not lead to competition between synapses onto the same postsynaptic neuron, and maintained synaptic weight distribution to a homogeneous distribution, also referred to as a unimodal distribution (**Figure 2.1C**). Introducing a (partial) switch to either aEVE or sEVE caused divergence between synaptic weights for the synapses of the high and low firing rate neurons. The gradual change in synaptic efficacy results in a heterogeneous synaptic efficacy distribution in the network, with synapses that were either weak or strong, but fewer of the intermediate strength (referred to as multimodal). The amount of divergence (the degree of separation between high and low synaptic weights) between synapses of the low- and high firing rate neurons depended on the SVE-EVE balance (**Figure 2.1D**). When vesicle exocytosis was dominated by EVE we found that asynchronous exocytosis resulted in a moderate, and synchronous exocytosis resulted in a strong drive to increase the synaptic weights of the higher firing presynaptic neurons at the expense of synapses of the lower firing rate neurons (**Figure 2.1E**). The SVE-EVE balance regulated the rate at which synaptic competition occurred (**Figure 2.1F**). Cor-

related input could thus shape the structure of the network via EVE. As the rates of vesicle exocytosis onto the postsynaptic neuron were normalized such that they are equal for the three modes, this difference in outcome is caused by their spatiotemporal structure of the synaptic inputs to the postsynaptic neuron. This model of vesicle-timing dependent plasticity shows that the SVE-EVE balance can regulate the rate with which new patterns of action potentials are imprinted into synaptic weights. A switch from SVE to EVE enables a discrete onset for Hebbian plasticity and initiates a period at which synaptic weights rapidly rewire to represent the dominant sensory activity. The SVE-EVE balance can control the rate of Hebbian plasticity.

2.3.3 Additional functional roles for SVE

In addition to the above described functional role for SVE to control the rate of Hebbian plasticity, we explored other functional roles for SVE. We first compared the effect of SVE (**Figure 2.2A**) to that of EVE with uncorrelated spiking activity (**Figure 2.2B**) on the distribution of synaptic weights. We found that SVE homogenizes the synaptic weights into a tighter weight distribution compared to EVE (**Figure 2.2C**). SVE events occur more diffusely compared to EVE, and furthermore the larger EPSC inputs from EVE result in stronger correlations between pre- and postsynaptic spiking. Thus, an additional functional role of SVE is homogenization into a tight synaptic weight distribution and increased stability against synaptic weight fluctuations compared to EVE. Homogenization is also important for synaptogenesis, because newly formed synapses with small initial weights grow stronger and become incorporated into the synaptic pool (**Figure 2.2D**).

Next we asked whether SVE during early development was necessary at all; and what would happen for a gradual increase in EVE in the absence of SVE. Synaptic fluctuations as well as divergence in synaptic weights due to differences in firing rate can be prevented by completely abolishing vesicle release (no SVE, no EVE). However, if neither SVE nor EVE are present, synaptic weights become saturated due to the homeostatic mechanism (**Figure 2.2E**, Equation 2.8). If EVE increases gradually during development, synaptic weights also increase due to the homeostatic mechanism, while retaining the heterogeneous distribution (**Figure 2.2F**). Thus SVE is necessary to maintain synaptic weights in the appropriate dynamic range. SVE and EVE release mechanisms thereby both serve a biological role in synapse formation and synaptic maintenance [9–11].

2.3.4 Rewiring an established neuronal circuit after the SVE to EVE switch requires prolonged synaptic communication

After the switch from SVE to EVE and the subsequent changes in synaptic weight distribution across synapses, the network consists of a few strong synapses among

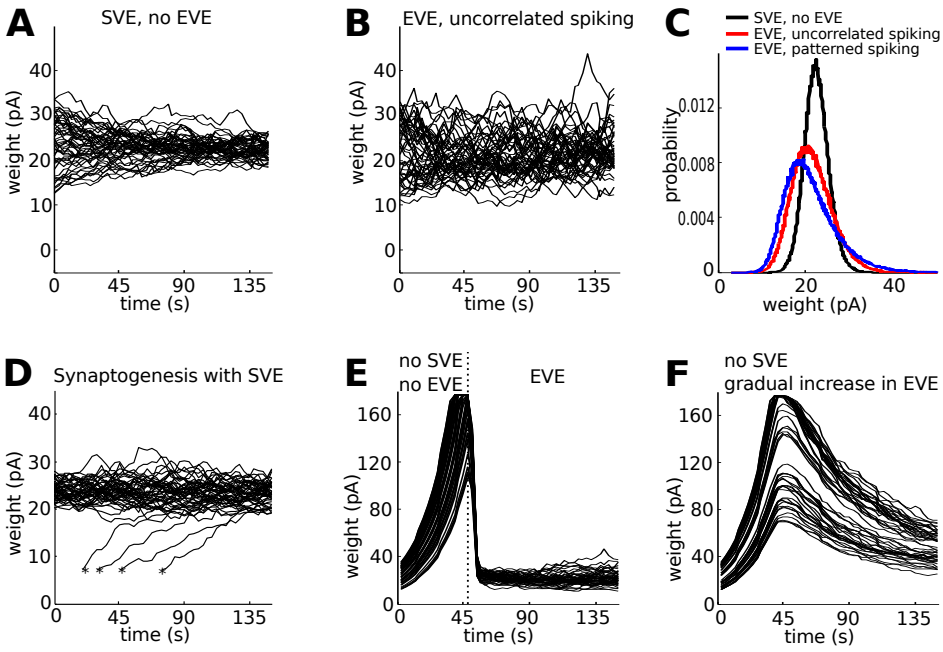

Figure 2.2: Additional functional roles of spontaneous vesicle exocytosis (SVE). ***A****: Synaptic weights that are initially heterogeneous, homogenize into a tight synaptic weight distribution in the case of SVE. Black lines are traces of 50 synaptic weights randomly selected from a network of 500 presynaptic neurons that connect to 10 postsynaptic neurons.* ***B****: Synaptic weights show large fluctuations in the case of EVE. Here all neurons fire uncorrelated action potentials at the same mean firing rate.* ***C****: Distribution of synaptic weights for SVE (black line), EVE with uncorrelated spiking activity (4.8 Hz, blue line) and EVE with patterned spiking activity (red line). For the patterned activity, a subset of the neurons (20%) have higher firing rates (8 Hz) compared to the others (4 Hz). Notice the broadening for uncorrelated and patterned spiking activity in the case of EVE.* ***D****: Synaptogenesis creates new synapses with small initial synaptic weights (denoted with a *). SVE incorporates the newly generated synapses into the homogeneous pool of all synaptic weights.* ***E****: In the absence of SVE, the synaptic weights increase due to the homeostatic mechanism until they reach the maximum synapse size. Synaptic weights are heterogeneous when the switch to evoked vesicle exocytosis (EVE) occurs.* ***F****: For a gradual increase of EVE, in the absence of SVE, the synaptic weights span a large dynamic range and are heterogeneous.*

many other weak ones [20, 22]. This change in synaptic weight distribution shapes the network's ability to encode patterns of action potentials and translate them into memory traces. We aimed to establish the differential roles of the exocytosis modes in the activity dependent organization of cortical circuits. The VTDP model implements the plasticity terms and vesicle exocytosis times separately for each synapse. Such operations are on matrices of size $N_i \cdot N_o$ (number of input neurons · number of output neurons), which is computationally more demanding than the classical STDP modeling which generates spike times and thus works with operations on vectors of size N_i and N_o. We therefore used a rate model that represents vesicle-timing dependent plasticity, consisting of a similar structure and one that can be implemented with better computational efficiency (**Figure 2.3A**). The rate model will help other investigators who want to conduct follow-up studies to implement our model efficiently. The exocytosis rates are a combination of SVE (randomly distributed across synapses) and EVE (strong for the subset of highly active presynaptic neurons). The evolution of synaptic weights is then followed over time. Synaptic efficacy is potentiated for synapses with high vesicle exocytosis rates at the expense of synapses that have lower rate of exocytosis (**Figure 2.3B**).

Each network was initialized either without any particular structure, with each synaptic strength set randomly according to a unimodal distribution, or with a previously encoded weight pattern, comprised of a bimodal distribution of low and high values, that is different from the pattern presented (**Figure 2.3C**). While no pattern of action potentials could be stored during SVE, synaptic communication through EVE introduces competition that enables storage of the patterns of action potentials (**Figure 2.3D**). A switch from SVE to EVE thus generates a window of opportunity for a cortical network to rewire as instructed by experience. Rewiring an established circuit after the switch takes significantly more time than starting from a homogeneous state without patterns of action potentials imprinted (**Figure 2.3E**).

SVE can thus be used to maintain baseline network activity and unspecific network connectivity, and the SVE-EVE balance regulates the rate at which time neural circuits are shaped by patterns of action potentials.

2.3.5 The developmental switch from SVE to EVE during human brain development

How is the SVE-EVE balance regulated? An initial suggestion that SVE and EVE might utilize distinct vesicle pools [23] was accompanied by a concerted research effort to characterize the differential regulatory pathways that impact vesicle exocytosis (for reviews, see [15, 24]). Optical recordings from developing neurons *in vitro* demonstrated a switch from SVE to predominantly EVE as neurons matured [12]. The switch to EVE at the synaptic terminal occurs independent of whether there is functional communication with a postsynaptic neuron, suggesting a cell-autonomous process [12]. Investigations on cell-autonomous regulation of vesicle

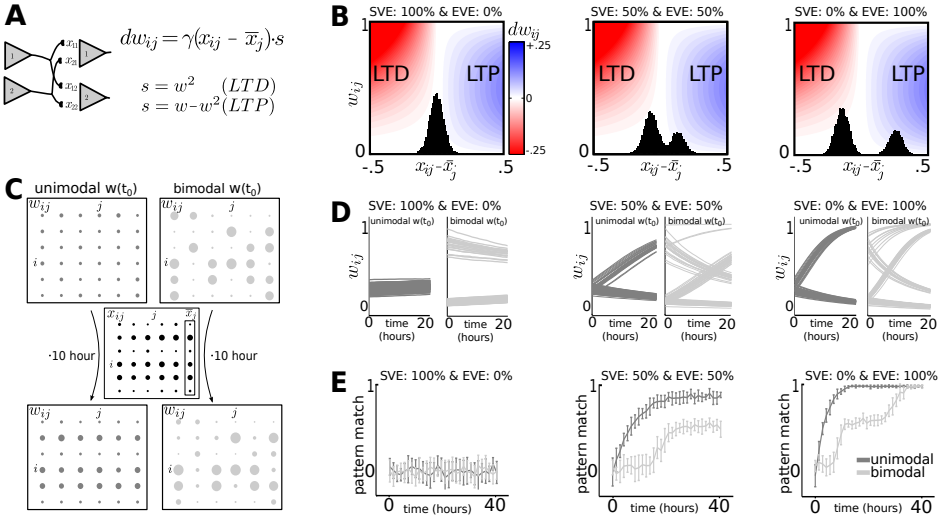

Figure 2.3: The rate at which a pattern of action potentials is imprinted onto a configuration of synaptic weights depends on the initial weight distribution and the SVE-EVE balance. We used the rate model described by Equations 2.11-2.12. ***A****: Presynaptic neurons i connect to postsynaptic neurons j, for which the synaptic weights are shaped by local competition between the vesicle exocytosis rates (x_{ij} relative to the average exocytosis rate onto the postsynaptic neuron ($\bar{x}_j$)). The exocytosis rates are a combination of SVE (randomly distributed across synapses) and EVE (strong for the subset of highly active presynaptic neurons).* ***B****: The degree of potentiation (blue, positive rate of change in dw_{ij}) and depression (red, negative rate of change) depends on whether the relative exocytosis rate is bimodal versus unimodal (black histograms).* ***C****: The initial synaptic weights (w) have either a unimodal distribution (left) or a bimodal distribution (right). A pattern of activity (x) is presented to both networks. Using the rate model, we can clearly see the activity pattern is represented in the weights of the network that started with the unimodal distribution, but not for the initial bimodal distribution. Dot size represents weight (w_{ij}) or exocytosis rate (x_{ij}).* ***D****: The rate at which synaptic weights converge to a configuration corresponding to the applied patterns of action potentials depends on the SVE-EVE balance. Dark and light gray traces start from an initial unimodal and bimodal distribution respectively.* ***E****: Matching the synaptic weights to the pattern of action-potential activity (pattern match, Equation 2.13) takes significantly longer when the initial weights have a bimodal distribution.*

exocytosis focus on the functional properties of the proteins involved in the docking of vesicles to the presynaptic membrane such as the SNARE proteins Syntaxin, SNAP-25, and VAMP2/Synaptobrevin and a core set of SNARE-binding proteins: Synaptotagmin, Munc13, Munc18, Doc2 and Complexin [24].

Exocytosis of vesicles docked at the active zone in the presynaptic terminal is mediated by calcium-sensitive proteins. Calcium sensitivity and kinetics of vesicle exocytosis depends on the calcium sensors expressed. The presence of high-affinity calcium sensor Doc2b increases the fraction of SVE exocytosis [25], which might also act completely independent of presynaptic action potential induced calcium entry [26]. Doc2a on the other hand facilitates aEVE [27]. sEVE is mediated by Synaptotagmin1, which is selectively enhanced by Complexin that can act as a fusion clamp or adaptor to inhibit SVE and aEVE [28, 29] (**Figure 2.4A**).

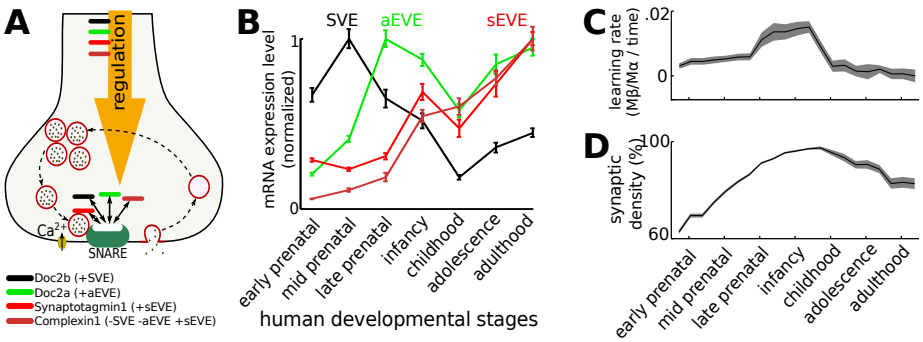

Figure 2.4: During cortical development there is a switch from exocytosis dominated by spontaneous exocytosis to asynchronous and synchronous vesicle exocytosis. ***A****: The SVE-EVE balance is regulated by Ca^{2+} sensing proteins (Doc2s and synaptotagmins). Complexin promotes Synaptotagmin1 mediated synchronous exocytosis while blocking spontaneous and asynchronous exocytosis [28].* ***B****: In humans, the relative mRNA expression of these sensors varies in time. Early in development there are high levels of Doc2b (SVE, black line), which decay during the intermediate developmental stage at which time there is an increase in Doc2a (aEVE, green line) expression. The expression of Synaptotagmin1/Complexin1 (sEVE, red lines) increases throughout neurodevelopment, reaching their maximal expression levels during late development [30].* ***C****: By implementing the mRNA expression levels as ratios for SVE, aEVE and sEVE, a period of rapid learning is observed early in development during which SVE decreases and aEVE and sEVE increase. During this period the wiring in the neural circuitry is formed, after which the learning rate decreases. Gray shade is standard deviation.* ***D****: During early developmental periods synaptogenesis is prominent, until activity-dependent pruning reduces the synaptic density later in life.*

The expression of these calcium sensors varies across time, which is reflected

in the corresponding mRNA expression levels. We re-analyzed the human transcriptome [30] for mRNA expression profiles of the calcium sensitive proteins during neurodevelopment and found high Doc2b expression early in development was followed by a peak in Doc2a, while Synaptotagmin-1/Complexin-1 became prominent during early childhood (**Figure 2.4B**). These profiles are consistent with a switch from high SVE to aEVE early in development and dominant sEVE at later developmental stages. To study the developmental learning rate, the SVE, aEVE and sEVE ratio profiles were used to mimic the biological situation. The synapses belonging to the higher firing rate neurons strengthen at the expense of the synapses belonging to the lower firing rate neurons (for EVE, not for SVE). The learning rate (see Equation 2.9 in the Materials & Methods) diminishes if the synaptic weights approach their upper and lower bounds, which resulted in a learning rate peak around infancy (**Figure 2.4C**). During development, new synapses were formed [31] and weak synapses were pruned ([32], see Materials & Methods). Early in development the rate of synaptogenesis was larger than the rate of synaptic pruning, which caused a rise in synaptic density (**Figure 2.4D**). After EVE became more dominant, the rate of synaptic pruning became larger than synaptogenesis, which caused a decrease in synaptic density.

The SVE-EVE switch thus coincides in time with the early stages in human neurodevelopment [33, 34]. There is a rapid increase in synaptogenesis around the time of birth for all cortical areas, while a burst of synapse formation occurs at different ages in cortical regions [33]. In the visual cortex, for example, synapse formation is accelerated between 3 and 4 months and the maximum density is reached between 4 and 12 months, while synaptogenesis in the prefrontal cortex reaches its peak well after the first year [33]. After the peak in synaptic density, corresponding to about 150% of adult levels, a sensitive period with high levels of associative plasticity occurs, whereas plasticity that occurs beyond the end of this sensitive period alters connectivity patterns within the architectural constraints established during the sensitive period [33, 34]. These developmental patterns are highly conserved throughout many species [35].

2.3.6 The maturation of the STDP rule during development

A transition from an immature to mature STDP rule is observed during early cortical development of the rat somatosensory cortex (**Figure 2.5C**, [19]). The transition coincides in time with a critical period in circuit formation in the barrel cortex, during which extensive activity-dependent pruning occurs confining neuronal arborizations to the columnar structure in the barrel cortex ([1], **Figure 2.5A**). At the same time, a functional transition occurs from predominantly spontaneous, stimulus-independent exocytosis early in development to stimulus-dependent exocytosis later in development ([2], **Figure 2.5B**). The action potential-dependent responses in the intermediate stages are typically prolonged and with high variability, which matures to a responsiveness that is tightly

synchronized to the stimulus. By modeling the corresponding changes in exocytosis using the VTDP model (see above), we found that STDP expression matures because of the switch to vesicle exocytosis that is increasingly time-locked to the stimulus ([19], **Figure 2.5C**).

2.4 Discussion

The switch from SVE to EVE triggers a period of rapid synaptic competition, mediated by synaptic depression and potentiation according to Hebbian plasticity rules. This may seem trivial, but it has important functional consequences for neural circuit development, as we will highlight here. In general, the switch provides a framework for understanding the onset of synaptic plasticity in circuit formation during neurodevelopment by mechanistically linking the onset to the developmental changes in vesicular exocytosis of neurotransmitters.

While the molecular mechanisms for vesicle exocytosis are well described, the functional roles of SVE and aEVE are unclear [15–17]. Our VTDP model showed that early in development, in the absence of relevant sensory input, SVE maintains synaptic weights in a homogeneous distribution and within the appropriate dynamic range. Molecular changes at the presynaptic terminal can then switch vesicle release from SVE to EVE. We propose that this SVE to EVE switch enables sensory inputs to fine-tune the circuit connectivity using activity dependent synaptic reorganization (**Figure 2.5**, [37]). The transition from SVE to EVE can initiate a window of strong associative plasticity, during which for example local connectivity can be reorganized extensively by activity-dependent mechanisms of plasticity such that the appropriate feature selectivity is established in the network [5]. Similar to the switch from immature (P9-11 in mice) to mature (P12+) visual responses, a switch from endogenous network oscillations to mature visual responses occurs at birth in human [38]. Children born prematurely have deficits in visual acuity and contrast sensitivity compared to children born at full term [39].

The SVE to EVE switch involves molecular changes at the presynaptic terminal and brain regions could open windows for rapid synaptic reorganization in a specifically programmed temporal order. Hierarchical organization of sensorymotor pathways may develop through a cascade of such windows for plasticity [40]. The sequential opening of such windows was for example observed for the visual cortex, where plasticity for inputs to L2/3 extends beyond the window of plasticity for thalamic inputs to L4 [41].

For an understanding of circuit plasticity during development, one needs to take into account the synaptic learning rule, the spike activity patterns present, and the timescales of their information content [42]. For example, the timescales at which STDP operates can change the effectiveness of synapse refinement, and specifically STDP over short timescales does not necessarily lead to the appropriate circuit refinement during early development [43]. During development

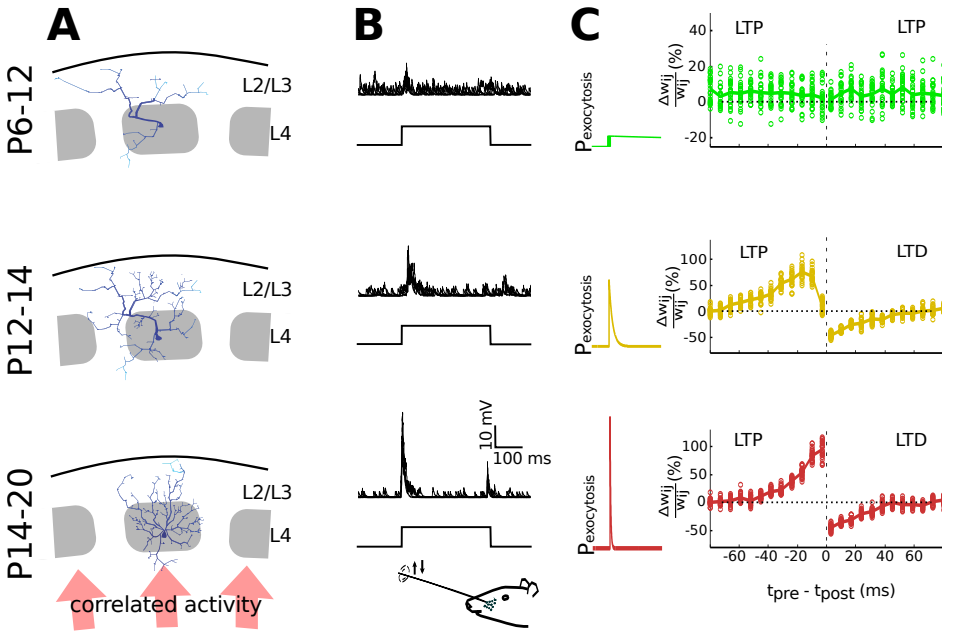

Figure 2.5: Predictions for the role of the SVE to EVE switch in the refinement of cortical neural circuits. ***A****: During early development arborization of barrel cortical neurons is sparse, and does not respect the columnar boundaries. Neurite outgrowth occurs during the intermediate developmental period and in late development, as synapses mature, the extensive arborizations outside the column are pruned in an activity dependent manner (illustration based on the results from [1], using the Trees Toolbox [36]).* ***B****: Whisker deflection induces synaptic responses in layer 2/3 of the barrel cortex. The input to L2/3 is largely uncorrelated at P12, with a rapid switch to stimulus-driven responses during development [2]. At P12-P14 the stimulus-induced activity is typically prolonged and with high variability, whereas at a later stage (P20) the responses are more precisely time-locked to the stimulus [2].* ***C****: By modeling changes in the release probability from SVE to highly time-locked release during development, Hebbian plasticity behavior changes from an immature to mature STDP rule. The maturation process of the STDP rule is described in vitro for layer 4 – layer 2/3 synapses during these critical developmental stages [19]. The calcium time constant (Equation 2.4) was 1 second (top), 7 millisecond (middle) and 2 millisecond (bottom), and 50 stimuli were given for each* $t_{pre} - t_{post}$ *bin.*

correlations in spike activity patterns become faster, which can further change the efficacy of STDP [42]. Importantly, the developmental switch that we found was observable for different timescales of STDP and thus timescale independent (data not shown).

Burst-based Hebbian learning rules, which integrate spike activity patterns over longer timescales, play a role in cortical refinement [44]. For burst-based plasticity, LTP is favored over LTD [45]. Vesicle exocytosis in the form of aEVE (vesicles are released asynchronously after an action potential) could be considered a miniburst of vesicle exocytosis. Such a miniburst of vesicles introduces multiple pairings of vesicles with a postsynaptic spike as opposed to sEVE (vesicles are released directly after an action potential and have the same temporal relation to the postsynaptic spike). The release in the form of aEVE could thus bias the VTDP rule towards LTP over LTD early in development [45].

Neural responses become increasingly time-locked to stimuli during development [2, 38]. Using the VTDP model, we show that the transition to action potential-dependent vesicle release can explain the maturation of the STDP rule observed in the somatosensory cortex ([19], **Figure 2.5C**). The VTDP model thus links together the experimental observation of increased action potential-dependent input, receptive field refinement to the home column of sensory input and maturation of STDP that coincide in time during early postnatal development. Although plasticity mechanisms in the postsynaptic neuron change during development [46], our model does not depend on the molecular machinery for plasticity in the postsynaptic neuron. Solely by introducing changes in the presynaptic release machinery, our VTDP model can mechanistically elucidate the functional changes, structural reorganization and maturation of activity-dependent plasticity that occur during early neurodevelopment.

The early postnatal development is accompanied by periods with rapid, often irreversible changes [47], including but not limited to maturation of inhibition [48, 49]. A modeling study shows that the maturation of inhibition can initiate a critical period by preferentially suppressing spontaneous spiking activity relative to visually evoked activity [40]. For this mechanism to be effective it should occur after the SVE-EVE switch, otherwise no evoked activity could be preferentially selected. Furthermore, the maturation of inhibition effectively increases the spiking threshold which affects all synapses simultaneously, whereas a SVE-EVE switch could initiate competition between synapses based on the identity of the presynaptic populations, thereby regulating synaptic plasticity in a region, layer or neuron type specific manner. The balance between SVE and EVE was shown to segregate between synapses, allowing the SVE-EVE switch to occur in a synapse specific manner [50, 51]. The increase in inhibition could further functionalize the SVE-EVE switch by the selective suppression of SVE relative to EVE [40]. However, the increased threshold caused by the maturation of inhibition could be compensated by homeostatic upscaling of all synapses, potentially abolishing the effect of inhibition.

The results presented herein shows that SVE independently and single-handedly

places synaptic rewiring on hold, and switching to EVE induces a period of rapid, activity-dependent changes. Once the neural circuit is wired to represent particular sensory features, rewiring is significantly more difficult and requires disproportionately more vesicular neurotransmission.

The cell-autonomous regulation of the SVE-EVE balance

At the presynaptic terminal, proteins involved in the exocytotic machinery determine the SVE-EVE balance. The expression of the relevant calcium sensitive proteins can be genetically regulated, and evidence for a cell-autonomous switch from SVE to EVE has previously been shown *in vitro* [8, 12].

Despite the fact that both SVE and EVE have the potential to drive Hebbian plasticity across the synapse, it is unclear how, where and when Hebbian plasticity develops in the first place [7]. The model presented here mechanistically links the mode of vesicular exocytosis to Hebbian plasticity during neural development. As the switch from SVE to EVE is genetically regulated, it is an ideal candidate mechanism to initiate region, layer and cell specific onset of Hebbian plasticity. Specific regulation of the onset of Hebbian plasticity is, for example, important for a hierarchical system in order to optimally deal with the input statistics, such that sensitivity to low-level features (i.e. orientation) develop prior to rewiring the circuits that deal with high-level features (i.e. object recognition) [41].

Neural circuits dealing with sensory information first establish diffuse connectivity with broad receptive fields, followed by selection and refinement of the projections (**Figure 2.5A**, [1, 5]). Because electrophysiological recordings of neural circuit development can be biased towards characterizing high firing rate neurons, the role of the SVE-EVE balance is optimally studied with optical and molecular techniques that can assess specific cell activity and collect large population statistics without bias [52]. Further development of molecular techniques to regulate and track the cellular content of the SVE-EVE balance together with optical recording techniques is necessary for fundamental insights in the role of vesicular exocytosis on the structural and functional aspects of synapse maturation and maintenance during neural development.

Our results predict that SVE plays a permissive role in the expression of synaptic plasticity and is important for the maintenance of synaptic strengths by disconnecting the action potential-dependent activity during early neurodevelopment. In agreement with this proposition, selective disturbance of SVE release in *Drosophila* neuromotor junction alters the structural organization of the synapses during development [53].

Understanding the specificity of cell-autonomous regulation of the SVE-EVE balance across time and brain region will provide important insights into the maturation of synaptic wiring and creation of functional networks during brain development. An SVE-EVE imbalance might result in learning deficits because functional circuits would not be appropriately formed by sensory experience in the absence of the regulated switch in the mode of neurotransmitter release. As such,

deregulation of the molecular pathways of the three modes of vesicle exocytosis might contribute to the etiology of neurodevelopmental disorders. For example, the expression of Complexin1, a protein that suppresses SVE and enhances EVE, is dysregulated in patients with schizophrenia, depression and bipolar disorder [54]. Furthermore, Complexin1 knock-out mice show developmental deficits [54]. Hence understanding the molecular mechanisms underlying vesicle exocytosis in relation to developmental regulation of Hebbian plasticity may lead to the rational design of treatments that could alleviate learning deficits early in neural development.

2.5 Materials & Methods

To study the role of exocytosis mode on Hebbian plasticity without assumptions regarding structure of the network, we use a feed-forward connection scheme. An input pattern consists of a subset of upstream (presynaptic) excitatory neurons with higher firing rates relative to the rates of the other neurons. The competitive input in vivo can originate from an over-representation of particular sensory inputs or variability in neural excitability [55]. We apply homeostatic plasticity [56] to maintain the firing rates of the postsynaptic neurons within a certain range (∼5 Hz), which also ensures competition between the synaptic inputs.

The vesicles can be exocytosed according to three different mechanisms each represented by a fraction, which can vary because it reflects the presynaptic protein content of the relevant Ca^{2+} sensitive proteins for SVE, aEVE and sEVE (**Figure 2.4A**, [15, 24]). After vesicle exocytosis, the postsynaptic membrane is depolarized, through which each released vesicle can contribute to a time-dependent learning effect. In the case of aEVE and sEVE, the resulting connectivity pattern is comprised of a few strong connections among many weak connections (**Figure 2.1, 2.2** and [20]).

2.5.1 Vesicle Timing Dependent Plasticity model

To study Hebbian plasticity in a feed-forward network architecture we use leaky integrate-and-fire neurons:

$$\frac{dV}{dt} = -\frac{(V - V_{rest})}{\tau_m} + \frac{I_{ves}}{C_m} \tag{2.1}$$

The neurons have a resting membrane potential V_{rest}, a membrane time constant τ_m and a capacitance C_m (for parameter values see Table 2.1). Each vesicle induces a postsynaptic current I_{ves} (See Equation 2.6 below). Refractoriness was modeled with an adaptive action potential threshold:

$$\frac{d\theta_m}{dt} = -\frac{(\theta_m - \theta_{rest})}{\tau_\theta} \tag{2.2}$$

The adaptive threshold θ_m is reset to θ_{max} directly after an action potential and returns with a time constant τ_θ to the threshold value at rest, θ_{rest} (for parameter values see Table 2.1).

We describe vesicle exocytosis in terms of the rate of Poisson processes for SVE, aEVE and sEVE. The resulting probability of exocytosis depends on the number of molecules that are available to support each of the different exocytosis modes, described here in terms of the fraction ξ_{SVE}, ξ_{aEVE}, and ξ_{sEVE}, the sum of which is one for each synapse. The switch from SVE to EVE is implemented by reducing ξ_{SVE} and increasing ξ_{aEVE} or ξ_{sEVE}, according to the equation ξ_{SVE} = 1 - ξ_{aEVE} - ξ_{sEVE}. The probability of exocytosis (v) during a short interval (we used the Euler Method to solve the differential equations with time steps of $\Delta t = 1$ ms), from presynaptic neuron i to postsynaptic neuron j, depends on the fraction of the available ($P_{a,ij}$, see Equation 2.5) over the total (P_c) vesicle pool:

$$\begin{aligned} v_{SVE,ij} &= n \cdot r_m \cdot \xi_{SVE} \frac{P_{a,ij}}{P_c} \Delta t \\ v_{aEVE,ij} &= Ca_{ij} \cdot \xi_{aEVE} \frac{P_{a,ij}}{P_c} \Delta t \\ v_{sEVE,ij} &= n \cdot r_i \cdot \xi_{sEVE} \frac{P_{a,ij}}{P_c} \Delta t \end{aligned} \tag{2.3}$$

For a fair comparison of the different exocytosis modes, each was made to have the same average release rate; hence v_{SVE} is scaled by the mean firing rate that would drive the number of vesicles released through sEVE ($r_m = \Sigma\ r_i\ /\ N$) averaged across all N presynaptic neurons and v_{aEVE} depends on the amount of residual Ca^{2+} expressed in dimensionless form, which decays exponentially with time constant τ_{Ca} (parameter values in Table 2.1):

$$\tau_{Ca} \frac{dCa(t)}{dt} = -Ca(t) \tag{2.4}$$

The total amount of Ca^{2+} entering the presynaptic terminal in response to a single action potential is given by $A = n \cdot dt\ /\ \tau_{Ca}$, such that each action potential is modeled to exocytose 4 vesicles for $\xi_{\mathrm{aEVE}} = 1$. Likewise, the same number ($n = 4$) vesicles is released by sEVE for each action potential. Firing rate is high (8 Hz) for a subpopulation (20%) of the presynaptic neurons compared to the other neurons (4 Hz). The release probabilities are normalized such that for each release mode the average rate of vesicles release is the same, only the

spatiotemporal structure of the synaptic inputs onto the postsynaptic neuron is different.

Most synapses in the brain maintain a single active zone [57] with vesicles docked for exocytosis [58], while an axon can make multiple connections between cells. The active zone increases in size during development [59], and the number of docked vesicles is linked to the size of the active zone [60]. We study vesicle pool utilization in the different modes, and set the total vesicle pool per synapse (P_c) to 100. A vesicle that is exocytosed, is moved from the active pool (P_a) to the recycling pool (P_r) and returns to the active pool according to:

$$\tau_{rec}\frac{dP_a}{dt} = P_r \tag{2.5}$$

With τ_{rec} being the vesicle recycling rate (parameter value in Table 2.1).

The postsynaptic current ($I_{ves}(j)$) on neuron j is the sum of currents caused by vesicles released from the presynaptic neurons i at time $t_{ves,i}$. Each vesicle caused a current $I_{ves}(i,j)$ which is described by:

$$I_{ves}(i,j) = w_{ij} \cdot e^{\frac{-(t-t_{ves})}{\tau_\alpha}} \text{ for } t_{ves} < t < t_{ves} + t_{window} \tag{2.6}$$

With time constant $\tau_\alpha = 3$ ms. For computational efficiency only the currents generated by recently exocytosed vesicles are used, with t_{window}= 20 ms. For this setting less than 0.2% of the initial current remains at the end of the window.

Synaptic weights are modified according to the Hebbian learning rules:

$$\begin{aligned} dw_{\text{ij+}} &= \lambda w_0^{1-\mu} w_{ij}^{\mu} e^{\frac{-|\Delta s|}{\tau}} \text{ if } \Delta s > 0 \\ dw_{\text{ij-}} &= -\lambda \alpha w_{ij} e^{\frac{-|\Delta s|}{\tau}} \text{ if } \Delta s < 0 \end{aligned} \tag{2.7}$$

With $\mu = 0.4$, $w_0 = 5\%$ of mean initial weights ($w_{ij}(0)$), $\lambda = 0.1$, $\alpha = 0.11$, $\tau = 20$ ms [61], and here Δs denotes the delay between vesicle exocytosis and the postsynaptic action potential, rather than the integration time step in the preceding text.

We use homeostatic scaling to maintain the overall firing rate of the postsynaptic neuron at a fixed level across longer periods [56]. This results in competition because strongly activated synaptic connections undergo potentiation at the expense of other synaptic connections projecting to the same postsynaptic neuron, balancing the total incoming synaptic activity to maintain the desired output firing rate [62]:

$$\tau_h \frac{dw_{ij}}{dt} = (r_m - r_j) \cdot w_{ij} \tag{2.8}$$

With τ_h the timescale of homeostatic scaling, r_m the desired firing rate (which we set to the mean input firing rate) and r_j the firing rate of postsynaptic neuron j (the running average is across the last 12 spikes). For parameter values see Table 2.1.

The network consists of 500 input neurons that are connected to 10 output neurons. A subset of neurons that has high firing rates represent neurons with receptive fields that are strongly activated by external stimuli. The presynaptic neurons produce Poisson distributed action potentials according to a probability $\mathrm{p_s} = \mathrm{r_i} \cdot \Delta\mathrm{t}$. Initially, SVE equilibrates the network to the desired firing rate (r_m), leading to a mean synaptic weight $w_{ij}(0)$. Synaptic strength has hard bounds at 0 and $8 \cdot w_{ij}(0)$, when it exceeds these extreme values it is reset to 0 or $8 \cdot w_{ij}(0)$, as appropriate.

Learning has occurred when the distribution of synaptic weights has become bimodal. We quantified the learning rate as the time change of the ratio of the median synaptic weight of the higher firing rate synaptic connections (M_{high}) over that of the lower firing rate synaptic connections (M_{low}):

$$\Lambda(t) = \frac{dD(t)}{dt} \tag{2.9}$$

Here $\Lambda(t)$ is the learning rate, $D(t) = M_{high}(t) \ / \ M_{low}(t)$. We used median synaptic weights because it is more robust than the mean and we used a ratio to make the measure independent of the overall scale of M.

To mimic a biological developmental profile, we used mRNA expression levels for Doc2b (SVE), Doc2a (aEVE) and Synaptotagmin1 · Complexin1 (sEVE) from a database of experimentally measured mRNA expresssion levels [30]. During maturation, in the model new synapses were formed with strength $0.3 \cdot \bar{w}_{ij}(0)$ and probability (P):

$$P_{ij} = k \cdot \Delta t \tag{2.10}$$

New synapses form between unconnected neurons i and j at a rate of 8% newly formed synapses per 2 weeks for early development ($\mathrm{k} = 6.6 \cdot 10^{-8}$), 5% early childhood ($\mathrm{k} = 5.0 \cdot 10^{-8}$) and 3% during adolescence and later ($\mathrm{k} = 2.5 \cdot 10^{-8}$) [31]. The generation rates were increased by a factor 10^6 for computational efficiency, while the relative duration of each developmental stage was preserved [30]. Synaptic stabilization is activity-dependent [63], and weak synapses are in general easily pruned [32]. Hence, weak synapses with strength $w_{ij} < 0.7 \cdot \bar{w}_{ij}(0)$, were eliminated and large synapses were limited to strength $8 \cdot \bar{w}_{ij}(0)$.

2.5.2 Competitive rate model

We used a rate model incorporating the dynamics due to vesicle-timing dependent plasticity to study the effect of the initial weight distribution on the ability

to encode patterns of action potentials. It incorporates competition between the exocytosis rates from all presynaptic neurons i that project to the same postsynaptic neuron j:

$$\frac{d}{dt}w_{ij} = \gamma(x_{ij} - \bar{x}_j) \cdot s \tag{2.11}$$

Where w_{ij} is the synaptic strength, x_{ij} is the rate of vesicle exocytosis (see Equation 2.12 below), $\bar{x}_j$ is the average input rate to postsynaptic neuron j, γ the rate constant and s is defined below (parameter values in Table 2.1). We use homeostatic scaling to maintain the overall firing rate of the postsynaptic neurons at a fixed level across longer periods (see 2.8, [56]). To keep synaptic weights within a specific range, the rate at which weights change is scaled [64], here by choosing $s = {w_{ij}}^2$ for LTD ($x_{ij} < x_j$) and $s = w_{ij}$ - ${w_{ij}}^2$ for LTP ($x_{ij} > x_j$). Hence large synapses undergo stronger depression during periods with reduced activity, whereas medium sized synapses are most strongly potentiated in times of correlated activity [65]. This scaling factor affects the overall magnitude of the rate of change of dw_{ij}, but the direction of change, whether it gets weakened or strengthened, depends on the rate of exocytosis at each synapse, which is modeled as a combination of SVE and EVE:

$$x_{ij} = \xi \cdot x_{ij,sve} + (1 - \xi) \cdot x_{ij,eve} \tag{2.12}$$

Where ξ is the contribution of SVE ($x_{ij,sve}$) and $1 - \xi$ being the contribution of EVE ($x_{ij,eve}$). The EVE distribution for $x_{ij,eve}$ is bimodal, with a subset of presynaptic neurons having high rates ($x_{ij,eve} = 0.8$) and other neurons firing at a lower rate ($x_{ij,eve} = 0.4$). The rate $x_{ij,sve}$ for SVE is taken from a Gaussian distribution ($\mu = \Sigma x_{ij,eve} \,/\, N^2$) and standard deviation 0.05. The initial synaptic weights are either unimodal Gaussian distributed ($\mu \pm 0.05$) or bimodal ($\mu_{weak} = 0.2 \pm 0.02$, $\mu_{strong} = 0.8 \pm 0.08$). To quantify the degree to which weights represent the pattern of presynaptic spiking, we calculate the overlap between the resulting weights and the applied patterns of action potentials using the Heaviside step function (Θ):

$$P = \frac{1}{N^2} \sum_{i,j=1}^{N} (2\Theta[w_{ij} - \bar{w}] - 1) \cdot (2\Theta[x_{ij} - \bar{x}_0] - 1) \tag{2.13}$$

This measures the fraction of synapses with a higher than average strength that belong to a presynaptic neuron with a higher than average activity. Here w_{ij} and x_{ij} are the synaptic weight and vesicle exocytosis rate from presynaptic neuron i to postsynaptic neuron j, respectively. The thresholds inside the Heaviside step

Variable description	Symbol	Value	Citation
Membrane rest potential	V_{rest}	-70.6 mV	[20]
Membrane time constant	τ_{mem}	9.4 ms	[20]
Membrane capacitance	C_{mem}	281 pF	[20]
Spike threshold at rest	θ_{rest}	-50.4 mV	[20]
Spike threshold max	θ_{max}	30.4 mV	[20]
Spike threshold relaxation constant	τ_{θ}	50 ms	[20]
Calcium decay time constant	$\tau_{Ca^{2+}}$	100 ms	[15]
STDP time constant	τ_{STDP}	20 ms	[61]
Vesicle recycling rate	τ_{rec}	800 ms	[66]
Homeostatic plasticity time constant	τ_h	100 s	
Rate constant of rate model	γ	10^{-4} s^{-1}	
Number of presynaptic neurons	N	500	
Firing rate low / high	r_j	4 / 8 Hz	

Table 2.1: Parameters for the VTDP model.

functions are the average synaptic weight and average presynaptic spiking x_0. The overlap between the presynaptic spiking and synaptic weights is normalized by the total number of synapses (N^2). If the synaptic weights correlate perfectly with presynaptic spiking, P will attain its maximal value of one. If the weights are uncorrelated with the presynaptic spiking, P will approach zero for large enough networks.

References

[1] KJ Bender, J Rangel, and DE Feldman. "Development of Columnar Topography in the Excitatory Layer 4 to Layer 2/3 Projection in Rat Barrel Cortex". In: *The Journal of Neuroscience* 23.25 (2003), pp. 8759–8770.

[2] EA Stern, M Maravall, and K Svoboda. "Rapid Development and Plasticity of Layer 2/3 Maps in Rat Barrel Cortex In Vivo". In: *Neuron* 31 (2002), pp. 305–315.

[3] N Narboux-Nûme et al. "Neurotransmitter Release at the Thalamocortical Synapse Instructs Barrel Formation But Not Axon Patterning in the Somatosensory Cortex". In: *The Journal of Neuroscience* 32.18 (2012), pp. 6183–6196.

[4] S Cohen-Cory. "The Developing Synapse: Construction and Modulation of Synaptic Structures and Circuits". In: *Science* 298.5594 (2002), pp. 770–776.

[5] H Ko et al. "The emergence of functional microcircuits in visual cortex". In: *Nature* 496.7443 (2013), pp. 96–100.

[6] C Lohmann and HW Kessels. “The developmental stages of synaptic plasticity”. In: *The Journal of Physiology* 592.1 (2014), pp. 13–31.
[7] P Caroni, F Donato, and D Muller. “Structural plasticity upon learning: regulation and functions”. In: *Nat Rev Neurosci* 13.7 (2012), pp. 478–490.
[8] L Kay, L Humphreys, BJ Eickholt, and J Burrone. “Neuronal activity drives matching of pre- and postsynaptic function during synapse maturation”. In: *Nature Neuroscience* 14.6 (2011), pp. 688–690.
[9] RA McKinney, M Capogna, R Durr, BH Gahwiler, and SM Thompson. “Miniature synaptic events maintain dendritic spines via AMPA receptor activation”. In: *Nature Neuroscience* 2.1 (1999), pp. 44–49.
[10] MA Sutton et al. “Miniature Neurotransmission Stabilizes Synaptic Function via Tonic Suppression of Local Dendritic Protein Synthesis”. In: *Cell* 125.4 (2006), pp. 785–799.
[11] LC Andreae and J Burrone. “The role of neuronal activity and transmitter release on synapse formation”. In: *Current Opinion in Neurobiology* 27 (2014), pp. 47–52.
[12] LC Andreae, NB Fredj, and J Burrone. “Independent Vesicle Pools Underlie Different Modes of Release during Neuronal Development”. In: *Journal of Neuroscience* 32.5 (2012), pp. 1867–1874.
[13] R Tyzio et al. “Membrane Potential of CA3 Hippocampal Pyramidal Cells During Postnatal Development”. In: *Journal of Neurophysiology* 90.5 (2003), pp. 2964–2972.
[14] Sarah J Etherington and Stephen R Williams. “Postnatal Development of Intrinsic and Synaptic Properties Transforms Signaling in the Layer 5 Excitatory Neural Network of the Visual Cortex”. In: *The Journal of Neuroscience* 31.26 (2011), pp. 9526–9537.
[15] PS Kaeser and WG Regehr. “Molecular Mechanisms for Synchronous, Asynchronous, and Spontaneous Neurotransmitter Release”. In: *Annual Review of Physiology* 76.1 (2014), pp. 333–363.
[16] ET Kavalali et al. “Spontaneous Neurotransmission: An Independent Pathway for Neuronal Signaling?” In: *Physiology* 26.1 (2011), pp. 45–53.
[17] ET Kavalali. “The mechanisms and functions of spontaneous neurotransmitter release”. In: *Nat Rev Neurosci* 16.1 (2015), pp. 5–16.
[18] V Volman, H Levine, and TJ Sejnowski. “Shunting Inhibition Controls the Gain Modulation Mediated by Asynchronous Neurotransmitter Release in Early Development”. In: *PLoS Comput Biol* 6.11 (2010), e1000973.
[19] C Itami and F Kimura. “Developmental Switch in Spike Timing-Dependent Plasticity at Layers 4-2/3 in the Rodent Barrel Cortex”. In: *The Journal of Neuroscience* 32.43 (2012), pp. 15000–15011.
[20] C Clopath, L Busing, E Vasilaki, and W Gerstner. “Connectivity reflects coding: a model of voltage-based STDP with homeostasis”. In: *Nat Neurosci* 13.3 (2010), pp. 344–352.
[21] DE Feldman. “The Spike-Timing Dependence of Plasticity”. In: *Neuron* 75.4 (2012), pp. 556–571.

[22] S Song, PJ Sjöström, M Reigl, S Nelson, and DB Chklovskii. "Highly Nonrandom Features of Synaptic Connectivity in Local Cortical Circuits". In: *PLoS Biol* 3.3 (2005), e68.

[23] Y Sara, T Virmani, F Deak, X Liu, and ET Kavalali. "An Isolated Pool of Vesicles Recycles at Rest and Drives Spontaneous Neurotransmission". In: *Neuron* 45.4 (2005), pp. 563–573.

[24] R Jahn and D Fasshauer. "Molecular machines governing exocytosis of synaptic vesicles". In: *Nature* 490.7419 (2012), pp. 201–207.

[25] AJ Groffen et al. "Doc2b Is a High-Affinity Ca2+ Sensor for Spontaneous Neurotransmitter Release". In: *Science* 327.5973 (2010), pp. 1614–1618.

[26] Z Pang et al. "Doc2 supports spontaneous synaptic transmission by a Ca^{2+}-independent mechanism". In: *Neuron* 70.2 (2011), pp. 244–251.

[27] J Yao, JD Gaffaney, SE Kwon, and ER Chapman. "Doc2 Is a Ca2+ Sensor Required for Asynchronous Neurotransmitter Release". In: *Cell* 147.3 (2011), pp. 666–677.

[28] J Tang et al. "A Complexin/Synaptotagmin 1 Switch Controls Fast Synaptic Vesicle Exocytosis". In: *Cell* 126.6 (2006), pp. 1175–1187.

[29] E Neher. "Complexin: Does It Deserve Its Name?" In: *Neuron* 68.5 (2010), pp. 803–806.

[30] MJ Hawrylycz et al. "An anatomically comprehensive atlas of the adult human brain transcriptome". In: *Nature* 489.7416 (2012), pp. 391–399.

[31] TF Roberts, KA Tschida, ME Klein, and R Mooney. "Rapid spine stabilization and synaptic enhancement at the onset of behavioural learning". In: *Nature* 463.7283 (2010), pp. 948–952.

[32] GF Woods, WC Oh, LC Boudewyn, SK Mikula, and K Zito. "Loss of PSD-95 Enrichment Is Not a Prerequisite for Spine Retraction". In: *The Journal of Neuroscience* 31.34 (2011), pp. 12129–12138.

[33] MH Johnson. "Functional brain development in humans". In: *Nat Rev Neurosci* 2.7 (2001), pp. 475–483.

[34] EI Knudsen. "Sensitive Periods in the Development of the Brain and Behavior". In: *Journal of Cognitive Neuroscience* 16.8 (2004), pp. 1412–1425.

[35] AD Workman, CJ Charvet, B Clancy, RB Darlington, and BL Finlay. "Modeling Transformations of Neurodevelopmental Sequences across Mammalian Species". In: *The Journal of Neuroscience* 33.17 (2013), pp. 7368–7383.

[36] H Cuntz, F Forstner, A Borst, and M Häusser. "One Rule to Grow Them All: A General Theory of Neuronal Branching and Its Practical Application". In: *PLoS Comput Biol* 6.8 (2010), e1000877.

[37] T Celikel, VA Szostak, and DE Feldman. "Modulation of spike timing by sensory deprivation during induction of cortical map plasticity". In: *Nat Neurosci* 7.5 (2004), pp. 534–541.

[38] MT Colonnese et al. "A Conserved Switch in Sensory Processing Prepares Developing Neocortex for Vision". In: *Neuron* 67.3 (2010), pp. 480–498.

[39] AR O'Connor et al. "Visual function in low birthweight children". In: *British Journal of Ophthalmology* 88.9 (2004), pp. 1149–1153.

[40] T Toyoizumi et al. "A Theory of the Transition to Critical Period Plasticity: Inhibition Selectively Suppresses Spontaneous Activity". In: *Neuron* 80.1 (2013), pp. 51–63.

[41] B Jiang, M Treviño, and A Kirkwood. "Sequential Development of Long-Term Potentiation and Depression in Different Layers of the Mouse Visual Cortex". In: *The Journal of Neuroscience* 27.36 (2007), pp. 9648–9652.

[42] DA Butts and PO Kanold. "The applicability of spike time dependent plasticity to development". In: *Frontiers in Synaptic Neuroscience* 2.30 (2010).

[43] J Gjorgjieva, T Toyoizumi, and SJ Eglen. "Burst-Time-Dependent Plasticity Robustly Guides ON/OFF Segregation in the Lateral Geniculate Nucleus". In: *PLoS Comput Biol* 5.12 (2009), e1000618.

[44] DA Butts, PO Kanold, and CJ Shatz. "A Burst-Based "Hebbian" Learning Rule at Retinogeniculate Synapses Links Retinal Waves to Activity-Dependent Refinement". In: *PLoS Biology* 5.3 (2007), e61.

[45] PJ Sjöström, GG Turrigiano, and SB Nelson. "Rate, Timing, and Cooperativity Jointly Determine Cortical Synaptic Plasticity". In: *Neuron* 32.6 (2001), pp. 1149–1164.

[46] H Yasuda, AL Barth, D Stellwagen, and RC Malenka. "A developmental switch in the signaling cascades for LTP induction". In: *Nature Neuroscience* 6.1 (2003), pp. 15–16.

[47] DH Bhatt, S Zhang, and W Gan. "Dendritic Spine Dynamics". In: *Annual Review of Physiology* 71.1 (2009), pp. 261–282.

[48] TK Hensch et al. "Local GABA Circuit Control of Experience-Dependent Plasticity in Developing Visual Cortex". In: *Science* 282.5393 (1998), pp. 1504–1508.

[49] S Sugiyama et al. "Experience-Dependent Transfer of Otx2 Homeoprotein into the Visual Cortex Activates Postnatal Plasticity". In: *Cell* 134.3 (2008), pp. 508–520.

[50] D Atasoy et al. "Spontaneous and Evoked Glutamate Release Activates Two Populations of NMDA Receptors with Limited Overlap". In: *The Journal of Neuroscience* 28.40 (2008), pp. 10151–10166.

[51] JE Melom, Y Akbergenova, JP Gavornik, and JT Littleton. "Spontaneous and Evoked Release Are Independently Regulated at Individual Active Zones". In: *The Journal of Neuroscience* 33.44 (2013), pp. 17253–17263.

[52] AL Barth and JFA Poulet. "Experimental evidence for sparse firing in the neocortex". In: *Trends in Neurosciences* 35.6 (2012), pp. 345–355.

[53] BJ Choi et al. "Miniature Neurotransmission Regulates Drosophila Synaptic Structural Maturation". In: *Neuron* 82.3 (2014), pp. 618–634.

[54] D Glynn, RJ Sizemore, and AJ Morton. "Early motor development is abnormal in complexin 1 knockout mice". In: *Neurobiology of Disease* 25.3 (2007), pp. 483–495.

[55] JS Espinosa and MP Stryker. “Development and Plasticity of the Primary Visual Cortex”. In: *Neuron* 75.2 (2012), pp. 230–249.
[56] GG Turrigiano. “The Self-Tuning Neuron: Synaptic Scaling of Excitatory Synapses”. In: *Cell* 135.3 (2008), pp. 422–435.
[57] TC Südhof. “The Presynaptic Active Zone”. In: *Neuron* 75.1 (2012), pp. 11–25.
[58] T Schikorski and CF Stevens. “Quantitative Ultrastructural Analysis of Hippocampal Excitatory Synapses”. In: *The Journal of Neuroscience* 15.17 (1997), pp. 5858–5867.
[59] GL Clarke, J Chen, and H Nishimune. “Presynaptic active zone density during development and synaptic plasticity”. In: *Frontiers in Molecular Neuroscience* 5.12 (2012).
[60] N Holderith et al. “Release probability of hippocampal glutamatergic terminals scales with the size of the active zone”. In: *Nature Neuroscience* 15.7 (2012), pp. 988–997.
[61] A Morrison, A Aertsen, and M Diesmann. “Spike-Timing-Dependent Plasticity in Balanced Random Networks”. In: *Neural Computation* 19.6 (2007), pp. 1437–1467.
[62] JN Bourne and KM Harris. “Coordination of size and number of excitatory and inhibitory synapses results in a balanced structural plasticity along mature hippocampal CA1 dendrites during LTP”. In: *Hippocampus* 21.4 (2011), pp. 354–373.
[63] M De Roo, P Klauser, P Mendez, L Poglia, and D Muller. “Activity-Dependent PSD Formation and Stabilization of Newly Formed Spines in Hippocampal Slice Cultures”. In: *Cerebral Cortex* 18.1 (2008), pp. 151–161.
[64] W Gerstner and WK Kistler. *Spiking Neuron Models*. book. Cambridge University Press, 2002.
[65] M Gilson and T Fukai. “Stability versus Neuronal Specialization for STDP: Long-Tail Weight Distributions Solve the Dilemma”. In: *PLoS ONE* 6.10 (2011), e25339.
[66] M Tsodyks, A Uziel, and H Markram. “Synchrony Generation in Recurrent Networks with Frequency-Dependent Synapses”. In: *The Journal of Neuroscience* 20.RC50 (2000), pp. 1–5.

Chapter 3

Anti-correlations in the degree distribution increase stimulus detection performance in noisy spiking neural networks

This chapter is currently under review:

M.B. Martens, A.R. Houweling, P.H.E. Tiesinga (2016). *Anti-correlations in the degree distribution increase stimulus detection performance in noisy spiking neural networks.* Journal of Computational Neuroscience

3.1 Abstract

Neuronal circuits in the rodent barrel cortex are characterized by stable low firing rates. However, recent experiments show that short spike trains elicited in single neurons can induce behavioral responses. Hence, the underlying neural networks provide stability against internal fluctuations in the firing rate, while simultaneously making the circuits sensitive to small external perturbations. Here we studied whether stability and sensitivity was affected by connectivity structure in recurrently connected spiking networks. We found that anti-correlation between the number of afferent (in-degree) and efferent (out-degree) synaptic connections of neurons increases stability because it led to a reduction in burst discharges, relative to networks with a positively correlated or uncorrelated degree distribution. In the stable network state, stimulation of a few cells could lead to a detectable change in the firing rate. To quantify the ability of networks to detect the stimulation, we used a receiver operating characteristic (ROC) analysis. For a given level of background noise, networks with an anti-correlated degree distribution displayed the lowest false positive rates, and consequently had the highest stimulus detection performance. We propose that an anti-correlated degree distribution may be a computational strategy employed by sensory cortices to increase the detectability of external stimuli. We show that networks with an anti-correlated degree distribution can in principle be formed by applying to networks with an uncorrelated degree distribution, learning rules comprised of a combination of spike-timing dependent plasticity, homeostatic plasticity and pruning. To test our prediction we suggest a novel experimental method to estimate correlation in the degree distribution.

3.2 Introduction

A fundamental goal of neuroscience is to elucidate how neural circuits respond to small external inputs, while simultaneously remaining stable against neuronal noise. This is especially a problem for cortical networks producing sparse activity, because weak external inputs involve a number of spikes that is comparable to the number of spikes produced by spontaneous activity. Neuronal noise can arise from intrinsic and extrinsic sources and influences every level of the nervous system [1, 2]. Noise has in some cases been found to limit the information capacity of neurons [3, 4], but could also enhance the computational capability of neurons in other circumstances [5, 6].

With the advent of recording and imaging techniques that are not biased to record from neurons with a high firing rate, experiments revealed sparse firing in the neocortex [7–9]. For example, the barrel cortex shows spontaneous spiking at low firing rates, ranging from less than 1 Hz in the superficial layers to a few Hz in the deep layers [8, 10, 11]. A single extra spike in one neuron in the barrel cortex is amplified and produces approximately 28 additional spikes in its postsynaptic

targets, thereby causing a detectable increase in firing rate in the local network [12]. The brain thus requires strategies to remain stable against noise in the form of spontaneous spiking activity.

At the same time sensory systems have to be sensitive to relevant external input. Rodents can be trained to use their whiskers to detect an object that predicts a reward and respond with licking to obtain this reward [13]. The neural responses in barrel cortex to whisker stimulation are hypothesized to play an important role in performing sensory tasks [14]. Whisker stimulation results in a stimulus-locked neuronal response that can be measured in the rat barrel cortex [15]. It is even possible to train rats to respond when they detect a small number of spikes elicited by electrical stimulation of a single neuron in the sensory cortex [7, 16].

Thus, neuronal networks need to be stable against intrinsic fluctuations and unrelated spiking input from other brain areas, while the aforementioned experiments showed that these networks are also sensitive to small perturbations. Sensitivity and stability are connected and can in general not be optimized simultaneously, as the increase in one causes a decrease in the other. Increases in sensitivity to external stimuli are mostly studied in terms of modulation of neuronal activity, for example by attention mechanisms (for reviews see [17, 18]). Here we examine whether specific structures in network connectivity can improve the sensitivity to stability trade-off in spiking neural networks (SNNs). Experimentally, SNNs show spontaneous spiking, which can be amplified through recurrent connectivity into synchronous network-wide activity, referred to as a burst [19, 20]. Such bursts can also be evoked in SNNs by external stimulation [20]. We investigated recurrent SNNs and used simulations to determine the effects of correlation between the number of afferent (in-degree) and efferent (out-degree) connections in neurons on the generation of bursts as part of spontaneous activity and in response to external stimulation. We studied whether stimulation would lead to a detectable change in the firing rate, which in our model would often involve amplification into a burst response. Within the context of our model, a large fraction of the neurons in the network participate in the burst. When comparing to barrel cortex, this core network should be considered embedded in a much lager network. Hence, for that network detection corresponds to a small fraction of the network becoming active, which is more representative for the experimental situation.

This computational study is the first to focus on the trade-off between sensitivity and stability with correlations between the in- and out-degree in SNNs, rather than in simplified binary networks [21]. The SNNs in this study consist of neuronal types and connection probabilities representative of cortical networks, and show stable low firing rate and/or brief burst responses, whereas neural networks with binary neurons will converge to either a high or a low firing rate after a single stimulation [21]. To test network sensitivity we apply nanostimulation (single neuron stimulation) or stimulation of a few neurons (typically four). Our guiding hypothesis is that improved stimulus detection can be achieved through

anti-correlations in the degree distribution.

We focus on correlations within the same neurons, rather than degree-correlations between different neurons, which is referred to as assortativity [22]. Most biological networks are disassortative, such that nodes with many edges preferentially connect to nodes with a few edges [22]. Assortative networks appear less stable [23], but at the same time assortative neural networks perform better in detecting subthreshold stimuli and outperform disassortative networks in the case of memory retrieval [24, 25]. Multi-unit recordings in organotypic brain slices suggest a frequency-dependent network architecture, and showed that cortical and hippocampal connectivity is disassortative for low frequencies and cortical connectivity is assortative for the high frequency range in cortex [26]. These studies thus show that whether high degree neurons preferentially connect to other neurons with low or high degree plays a role in network functioning, and that (dis)assortativity can be found in neuronal networks. However, few studies have focused on correlation in the in-degree and out-degree in the same neurons.

Neuronal network connectivity is not static, but can vary on a timescale of hours [27] or days [28, 29], during which synaptic contacts can form and disappear [30]. Plasticity has an important role in neuronal circuit formation, in particular in the form of spike-timing dependent plasticity (STDP) which induces competitive learning [31]. We studied networks that were formed randomly (without correlation in the degree distribution) and found that STDP shapes the network such that after pruning the weakest synapses a stable network with an anti-correlation in the degree distribution is obtained.

When we quantified network stability in the presence of noise, we found that the onset of the bursting state, where noise continuously evokes bursts at a low rate, was delayed to higher levels of background noise for networks with anti-correlated degree distribution compared to networks with positive correlations in the degree distribution. Networks with anti-correlations in the degree distribution are thus more stable against background noise. We also tested the sensitivity to stimulation for low noise levels, when the networks were not spontaneously bursting, and found that positively correlated networks were the most sensitive as they produced a burst response for the lowest level of recurrent excitatory connection strength. We then tested stimulus detection, which requires simultaneous stability and sensitivity, by applying stimulation to a few neurons (1-6) under noise levels for which spontaneous network bursts occurred at low rates. The anti-correlated networks outperformed networks with positive correlations. Taken together, these results suggest that the correlation structure is important for the stability and stimulus detection in neuronal networks. Furthermore, we demonstrate that the necessary anti-correlation in the degree distribution can emerge as the result of a simple plasticity rule.

3.3 Materials and Methods

In this study, we determine whether correlations in the joint in- and out-degree distribution affect stability, sensitivity and/or stimulus detection performance. We test this in sparsely connected networks of spiking neurons. Here we state the network dynamics and connectivity rules used, and describe how the analyses were performed.

3.3.1 Network dynamics

The dynamics of the neurons in the model are described by equations proposed by Izhikevich [32]. The dynamics of these neurons combine the biophysical accuracy of Hodgkin-Huxley-type dynamics and computational efficiency of integrate-and-fire neurons. Equations 3.1 - 3.3 give the general form for Izhikevich-type neurons.

$$\frac{dv}{dt} = 0.04v^2 + 5v + 140 - u + I \tag{3.1}$$

$$\frac{du}{dt} = a(bv - u) \tag{3.2}$$

With the following after-spike reset conditions:

$$\text{if } v \geq 30 \text{ mV, then } \begin{cases} v \leftarrow c \\ u \leftarrow u + d \end{cases} \tag{3.3}$$

where v represents the membrane potential (in mV) and u represents the membrane recovery variable, which accounts for the activation of the K^+ currents and inactivation of Na^+ currents [32]. The input current I (in pA) is described in Equation 3.4 below. We used the Euler method for integration of the differential equations with smaller integration time steps than in the aforementioned references in order to ensure sufficient accuracy, specifically 0.05 ms for the membrane potential and $dt = 0.1$ ms for the other variables. The dimensionless parameters a, b, c and d describe the neuronal type, in our model we use the settings for regular spiking (RS), fast spiking (FS) or low-threshold spiking (LTS) model neurons. These parameters are listed in Table 3.1.

The parameter a is the time constant of the recovery variable u, smaller values result in slower recovery.

The parameter b represents the sensitivity of the recovery variable u to the subthreshold fluctuations of the membrane potential v, where larger values yield a stronger coupling between u and v.

The parameter c is the reset value of the membrane potential after a spike.

The parameter d represents the change in recovery variable u, caused by spike-activated Na^+ and K^+ conductances.

Name	Type	N	a	b	c	d	I_{fluc} (pA)
Pyr	RS	480	0.02	0.2	-65 ± 5	8	3 ± 0.5
PV	FS	60	0.1	0.2	-65 ± 5	2	0 ± 0.5
Sst	LTS	60	0.02	0.25	-65 ± 5	2	0 ± 0.5

Table 3.1: Parameter settings proposed by Izhikevich to model different neuronal classes found in the cortex [32]. Pyramidal neurons (Pyr) are modeled as regular spiking (RS). The inhibitory population consists of different cell classes: we modeled parvalbumin postive neurons (PV) as fast spiking (FS) and somatostatin positive neurons (Sst) as low-threshold spiking (LTS). ± denotes variance of the underlying normal distribution.

We model two sources of noise. The first is the variability associated with small random events, such as ion channel noise and stochastic synaptic release and weak synaptic inputs due to uncorrelated spiking [1, 33]. These sources of noise contribute only a small fraction to the variability in the input (represented by I_{fluc} in Equation 3.4 below). The other form of noise we simulate is an occasional larger event, such as correlated spiking input events from other brain areas that are unrelated to the sensory stimulus [12], and is referred to as background noise (I_{bg} in Equation 3.4 below). The cells receive the total input I (in pA) given as:

$$I = I_{fluc} + I_{bg} + I_{syn} + I_{stim} \tag{3.4}$$

I_{fluc} is modeled as white noise (for mean and variance see Table 3.1), and I_{bg} is modeled as a Poisson process where each background spike event causes a brief current pulse to the excitatory neurons with an amplitude of 15 pA and a duration of 0.1 ms. I_{syn} is the conductance-based synaptic input between the recurrently connected neurons (Equation 3.5). The stimulation for our sensitivity measurements is represented by I_{stim} (parameter settings are given in section 3.3.5).

$$I_{syn,j}(t) = \sum_i w_{ij} \cdot g_i(t)[E_{i,rev} - v_j(t)] \tag{3.5}$$

Here w_{ij} is the synaptic strength between presynaptic neuron i and postsynaptic neuron j, g is the conductance (nS), E_{rev} the reversal potential for a particular synaptic current (0 mV for excitatory and -80 mV for inhibitory neurons) and v is the postsynaptic membrane potential (mV). The conductance g is increased with 1 nS for each presynaptic spike and falls off with a time constant of 2 ms for excitatory, and 10 ms for inhibitory neurons (**Figure 3.1A**).

3.3.2 Network connectivity

The model network was composed of 600 neurons, of which 80% were excitatory (pyramidal cells, Pyr) and 20% were inhibitory neurons. The cortex consists

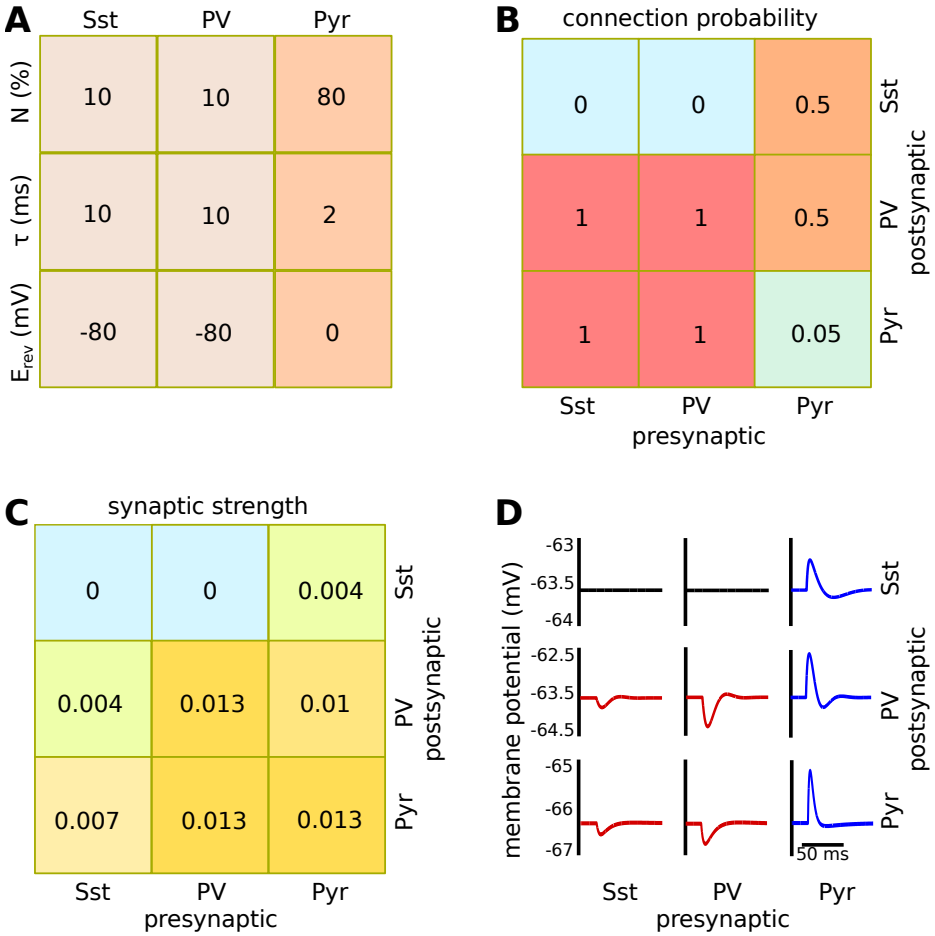

Figure 3.1: The model network was comprised of one type of excitatory (Pyr) neuron and two inhibitory classes (PV and Sst). ***A****: The majority of cells was excitatory and made fast glutamatergic synapses with a reversal potential of 0 mV. The two types of inhibitory neurons projected fast GABAergic synapses with a reversal potential of -80 mV. The synaptic decay constant τ depended on the presynaptic neuronal class. Table 3.1 contains a full description of the neuronal model parameters.* ***B****: The pyramidal cells have a sparse recurrent connectivity to other pyramidal cells but connect with a high probability to the interneuron populations. In return, both PV and Sst interneurons connected to all Pyr and PV cells, but not to Sst interneurons.* ***C****: We used the relative connection strength that was found for the inhibitory populations [34].* ***D****: The voltage deflection in response to a single presynaptic action potential when the cells are held at resting potential. The model is conductance based, hence the deflection caused by inhibition is relatively low compared to excitation when the cells are at resting potential.*

of many functionally distinct inhibitory neuron classes that can be identified by molecular markers [34–36]. Here we used two main inhibitory cell types, namely the fast-spiking parvalbumin-expressing interneurons (PV) and the low threshold somatostatin-expressing interneurons (Sst), (**Figure 3.1A**). For a local network of rat neocortical neurons the Pyr-Pyr connection probability is about 5%, whereas each interneuron projects to most of the local Pyr cells [34, 37, 38], (**Figure 3.1B**). PV neurons are modeled here to receive inhibition from both PV and Sst neurons, whereas Sst neurons only receive excitatory input [34, 39]. The relative fraction of synaptic drive that the interneurons provide is taken from experimental data [34] (**Figure 3.1C-D**).

3.3.3 Correlations in the degree distribution

Our goal is to determine whether correlations in the in- and out-degree distribution are beneficial in that they increase stability and stimulus detection performance relative to uncorrelated networks. We studied the effect of correlations in the degree distribution for the excitatory neurons, whereas interneurons were connected densely but without correlations in the degree distribution [38]. We generated networks from a truncated bivariate Gaussian for the joint in- and out-degree distribution, this allowed the generation of networks with large variance in the in- and out-degree distribution [21]. We start from a bivariate Gaussian with a diagonal covariance matrix given in Equation 3.6.

$$p(x,y) = \frac{1}{\sqrt{4\pi^2}\sigma_x\sigma_y} \cdot e^{\left(-\frac{(x-\mu)^2}{2\sigma_x^2} - \frac{(y-\mu)^2}{2\sigma_y^2}\right)} \tag{3.6}$$

The bivariate Gaussian can be rotated 45 degrees clockwise or anticlockwise to obtain a distribution with positive (PCOR) and negative (ACOR) correlations, respectively. The mean degree (μ) depended on the network size (N) and the connection probability (p) as $\mu = N \cdot p$. The long axis was $\sigma_y = \mu/3$ and the short axis σ_x was set to $0.3 \cdot \sigma_y$. The distributions were truncated at 1 (since a zero degree neuron would not be considered part of the network) and at twice the mean degree to make the distribution symmetric.

Degree distributions were obtained by sampling for each neuron i, the in- and out-degree from the corresponding bivariate Gaussian, d_i^{in} and d_i^{out}, respectively. For the uncorrelated control network (UCOR) the list of d_i^{out} values was randomly permuted. For the networks with mixed positive and anti-correlations (XCOR), d_i^{in} and d_i^{out} were sampled for 50% of the cells from PCOR, and for 50% of the cells from ACOR distributions. The simplest method for generating a realization of the corresponding network is the configuration method [40]. A list with d_i^{out} stubs for each neuron is made and concatenated into a list s_k^{out}. Likewise, a list with d_i^{in} stubs is made and concatenated into a list s_k^{in} and randomly permuted. From these two lists, pairs are picked from the same position, i.e., the kth stub on the out-list is matched to the kth stub on the in-list to make the connection s_k^{out} to s_k^{in}.

After the initial connectivity was made, we searched for multiple overlapping and self connections. The overlapping and self connections were mutually permuted using k-permutation (sampling without replacement). This procedure was repeated until no overlapping or self connections were found. In the rare case that there was no solution possible, other connections were included in the permutation until we arrived at a connectivity matrix without double or self connections. The probability of obtaining multiconnections were not significantly different between PCOR and ACOR networks (two-sided t-test on $n = 1000$ networks, probabilities are 2.5 $\pm$ 0.2% and 2.5 $\pm$ 0.2%, respectively). However, PCOR networks, which contain neurons with high in- and out-degree, have a significantly higher probability for self-connection than ACOR networks ($p < 0.001$ for two-sided t-test on $n = 1000$ networks, probabilities are 0.15 $\pm$ 0.04% and 0.14 $\pm$ 0.04%, respectively). Because overlapping and self connections were mutually permuted, these high in- and out-degree neurons in PCOR networks have a minor bias to preferentially connect to each other due to there being more self connections. However, since we study correlations between in- and out-degree, we prefer to maintain the distribution of the in- and out-degrees compared to, for example, discarding double and self-connections which would lead to a more detrimental bias because more connections will need to be discarded in PCOR networks compared to ACOR networks.

3.3.4 Network stability

Cortical neuronal networks need to be stable in the sense that stochastic fluctuations should not lead to large increases in the firing rate that could be detected as a stimulation. The stability of the network is quantified in the model by the rate at which background activity triggers synchronous network-wide activity, also called a network burst. For burst detection we used the spike density method, where a spike density trace is calculated by convolving each spike with a Gaussian (Equation 3.7), [19, 41]. The start of a burst is defined as the time at which the spike density trace crosses a threshold (10 Hz, which requires about 3% of the neurons to be active within a 5 ms interval), and the end of the burst is given by the time at which the spike density drops below this threshold.

$$G(t) = A \cdot e^{\frac{-(t-\tau)^2}{2\sigma^2}} \tag{3.7}$$

Where τ is the time at which the spike occurred, A is the amplitude of the Gaussian (set to 1) and σ the width of the Gaussian (2.5 ms).

3.3.5 Network sensitivity

We tested the sensitivity of cortical neuronal networks to external stimulation. The sensitivity of the network is tested in the model by detecting whether stimulation in a few selected neurons for a fixed duration evokes a network response above a fixed threshold (i.e. 10 Hz); the stimulated neurons were excluded from

the burst detection. We selected the stimulated neurons from 10 neurons with an out-degree closest to the average out-degree. Depending on the experiment, a number of neurons (n_p) were sampled from these 10 neurons. For each stimulation a new set of n_p neurons were sampled. A stimulus input (I_{stim}, Equation 3.4) was applied to the sampled neurons by injection of $I_{stim} = 8$ pA for 25 ms, while the networks were not bursting spontaneously (that is for very low background noise).

3.3.6 ROC analysis

To produce the receiver-operating curve (ROC), we need to determine the true and false positive rate for a set of detection thresholds. Stimulation was applied every 70 ms. We used a detection window of 60 ms, where we discarded the 5 ms before the stimulation and the 5 ms at the end of the stimulus window. This was performed to avoid the leaking in of the spike density from another stimulus window due to smoothing. We simulated the networks with and without stimulation. A false positive was called when the firing rate exceeded the specified threshold in the unstimulated condition. A true positive was called when the firing rate exceeded the threshold in the stimulated condition. At the start of each stimulus window, all network variables and random number generator seeds were restored to those corresponding to the unstimulated trial; for a fair comparison, the network state and noise at the start of the stimulus trial was thus identical to the stimulus-free trial.

The ROC curve was then obtained by plotting the fraction of false positives against the fraction of true positives for many different thresholds. When there is no effect of the applied stimulus, the number of true positives equals the number of false positives, hence the ROC is the diagonal with an area under the curve (AUC) of 0.5. We tested this protocol by stimulating 0 neurons (i.e. the network behaviour should be exactly the same as for a stimulus-free trial) and found an AUC of exactly 0.5. The deviation of the ROC curves from the diagonal, or equivalently deviation of the AUC from 0.5, is a measure for how different the distributions are and maps for Gaussian distributions on to the effect size of d', which is the difference in means of the distributions divided by their standard deviation [42].

3.3.7 Plasticity

The number of synaptic connections increases during early development, and subsequent associative plasticity supervises the maturation of cortical circuits, decreasing the number of synaptic connections [43–45]. Synaptic stabilization is activity-dependent and involves the formation of PSD-95 [46]. PSD-95 is associated with spine stability; weak synapses containing little PSD-95 are in general easily pruned [47, 48].

The number of synapses peaks before the critical rewiring period, and subsequently decreases during further development [45, 49]. To mimic the reduction in synapses we initialized UCOR type networks with an excitatory connection probability of 10%, twice that of the final value of 5%. The networks were presented with random input in the form of spontaneous release and background spiking (see I_{fluc} and I_{bg}, respectively in Equation 3.4 for details). We applied a spike-timing dependent plasticity (STDP) rule [31], while the overall level of network activity was maintained by a network homeostasis rule (see below). The simulations were then run for 20 s. The amplitude of STDP was increased and homeostatic plasticity was made faster in order to reduce the length of the simulation period. The results were comparable to those that were obtained for simulations that were run for a longer duration of 50 s. At the end of the simulation the weakest synapses were removed until a connectivity of exactly 5% remained.

Spike-timing dependent plasticity

For the STDP rule we used a function F(Δt) that determined the amount of synaptic modification arising from a single pair of pre- and postsynaptic spikes separated by a time Δt:

$$F(\Delta t) = \begin{cases} A_+ e^{\frac{-\Delta t}{\tau_+}}, & \text{if } \Delta t < 0 \\ -A_- e^{\frac{-\Delta t}{\tau_-}}, & \text{if } \Delta t > 0 \end{cases} \tag{3.8}$$

Where $\tau_+ = \tau_- = 20$ ms, $A_+ = \frac{A_-}{1.05} = 0.005$ [31]. We used a hard upper bound of synaptic strength equal to 0.013. We found that for this synaptic strength neurons fire at rates similar to the target firing rate (Equation 3.9), for the supplied noise level of 0.1 Hz.

Network homeostasis

Applying the STDP rule (Equation 3.8) has a strong effect on the postsynaptic firing rate [31]. We therefore maintained the network mean firing rate with:

$$\tau_h \frac{dW}{dt} = (R_{tar} - \bar{R}) \cdot W \tag{3.9}$$

Where W is the connectivity matrix containing the postsynaptic weights of all neurons in the network. According to this rule all synaptic weights in the matrix W are adjusted multiplicatively when the current mean firing rate over the last 500 ms ($\bar{R}$) diverges from the target mean firing rate ($R_{tar} = 1.5$ Hz); for this process we used a (sped-up) timescale of $\tau_h = 2$ s. Experimentally homeostatic plasticity timescales are generally in the range of hours to days [50, 51].

3.3.8 Statistical analysis

To test for significant differences between ACOR and PCOR networks we used the 2-sided t-test, implemented as ttest2 in Matlab (Mathworks).

We used two methods to test whether correlations in the degree distributions arise when we applied the plasticity rules described above.

For the first method (referred to as the LSR-method) we evaluated the degree correlation using the least square regression on the in- and out-degree of the neurons; we used the Matlab (Mathworks) function polyfit and we tested whether the coefficient of the linear fit was significantly different from a horizontal line (uncorrelated degree distribution).

For the second method (referred to as the quadrant-method) we plotted the in- and out-degree of the neurons and divided this plot into four quadrants. For the top-right quadrant both the in- and out-degree of the neurons are larger than the mean in- and out-degree, respectively. For the bottom-left quadrant, both the in- and out-degree are smaller than their mean. The number of neurons in these two quadrants (P_n) contribute to a positive correlation in the degree distribution. Similarly, the number of neurons in the top-left and bottom-right quadrants (A_n) are counted, which contribute to an anti-correlation in the degree distribution. We tested whether ($\frac{P_n}{A_n}$ - 1) was significantly different from zero using a two-sided t-test.

3.4 Results

3.4.1 Networks with anti-correlated degree distribution have the lowest spread in the number of synaptic contacts

Here we examined the in- and out-degree distribution of four network types with correlated in- and out-degrees for the neurons: no correlation (UCOR), anti-correlation (ACOR), positive correlation PCOR or a mix of anti- and positive correlation (XCOR, **Figure 3.2A**). The marginal distribution of pre- or postsynaptic connections per neuron is identical for these different networks (**Figure 3.2B**). However, the distribution for the sum of in- and out-degrees shows that ACOR networks have a tight distribution for the sum of pre- and postsynaptic connections per cell, whereas PCOR networks show a wide range of values of the summed degrees, with some cells that make few pre- and postsynaptic contacts and others that have many synaptic contacts (**Figure 3.2C**, in Section 3.5 we relate these differences to metabolic demands on the cell).

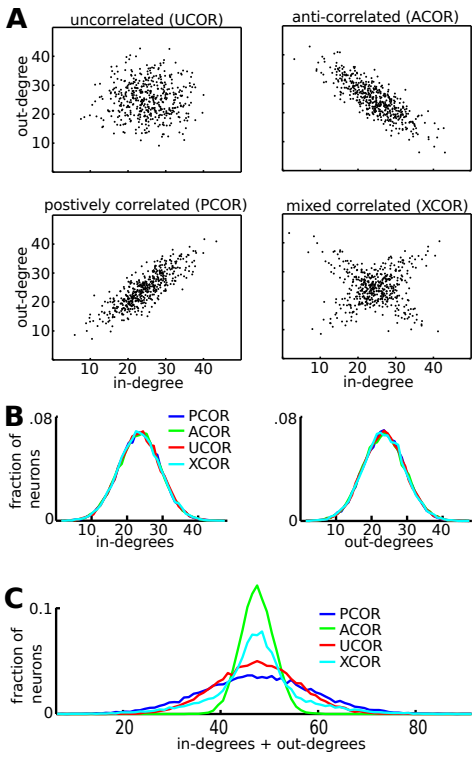

Figure 3.2: Construction of networks with a correlation between in- and out-degree. ***A****: Scatter plots of the in- vs. out-degree for the four network types. The degree distributions were sampled from a truncated bivariate Gaussian, with for each network type a different covariance matrix. For the uncorrelated (UCOR) networks, the covariance matrix was diagonal, with equal variance of the marginal distributions for the in- and out-degrees. To generate correlations we start from a diagonal covariance matrix with unequal variances and rotated it by 45 degrees anticlockwise to obtain anti-correlated (ACOR) networks and by 45 degrees clockwise to obtain positively correlated (PCOR) networks. We also constructed networks where half of the in- and out-degree pairs were picked from an anti-correlated distribution and the other half from a positively correlated distribution (XCOR).* ***B****: The networks were constructed so that the marginal distributions for the in- and out-degree were the same for the four network types.* ***C****: The distributions of the sum of in- and out-degree for each neuron shows that ACOR networks have a tight distribution for the total number of connections per cell, whereas PCOR networks show a wider range, with some cells that have few pre- and postsynaptic contacts and others that have many incoming and outgoing synaptic contacts.*

3.4.2 Networks with anti-correlated degree distribution have longer path lengths between pairs of neurons and larger structural cores

Having constructed networks with unique correlations in the degree distribution, we wanted to know whether and in what ways the structural connectivity of these networks was different. We used concepts from graph theory that are described in textbooks [40]. We studied the mean shortest path between the excitatory neurons, which is the shortest path between two nodes, averaged across all pairs and therefore provides a measure of the effective connectivity in the network. Mean path length could be a relevant quantity because it describes how activity can spread across the network to induce a network burst. An increase in connection probability decreased the mean shortest path length (**Figure 3.3A**). By maintaining a constant connection probability and varying the network size, we observed that the mean shortest path also decreases with network size (**Figure 3.3B**). We tested whether the mean shortest path length was affected by correlations in the degree distribution and found that for the typical networks used here (480 excitatory neurons and connection probability 0.05), ACOR networks had a significantly longer mean shortest path length, with an increase of 1-2% compared to PCOR networks ($p < 0.001$, significance was tested using a two-sided t-test, **Figure 3.3C**). These differences are small, but become larger for more sparsely connected networks.

Intuitively, a network structural core consists of highly interconnected neurons. To study whether correlations in the degree distribution affected the network structural core size, we performed a k-core analysis [52]. The k-core is the largest subgraph comprised of neurons with a summed in- and out-degree of at least k, which is determined by recursively removing neurons that have a summed in- and out-degree lower than k. At the macroscopic level, when applying k-core decomposition to the connectivity at the level of anatomical brain regions, a structural core remains characterized by high metabolic activity that overlaps with the activity in the human brain during the resting state (i.e. the human default mode network), suggesting that a structural core is the basis for shaping brain dynamics [53]. At the microscopic level we found that ACOR resulted in a significantly larger structural core (**Figure 3.3D**).

Taken together, we found graph theoretical differences between the different network types. The number of synaptic connections is more homogeneously distributed in ACOR compared to PCOR networks, which led to a larger structural core size. However, the average shortest path length was increased in ACOR networks compared to PCOR networks. PCOR networks have neurons with high in- and out-degree that function as hubs that reduce the shortest path length. The question is whether these differences have dynamical consequences in terms of stability and sensitivity.

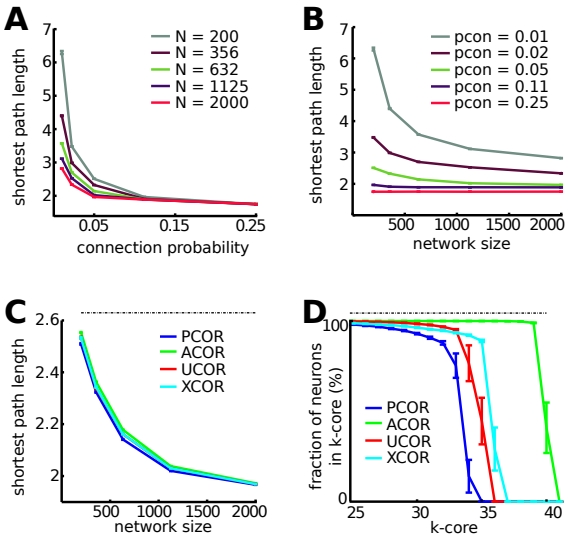

Figure 3.3: The anti-correlated degree distribution leads to a higher mean shortest path length between two excitatory neurons and a larger core size. ***A****: The shortest path length, which is the mean distance between all pairs in the network, decreases with increasing connection probability.* ***B****: The shortest path length also decreased with increasing network size. This reduction is most notable for sparsely connected networks (connection probability 0.01).* ***C****: The four network types were compared for varying network sizes, while the connection probability was fixed to 0.05. ACOR networks have a significantly increased (1-2 %) mean shortest path length.* ***D****: The results of a k-core decomposition are shown for networks with 480 pyramidal cells and connection probability 0.05. ACOR led to a larger core of highly connected neurons compared to PCOR. For each correlation type the statistics were averaged across 60 networks, error bars are 1 standard error of the mean (SEM) and dotted lines indicate significant differences between ACOR and PCOR networks according to a two-sided t-test.*

3.4.3 Anti-correlated networks are most stable against background noise

In vivo recordings in the rat somatosensory cortex show that cortical neurons fire at a low frequency, ranging from less than 1 Hz in the superficial layers to a few Hz in the deep layers [8, 10, 11]. We are primarily interested in the state of low firing rate, in which each neuron is only active a small fraction of the time, because this state allows a stimulation to cause a detectable difference in the network firing rate. We therefore quantified the stability of each of the four network types (see **Figure 3.2A**).

In the absence of noise, no spiking activity was detected in any of the networks. For a low level of background noise, the networks remained stable and fired irregularly, while increased noise results in unstable, continuous network bursting (**Figure 3.4A**). The excitatory synaptic strength were such that low frequency spiking input could evoke a detectable response.

We found that ACOR networks showed fewer burst responses for the same level of noise compared to PCOR networks (**Figure 3.4B**). This also related to a lower firing rate in ACOR networks (**Figure 3.4C**). Thus PCOR networks were less stable than ACOR networks. Stability for UCOR and XCOR networks was in-between ACOR and PCOR networks.

We wanted to know whether these differences in stability could be explained by the different graph theoretical properties found above. For a given path length the properties such as firing rate were broadly distributed, but there was no statistical trend observable between the mean firing rate of the network and the mean shortest path length of the associated network (Pearson correlation values were not significantly different from zero, **Figure 3.4D**). We also did not find a correlation between k-core size and firing rate (**Figure 3.4E**). Thus, for the same number of connections in a network, the mean pair distance and structural core size did not influence the network stability.

We then studied the relation between in-degree and firing rate for individual neurons. A high in-degree led to a high firing rate (**Figure 3.4F**). Given the correlation structure in the network, this means that high out-degree neurons in a PCOR network have high firing rates, whereas the high out-degree neurons in the ACOR network have low firing rates. Hence, the anti-correlated degree distribution directly results in a reduced synaptic output to the network, indicating the mechanism by which the additional stability is generated.

3.4.4 Positively correlated networks are most sensitive to stimulation in the absence of spontaneous bursts

Whisker stimulation results in time-locked responses that can be measured in the rat somatosensory cortex [15]. These neuronal responses are hypothesized to play an important role in performing and learning sensory tasks [13, 14]. Rats are better at detecting external stimulation when multiple neurons are activated

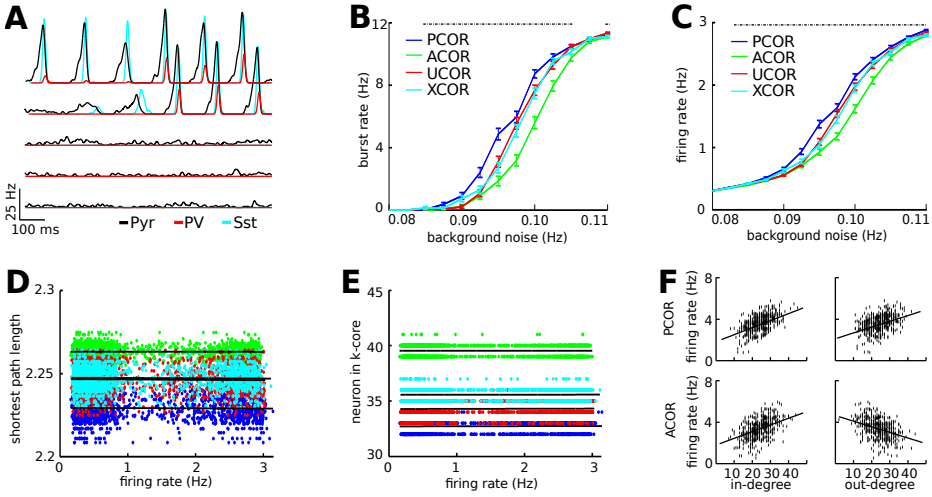

Figure 3.4: An anti-correlated degree distribution increases stability against noise. ***A****: Averaged firing rates of excitatory (black lines), PV (red traces) and Sst (cyan traces) neurons in response to background noise events at frequencies between 0.08 Hz and 0.1 Hz per neuron. The low noise input evokes background spiking activity without bursting (lower traces), whereas the high noise input rates trigger periodic synchronized bursting activity in the network (upper traces).* ***B****: The PCOR networks (blue) produce network burst activity for a lower noise rate than the ACOR networks (green). UCOR (red) and XCOR (cyan) correlated networks showed intermediate levels of stability.* ***C****: As expected for a lower burst rate, the ACOR networks also have a lower firing rate compared to the PCOR network for an equal amount of random input spikes.* ***D****: The ACOR networks have on average a longer shortest path length (also see Figure 3.3). The shortest path length for a given network was not correlated with the firing rate in that network, as the Pearson correlation value was not significantly different from zero ($p > 0.05$). Each dot represents the mean firing rate of the excitatory network; background noise rates varied between 0.075 and 0.11 Hz.* ***E****: No correlation was found between the mean firing rate of a network and the largest k-core in that network. Statistics and color convention were as in panel D.* ***F****: Dots represent the firing rate of a single neuron plotted against its in- and out-degree for one network in the bursting state (input rate 0.11 Hz per neuron). In panels B to E the statistics are averaged across 120 networks, error bars are 1 SEM and dotted lines indicate significant differences between ACOR and PCOR networks according to a two-sided t-test. Each network consisted of 480 pyramidal, 60 PV and 60 Sst neurons.*

compared to when a single neuron is stimulated [7, 54]. Here we studied the network responses upon stimulation of 6 neurons while the networks were not bursting spontaneously (0.07 Hz background noise). For weak excitatory coupling strength, only a few neurons in the network responded to stimulation in addition to the directly stimulated cells (**Figure 3.5A**). Neuronal recruitment increased with excitatory coupling strength (**Figure 3.5B**), where PCOR networks had a higher peak firing rate than ACOR networks (**Figure 3.5C**). Network-wide burst responses, detected when the firing rate crossed a predefined threshold, were realized for weaker coupling strengths in the case of PCOR networks (**Figure 3.5D**), and these networks were fastest to reach their peak activity (**Figure 3.5E**). Taken together, these data show that networks with positive correlations in the degree distribution, in the absence of spontaneous network bursting, are most sensitive to stimulation of a few neurons.

3.4.5 Stimulus detection is enhanced in anti-correlated networks for higher background noise

We showed that in the absence of spontaneous bursting the PCOR networks were most sensitive to stimulation, whereas ACOR networks were found to be more stable against noise. Here we investigate the sensitivity to external stimulation for varying degrees of background noise; this provides a direct quantification of detection performance. For our experiments we first supply the networks with background noise in the form of random spiking in each of the excitatory neurons of the network (see Methods, section 3.3.5). We then applied stimulation in 1 to 6 neurons and observed a moderate to clearly noticable increase in the firing rate. (**Figure 3.6A**).

We used these experiments to study whether stimulation had a detectable effect on the network activity (**Figure 3.6B**). For low detection thresholds, detection of both true and false positive network events is high. For intermediate detection thresholds we observed that ACOR had lower rates of false positive events compared to PCOR networks (**Figure 3.6B**). From the true and false positive rates we constructed ROC curves (**Figure 3.6C**). From these ROC curves we extracted the area under the curve (AUC) as a measure of stimulus detection in noisy conditions, and show that for stimulation of a few (1 - 6) neurons stimulus detection in ACOR networks was enhanced compared to PCOR networks (**Figure 3.6D**). Nanostimulation (single neuron) had a small but significant effect on stimulus detection. We then studied the stimulus detection under varying background noise levels (**Figure 3.6E**). We found that ACOR networks were able to detect stimuli for stronger background noise, which can be attributed to the increased stability against background noise as shown before (**Figure 3.4B-C**).

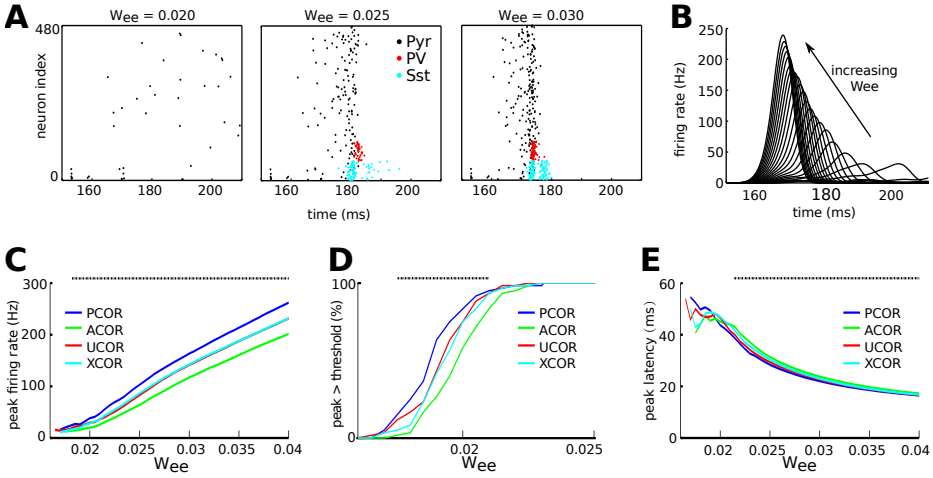

Figure 3.5: Networks with a positively correlated degree distribution are more sensitive to a small perturbation for the low noise condition, for which there are no spontaneous bursts. ***A****: Rastergrams wherein each dot represents a spike. The spikes of excitatory pyramidal cells are in black, PV interneuron spikes are in red and Sst interneurons spikes are in cyan. Depending on the strength of recurrent excitation (w_{ee}), external stimulation in 6 neurons of a UCOR network leads to either a weak response of varying duration that did not recruit inhibitory neurons, or a strong, sharp response that recruited inhibitory neuron activity that curtailed the burst. Each neuron received input from background spikes at a rate of 0.07 Hz. Interneurons were recruited only when a network burst occurred. The rastergrams also show the spikes of the stimulated neurons, but these were not included for the burst detection and post-stimulus time histograms to avoid stimulation artifacts.* ***B****: The smoothed post-stimulus time histogram of excitatory neurons for 25 different values of the recurrent excitatory strength, equally spaced between 0.015 and 0.04. For smoothing see Equation 3.6.* ***C****: Mean peak firing rate in the smoothed post-stimulus time histogram plotted against the recurrent excitatory strength. PCOR networks (blue) showed higher peak firing rates compared to the ACOR networks (green) for equal recurrent strength.* ***D****: Bursts were detected when the recurrent strength exceeded 0.015, and for recurrent strength 0.023 and higher the network consistently showed a burst response after each stimulation.* ***E****: The peak latency, which is the time between the onset of stimulation and the peak of the burst, decreased for stronger recurrent strength. For recurrent strength below 0.02, variability in the peak latency is high due to the low number of detected bursts. For each network type the statistics are averaged across 60 networks with one stimulation per network, error bars are 1 SEM and dotted lines indicate significant differences between ACOR and PCOR networks according to a two-sided t-test.*

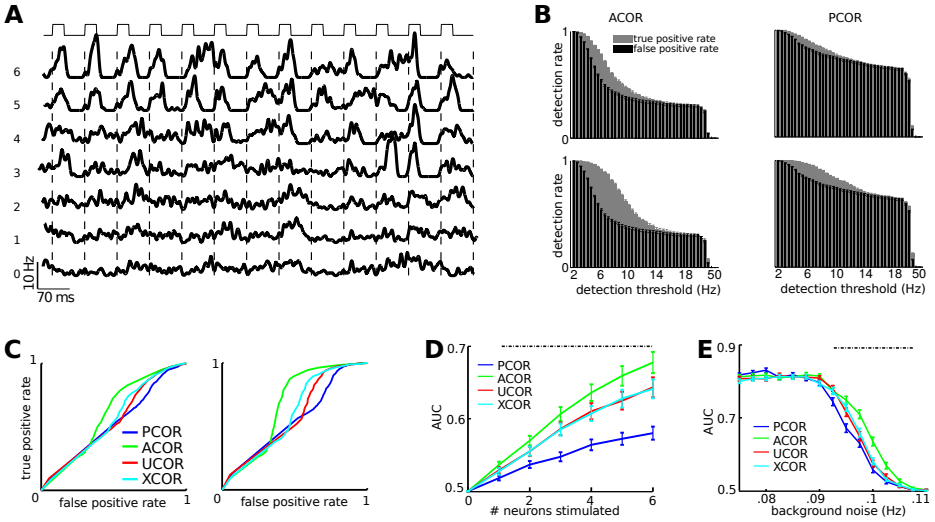

Figure 3.6: Stimulus detectability, as evaluated by ROC analysis, is higher for networks with anti-correlations in the degree distributions than for networks with positive degree correlation. ***A****: Spike density for the excitatory neurons in a stimulated ACOR network. Stimulation was applied every 70 ms to up to 6 neurons in the network; the stimulus duration is indicated by the block pattern (top). At the start of each stimulation, which is indicated by a dotted line, the network variables were reset to their baseline value (no stimulation, bottom). Under the same noise conditions as the baseline trace, the number of stimulated neurons increased from bottom to top with a step of one. In the top trace stimulation was applied to 6 neurons, which often initiated a detectable response including many neurons. Background noise was 0.098 Hz per neuron.* ***B****: Stimulation of 3 (top) and 6 (bottom) neurons was applied to ACOR (left) and PCOR networks (right), while the background noise was identical. Stimulation in the ACOR networks was better detectable than stimulation in the PCOR networks because the PCOR networks were less stable to noise.* ***C****: The corresponding ROC curves for 3 (left) and 6 (right) stimulated neurons quantify the stimulus detectability, such that curves further away from the diagonal relate to higher detection rates. Because neuronal networks respond non-linearly to noise, which occasionally initiated bursting in response to spontaneous activity, additional stimulation in that case did not increase the response amplitude further, therefore the bottom-left part of the ROC curves remain along the diagonal.* ***D****: The area-under-curve (AUC) of the ROC is a quantification of stimulus detectability. Detectability increases with the number of stimulated neurons and is highest for ACOR networks.* ***E****: We stimulated four neurons under different background noise levels. ACOR networks showed higher detectability in the high noise conditions compared to PCOR networks. For each correlation type the statistics are averaged across 120 networks, error bars are 1 SEM and dotted lines indicate significant differences between ACOR and PCOR networks according to a two-sided t-test.*

3.4.6 A minimal connection probability to detect external stimulation

We showed that ACOR networks outperform PCOR networks in detection of external stimulation under high levels of noise. Next we wondered what influence connection probability had on stimulus detection. We maintained constant synaptic strengths and observed that for a high connection probability (10%) network bursting occurred at noise levels around 0.07 Hz, whereas networks with a low connection probability (1%) did not burst until noise levels reached rates around 0.14 Hz (**Supplementary Figure 3.9**). For a clear comparison, we performed simulation of networks with these connection probabilities for the same range of noise levels. For connection probability 5% and 10% our previous results that ACOR outperforms PCOR were confirmed. When connection probability dropped to 3% and below the stimulation of a few neurons was difficult to detect and the advantage of ACOR to outperform PCOR disappeared. When connection probability was further reduced to 1%, the ability to detect external stimulation was almost completely abolished. We attribute these findings to the higher mean out-degree in the densely connected networks compared to sparsely connected networks, thereby allowing external stimulation of a few neurons to recruit a larger synaptic drive to the rest of the network. For our stimulation protocol involving 600 neurons, stimulation in four neurons and our setting of synaptic strength, the minimal connection probability to detect external stimulation was $\sim$5%.

3.4.7 Associative plasticity forms anti-correlations in the degree distribution

How could networks with anti-correlations in the degree distribution emerge? Several different models exist for the establishment of synaptic connections, but these do not take into account correlations in the degree distribution [55, 56]. We studied whether correlations in the degree distribution could emerge from associative plasticity.

Early in development the number of synaptic connections is high, and subsequent associative plasticity reorganizes the cortical circuits, decreasing the number of synaptic connections (see Section 3.3.7 for details). We constructed networks with 10% connection probability to represent the more densely connected networks early in development. These networks were of the UCOR type to mimic the random organization. Uncorrelated spontaneous spiking was supplied to the network as synaptic inputs with an amplitude of $I_{bg} = 15$ pA, duration of 0.1 ms and at a rate of 0.1 Hz for each neuron. The rate of 0.1 Hz was chosen because the ACOR networks that were generated from a bivariate Gaussian distribution then fired at $\sim$1.5 Hz, for which the occasional synchronized burst emerged. When in these networks the synaptic strength was modified by STDP and the set point rate for the homeostatic process was set to 1.5 Hz, spiking activity still

propagated throughout the network accompanied by the occasional synchronized network burst.

We observed that associative plasticity reorganized the synaptic weight distribution towards a bimodal distribution (**Figure 3.7A**). Synapses were pruned (removed), starting with the weakest synapses, until a connectivity of 5% was obtained (**Figure 3.7A**). We summed the synaptic inputs to each of the neurons and found that the distribution was comparable to explicitly constructed ACOR networks from a correlated bivariate Gaussian distribution (**Figure 3.7B**).

By plotting the in- and out-degree of the synaptic connections that remained after associative plasticity, we observed anti-correlation in the degree distribution (**Figure 3.7C**). We calculated the correlation (Section 3.3.7) for 60 networks with randomly initialized dynamics and connectivity, and found that anti-correlation in the degree distribution was consistently formed (**Figure 3.7D**).

In summary, for these parameter settings, dense and uncorrelated networks were consistently reorganized into more sparsely connected networks with anti-correlation in the degree distribution by synaptic pruning.

3.5 Discussion

The activity produced by cortical microcircuits in sensory areas provides the opportunity to detect external stimuli, provided that the circuits are stable against noise generated by spontaneous firing. Such simultaneous sensitivity and stability is difficult to achieve [21]. Previously, in a simple recurrent network of stochastic binary neurons, it was numerically shown that stability was increased for ACOR relative to PCOR networks. Nevertheless, these ACOR networks consisting of binary neurons had the same level of sensitivity compared to PCOR [21].

Here we studied the effects of correlation between in- and out-degree on stimulus detection in recurrent spiking neuronal networks. We found that ACOR networks had increased network stability, whereas in our simulations of the low noise state, without the spontaneous bursting activity, sensitivity was highest for PCOR networks. The rat somatosensory cortex shows spontaneous spiking at firing rates of up to a few Hz [8, 10, 11]. When we performed stimulation in the more realistic setting of spontaneous background spiking, representative of these experimentally observed network states, we found that detection performance was highest for the ACOR networks. High noise levels bring the recurrent networks to the spontaneous bursting regime, resulting in a high false positive rate. Anti-correlations in the degree distribution provide stability to the network, and as a consequence a lower false positive rate. At the same time, these ACOR networks remain sensitive to external stimulation, thus simultaneously improving stability and stimulus detection compared to PCOR networks. Our hypothesis is that stimulation detection corresponds to a nonlinear increase in neural activity in sensory areas. In our model, we use bursts as a proxy for such an event. As our model networks represent only a small part of the entire barrel cortex

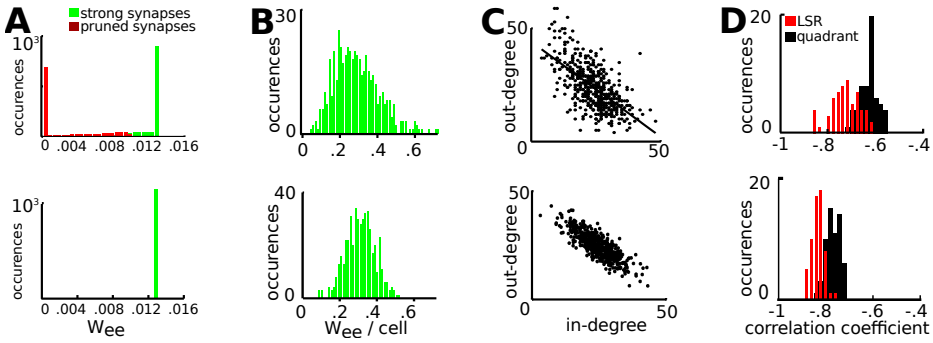

Figure 3.7: Associative plasticity forms networks with anti-correlation in the degree distribution. ***A****: Top: a UCOR network with a connection probability of 10% with an upper bound on synaptic strength of 0.013 was run for 20 seconds with spike-timing dependent plasticity. The amplitude of STDP was increased and timescale of homeostatic plasticity was decreased compared to their values in the literature in order to reduce the duration of the simulation. At the end of the simulation period the synaptic distribution was bimodal. The weak synapses (red) were pruned and removed from the distribution until a connectivity of exactly 5% was obtained. The synaptic strength of the remaining synapses (green bars) was comparable to an ACOR network explicitly constructed from a bivariate Gaussian distribution (bottom).* ***B****: The summed excitatory synaptic strength for the STDP-generated network (top) and the explicitly constructed ACOR network (bottom).* ***C****: In- and out-degrees of the STDP-generated network (top) and the explicitly constructed ACOR network (bottom). Black line is fitted using the LSR-method.* ***D****: 60 STDP-generated networks (top) and 60 explicitly constructed ACOR networks (bottom) were tested for correlations in the degree distribution using the LSR-method and the quadrant-method (see Materials and Methods). All STDP-generated networks showed anti-correlations in the degree distribution that were comparable to the generated ACOR networks. The LSR-method shows that the angle of the slope is similar for the explicitly generated and STDP-generated networks, whereas the lower values found for the STDP-generated networks using the quadrant-method are due to the increased variance across independent realizations.*

network, the bursts correspond to a more modest increase in the barrel cortex activity. Specifically, they should be experimentally observable as a modestly increased rate coupled to a strongly increased level of synchronization in sparsely active networks [7–9]. We further speculate that downstream neurons in areas that plan actions (i.e. the initiation of licking) have become more sensitive to these synchronously active neurons, for instance, through a Hebbian mechanism during training.

By dissecting the firing rate based on in-degree, we found that in the ACOR networks the neurons with high out-degrees had on average a lower firing rate; this effectively reduces the excitatory input to the network during spontaneous activity. Concurrently, the high in-degree neurons collect inputs from many neurons in the network, and have a higher than average firing rate, but project their output to a relatively small portion of the neurons so as to not destabilize the network. As a consequence, stimulating the average out-degree neurons in the ACOR networks result in a burst response even though the networks remained more stable against the noise-induced bursts compared to the PCOR networks. It was recently shown *in vivo* that network firing patterns are largely dictated by basic circuit variables [57, 58]. We suggest correlations in the degree distribution contribute as a basic network property to the maintenance of stable spiking activity in neuronal networks.

For the neuronal networks in this study we found that sensitivity to stimulation of a few neurons requires a minimal connection probability. Although many synaptic connectivity features are ubiquitous among cortical system, experimentally observed connectivities differ between species and sensory modality (for review see [59]). It is interesting whether the ability to detect nanostimulation is, for example, different between rats and mice, and whether visual, auditory and somatosensory regions show a difference in detection performance. We predict that densely connected regions show better performance compared to sparsely connected regions. Inhibitory neurons are less abundant in cortical circuits than excitatory neurons, but are more densely connected to the excitatory population [34]. Nanostimulation of inhibitory neurons might therefore have an increased detection performance compared to nanostimulation of excitatory neurons.

Synaptic communication places a disproportionally high demand on energy consumption [60, 61]. Pre- and postsynaptic parts of the neuron consume a comparable amount of energy [61, 62]. Cells that are stressed by excessive ATP consumption can produce damaging levels of reactive oxygen and nitrogen species (ROS/RNS) in the cell, leading to protein dysfunction and potential cell death (for review see [63]). Cell death by oxidative stress is linked to neurodegenerative diseases [63]. When networks have anti-correlations in the degree distribution, the energy demand is more homogeneously distributed over the neurons (**Figure 3.8A**). Thus, by making cellular demands on energy consumption more homogeneous, the anti-correlation in the degree distribution provides another level of robustness to brain networks.

For standard growth models the number of pre- and postsynaptic connections

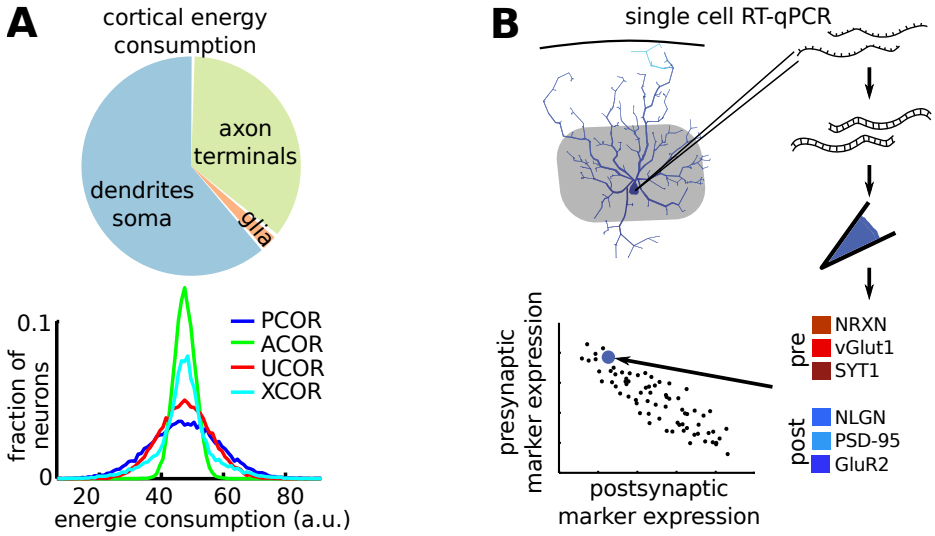

Figure 3.8: Metabolic consequences of, and a method to experimentally confirm, anti-correlated degree distributions in the cortex. ***A****: The pre- and postsynaptic parts of the neuron have a comparable energy consumption ([61, 62], estimates in the diagram are from [61]). By assigning equal levels of energy consumption to the pre- and postsynaptic part of each synapse, we find that energy demands are more homogeneously distributed over cells in ACOR networks compared to PCOR networks.* ***B****: To estimate the in- and out-degree of single neurons, we propose to use single cell RT-qPCR and compare the relative expression of pre- and postsynaptic markers. This can for example be performed for RNA encoding presynaptic proteins Neurolexin (NRXN), Vesicular glutamate transporter 1 (vGlut1) and Synaptotagmin-1 (SYT1) [64–66]; and postsynaptic proteins Neuroligin (NRGN), postsynaptic density-95 (PSD-95) and Glutamate receptor 2 (GluR2) [64, 65, 67].*

for each neuron is set to be independent, and there is no correlation in the in- and out-degrees. These networks will be of type UCOR. Previously, STDP was shown to lead to non-random structures [68, 69] and disassortivity in network connectivity [70]. These authors also studied the distribution of in-degree, out-degree and sum of in- and out-degree. They observed a general reduction in the out-degree, particularly for neurons with high in-degrees, but did not quantify the correlations in the degree distribution [70]. We demonstrated that STDP can reorganize UCOR networks into networks with anti-correlation in the degree distribution.

What could trigger this structural organization in a developing brain? One possibility is that the network restructuring towards anti-correlations occurs after the transition from immature to mature STDP [71]. For the rat somatosensory cortex, this developmental switch coincides with the critical learning period and a period of rapid reorganization of the cortical circuitry [44].

Alternatively, in the mature brain plasticity rules could form an anti-correlated degree distribution to obtain cortical circuits sensitive to (nano-)perturbation. After a training period rats respond significantly more to stimulation of a single neuron in the somatosensory cortex than to catch trials, consistent with a sparse cortical code for sensation [7, 16]. Thalamic activity that is triggered by whisker stimulation could project preferentially to neurons with high out-degrees. Here, an anti-correlated network configuration could provide simultaneous stability to noise, and sensitivity to (nano)stimulation.

In the networks studied here, synaptic strength was held constant. Consequently, the variability in in-degree results in variable firing rates. For our plasticity experiments, we applied homeostatic scaling such that the network scales towards a specific target firing rate. However, homeostatic scaling could also be applied to individual neurons [51]. Firing rates of individual neurons converging to a target firing rate could lead to variability in the synaptic strength, thereby reducing the stability of the ACOR network and abolishing the competitive advantage of ACOR compared to PCOR networks.

The recurrent networks were organized without any laminar structure. However, the cortex is organized as a layered structure, generally thought to be comprised of functional cortical columns [72, 73], which can improve computational efficiency beyond the capabilities of recurrent networks without such spatial organization [74–76]. As we showed here, correlations in the degree distribution can also provide additional capabilities for stimulus detection. Neurons in cortical networks with an anti-correlation in the degree distribution can perform unique roles in the network. The neurons with low in-degree and high out-degree could project to amplify a signal by projecting to many neurons within a layer or across layers. The neurons with high in-degree and low out-degree could provide improved detection of a network burst by integrating many inputs, and send the detection signal to specific target neurons.

Due to experimental limitations, correlations in the degree distribution have not been directly quantified experimentally [21]. Classical tracing techniques are

not appropriate for single neuron studies because they involve connections to or from multiple nearby neurons [77]. Electron microscopy (EM) based reconstruction of cortical circuitry could provide the complete connectivity structure of a local network. Analysis in a recent review paper [78] show that it could be experimentally feasible to image an appropriately sized block of cortical tissue. However, the main bottle neck is analysis: the detection of synapses and properly identifying the pre- and postsynaptic neuron. The combination of new technologies, such as crowd sourcing [79], interactive machine learning [80] and molecular biology [81] will make the EM more feasible within a decade. Alternatively, viral based techniques allow crossing of exactly one single synaptic connection which could help to visualize neurons [82, 83]. However, to obtain the pre- and postsynaptic connections, single cells should be infected with both anterograde and retrograde crossing viruses, making this a challenging approach. Another method is to simultaneously record from multiple cells and assess connections by inducing action potentials in one neuron at a time and recording the postsynaptic responses in other nearby cells [84, 85]. Such recordings can be used to estimate the degree distribution indirectly by subsampling. Alternatively, correlations in the degree distribution can be estimated by studying motifs, for example from triplets of neurons [21]. Taken together, we feel that these techniques do not provide a feasible strategy for experimentally confirming our hypothesis on connectivity. We have therefore formulated an alternative approach.

The diversity of interneuron subtypes, generally defined by particular molecular markers such as parvalbumin and somatostatin, have been elegantly interrogated by simultaneous use of molecular, anatomical and electrophysiological techniques on single neurons [86, 87]. For the excitatory cells here we propose a similar approach: by patch clamping single neurons (1) the electrophysiological profile can be tested, (2) color the cell by dye or virus injection such that the anatomical structure can be reconstructed and (3) by single-cell Reverse Transcriptase-quantative Polymerase Chain Reaction (RT-qPCR) [88], or RNA sequencing (RNA seq) [89], the mRNA content of the cell could be quantified. The mRNA quantity is an indirect measure of protein expression in the cell. By quantifying the mRNA that code for proteins that are typically found in the presynaptic terminal (such as Neurolexin, Vesicular glutamate transporter 1 and Synaptotagmin-1 [64–66]) and proteins that are typically found in the postsynaptic spines (such as Neuroligin, PSD-95, and GluR2 [64, 65, 67]), the in- and out-degree of single neurons can be estimated (**Figure 3.8B**). Thus, by combining the molecular, anatomical and electrophysiological blueprint of the cell's degree distribution, a (layer-specific) subclassification could be made for single excitatory neurons.

In this study, we showed that correlations in the degree distribution can add computational capabilities for neuronal networks. While intuitively networks that have neurons with high in- and out-degree seem ideal for stimulus detection, we showed that when taking network stability into consideration the detectability was enhanced for networks with an anti-correlated degree distribution. We pro-

pose experimental methods to investigate the correlation of in- and out-degree in individual neurons. Furthermore, we have shown how a simple plasticity rule can organize cortical networks to obtain anti-correlations in the degree distribution. Our results suggest that anti-correlated degree distributions could be an important strategy to increase stimulus detectability in recurrent cortical networks.

3.6 Supplementary Figure

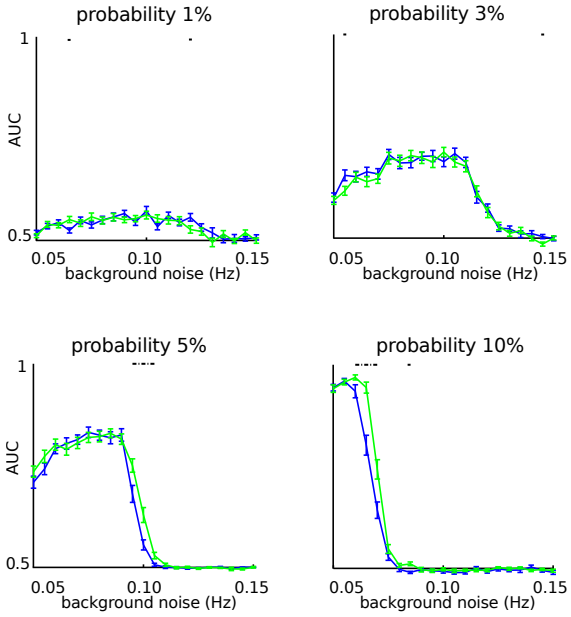

Figure 3.9: Stimulus detectability is abolished for low connection probability. All networks were stimulated while the noise ranged from 0.04 Hz to 0.15 Hz. The area-under-curve (AUC) was calculated as before: in short, for each stimulation the network activity was compared to the activity of the network without stimulation. The state of the network variables and random noise generator were identical between the two conditions. An AUC value of 0.5 represents a network that is unable to detect stimulation. For each correlation type the statistics are averaged across 60 networks, error bars are 1 SEM and dotted lines indicate significant differences between ACOR and PCOR networks according to a two-sided t-test.

References

[1] GA Jacobson et al. “Subthreshold voltage noise of rat neocortical pyramidal neurones”. In: *J Physiol* 564.1 (2005), pp. 145–160.

[2] AA Faisal, LPJ Selen, and DM Wolpert. “Noise in the nervous system”. In: *Nat Rev Neuroscience* 9.4 (2008), pp. 292–303.

[3] E Schneidman, B Freedman, and I Segev. “Ion Channel Stochasticity May Be Critical in Determining the Reliability and Precision of Spike Timing”. In: *Neural Computation* 10.7 (1998), pp. 1679–1703.

[4] M London, A Schreibman, M Hausser, ME Larkum, and I Segev. “The information efficacy of a synapse”. In: *Nat Neurosci* 5.4 (2002), pp. 332–340.

[5] M Rudolph and A Destexhe. “Correlation Detection and Resonance in Neural Systems with Distributed Noise Sources”. In: *Phys. Rev. Lett.* 86.16 (2001), pp. 3662–3665.

[6] WC Stacey and DM Durand. “Synaptic Noise Improves Detection of Subthreshold Signals in Hippocampal CA1 Neurons”. In: *Journal of Neurophysiology* 86.3 (2001), pp. 1104–1112.

[7] AR Houweling and M Brecht. “Behavioural report of single neuron stimulation in somatosensory cortex”. In: *Nature* 451.7174 (2008), pp. 65–68.

[8] AL Barth and JFA Poulet. “Experimental evidence for sparse firing in the neocortex”. In: *Trends in Neurosciences* 35.6 (2012), pp. 345–355.

[9] J Wolfe, AR Houweling, and M Brecht. “Sparse and powerful cortical spikes”. In: *Current Opinion in Neurobiology* 20.3 (2010), pp. 306–312.

[10] DS Greenberg, AR Houweling, and JND Kerr. “Population imaging of ongoing neuronal activity in the visual cortex of awake rats”. In: *Nat Neurosci* 11.7 (2008), pp. 749–751.

[11] CPJ de Kock and B Sakmann. “Spiking in primary somatosensory cortex during natural whisking in awake head-restrained rats is cell-type specific”. In: *Proceedings of the National Academy of Sciences* 106.38 (2009), pp. 16446–16450.

[12] M London, A Roth, L Beeren, M Hausser, and PE Latham. “Sensitivity to perturbations in vivo implies high noise and suggests rate coding in cortex”. In: *Nature* 466 (2010), pp. 123–127.

[13] D Huber et al. “Multiple dynamic representations in the motor cortex during sensorimotor learning”. In: *Nature* 484.7395 (2012), pp. 473–478.

[14] CCH Petersen and S Crochet. “Synaptic Computation and Sensory Processing in Neocortical Layer 2/3”. In: *Neuron* 78.1 (2013), pp. 28–48.

[15] EA Stern, M Maravall, and K Svoboda. “Rapid Development and Plasticity of Layer 2/3 Maps in Rat Barrel Cortex In Vivo”. In: *Neuron* 31 (2002), pp. 305–315.

[16] G Doron, M von Heimendahl, P Schlattmann, AR Houweling, and M Brecht. “Spiking Irregularity and Frequency Modulate the Behavioral Report of Single-Neuron Stimulation”. In: *Neuron* 81.3 (2014), pp. 653–663.

[17] PHE Tiesinga, J Fellous, and TJ Sejnowski. “Regulation of spike timing in visual cortical circuits”. In: *Nat Rev Neurosci* 9.2 (2008), pp. 97–107.
[18] P Fries. “Neuronal Gamma-Band Synchronization as a Fundamental Process in Cortical Computation”. In: *Annual Review of Neuroscience* 32.1 (2009), pp. 209–224.
[19] MB Martens, M Chiappalone, D Schubert, and PH Tiesinga. “Separating burst from background spikes in multichannel neuronal recordings using return map analysis”. In: *Int J Neural Syst* 4.24 (2014), p. 1450012.
[20] M Chiappalone, A Vato, L Berdondini, M Koudelka-hep, and S Martinoia. “Network dynamics and synchronous activity in cultured cortical neurons”. In: *International Journal of Neural Systems* 17.02 (2007), pp. 87–103.
[21] JC Vasquez, AR Houweling, and PHE Tiesinga. “Simultaneous stability and sensitivity in model cortical networks is achieved through anti-correlations between the in- and out-degree of connectivity”. In: *Frontiers in Computational Neuroscience* 7.156 (2013).
[22] MEJ Newman. “The structure and function of complex networks”. In: *SIAM Review* 45 (2003), pp. 167–256.
[23] M Brede and S Sinha. “Assortative mixing by degree makes a network more unstable”. arXiv, eprint 0507710/cond-mat. 2005.
[24] S de Franciscis, S Johnson, and JJ Torres. “Enhancing neural-network performance via assortativity”. In: *Phys. Rev. E* 83.3 (2011), p. 036114.
[25] C Schmeltzer, AH Kihara, IM Sokolov, and S Rudiger. “Degree Correlations Optimize Neuronal Network Sensitivity to Sub-Threshold Stimuli”. In: *PLoS ONE* 10.6 (2015), e0121794.
[26] S Ito et al. “Large-Scale, High-Resolution Multielectrode-Array Recording Depicts Functional Network Differences of Cortical and Hippocampal Cultures”. In: *PLoS ONE* 9.8 (2014), e105324.
[27] A Minerbi et al. “Long-Term Relationships between Synaptic Tenacity, Synaptic Remodeling, and Network Activity”. In: *PLoS Biol* 7.6 (2009), e1000136.
[28] JT Trachtenberg et al. “Long-term in vivo imaging of experience-dependent synaptic plasticity in adult cortex”. In: *Nature* 420.6917 (2002), pp. 788–794.
[29] AJGD Holtmaat et al. “Transient and Persistent Dendritic Spines in the Neocortex In Vivo”. In: *Neuron* 45.2 (2005), pp. 279–291.
[30] R Yuste and T Bonhoeffer. “Genesis of dendritic spines: insights from ultrastructural and imaging studies”. In: *Nat Rev Neurosci* 5.1 (2004), pp. 24–34.
[31] S Song, KD Miller, and LF Abbott. “Competitive Hebbian learning through spike-timing-dependent synaptic plasticity”. In: *Nat Neurosci* 3.9 (2009), pp. 919–926.
[32] EM Izhikevich. “Simple model of spiking neurons”. In: *Neural Networks, IEEE Transactions on* 14.6 (2003), pp. 1569–1572.

[33] C O'Donnell and MCW van Rossum. "Systematic analysis of the contributions of stochastic voltage gated channels to neuronal noise". In: *Frontiers in Computational Neuroscience* 8.105 (2014), fncom.2014.00105.

[34] CK Pfeffer, M Xue, M He, ZJ Huang, and M Scanziani. "Inhibition of inhibition in visual cortex: the logic of connections between molecularly distinct interneurons". In: *Nat Neurosci* 16.8 (2013), pp. 1068–1076.

[35] The Petilla interneuron nomenclature Group. "Petilla terminology: nomenclature of features of GABAergic interneurons of the cerebral cortex". In: *Nat Rev Neurosci* 9.7 (2008), pp. 557–568.

[36] J DeFelipe et al. "New insights into the classification and nomenclature of cortical GABAergic interneurons". In: *Nat Rev Neurosci* 14.3 (2013), pp. 202–216.

[37] C Holmgren, T Harkany, B Svennenfors, and Y Zilberter. "Pyramidal cell communication within local networks in layer 2/3 of rat neocortex". In: *The Journal of Physiology* 551.1 (2003), pp. 139–153.

[38] AM Packer and R Yuste. "Dense, Unspecific Connectivity of Neocortical Parvalbumin-Positive Interneurons: A Canonical Microcircuit for Inhibition?" In: *The Journal of Neuroscience* 31.37 (2011), pp. 13260–13271.

[39] JR Gibson, M Beierlein, and BW Connors. "Two networks of electrically coupled inhibitory neurons in neocortex". In: *Nature* 402.6757 (1999), pp. 75–79.

[40] MEJ Newman. *Networks: an Introductions*. Oxford: Ofxord University press, 2010.

[41] J van Pelt, PS Wolters, MA Corner, WLC Rutten, and GJA Ramakers. "Long-term characterization of firing dynamics of spontaneous bursts in cultured neural networks". In: *Biomedical Engineering, IEEE Transactions on* 51.11 (2004), pp. 2051–2062.

[42] FAA Kingdom and N Prins. *Psychophysics: A Practical Introduction*. Academic Press: an imprint of Elsevier, London, 2010.

[43] D Ko, CJ Wilson, CJ Lobb, and C Paladini. "Detection of bursts and pauses in spike trains". In: *Journal of Neuroscience Methods* 211.1 (2012), pp. 145–158.

[44] MB Martens, T Celikel, and PHE Tiesinga. "A developmental switch for Hebbian plasticity". In: *PLoS Computational Biology* 11.7 (2015), e1004386.

[45] MH Johnson. "Functional brain development in humans". In: *Nat Rev Neurosci* 2.7 (2001), pp. 475–483.

[46] M De Roo, P Klauser, P Mendez, L Poglia, and D Muller. "Activity-Dependent PSD Formation and Stabilization of Newly Formed Spines in Hippocampal Slice Cultures". In: *Cerebral Cortex* 18.1 (2008), pp. 151–161.

[47] A Holtmaat, L Wilbrecht, GW Knott, E Welker, and K Svoboda. "Experience-dependent and cell-type-specific spine growth in the neocortex". In: *Nature* 441.7096 (2006), pp. 979–983.

[48] GF Woods, WC Oh, LC Boudewyn, SK Mikula, and K Zito. "Loss of PSD-95 Enrichment Is Not a Prerequisite for Spine Retraction". In: *The Journal of Neuroscience* 31.34 (2011), pp. 12129–12138.

[49] EI Knudsen. "Sensitive Periods in the Development of the Brain and Behavior". In: *Journal of Cognitive Neuroscience* 16.8 (2004), pp. 1412–1425.

[50] HS Bateup, CL Denefrio, CA Johnson, JL Saulnier, and BL Sabatini. "Temporal dynamics of a homeostatic pathway controlling neural network activity". In: *Frontiers in Molecular Neuroscience* 6.28 (2013).

[51] GG Turrigiano. "The Self-Tuning Neuron: Synaptic Scaling of Excitatory Synapses". In: *Cell* 135.3 (2008), pp. 422–435.

[52] JI AlvarezHamelin, L Dall'Asta, A Barrat, and A Vespignani. "Large scale networks fingerprinting and visualization using the k-core decomposition". In: *Advances in Neural Information Processing Systems* 18 (2006), pp. 41–50.

[53] P Hagmann et al. "Mapping the Structural Core of Human Cerebral Cortex". In: *PLoS Biol* 6.7 (2008), e159.

[54] R Romo, A Hernandez, A Zainos, and E Salinas. "Somatosensory discrimination based on cortical microstimulation". In: *Nature* 392.6674 (1998), pp. 387–390.

[55] Y Yoshihara, M De Roo, and D Muller. "Dendritic spine formation and stabilization". In: *Current Opinion in Neurobiology* 19.2 (2009), pp. 146–153.

[56] P García-López, V García-Marín, and M Freire. "Dendritic Spines and Development: Towards a Unifying Model of Spinogenesis". In: *Neural Plasticity* 2010 (2010), pp. 1–29.

[57] M Okun et al. "Diverse coupling of neurons to populations in sensory cortex". In: *Nature* 521.7553 (2015), pp. 511–515.

[58] KD Harris and TD Mrsic-Flogel. "Cortical connectivity and sensory coding". In: *Nature* 503.7474 (2013), pp. 51–58.

[59] J Chapeton, T Fares, D LaSota, and A Stepanyants. "Efficient associative memory storage in cortical circuits of inhibitory and excitatory neurons". In: *Proceedings of the National Academy of Sciences* 109.51 (2012), E3614–E3622.

[60] JW Mink, RJ Blumenschine, and DB Adams. "Ratio of central nervous system to body metabolism in vertebrates: its constancy and functional basis". In: *American Journal of Physiology* 241.3 (1981), R203–R212.

[61] JJ Harris, R Jolivet, and D Attwell. "Synaptic Energy Use and Supply". In: *Neuron* 75.5 (2012), pp. 762–777.

[62] D Attwell and SB Laughlin. "An Energy Budget for Signaling in the Grey Matter of the Brain". In: *J Cereb Blood Flow Metab* 21.10 (2001), pp. 1133–1145.

[63] X Wang and EK Michaelis. "Selective Neuronal Vulnerability to Oxidative Stress in the Brain". In: *Frontiers in Aging Neuroscience* 2.12 (2010), pp. 1663–4365.

[64] TC Sudhof. “Neuroligins and neurexins link synaptic function to cognitive disease”. In: *Nature* 455.7215 (2008), pp. 903–911.
[65] GMJ Beaudoin et al. “Culturing pyramidal neurons from the early postnatal mouse hippocampus and cortex”. In: *Nature Protocols* 7.9 (2012), pp. 1741–1754.
[66] J Tang et al. “A Complexin/Synaptotagmin 1 Switch Controls Fast Synaptic Vesicle Exocytosis”. In: *Cell* 126.6 (2006), pp. 1175–1187.
[67] R Dingledine, K Borges, D Bowie, and SF Traynelis. “The Glutamate Receptor Ion Channels”. In: *Pharmacological Reviews* 51.1 (1999), pp. 7–62.
[68] H Kato and T Ikeguchi. *Emergence of Highly Nonrandom Functional Synaptic Connectivity Through STDP*. Vol. 6443. Lecture Notes in Computer Science. Springer Berlin Heidelberg, 2010, pp. 116–123.
[69] N Masuda and H Kori. “Formation of feedforward networks and frequency synchrony by spike-timing-dependent plasticity”. In: *Journal of Computational Neuroscience* 22.3 (2007), pp. 327–345.
[70] H Kato, T Ikeguchi, and K Aihara. *Structual analysis on stdp neural networks using complex network theory*. Vol. 5768. ICANN. Springer Berlin Heidelberg, 2009, pp. 306–314.
[71] C Itami and F Kimura. “Developmental Switch in Spike Timing-Dependent Plasticity at Layers 4-2/3 in the Rodent Barrel Cortex”. In: *The Journal of Neuroscience* 32.43 (2012), pp. 15000–15011.
[72] VB Mountcastle. *Perceptual neuroscience: the cerebral cortex*. Cambridge, MA: Harvard University Press, 1998.
[73] RJ Douglas and KAC Martin. “Neuronal circuits of the neocortex”. In: *Annual Review of Neuroscience* 27.1 (2004), pp. 419–451.
[74] A Treves. “Computational Constraints that may have Favoured the Lamination of Sensory Cortex”. In: *Journal of Computational Neuroscience* 14.3 (2003), pp. 271–282.
[75] RDS Raizada and S Grossberg. “Towards a Theory of the Laminar Architecture of Cerebral Cortex: Computational Clues from the Visual System”. In: *Cerebral Cortex* 13.1 (2003), pp. 100–113.
[76] S Haeusler and W Maass. “A Statistical Analysis of Information-Processing Properties of Lamina-Specific Cortical Microcircuit Models”. In: *Cerebral Cortex* 17.1 (2007), pp. 149–162.
[77] JL Lanciego and FG Wouterlood. “A half century of experimental neuroanatomical tracing”. In: *Journal of Chemical Neuroanatomy* 42.3 (2011), pp. 157–183.
[78] M Helmstaedter. “Cellular-resolution connectomics: challenges of dense neural circuit reconstruction”. In: *Nature Methods* 10.6 (2013), pp. 501–507.
[79] I Arganda-Carreras et al. “Crowdsourcing the creation of image segmentation algorithms for connectomics”. In: *Frontiers in Neuroanatomy* 9.142 (2015).
[80] C Sommer, C Strähle, U Köthe, and FA Hamprecht. “ilastik: Interactive Learning and Segmentation Toolkit”. In: *Eighth IEEE International Sym-*

posium on Biomedical Imaging (ISBI 2011). Proceedings. 1. 2011, pp. 230–233.

[81] N Hirokawa. "From electron microscopy to molecular cell biology, molecular genetics and structural biology: intracellular transport and kinesin superfamily proteins, KIFs: genes, structure, dynamics and functions". In: *Journal of Electron Microscopy* 60.1 (2011), S63–S92.

[82] IR Wickersham et al. "Monosynaptic Restriction of Transsynaptic Tracing from Single, Genetically Targeted Neurons". In: *Neuron* 53.5 (2007), pp. 639–647.

[83] F Osakada et al. "New Rabies Virus Variants for Monitoring and Manipulating Activity and Gene Expression in Defined Neural Circuits". In: *Neuron* 71.4 (2015), pp. 617–631.

[84] S Song, PJ Sjöström, M Reigl, S Nelson, and DB Chklovskii. "Highly Nonrandom Features of Synaptic Connectivity in Local Cortical Circuits". In: *PLoS Biol* 3.3 (2005), e68.

[85] R Perin, TK Berger, and H Markram. "A synaptic organizing principle for cortical neuronal groups". In: *Proceedings of the National Academy of Sciences* 108.13 (2011), pp. 5419–5424.

[86] L Tricoire et al. "A Blueprint for the Spatiotemporal Origins of Mouse Hippocampal Interneuron Diversity". In: *Journal of Neuroscience* 31.30 (2011), pp. 10948–10970.

[87] M Toledo-Rodriguez and H Markram. *Single-Cell RT-PCR, a Technique to Decipher the Electrical, Anatomical, and Genetic Determinants of Neuronal Diversity*. Vol. 1183. Methods in Molecular Biology. Springer New York, 2014, pp. 143–158.

[88] WM Freeman, SJ Walker, and Vrana KE. "Quantitative RT-PCR: pitfalls and potential". In: *Biotechniques* 26.1 (1999), pp. 112–122.

[89] A Zeisel et al. "Cell types in the mouse cortex and hippocampus revealed by single-cell RNA-seq". In: *Science* 347.6226 (2015), pp. 1138–1142.

Chapter 4

Stimulus detection probability is increased by spike train irregularity

This chapter is in preparation for publication.

T. van Gils, P.H.E. Tiesinga, M.B. Martens

4.1 Abstract

Recent experiments have shown that short spike trains elicited in single neurons of the somatosensory cortex were able to induce a behavioural response. Interestingly, the rats showed an increased response rate for stimulations with pulse trains that led to spike trains with irregular interspike intervals (ISIs). However, the neuronal circuits in the somatosensory cortex are also spontaneously active, providing similarly-sized input that is not related to the stimulus. We computationally studied whether sensitivity was effected by the spike train irregularity in spiking neural networks (SNNs). In SNNs, we found that the probability to induce a detectable event in the form of a network burst was increased for single-neuron injection of irregular relative to regular spike trains. The increased detection rate depended on the short-term plasticity profile, providing a possible mechanism for neural networks to tune sensitivity to stimulus irregularity. Furthermore, using binary networks to study the role of action potential interaction, we found that sensitivity to spike train irregularity is inherent to recurrent networks. Taken together, we hypothesize that the sensitivity to spike train irregularity in neural networks relates to the short ISIs that are present in irregular stimulation. Short ISIs lead to increased synaptic integration, which can be modified by the short-term plasticity profile, and a higher probability of coincidence detection. Brain circuits could use this as a strategy to increase the detection probability of natural stimuli, which are often composed of irregular spike trains.

4.2 Introduction

Noise, in the form of biochemical and biophysical stochastic processes that affect information transfer, permeates every level of the nervous system [1]. Brain circuits are stable to noise perturbations that represent sensory input to which they need to respond, while simultaneously remaining sensitive to equally sized externally induced perturbations. Several mechanisms are proposed to enhance neuronal communication, for example coherence in neuronal oscillations (for reviews see [2, 3]) or wiring schemes of the circuitry [4].

Noise is not always a problem for neurons, as it can also be a solution to information processing problems: intermediate levels of noise can improve stimulus detection [1]. Recording and imaging techniques that do not select the recorded neurons, and thereby provide unbiased measurement of the firing rates show that sensory areas are sparsely and spontaneously active [5, 6]. Neurons in the rat barrel cortex for example shows spontaneous spiking at a rate of a few Hz [5, 7, 8]. It is therefore of interest to determine whether externally induced perturbations can influence behaviour. Relatively strong external stimulations of hundreds of neurons in the form of microstimulation have already established a direct link from spiking activity to behaviour [9, 10]. However, it was even possible to condition rats to report stimulation of single neurons in the sensory cortex

[11]. These experimental results suggest that perturbations of single neurons can influence decision making.

Recently, Doron and coworkers showed that the discharge pattern of evoked spikes in single neuron stimulation affected detection probability [12]. Injections of irregular spike trains were able to evoke behavioural responses, whereas regular spike trains were not able to influence behaviour [12]. Furthermore, rats are more sensitive to irregular patterns in whisker deflection compared to regularly ordered deflections [13]. It is unclear by which mechanism cells have a stronger impact when they fire irregularly [12]. Our guiding hypothesis is that irregular spike trains have a higher probability to evoke a neuronal network responses compared to the same number of spikes in regular spike trains.

To investigate this, we first explored detectability of irregular spike trains in SNNs. The single-neuron stimulation detection task used by [12] starts with training the rats to detect microstimulation [14] over several days before switching to single-neuron stimulation trials. To mimic this situation in our experiments, and obtain a baseline response rate, we trained *in silico* SNNs to respond to spike trains with an intermediate regularity at a response rate of 50%, before applying irregular or regular stimulation. During the training period, we applied network scaling [15]. Adjustment of the synaptic weights to maintain a certain level of action potential activity can be achieved by homeostatic plasticity mechanisms that dynamically set synaptic strengths [16], ion-channel expression [17] or the release of neuromodulators [18]. Stimulation of the networks after the training period showed that irregular spike trains increased and regular spike trains decreased the stimulus detection rate. Using this setup, we found that short-term plasticity (STP) could modify the sensitivity to stimulus irregularity. We studied the interspike intervals (ISIs) in a window leading up to the burst and found that short ISIs, and pairs of short ISIs, were more likely to precede a burst. Together, these results suggest that short ISIs in irregular stimuli have an increased probability to generate a burst, and that synaptic dynamics effect the impact of short ISIs on burst generation. Furthermore, we stimulated recurrent networks of binary neurons, showing that sensitivity to stimulus irregularity can occur irrespective of neuronal dynamics. In a probabilistic model for the binary neurons, we find that two consecutive ISIs resulted in higher burst probability due to a network interaction term, whereas the same amount of spikes in isolation had a lower burst probability, suggesting a strong contribution of the recurrent network structure to respond to short ISIs.

In cortical neurons, the degree of spike train variability and regularity varies, where in some cases the variability in response patterns is high, and under other conditions neurons fire more consistently (for review, see [1]). More short ISIs are found in irregular relative to regular spike trains. Here, we propose that the increased sensitivity to spike train irregularity in neural networks can be explained by (1) synaptic signal integration for short ISIs, which can be tuned by the STP profile, and (2) an increased coincidence detection for short ISIs in recurrent networks.

Variable description	Symbol	Value	Citation
Membrane rest potential	V_{rest}	-70.6 mV	[19]
Membrane time constant	τ_m	9.4 ms	[19]
Membrane capacitance	C_m	281 pF	[19]
Spiking threshold at rest	θ_{rest}	-50.4 mV	[19]
Maximum spiking threshold	θ_{max}	30.4 mV	[19]
Adaptive threshold time constant	τ_θ	50 ms	[19]
Vesicle recovery constant	τ_{rec}	800 ms	[20]
Alpha function time constant	τ_α	3 ms	
Maximum vesicle exocytosis	N_T	10	
Vesicle pool capacity	P_c	75	

Table 4.1: Parameter values of the SNNs.

4.3 Methods

We studied the role of spike train irregularity in the generation of a network-wide burst of action potentials (network response) in recurrent SNNs, consisting of leaky integrate-and-fire (LIF) neurons with adaptive synapses. To highlight the role of network structure on the generation of network responses, we also used binary simulations and calculations.

4.3.1 Neuron model

For the SNN simulations we used LIF neurons:

$$\frac{dV}{dt} = -\frac{(V - V_{rest})}{\tau_m} + \frac{I_{ves}}{C_m} \tag{4.1}$$

Where V_{rest} is the resting membrane potential, τ_m the membrane time constant, C_m the membrane capacitance and I_{ves} the synaptic input current as defined in Equation 4.3 below (parameter values are listed in Table 4.1). After an action potential occurred, the membrane potential was reset to V_{rest}. We used the Euler method to solve the differential equation with time steps of $dt = 0.5$ ms. An action potential was modelled to occur when the membrane voltage became larger than an adaptive threshold τ_m which satisfied the following equation:

$$\frac{d\theta_m}{dt} = -\frac{(\theta_m - \theta_{rest})}{\tau_\theta} \tag{4.2}$$

Where θ_m returns to the threshold value θ_{rest} at rest with time constant τ_θ. After an action potential occurred, the threshold is set to $\theta_m = \theta_{max}$ (parameter values are listed in Table 4.1).

4.3.2 Synapse model: vesicle exocytosis

Synaptic transmission was implemented as vesicle exocytosis from the presynaptic neuron, leading to the depolarization of the postsynaptic membrane (Figure 4.1). The resulting excitatory postsynaptic current (EPSC) is modelled as an alpha function, resulting in a postsynaptic current (I_{ves}) in neuron j at time t:

$$I_{ves}(j,t) = \sum_{i=1}^{N} \left[w_{ij} \cdot \sum_{\Delta t} v_{ij}(t - \Delta t) \cdot \alpha(\Delta t) \right] \tag{4.3}$$

Where w_{ij} is the synaptic strength between presynaptic neuron i and postsynaptic neuron j, v_{ij} the number of vesicles that were exocytosed from presynaptic neuron i onto postsynaptic neuron j at time Δt before the current time t (parameter values are listed in Table 4.1). Vesicles were omitted at $\Delta t > 20$ ms, at which time less than 1% of the maximal current remained. The currents generated by a single vesicle were modelled as a normalized alpha function $\alpha(t)$:

$$\alpha(t) = \frac{t}{\tau_\alpha} \cdot e^{1 - \frac{t}{\tau_\alpha}} \tag{4.4}$$

With τ_α being the time constant for synaptic decay (parameter value is listed in Table 4.1).

The probability that vesicle exocytosis occurred in response to an action potential in the presynaptic neuron was modelled as a binomial distribution:

$$p_{ij}(v_{ij} \mid N_T, \Theta) = \binom{N_T}{v_{ij}} \Theta^{v_{ij}} (1 - \Theta)^{N_T - v_{ij}} \tag{4.5}$$

With v_{ij} being the number of vesicles that is exocytosed and N_T the maximum number of released vesicles in response to a single action potential (parameter values are listed in Table 4.1). We simulated two types of release models, for which $\Theta = P_f$ was the default, where P_f is the fraction of available vesicles in the vesicle pool (Equation 4.6 below). To evaluate the properties of a large variety of short-term plasticity profiles, we also used $\Theta = F \cdot D \cdot P_f$, with F a facilitation term (Equation 4.7 below) and D a depression term (Equation 4.8 below).

An exocytosed vesicle was moved from the active pool (P_a) to the recycling pool (P_r), and vesicles return to the active pool according to:

$$\frac{dP_a}{dt} = \frac{P_r}{\tau_{rec}} \tag{4.6}$$

Where P_c is the total vesicle pool capacity per synapse and τ_{rec} is the vesicle recycling rate. Vesicle pools were initialized at 80% of the vesicle pool capacity P_c (parameter values are listed in Table 4.1). The fraction of available vesicles is calculated as $P_f = \frac{P_a}{P_c}$.

To study spike train detectability under noisy conditions, we implemented synaptic noise in the form of a Poisson process for spontaneous vesicle exocytosis, η, at a default rate of 10 Hz.

Name	F_1	K_F	τ_F	K_D	k_0	k_{max}	τ_D	P_c
Default	-	-	100 ms	2	$2s^{-1}$	$30s^{-1}$	50 ms	75
SF	0.05	7.4	”	”	”	”	”	20
SD	*off*	*off*	”	”	$0.7s^{-1}$	$20s^{-1}$	”	75
D	0.4	8	”	”	”	”	”	50
F	0	16	”	”	”	”	”	150
FD	0.2	0.5	”	”	”	”	”	75

Table 4.2: Parameter values for simulations with short-term facilitation and depression mechanisms as described in [21]. The ” indicate the default values given in the first row.

4.3.3 Synapse model: Ca^{2+}-dependent short-term plasticity

To study a large variety of short-term plasticity profiles, we implemented, in addition to the dynamical synapses described above, a facilitation and depression term based on residual Ca^{2+} in the presynaptic terminal [22, 23], and used the model proposed by Dittman et. al. [21](**Figure 4.1**):

$$F(t) = F_1 + \frac{1 - F_1}{1 + K_F/CaX_F(t)} \tag{4.7}$$

$$\frac{dD}{dt} = (1 - D(t)) \cdot k_{recov}(CaX_d) - \frac{v_{ij}(t)}{N_T} \cdot \delta(t - t_{sp}) \tag{4.8}$$

$$k_{recov}(CaX_D) = \frac{k_{max} - k_0}{1 + K_D/CaX_D(t)} + k_0 \tag{4.9}$$

Where F_1 is the strength of facilitation after the first action potential, K_F and K_D denote the strength of facilitation and depression, respectively, $v_{ij}(t)$ is the number of exocytosed vesicles (Equation 4.5 and synaptic noise in the form of spontaneously exocytosed vesicles) from presynaptic neuron i to postsynaptic neuron j and δ is the dirac delta function (parameter values are listed in Table 4.2). The residual calcium binding is described by CaX_F and CaX_D as follows:

$$\frac{dCaX_F}{dt} = -CaX_F(t)/\tau_F + \Delta_F \cdot \delta(t - t_{sp}) \tag{4.10}$$

$$\frac{dCaX_D}{dt} = -CaX_D(t)/\tau_D + \Delta_D \cdot \delta(t - t_{sp}) \tag{4.11}$$

Where Δ_F, Δ_D and K_F are related to each other: $\frac{K_F}{\Delta_F} = C$ and $\Delta_F = \Delta_D$ (parameter values are listed in Table 4.2). Using this calcium-based model for short-term facilitation and depression we generated several distinct profiles of facilitatory and depressing neurons (parameter values are listed in Table 4.2).

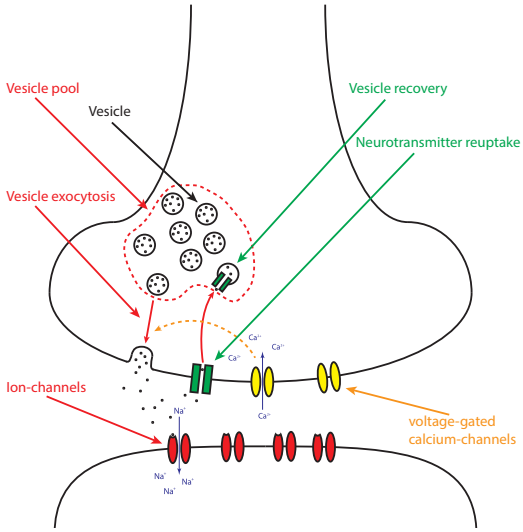

Figure 4.1: Calcium induction of short-term plasticity. Action potentials that arrive in the axonal terminal open voltage-gated calcium channels. Residual calcium at the time of the next action potential can have a facilitatory or depressing effect on the probability of vesicle release [21].

4.3.4 Burst detection

Network bursts were detected using a spike density method. Spikes from all neurons were combined intro a single spike train (S) with time bins of 0.5 ms, and convolved with a rectangular kernel that was of width 10 ms:

$$\rho_{spike}(t) = \sum_{\Delta t=0}^{19} S(t - \Delta t) \tag{4.12}$$

The burst onset was defined as the time when $\rho_{spike}(t)$ first became larger than 100 spikes in the 10 ms window, and the end of a burst was defined as the time when ρ_{spike} first became lower than 50 spikes in the 10 ms window. A burst onset within the detection window of 500 ms after the stimulus onset was regarded as having been caused by this stimulus (true positive). During catch trials, a burst that was related to synaptic noise could also occur during the detection window (false positive). The network response rate is taken as the true positive rate in response to the stimulations.

4.3.5 Stimulus generation

For each network, one neuron (single-neuron stimulation) and a set of neurons (multi-neuron stimulation, 5 neurons unless indicated otherwise) were randomly

selected and used throughout the experiment for stimulation. For the conditions without noise, the network state was reset to default values at the start of each stimulation trial. Stimulation was applied for 250 ms and simulations were run for the duration of the detection window of 500 ms. For the simulations with noise, 250 ms stimulation was applied every 2 seconds, without resetting the network state.

The interspike intervals (ISIs) of the stimulus spike trains were sampled from a gamma distribution with a variable renewal constant ($K_{stim} = 1$ and 10 for irregular and regular stimuli, respectively) at rate 50 Hz. The number of stimulations per network was 30 for the conditions without noise and 20 in the case of noise, with permutations in the ISIs between networks to generate unique stimulus trains while maintaining the same coefficient of variation (CV_{ISI}).

4.3.6 Sensitivity to Stimulus Irregularity

To assess the differential impact of stimulus irregularity, we calculate the sensitivity to stimulus irregularity (SSI). The SSI is the difference between network response rate for irregular stimuli ($K_{stim} = 1$) and regular stimuli ($K_{stim} = 10$). A high SSI relates to networks that are highly sensitive to irregular stimuli, whereas for a low SSI the networks respond similarly to irregular and regular stimuli. A negative SSI would indicate that the network is more sensitive to stimulation by regular simuli compared to irregular stimuli.

4.3.7 Network generation

The model network was composed of $N = 500$ excitatory neurons that were connected with probability $P_{con} = 5\%$ [24]. Synaptic weights were picked from a uniform distribution between 20 and 60 pA.

We used an iterative global scaling of the synaptic strength, implemented as:

$$dw_{ij}(\tau) = \Gamma(\tau) \cdot \lambda(s) \cdot w_{ij}(\tau - 1) \tag{4.13}$$

Where Γ determines the direction of change (Equation 4.14) and λ is a damping rate factor that iteratively decreases with the number of sign changes (s) that occured in $\Gamma(\tau)$, implemented as $\lambda(s) = 0.7^s$. Networks were scaled for 60 stimulations, τ is the stimulus index and Γ is calculated as:

$$\Gamma(\tau) = \begin{cases} -0.2, & \text{if } R(\tau) > 50\% \\ 0, & \text{if } R(\tau) = 50\% \\ 0.2, & \text{if } R(\tau) < 50\% \end{cases} \tag{4.14}$$

Where R is the network response rate, taken as the true positive rate over the last two stimuli. The scaling method is thus set to iteratively approach a network response rate of 50%. After the scaling phase, the network reponse rates were tested with irregular and regular stimulus spike trains.

4.3.8 Binary networks: simulation

Binary networks were composed of $N = 500$ excitatory neurons that were connected with probability $P_{con} = 5\%$ [24]. Synaptic strengths were picked from a uniform distribution between 0.75 and 1.25. The network activity is given by:

$$V_j(t) = \sum_{i=1}^{N} w_{ij} \cdot s_i(t-1) \tag{4.15}$$

Where V_j represents the input to postsynaptic neuron j, w_{ij} the synaptic strength between presynaptic neuron i and postsynaptic neuron j and s_i the state (firing an action potential or silent) of the neuron i, given by the condition:

$$s_i(t) = \begin{cases} 1 & \text{for } V_i(t) \geq \Theta \\ 0 & \text{otherwise} \end{cases} \tag{4.16}$$

With Θ being a variable action potential threshold given by

$$\Theta = 1.25 - \frac{\theta_{sim}}{2N \cdot P_{con}} \tag{4.17}$$

Where θ_{sim} is the value that was varied to adjust network excitability. We calculate the action potential threshold Θ with respect to the maximal synaptic strength (1.25). Network activity was set to $V = 0$ and $s = 0$ for all neurons at the start of each stimulation trial. The network was considered to burst when more than 90% of the neurons were active in a single time bin.

4.3.9 Binary networks: probabilistic model

We used a probabilistic model to calculate the increase in burst probability as a function of action potential interaction in binary neurons. First, we calculate the probability that a single action potential leads to one or multiple action potentials. Then, we calculate the probability that two action potentials interact in a way that also leads to an action potential. To calculate these values we use as an approximation the hypergeometric probability distribution [25], because we wanted to have an explicit expression to make the subsequent analytical derivations clearer. It does therefore not correspond exactly to the simulations of the binary networks in the preceding section.

For a single active neuron in the network we use the hypergeometric probability distribution to obtain the probability of it activating one or multiple neurons:

$$p(s \mid M, \Theta_{model}, N_{out}) = \frac{\binom{\Theta_{model}}{s} \cdot \binom{M-\Theta_{model}}{N_{out}-s}}{\binom{M}{N_{out}}} \tag{4.18}$$

Where M is the number of available neurons in the network, $N_{out} = 25$ is the average number of synaptic connections per neuron and Θ_{model} the number of

neurons that are excited enough to spike when they get an input. There are no autaptic connections, as such the current active neuron is not in the sample pool and $M = N$ - 1 = 499. Because the calculation of these values is computationally intensive, we used the HyperQuick implementation of the hypergeometric distribution [25].

When there are two coincident synaptic inputs to a neuron, we assume that it will spike. Hence we look at the number of states in which s neurons are in the $N_{out,1}$ and $N_{out,2}$ set, ignoring the effects of excitability (in the previous formula):

$$c(s \mid M, N_{out,1}, N_{out,2}) = \frac{\binom{N_{out,1}}{s} \cdot \binom{M-N_{out,1}}{N_{out,2}-s}}{\binom{M}{N_{out,2}}} \tag{4.19}$$

Where, as before, M is the number of neurons in the network, $N_{out,1} = N_{out,2}$=25 is the average number of synaptic connections per neuron. This distribution thus calculates the probability that an active neuron projects to a fraction of the same postsynaptic neurons that the other active neuron projects to. In the Markov chain we combine these two effects (Equation 4.18 & Equation 4.19). For instance, a transition from a state with two active neurons to a state with one active neuron, m_{21}, can take place in two ways, (1) when either one of the actived neurons causes a spike, but the other neuron does not, nor does the coincidence of two synaptic inputs: 2·p(0)p(1)c(0) (the two reflects that it can be either neuron), or (2) when two coincident synaptic inputs recruit a spike but the individual ones do not: p(0)p(0)c(1). The other coefficients are derived in a similar way.

$$M = \begin{bmatrix} 1 & 0 & 0 & 0 \\ p(0) & p(1) & p(2) & 1-p(0)-p(1)-p(2) \\ m_{20} & m_{21} & m_{22} & 1-m_{20}-m_{21}-m_{22} \\ 0 & 0 & 0 & 1 \end{bmatrix} \tag{4.20}$$

Where $m_{20} = p(0)^2c(0)$, $m_{21} = 2p(0)p(1)c(0) + p(0)^2c(1)$ and $m_{22} = p(0)^2c(2) + p(1)^2c(0) + 2p(1)p(0)c(1) + 2p(2)p(0)c(0)$. For example, using the default values given for Equation 4.18 and $\Theta_{model} = 5$, we calculate the probability that one action potential leads to exactly one (s=1) other action potential in the next step, for which we obtain $p(1) = \frac{\binom{5}{1}\cdot\binom{499-5}{25-1}}{\binom{499}{25}}$=0.21=21%. We assume that more than 2 action potentials will eventually lead to a network burst, such that the M is constrained to be of size 4×4.

The first action potential of the stimulus spike train that is injected into the network sets the probability to find a single action potential in the network at $P(1) = 1$. $P(0)$, $P(2)$ and $P(3)$ are initialized at value 0. After a stimulus spike train consisting of N ISIs, the final P is calculated as:

$$P(M, \tau) = P_{init} \cdot \left(\prod_{n=1}^{N} M^{\tau(n)} \cdot S \right) \cdot \lim_{t \to \infty} M^t \tag{4.21}$$

With P being a vector containing the probabilities for 0, 1, 2 or more spikes being found in the network, M the transition matrix (Equation 4.20), $\tau(n)$ the length of the n-th ISI in the stimulus spike train and S the injection of an action potential after each ISI, achieved by shifting the values in the vector P:

$$S = \begin{bmatrix} 0 & 1 & 0 & 0 \\ 0 & 0 & 1 & 0 \\ 0 & 0 & 0 & 1 \\ 0 & 0 & 0 & 1 \end{bmatrix} \tag{4.22}$$

In this probabilistic model, $P(3)$ is then taken as the probability for a stimulus spike train to initiate a network burst.

4.4 Results

We studied conditions that could influence the network response rate to single-neuron stimulation, for which we compared stimulation in the form of irregular spike trains to stimulation with regular spike trains. A network response is taken as a network-wide, synchronous burst of action potentials that occurred within a 500 ms post-stimulus detection window.

4.4.1 Sensitivity to single-neuron stimulation under noisy conditions

We first studied the network response rate to nonstimulation (catch trials), single-neuron stimulation and multi-neuron stimulation in SNNs under noisy conditions. Previously, it was shown that rats could be trained to respond to single-neuron stimulation in the somatosensory cortex with a tongue lick response [11]. Follow-up studies showed that the response rate was significantly enhanced for irregularity in the spike trains [12]. During the training phase (duration 8.1 $\pm$ 2.1 days), the stimulation strength was reduced for each rat until their minimal detection threshold (2-5 μA) was reached [12]. The rats thus required extensive training to be able to detect single-neuron stimulation, and stimulation strength was adjusted per cell [12].

For the networks that were used in this study, we applied an iterative method to approach a 50% response rate to stimulus spike trains with intermediate regularity (ISIs from gamma distribution with renewal constant $K_{stim} = 5$), using network-wide scaling of the synaptic strength. We indeed found that in the 252 networks that were tested, the network response rate correctly scaled to $\sim$50% for stimuli with intermediate regularity, with an average response rate after scaling of 51.71% and standard deviation 14.45% (not significantly different from 50%, tested using ttest, the one-tailed t-test function in MATLAB (The Mathworks, Natick, MA, USA)).

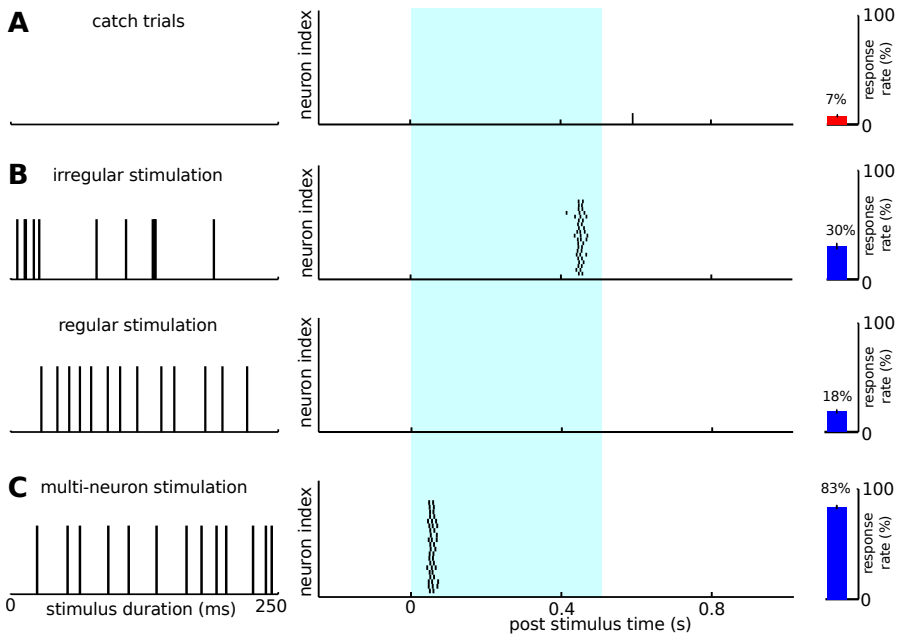

Figure 4.2: Spike train irregularity increases the network response rate for single-neuron stimulation under noisy conditions. ***A****: Synaptic noise in the form of spontaneous vesicle exocytosis can evoke network-wide bursts of action potentials. Spontaneous bursts during the detection window are considered false positives (red bar). Detection window indicated in cyan.* ***B****: The true positive detection rate (blue bars) was higher for single-neuron stimulation with irregular spike trains than for stimulation with regular spike trains (vertical axis is neuron index, small black bars indicate the timing of an action potential, long black bars indicate the stimulus spike train).* ***C****: Multi-neuron (5 neurons) stimulation resulted in a high true positive rate. Networks consisted of 500 LIF neurons with dynamical synapses with STP settings $F_1 = 0.24$, $K_F = 0.67$, and default values in Table 4.2. Data are obtained from 36 networks with 20 stimulations per condition.*

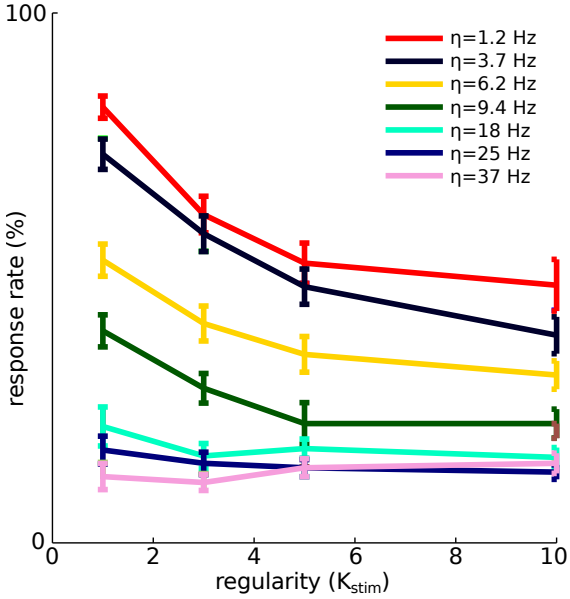

Figure 4.3: Noise reduces the SSI. The response rate was comparable between high and low regularity for high levels of noise. For the decrease in overall response rate, see main text. Noise was added in the form of spontaneous vesicle release, for which the rates are given in the figure legend. Network settings as in Figure 4.2.

We tested nonstimulation (catch trials) and single-neuron stimulation in these iteratively adapted and randomly connected SNNs. Model networks (default parameter settings) that were tested in the presence of synaptic noise induced a network response rate of 7% in the nonstimulation (catch) trials (**Figure 4.2A**). We found that networks that were stimulated with irregular ($K_{stim} = 1$) spike trains showed a network response rate of 30%, higher than the 18% network response rate for regular ($K_{stim} = 10$) stimulus spike trains (**Figure 4.2B**). In the noise simulations, the networks were scaled to an overall burst rate of 50%, which included spontaneous bursts that could occur also outside the 500 ms detection time window. Therefore, for the noise conditions, the reported network response rates are lower than 50%.

We also applied multi-neuron stimulation to SNNs that were trained to single-neuron stimulation. Stimulation in 10 neurons resulted in a 83% network response rate (**Figure 4.2C**), which is comparable to multi-neuron stimulation in rats for which a 92% tongue lick response rate was observed [12].

We were interested in whether the increased detection rates to irregular stimuli remained for high levels of synaptic noise. We found that for the parameter settings used here, the detection rates were comparable between irregular and regular stimuli in the case of high noise levels (**Figure 4.3**).

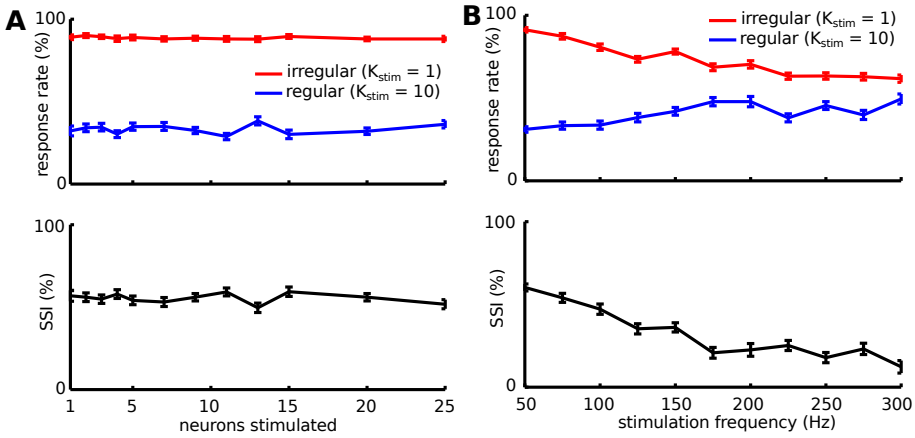

*Figure 4.4: Sensitivity to stimulus irregularity (SSI) was constant over network sizes (**A**), but diminished for high stimulation frequency (**B**). Data are presented as mean ± SEM and obtained from 24 networks with 30 stimulations per condition. For these simulations, the noise parameter η was set to zero.*

These results thus show that SNNs could be scaled to respond to single-neuron stimulation under noisy conditions. Furthermore, the network response rate was higher for stimulation with irregular spike trains compared to regular spike trains.

4.4.2 Sensitivity to stimulus irregularity

Next, we asked whether the specific stimulation settings had an effect on the sensitivity to stimulus irregularity (SSI). As shown above, multi-neuron stimulation in networks that were trained to single-neuron stimulation led to a high response rate. Here, we were interested in whether networks that were sensitive to multi-neuron stimulation were different in terms of SSI compared to networks that were sensitive to single-neuron stimulation. Therefore, to selectively evaluate the SSI, the networks were scaled for each property value to a response rate of approximately 50% for stimuli of intermediate regularity. In these networks, the SSI is defined as the difference between the response rate to irregular stimuli and regular stimuli, and was thus used as a measure of the degree to which the networks are more sensitive to irregular stimulation compared to regular stimulation.

We first studied the SSI in single- and multi-neuron stimulation. We found that for irregular stimulation the response rate was consistently higher compared to regular stimuli, with no correlation between the SSI and the number of stimulated neurons (**Figure 4.4A**). These results show that the SNNs were more sensitive to irregular spike trains compared to regular spike trains for both single-

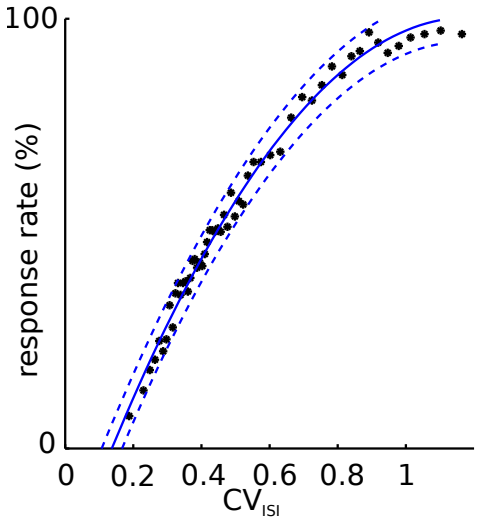

Figure 4.5: Positive correlation between the coefficient of variation of the stimulus ISIs (CV_{ISI}) and the network response rate. Data are presented as mean ± SEM and were obtained from 20 stimuli per condition for K_{stim} = 1, 5 and 10; each dot represents one stimulus, with the ISIs of the stimulus shuffled and tested in 252 networks. Blue line is a 2nd-order polynomial fit with confidence intervals indicated by the dotted blue lines. For these simulations, the noise parameter η was set to zero.

neuron as well as strong sensory input in the form of action potential activity in multiple neurons.

We found that high frequency stimulation resulted in a reduction in SSI compared to low frequency stimulation (**Figure 4.4B**). The SSI was highest for a stimulus frequency of 50 Hz (mean ISI 20 ms), and lowest for 300 Hz (mean ISI 3.3 ms). We hypothesize that the relatively high response rate for the high frequency stimulation is caused by the overlap between the short mean ISIs (3.3 ms) and the EPSC time constant (3 ms). As such, the relatively short mean ISIs of the regular spike trains can sufficiently integrate EPSC currents, leading to a reduction in the SSI of the neurons.

4.4.3 Short ISIs had a high probability to be followed by a network burst

We found that stimulation with irregular spike trains resulted in a higher response rate compared to stimulation with regular spike trains. We were therefore interested in the relation between the coefficient of variation of the stimulus ISIs (CV_{ISI}) and the network response rate. Single-neuron stimulation in rats showed that the response rate positively correlated with the CV_{ISI} [12]. Here, in

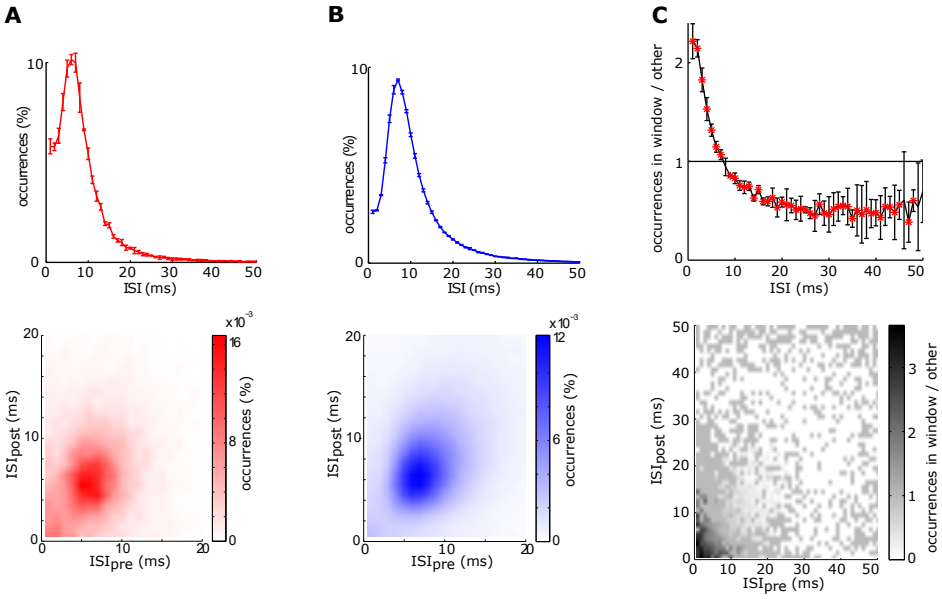

Figure 4.6: Short ISIs have a relatively high probability to be followed by a network burst. ***A****: Distribution of ISIs (top) and return map (bottom) of the ISIs that occurred during a 50 ms window directly before each burst.* ***B****: As in (A), but for the ISIs (top) and return map (bottom) of all other spikes outside the 50 ms window.* ***C****: The ratio of the distributions in (A) to (B). There are more short ISI (top) and pairs of short ISIs (bottom) in the 50 ms window preceding a burst compared to the other ISIs outside this window. Red * indicates significantly different from 1 (t-test, p<0.05). Data are presented as mean ± SEM and were obtained from 36 networks that were tested for 11 different frequencies with 20 stimulations per condition.*

SNNs we also found a correlation between network response rate and CV_{ISI} for single-neuron stimulation (**Figure 4.5**). The response rate to spike trains with CV_{ISI} ≈1 (Poisson distributed) approached 100%, whereas a CV_{ISI} below ∼0.5 corresponded to network response rates of less than 50% (**Figure 4.5**).

We were interested in whether there was a difference in the ISI distribution shortly before a burst, compared to the distribution of the other ISIs that did not directly precede a burst. We first plotted the distribution of ISIs in a 50 ms window preceding each burst, and the return map of all spikes in this window (**Figure 4.6A**), as well as the distribution of ISIs and the return map of all spikes that were not in this window (**Figure 4.6B**). By taking the ratio of these two distributions, we found that there are significantly more short ISIs (<10 ms), and pairs of short ISIs, in the 50 ms window preceding a burst (**Figure 4.6C**).

Taken together, the coefficient of variation of the stimulus spike trains tightly

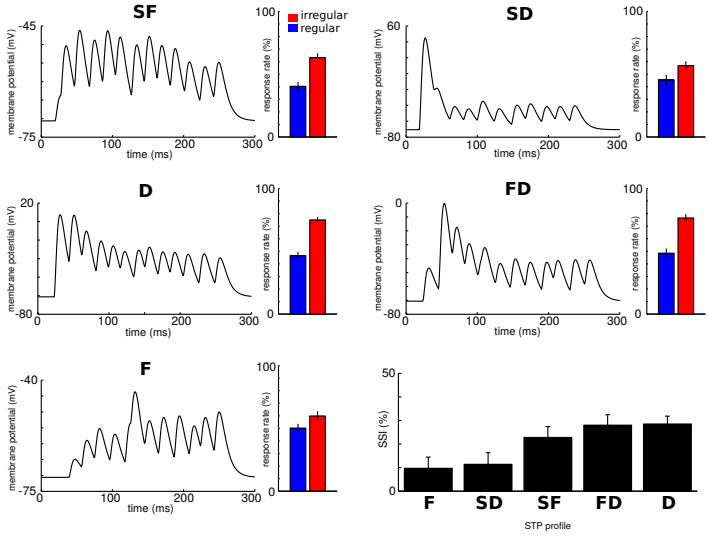

Figure 4.7: The short-term plasticity profile modulates the selectivity to stimulus irregularity. Example EPSC traces for several distinct STP profiles. These profiles were stimulated with irregular (response rates in red bars) and regular (response rates in blue bars) stimuli. The SSI values for the different STP profiles are shown as black bars. Data are mean ± SEM and were obtained from 24 networks, each network was tested for 30 stimulations per condition. For these simulations, the noise parameter η was set to zero.

correlated with the network response rate. Short ISIs, alone or in pairs, have a higher probability to be followed by a network burst than longer ISIs.

4.4.4 SSI depended on STP profile

Next, we studied whether calcium-induced changes in the synaptic release probability, either facilitating or depressing the release probability in response to subsequent spikes, had an effect on SSI. First, we manually selected several distinct STP profiles, namely depressing (D), facilitating (F), strong depressing (SD), strong facilitatory (SF) and facilitatory + depressing (SD); for parameters see Table 4.2. The SSI for facilitatory synapses was lowest, and depressing synapses showed the strongest SSI. These results imply that SSI can be modulated by the neurotransmitter release dynamics (**Figure 4.7**).

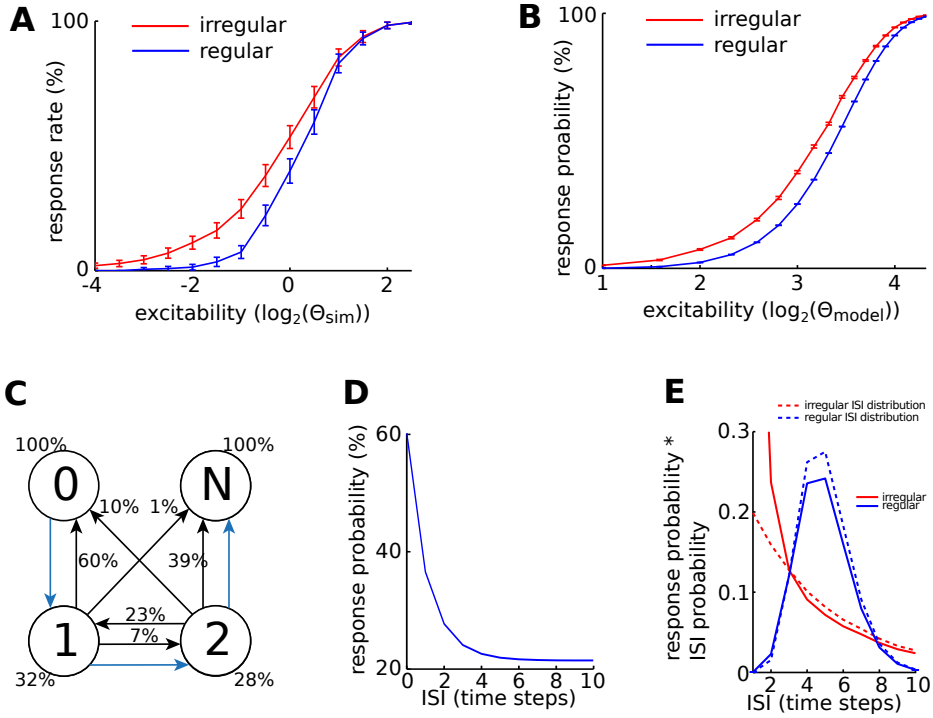

Figure 4.8: Binary network simulations and a probabilistic model for binary neurons show selectivity to stimulus irregularity. ***A****: SSI to single-neuron stimulation was observed in binary network simulations for a large range of neuronal excitability values. Data are presented as mean ± SEM and are obtained from 16 networks, where 10 stimuli were applied to each of 100 different neurons per network.* ***B****: SSI to single-neuron stimulation was also observed in a probabilistic model of binary neurons for a large range of neuronal excitability values. Data are presented as mean ± SEM and are obtained from 200 ISI spike trains.* ***C****: Example Markov chain for $\Theta_{model} = 10$. Black arrows with corresponding percentages indicate the probability to move from one state to another, blue arrows indicate stimulus injection of a single action potentail.* ***D****: Response probability to two action potentials that could interact in the network (short ISIs < 5 time steps) or could be considered to generate bursts independently (long ISIs > 10 time steps). $\Theta_{model} = 10$.* ***E****: The ISI response probabilities from (D), multiplied with the corresponding ISI distribution (dotted lines), yield the total response rates (solid lines). Total response rate was higher for irregular (area under the curve = 1.59) than for regular (area under the curve = 0.91) stimuli. Neural excitability parameter Θ_{model} was set to 5.*

4.4.5 Binary networks: SSI occurred in the absence of dynamical synapses

We wanted to know whether the SSI that we found in SNNs depended on the neuronal dynamics that operate at several time scales (such as relative synaptic time scale, depression and facilitation). Therefore, we used binary networks, which allowed us to study action potential propagation in recurrent networks without any time scales to consider. We varied the neuronal excitability parameter (θ_{sim}, Equation 4.17) in the binary networks and found that single-neuron stimulation led to a higher network response rate for irregular stimulus spike trains compared to regular stimuli (**Figure 4.8A**).

Binary network models can also be described analytically in terms of probabilities. Indeed, using a simplified probabilistic model described in subsection 4.3.9, we find that irregular single-neuron stimulation resulted in higher response rates compared to regular stimulation (**Figure 4.8B**). The probability for action potentials to propagate, amplify or diminish in the probabilistic network is described by a Markov Chain, which depends on the neuronal excitability (**Figure 4.8C**). We varied the duration of the ISI between two consecutive action potentials, and found an increased burst probability for short ISIs. For an ISI duration of a single time step the probability is relatively high that the two action potentials occur simultaneously in the network, thereby increasing the chance of coincidence detection. Indeed, the response probability of an ISI of 1 time step was 38% higher than for an ISI duration of more than 10 time steps, for which the response probability is predominantly determined by the sum of two individual action potentials that are injected into the network, with very low probability of interaction between these two action potentials (**Figure 4.8D**). Within the analytical model, one time step relates to the time it takes for one action potential to propagate to a connected neuron, and induce an action potential in that neuron, which is on the order of several ms [26].

We were interested whether the relatively high response rate of irregular spike trains could be related to a non-linear interaction between the ISI distribution and the response probability. To test this we multiplied the ISI distributions of irregular, which have more short ISIs, and regular stimuli, with the ISI response probability (**Figure 4.8D**). For network excitability parameter θ_{model}=5 we showed a 75% aggregate increase in response probability for irregular relative to regular stimuli (**Figure 4.8E**).

Together, we showed that SSI occurs in binary networks that contain no dynamics in synaptic function; these results support the hypothesis that SSI relates to coincidence detection in the network caused by short ISIs.

4.5 Discussion

Recently, the response rate to single-neuron stimulation in the somatosensory cortex of rats, as measured by tongue lick responses, was found to be higher for

stimulation with irregular than with regular spike trains [12]. We now found that in SNNs the response rate, as measured by a detectable and synchronous increase in action potential activity in the form of a burst, was also increased for irregular relative to regular spike trains. Furthermore, we found that the amplitude of SSI, an index for the sensitivity to the stimulus irregularity, could be modulated by the short-term plasticity profile of the synapses.

Under natural conditions, sensory stimuli often consist of a temporally irregular sequence of events [13], and cortical spike trains are highly irregular [1, 27]. Neurons can act as integrators or function as coincidence detectors (for review see [28]). As discussed below, we found that both signal integration as well as coincidence detection in recurrent networks contribute to the sensitivity to irregularity.

In the case of single-neuron stimulation it is necessary that the postsynaptic targets of the stimulated neuron fire at least one action potential, which occurs when the summed currents exceed a spike threshold. As such, the signal integration depends on the ISIs of the stimulated neuron. In our simulations the SSI diminished towards the highest stimulation frequency of 300 Hz. At these stimulation frequencies, the average ISI is comparable to the time constant of the EPSC, and the benefit of short ISIs found in irregular stimulation is reduced. The relation between ISI, and synaptic and membrane time scales, is thus important for signal integration and stimulus detection.

STP refers to the changes in synaptic efficacy of vesicle release due to the recent history of presynaptic activity (for overview see Chapter 1). The degree to which facilitation and depression occurs for each action potential, relates to the ISI with the previous action potential, and depends on the STP profile. We found that the SSI could be modulated by the STP profile, which was dictated by its facilitation and depression response to residual calcium. The degree of facilitation and depression depends on the protein composition at the axonal terminal and can be regulated in a cell and synapse-type specific way (for reviews see [29, 30]). By appropriately adjusting the molecular mechanisms for synaptic release, neural networks can thus tune sensitivity to stimulus irregularity.

We studied the role of coincidence detection in recurrent networks of binary neurons. Using a probabilistic model, we calculated the response rate to one or several action potentials in the network. In this model, the coincidence detection of two action potentials arriving at the same neuron, contributed to an increase in the response probability. We showed that for short ISIs the coincidence detection was increased. Coincidence detection in recurrent networks thus contributes to the selectivity in detection of irregular stimulation.

Recently, Histed and coworkers performed optical stimulation in the visual cortex of mice and showed that the total light delivered, which is equivalent to the spike count for low intensity Channelrhodopsin-2 stimulation, best predicted the behavioural response rate [31]. These results suggest that the spike count, but not the frequency, is important for a reliable behavioural response. For these experiments, the behavioural data for all animals was first collected for the long

(100-ms) pulses, and for shorter pulses later, ending with 1-ms pulses [31]. During the long recording sessions, networks could have had sufficient time to adapt to the new stimulus parameters.

In the study performed by Doron and coworkers [12], the rats were first trained during multiple days to respond to the stimulations, while the stimulus strength was lowered towards single-neuron stimulation. This training session could provide sufficient time, i.e. for homeostatic scaling of the synaptic weights [16, 32], to appropriately adjust the response probability to the stimulus strength. After training, data were collected in which the different stimulation conditions were interleaved. In our simulations, we first trained the networks to a 50% response rate, for which we applied network scaling to the synaptic weights [15]. In psychophysical studies, responses are often quantified in terms of a sigmoidal function, with two parameters: the stimulus magnitude leading to a 50% response rate, and what is the slope at that point. The 50% baseline response rate used in our simulations positioned the system at a point at which the factors that influence the slope, and thus the response rate, can be determined. Our experimental design, in which synaptic weights are not adjusted between the stimulus conditions (irregular and regular) is in line with the experimental design of interleaved stimulation that was used in the study of Doron and coworkers [12], and a difference in experimental design could explain the different outcome of the study by Histed and coworkers, as discussed above [31].

In conclusion, we show that recurrent networks display inherent sensitivity to short ISIs, which are more likely to occur in irregular spike trains. We propose that effective neuronal communication can be established by generating spike trains that contain more short ISIs than similarly-sized regular input, and that neurons can use STP to tune sensitivity to the irregular spike trains.

Acknowledgements

We want to thank Dr. Arthur Houweling for the valuable discussions that contributed to this Chapter.

References

[1] AA Faisal, LPJ Selen, and DM Wolpert. "Noise in the nervous system". In: *Nat Rev Neuroscience* 9.4 (2008), pp. 292–303.

[2] PHE Tiesinga, J Fellous, and TJ Sejnowski. "Regulation of spike timing in visual cortical circuits". In: *Nat Rev Neurosci* 9.2 (2008), pp. 97–107.

[3] P Fries. "Neuronal Gamma-Band Synchronization as a Fundamental Process in Cortical Computation". In: *Annual Review of Neuroscience* 32.1 (2009), pp. 209–224.

[4] JC Vasquez, AR Houweling, and PHE Tiesinga. "Simultaneous stability and sensitivity in model cortical networks is achieved through anti-correlations between the in- and out-degree of connectivity". In: *Frontiers in Computational Neuroscience* 7.156 (2013).

[5] AL Barth and JFA Poulet. "Experimental evidence for sparse firing in the neocortex". In: *Trends in Neurosciences* 35.6 (2012), pp. 345–355.

[6] J Wolfe, AR Houweling, and M Brecht. "Sparse and powerful cortical spikes". In: *Current Opinion in Neurobiology* 20.3 (2010), pp. 306–312.

[7] DS Greenberg, AR Houweling, and JND Kerr. "Population imaging of ongoing neuronal activity in the visual cortex of awake rats". In: *Nat Neurosci* 11.7 (2008), pp. 749–751.

[8] CPJ de Kock and B Sakmann. "Spiking in primary somatosensory cortex during natural whisking in awake head-restrained rats is cell-type specific". In: *Proceedings of the National Academy of Sciences* 106.38 (2009), pp. 16446–16450.

[9] S Afraz, R Kiani, and H Esteky. "Microstimulation of inferotemporal cortex influences face categorization". In: *Nature* 442.7103 (2006), pp. 692–695.

[10] CD Salzman, KH Britten, and WT Newsome. "Cortical microstimulation influences perceptual judgements of motion direction". In: *Nature* 346.6280 (1990), pp. 174–177.

[11] AR Houweling and M Brecht. "Behavioural report of single neuron stimulation in somatosensory cortex". In: *Nature* 451.7174 (2008), pp. 65–68.

[12] G Doron, M von Heimendahl, P Schlattmann, AR Houweling, and M Brecht. "Spiking Irregularity and Frequency Modulate the Behavioral Report of Single-Neuron Stimulation". In: *Neuron* 81.3 (2014), pp. 653–663.

[13] A Lak, E Arabzadeh, and ME Diamond. "Enhanced Response of Neurons in Rat Somatosensory Cortex to Stimuli Containing Temporal Noise". In: *Cerebral Cortex* 18.5 (2008), pp. 1085–1093.

[14] MH Histed, V Bonin, and RC Reid. "Direct activation of sparse, distributed populations of cortical neurons by electrical microstimulation". In: *Neuron* 63.4 (2009), pp. 508–522.

[15] A Maffei and A Fontanini. "Network homeostasis: a matter of coordination". In: *Current Opinion in Neurobiology* 19.2 (2009), pp. 168–173.

[16] GG Turrigiano. "The Self-Tuning Neuron: Synaptic Scaling of Excitatory Synapses". In: *Cell* 135.3 (2008), pp. 422–435.

[17] JE Niven et al. “The contribution of Shaker K+ channels to the information capacity of Drosophila photoreceptors”. In: *Nature* 421.6923 (2003), pp. 630–634.

[18] Cyrus P. Billimoria, Ralph A. DiCaprio, John T. Birmingham, L. F. Abbott, and Eve Marder. “Neuromodulation of Spike-Timing Precision in Sensory Neurons”. In: *The Journal of Neuroscience* 26.22 (2006), pp. 5910–5919.

[19] C Clopath, L Busing, E Vasilaki, and W Gerstner. “Connectivity reflects coding: a model of voltage-based STDP with homeostasis”. In: *Nat Neurosci* 13.3 (2010), pp. 344–352.

[20] M Tsodyks, A Uziel, and H Markram. “Synchrony Generation in Recurrent Networks with Frequency-Dependent Synapses”. In: *The Journal of Neuroscience* 20.RC50 (2000), pp. 1–5.

[21] JS Dittman, AC Kreitzer, and WG Regehr. “Interplay between facilitation, depression, and residual calcium at three presynaptic terminals”. In: *The Journal of Neuroscience* 20.4 (2000), pp. 1374–1385.

[22] D Fioravante and WG Regehr. “Short-term forms of presynaptic plasticity”. In: *Current opinion in neurobiology* 21.2 (2011), pp. 269–274.

[23] AV Blackman, T Abrahamsson, RP Costa, T Lalanne, and PJ Sjostrom. “Target-cell-specific short-term plasticity in local circuits”. In: *Front Synaptic Neurosci* 5.11 (2013).

[24] C Holmgren, T Harkany, B Svennenfors, and Y Zilberter. “Pyramidal cell communication within local networks in layer 2/3 of rat neocortex”. In: *The Journal of Physiology* 551.1 (2003), pp. 139–153.

[25] A Berkopec. “HyperQuick algorithm for discrete hypergeometric distribution”. In: *Journal of Discrete Algorithms* 5.2 (2007), pp. 341–347.

[26] P Maršálek, C Koch, and J Maunsell. “On the relationship between synaptic input and spike output jitter in individual neurons”. In: *Proceedings of the National Academy of Sciences* 94.2 (1997), pp. 735–740.

[27] KM Stiefel, B Englitz, and TJ Sejnowski. “Origin of intrinsic irregular firing in cortical interneurons”. In: *Proceedings of the National Academy of Sciences* 110.19 (2013), pp. 7886–7891.

[28] S Ratté, S Hong, E DeSchutter, and SA Prescott. “Impact of Neuronal Properties on Network Coding: Roles of Spike Initiation Dynamics and Robust Synchrony Transfer”. In: *Neuron* 78.5 (2013), pp. 758–772.

[29] PS Kaeser and WG Regehr. “Molecular Mechanisms for Synchronous, Asynchronous, and Spontaneous Neurotransmitter Release”. In: *Annual Review of Physiology* 76.1 (2014), pp. 333–363.

[30] R Jahn and D Fasshauer. “Molecular machines governing exocytosis of synaptic vesicles”. In: *Nature* 490.7419 (2012), pp. 201–207.

[31] MH Histed and JHR Maunsell. “Cortical neural populations can guide behavior by integrating inputs linearly, independent of synchrony”. In: *Proceedings of the National Academy of Sciences* 111.1 (2014), E178–E187.

[32] GW Davis. “Homeostatic Signaling and the Stabilization of Neural Function”. In: *Neuron* 80.3 (2013), pp. 718–728.

Chapter 5

Separating burst from background spikes in multichannel neuronal recordings using return map analysis

This chapter was published as:

M.B. Martens, M. Chiappalone, D. Schubert, P.H.E. Tiesinga (2014). *Separating burst from background spikes in multichannel neuronal recordings using return map analysis.* International Journal of Neural Systems; 24(4):1450012

5.1 Abstract

Action potentials can occur in isolation or as a coherent burst of action potentials. We propose a pre-processing method to separate the isolated background from the coherent burst action potentials to improve burst detection. High background activity in neuronal recordings reduces the effectiveness of currently available burst detection methods. For long-term, stationary recordings, burst and background spikes have a bimodal ISI distribution which makes it easy to select a threshold to separate burst and background spikes. Finite, non-stationary recordings lead to noisy ISIs for which the bimodality is not that clear. We introduce a pre-processing method to separate burst from background spikes that improves burst detection reliability because it efficiently uses both single and multi-channel activity. The method is tested using a stochastic model constrained by data available in the literature and recordings from primary cortical neurons cultured on Multi-Electrode Arrays. The separation between burst and background spikes is obtained using the interspike interval return map. The cut-off threshold is the key parameter to separate the burst and background spikes. We compare two methods for selecting the threshold: (1) the 2-step method, in which threshold selection is based on fixed heuristics and (2) the iterative method, in which the optimal cut-off threshold is directly estimated from the data. The proposed pre-processing method significantly increases the reliability of several established burst detection algorithms, both for simulated and real recordings. The pre-processing method makes it possible to study the effects of diseases or pharmacological manipulations, because it can deal efficiently with non-stationarity in the data.

5.2 Introduction

Spontaneous periodic network activity is involved in neuronal network maturation, formation and signal processing. We refer to spontaneous coherent network activity as a network burst, or burst [1–3]. Bursts achieve a more reliable information transfer than single spikes [4] and can contain more information than single spikes, suggesting that they are more potent signal for downstream areas [5]. Bursts are also related to behavioural state changes, such as the transition from single spiking to burst spiking of relay neurons in the subiculum (hippocampus) and thalamus [6–8]. Burst stimulation is also involved in cortical potentiation [9, 10] and experience-independent spontaneous burst activity occurs early during development, where it is involved in setting up the topographic organization of sensory systems [11–13]. Bursts thus play an important role in cortical processing.

Networks of primary cortical neurons from embryonic rats cultured on Multi-Electrode Arrays deploy a rich repertoire of bursts. The properties of these bursts depend on age, cell density and network size [14]. Monitoring the properties of spontaneous burst activity in self-organizing neuronal in vitro networks over time is a valuable tool for investigating the role of specific genes in neuronal

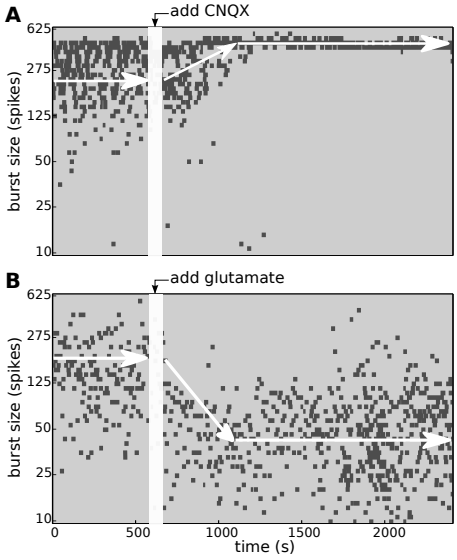

*Figure 5.1: Pharmacological manipulations introduce non-stationary network behaviour. Each black dot represents a network burst of coherent spiking activity in primary cortical cultures, recorded by a planar MEA (60 channels). (**A**): Bath application of the AMPA receptor antagonist CNQX (7 μM) increases the mean burst size. (**B**): Bath application of glutamate (30 μM) decreases the mean burst size. The wide range of burst characteristics requires a robust burst detection procedure.*

network formation [3, 15, 16]. In addition to slow changes in network behaviour, pharmacological treatments can induce rapid changes in network activity ([17, 18] and **Figure 5.1**), which can be used to probe the dynamical properties of networks from healthy subjects or animal models for disease.

A majority of burst detection methods currently available (Section 5.3.8) use a threshold for the interspike intervals, which is either fixed or adaptively determined [19–22]. Another burst detection method combines spikes on single channels into burstlets of consecutive spikes based on predefined criteria and searches for overlapping burstlets [23]. Burst detection methods can also use the surprise of the number of spikes within a predefined time interval, such as the Poisson Surprise [24, 25].

The aim of network burst detection is to distinguish the synchronized burst activity from regular background firing. For states with a high background activity, burst detection methods are less effective. Burst and background spikes do not lead to two easily distinguishable peaks in the single channel interspike interval histogram (**Figure 5.2A**). Peaks corresponding to burst and background

spikes are more clearly distinct when multiple channels are used (**Figure 5.2B**), and separation is further improved by constructing a multi-channel return map (**Figure 5.2C**). Using the Fuzzy Clustering Method (FCM, [26, 27]) we showed that burst and background spikes are significantly better separated in the multi-channel return map than using single channel interspike intervals ($p < 0.0001$, **Figure 5.2D**). Here we propose two methodological alternatives for our novel pre-processing method for multi-channel neuronal recordings: the 2-step method and the iterative method. Both pre-processing methods use the return map to separate the burst from background spikes to improve burst detection reliability. The 2-step and iterative method differ in how they select the threshold. The 2-step method uses fixed heuristics for threshold selection and the iterative method selects the thresholds in a data-driven manner. To evaluate the improved reliability of burst detection after pre-processing, we test the methods on a large dataset of experimental recordings and on artificial spike trains with spiking probabilities based on parameters estimated from real neuronal cultures.

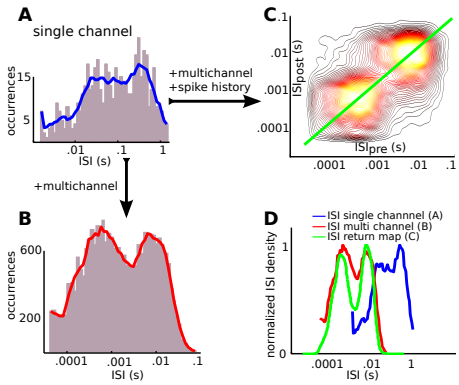

Figure 5.2: For simulated data, the reliability of separation into burst and background spikes is improved using multiple channels and the return map. ***A****: Interspike interval histogram for a single channel. Separation of burst and background spikes is difficult.* ***B****: When spike times from multiple channels are combined, the separation of burst and background spikes is improved.* ***C****: A contour of the multi-channel return map of the preceding (ISI_{pre}) and future (ISI_{post}) inter spike interval for each spike. The distribution is smoothed with a 2D Gaussian kernel, kernel density estimated from the data [28].* ***D****: Smoothed ISI distributions from panels A-C. The multi-channel return map (green) separates the burst and background spike significantly better than a single channel (blue) interspike interval distribution (Fuzzy Clustering Method, $p < 0.0001$).*

5.3 Materials and Methods

To test the reliability of the pre-processing methods, we used a stochastic model based on parameters from a large dataset of real neuronal culture recordings [14]. We also performed pharmacological manipulations to introduce non-stationarity in real neuronal recordings and test our pre-processing methods on this large dataset.

Simulations

Here we describe the stochastic spike generation model which we use to test our pre-processing methods.

5.3.1 Spike time generation

The burst and background spikes are generated as Bernoulli events at each time step ($\Delta t = 10^{-4}$ second) with the following non-stationary instantaneous probability:

$$p_{ch}\left(\text{spike in } [t; t+\Delta t]\right) = \left[\left(\sum_{b=1}^{N} A_b \cdot \Gamma_b(t - t_b)\right) + \alpha_{ch} \cdot \eta(t)\right] \cdot \Delta t. \tag{5.1}$$

Where Γ_b is the burst template function (Equation 5.2), which is a normalized double exponential with zero-clipped support. A_b is the burst amplitude (50 ± 17 spikes/sec). Background spiking probability $\eta(t)$ depends on a first-order auto-regressive process (Equation 5.5) in which heterogeneity between channels can be introduced by setting the value of α_{ch} for each channel separately.

$$\Gamma_b(\tau) = D\left(e^{-\frac{\tau}{\tau_{fall}}} - e^{-\frac{\tau}{\tau_{rise}}}\right) \tag{5.2}$$

The burst template function $\Gamma_b(t)$ depends on the rise (τ_{rise}, 75 ± 25 ms) and fall (τ_{fall}, 150 ± 50 ms) time and is normalized by D to make the peak firing rate probability independent of burst length.

$$D = \left(\left(\frac{\tau_{rise}}{\tau_{fall}}\right)^{\frac{\tau_c}{\tau_{fall}}} - \left(\frac{\tau_{rise}}{\tau_{fall}}\right)^{\frac{\tau_c}{\tau_{rise}}}\right)^{-1} \tag{5.3}$$

with

$$\tau_c = \frac{\tau_{fall}\tau_{rise}}{\tau_{fall} - \tau_{rise}} \tag{5.4}$$

The background firing rate $\eta(t)$ is a first-order auto-regressive process:

$$\eta(t) = C + \Phi \cdot \eta(t - \Delta t) + \epsilon(t) \tag{5.5}$$

Where C is the mean firing rate (0.6 spikes/s), Φ the model parameter representing the strength of the time correlation ($\Phi = 0.5 \pm 0.05$) and $\epsilon(t)$ Gaussian white noise with a standard deviation of 0.6 spikes/s.

The spike times generated here are convolved with a typical spike waveform from real neuronal recordings to obtain a simulated recording (Section 5.3.2 and **Figure 5.3A**).

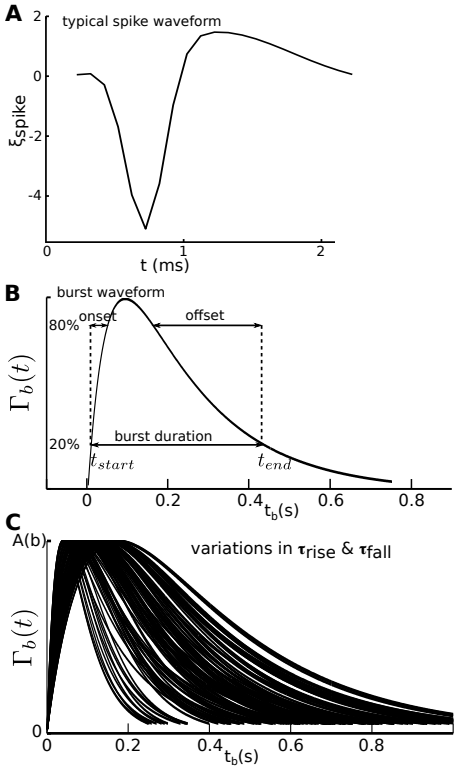

Figure 5.3: The stochastic model for spike generation, constrained by experimental data. ***A****: Typical simulated spike waveform (Equation 5.6). The amplitude is relative to the noise level.* ***B****: Schematic representation of the burst duration, onset and offset.* ***C****: Burst template probability distributions are represented by double exponential functions. Variations in fall and rise time yield realistic burst profiles [14]*

.

The times of burst initiation t_b are distributed according to a gamma renewal process with κ of order 4 and a frequency r of 1 Hz. If we normalize the area, long bursts will have a low peak firing rate and short bursts a high peak firing rate. Peak normalization better reflects experimental data [14]. In a large experimental

dataset [14], the burst duration was defined as the time between reaching 20% of the peak value from below during the rise phase (t_{start}), and crossing 20% from above during the fall phase (t_{end}, **Figure 5.3B**). Variations in the rise and fall time create the different burst profiles (**Figure 5.3C**). The onset duration is the time interval between t_{start} and the time at which 80% of the peak value is reached from below during the rise phase and the offset duration is the time interval between reaching of 80% of the peak from above and t_{end}. Spikes that occur within the burst, are labeled 'burst spikes'. Spikes that fall outside the burst interval are labeled 'background spikes'.

5.3.2 Continuous data simulation

In Section 5.3.1, we described the burst and background spike generation. Because MEAs typically record multiple cells on each electrode, spikes can be partially overlapping and thereby cause artifacts in spike detection. We obtained realistic voltage traces after we convolved the spikes with a spike waveform ($\xi_{spike}(t)$, Equation 5.6). The temporal dynamics of the waveform match the spike waveforms recorded in real data. Pink ($\frac{1}{f}$) electrical noise was added, with a power spectrum similar to real data. The continuous simulated data can be used to test spike detection and subsequent analysis steps.

$$\xi_{spike}(t) = A_p e^{-\frac{\left(t-\tau_{shift}\right)^2}{\sigma_p}} - A_n e^{-\frac{t^2}{\sigma_n}} \tag{5.6}$$

The template $\xi_{spike}(t)$ depends on the amplitude of the negative ($A_n = 6$) and positive ($A_p = 2$) deflection. These amplitudes are scaled relative to the median M of the absolute noise value, here $6 \cdot M(|noise|)$. The other deflection parameters are $\sigma_p = 0.8 \cdot 10^{-6}$ s^2, $\sigma_n = 0.2 \cdot 10^{-6}$ s^2, and the positive peak shift is $\tau_{shift} = 0.5$ milliseconds.

5.3.3 Cell culture protocol and experimental setup

To test our pre-processing methods on real neuronal recordings, we used dissociated neuronal cultures plated on Multi-Electrode Arrays (MEAs). Non-stationarity was introduced by pharmacological manipulations. Dissociated neurons were obtained from cerebral cortices of E18 embryonic rats. Experiments were performed in accordance with the European Community Council Directive of November 24th 1986 (86/609/EEC) for the care and use of laboratory animals and approved by MIUR (Ministero dell Universita e Ricerca Scientifica). All efforts were made to minimize the number of animals used and their suffering. Culture preparation was performed as previously described [17]. Under these conditions cortical neurons showed excellent growth and formation of synaptic connections that allowed us to record spontaneous electrical activity starting from week 2 up to week 4 in vitro.

The microelectrode arrays (Multi Channel Systems, Reutlingen, Germany) consist of 60 TiN planar round electrodes. The electrodes (30 μm diameter; spaced at 200 μm) are embedded in a glass substrate. Commercial recording software (MC-Rack, Multi Channel Systems) was used for data acquisition and online visualization. Data analysis was performed using custom Matlab scripts.

Data analysis

In this section, we describe the data analysis routines. We define the return map (Section 5.3.4) and describe the two pre-processing methods in detail (Section 5.3.5). In simulated data, the ground truth of the origin of the spikes is known and can be used to test the pre-processing methods, which we explain in Section 5.3.6. We define the spike detection method in Section 5.3.7 and burst detection methods in Section 5.3.8, and describe the applied statistics in Sections 5.3.9 and 5.3.10.

5.3.4 Return map analysis

The relation between the interspike interval of a past spike and a future spike can be plotted in a return map. In the return map, each dot represents the time interval between the (n-1)th and the nth spike (ISI$_{pre}$) as well as the time interval between the nth and the (n+1)th spike (ISI$_{post}$, see **Figure 5.4A**). Background spikes will generally have large ISI$_{pre}$ and ISI$_{post}$ values. The first spike of a burst will generally have a large ISI$_{pre}$ and small ISI$_{post}$, and the last spike will have a small ISI$_{pre}$ and large ISI$_{post}$. Spikes that are the core spikes of a burst are associated with both small ISI$_{pre}$ and ISI$_{post}$ values. The background spikes are first separated on each channel individually and secondly with spikes from all channels combined (**Figure 5.4B**).

5.3.5 Pre-processing methods

We tested two different methods to separate the burst from background spikes (**Figure 5.5**):

- 2-step method: in the first step, the spikes for each channel with ISI$_{pre}$ and ISI$_{post}$ larger than θ_1 (typical value 50 milliseconds) are labeled as 'background spikes' and removed from the distribution. In a second step, spikes from all channels are combined and spikes with ISI$_{pre}$ and ISI$_{post}$ larger than θ_2 (typical value 2 milliseconds) are labeled as 'background spikes'. The cut-off thresholds, θ_1 and θ_2 are the key parameters for the 2-step method.
- Iterative method: the multi-channel return map is used to find the optimal cut-off threshold $\theta_{2,optimal}$. The iterative method starts with a large θ_2. For the selection of θ_1, a fixed $\frac{\theta_1}{\theta_2}$ ratio is used together with θ_2. The

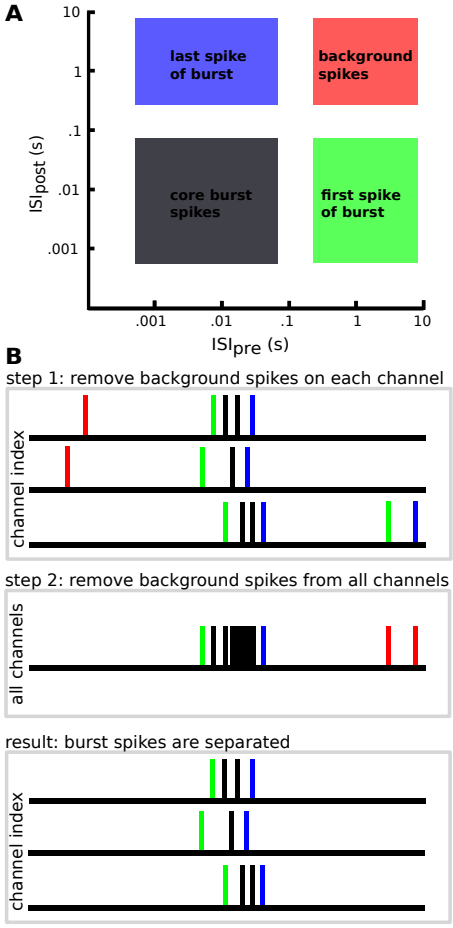

Figure 5.4: Schematic of the pre-processing method. ***A****: The return map of burst and background spikes. Red spikes are likely to be a background spike, with large* ISI_{pre} *and* ISI_{post}*. Green and blue spikes mark the start and end of a burst, respectively. Black spikes are likely to be spikes within a burst with small* ISI_{pre} *and* ISI_{post}*.* ***B****: First, spikes are separated on a per-channel basis using* θ_1*. All spikes from all channels are combined into a single spike train, after which a more stringent cut-off threshold* θ_2 *is applied. The result is a separation of burst from background spikes. The 2-step method and the iterative method differ in the threshold selection.*

heuristics for the $\frac{\theta_1}{\theta_2}$ are determined from simulated data and is shown to depend on the number of recording channels (**Figure 5.6**). The cut-off thresholds θ_1 and θ_2 are stepwise decreased and in each step the spikes with

ISI_{pre} and ISI_{post} exceeding θ_1 and θ_2 are labeled as background spikes and removed from the distribution. Spikes in the return map belong to one of four groups: (1) a background spike, (2) a core burst spike, (3) the first or (4) last spike of a burst. These four groups of spikes move to a different quadrant in a return map when a neighbouring spike is removed from the distribution (**Figure 5.7B**). For example, if a spike next to a background spike is removed, the ISI_{pre} or ISI_{post} of a neighbouring background spike is likely to jump to the top-right quadrant (the quadrant with $\text{ISI}_{pre} > \theta_2$ and $\text{ISI}_{post} > \theta_2$). This behaviour is used to estimate at which cut-off threshold the burst and background spikes are optimally separated. We decrease θ_2 in logarithmic steps from 1000 to 1 milliseconds in 25 steps. The number of spikes that jump to the top-right quadrant for each iterative reduction of the cut-off threshold is $n(\theta_2)$. A local minimum in this distribution gives the optimal threshold $\theta_{2,optimal}$. The iterative method is then restarted until this optimal threshold is reached, using as threshold for step 1, $\theta_{2,optimal}$ multiplied by the heuristic $\frac{\theta_1}{\theta_2}$ estimate for the given number of channels.

5.3.6 Spike classification

Optimal heuristics were obtained by scoring the quality of the pre-processing steps. In this section, we describe how the quality of the pre-processing steps were scored. We labeled each simulated spike as either a burst or a background spike. The aim is to correctly detect burst spikes. A spike was labeled a burst spike if it occurred during the burst and a spike was labeled a background spike if it occurred outside a burst. We defined a true positive spike as a burst spike detected as a burst spike. A false positive is a background spike detected as a burst spike. The true positive rate tpr is the fraction of true detected burst spikes across all burst spikes. The false positive rate fpr is the fraction of falsely detected burst spikes across all background spikes. Also, a false negative is a burst spike detected as a background spike and a true negative is a background spike detected as a background spike. The corresponding rates are related as: $tnr = 1 - fpr$ and $fnr = 1 - tpr$.

Heuristics for the 2-step method depended on whether the 'greedy' or a more 'conservative' strategy was used in step 1. When the 'greedy' strategy was used, equal weight was assigned to a true positive and a true negative spike. If the 'conservative' strategy was used, we assigned more importance to preservation of a true positive spike in step 1. Equation 5.7 shows how the objective function d' depends on the relative importance of the true positive rate α.

$$d'(\alpha) = \alpha \cdot tpr - fpr \tag{5.7}$$

The objective function $d'(\alpha)$ (pronounced d-prime) is a statistic for the quality of the separation of burst and background spikes. The objective function is related to a summary statistic of the Receiver Operating Characteristic (ROC) curve.

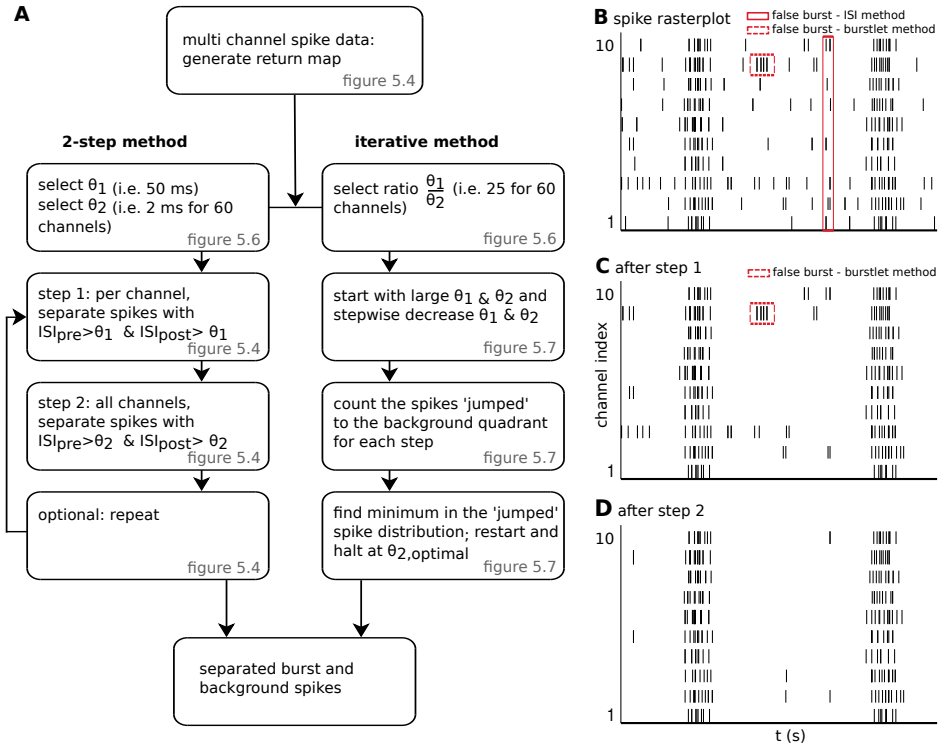

Figure 5.5: ***A****: Flowchart for the 2-step and iterative method. For the 2-step method, heuristics are used to separate the spikes for each channel individually (step 1) and with spikes from all channels combined (step 2). For the iterative method, the optimal cut-off threshold is determined from the distribution of 'jumped' spikes.* ***B****: A spike raster plot for 10 channels with burst and background spikes. Burst detection methods detect false positive bursts.* ***C****: For step 1 of the 2-step method, spikes with ISI_{pre} and ISI_{post} larger than θ_1 are separated and labeled background spikes for each channel individually. The number of false positive detected bursts is reduced.* ***D****: For step 2 of the 2-step method, spike times after step 1 are combined into a single spike train and spikes with ISI_{pre} and ISI_{post} larger than θ_2 are labeled background spikes. The number of false positive bursts is further reduced.*

The ROC curve for the 2-step method is obtained as follows: (1) perform step 1 for a wide range of θ_1 values (i.e. 1 millisecond to 10 seconds), (2) calculate for which θ_1 the objective function d'_{step1} is optimal, (3) use this $\theta_{1,optimal}$ to separate the spikes in step 1, followed by step 2 with a wide range of θ_2 values (i.e. 0.1 milliseconds to 10 seconds), (4) calculate for which θ_2 the objective function d'_{step2}

is optimal ($\alpha = 1$).

We introduced the factor α to weight the true positive rate relative to the false positive rate. For α larger than one, a burst spike detected as a burst spike was more important then correctly assigning a background spike as a background spike. To find out whether the score of the objective function can be improved by conservatively assigning spikes as background spikes, we studied the effect of changing α for step 1. For large α, the objective function will strongly penalize labeling burst spikes as background spikes in step 1, which required a relative large θ_1 (referred to as 'conservative'). For the objective function of step 2, α is always 1 to make an unbiased estimate for the quality of separation.

5.3.7 Spike detection

The spike detection used here is based on peak-to-peak spike detection [29]. The continuous signal is baseline corrected to centre around zero. The spike detection threshold is calculated as:

$$\Theta_{spike} = f \cdot M(|signal|) \cdot 1.5 \tag{5.8}$$

With f being the multiplying factor (typical value 8) and $M(|signal|)$ being the median of the absolute value of the signal. For typical MEA recordings, the median is related to the standard deviation by a factor of 1.5 [30]. To determine this factor, the standard deviation of high-pass filtered (300 Hz) recorded segments with no spikes were compared to the median of those same segments. Spikes in the recorded data have a large impact on the standard deviation but not on the median. The median is a good choice to set the spike detection threshold, because it is relatively insensitive to the short, but large amplitude spikes.

To reduce computational load on the spike detection, only signal samples larger and smaller than $\frac{\Theta_{spike}}{2}$ were considered. If the peak-to-peak value within the *peak lifetime* (1.5 milliseconds) exceeded Θ_{spike}, a spike was detected. No other spike could be called in a period before or after each detected spike equal to $(\frac{peak\ lifetime}{2})$.

5.3.8 Burst detection methods

To study the effect of pre-processing on burst detection, we used three previously-published burst detection methods before and after pre-processing:

- **isi method [21]**, which depends on two parameters: the minimal number of spikes per bursts (10 spikes) and the maximal interspike interval (100 milliseconds) at which a spike is considered part of the burst. Adaptive methods use the interspike interval distribution to select a maximal interspike interval.
- **burstlet method [23]**, which detects burstlets for each channel individually. A burstlet consists of 4 or more core and edge spikes. Core burst spikes

have an interspike interval of less than 100 milliseconds and $\frac{1}{4 \cdot firingrate}$, and edge burst spikes have an interspike interval of less than 200 milliseconds and $\frac{1}{3 \cdot firingrate}$. Overlapping burstlets on multiple channels are grouped into bursts.

- **spike density method, related to [31]**, for which spikes from all channels are convolved with a Gaussian (standard deviation 25 milliseconds), and peak-normalized to 1. The onset of a burst depends on crossing a predefined threshold (typically 10 spikes). The point where the spike density falls below the threshold marks the end of the burst. The size of the burst is the integral of the spike density between the burst onset and offset, normalized by the area of one spike.

5.3.9 Signal-to-noise estimation

Estimation of the signal-to-noise ratio is important to select the appropriate return map thresholds θ_1 and θ_2 and to decide if burst from background separation is necessary. We calculate the simulated signal-to-noise ratio as:

$$SNR = \left(\frac{n_{brs}}{n_{bgs}}\right) \cdot \left(\frac{\sum_i^{n_{bgs}} ISI(i)}{\sum_i^{n_{brs}} ISI(i)}\right) \tag{5.9}$$

Here, n_{brs} and n_{bgs} denote the number of spikes labeled as burst and background spikes, respectively. The SNR is the ratio of the mean ISI between burst spikes over the mean ISI between background spikes.

5.3.10 Statistics

To test quality of the pre-processing methods, we tested the three burst detection methods on a large dataset of real experimental recordings (number of cultures=71). The ground truth of experimental data is not known. As a measure of reliability, we performed two-sample F-tests for equal variance. We compared the variance (Equation 5.11) between the three burst detection methods before and after pre-processing. A large variance on the same experimental recording is related to a low consensus between the methods. For high reliability of burst detection, a low variance is desirable. The mean number of bursts for the three methods is calculated as:

$$\mu_{n,i} = \frac{1}{3} \cdot (\mu_{n,i,isi} + \mu_{n,i,burstlet} + \mu_{n,i,density}) \tag{5.10}$$

With $\mu_{n,i}$ the consensus bursts/minute for recording n and pre-processing method i (where i is: no pre-processing, the 2-step method or the iterative method).

$$\sigma_{i,j} = \sqrt{\sum_{n=1}^{N} \frac{(\nu_{n,i,j} - \mu_{n,i})^2}{N}} \tag{5.11}$$

With N the number of recordings and $\nu_{n,i,j}$ the bursts/minute for recording n. The standard deviation $\sigma_{i,j}$ is calculated for each burst detection method j (isi, burstlet or spike density method).

For simulated data, the ground truth of the burst and background spikes is known. The increased reliability of the three burst detection methods by the 2-step pre-processing method was tested with paired t-tests (tested on 15 segments of length 300 s each).

5.4 Results

We tested pre-processing methods on real and simulated data. First, we studied the optimal heuristics for the 2-step method and the quality of the iterative method (**Figure 5.6** and **Figure 5.7**). We tested three burst detection methods on real and simulated data before and after pre-processing (**Figure 5.9** and **5.10**).

For the pre-processing method the selection of the cut-off thresholds θ_1 and θ_2 are the key parameters to separate burst from background spikes. These thresholds can be fixed (2-step method, typical values of 50 and 2 milliseconds, respectively) or obtained in a data-driven way (iterative method). To calculate the heuristics for the optimal cut-off thresholds, we use the objective function $d'(\alpha)$ (Equation 5.7). For simulated data we find the optimal cut-off thresholds $\theta_{1,optimal}$ and $\theta_{2,optimal}$ for low (**Figure 5.6A**) and high (**Figure 5.6B**) signal-to-noise values. The black line represents the true positive rates (correctly labeled burst spikes as burst spikes) plotted versus the false positive rates (incorrectly labeled background spikes as burst spikes) for a wide range of θ_1 values, step 1 of the 2-step method. The red line (step 2) can start at the black dot ($\cdot$, greedy) or at the black asterisk (*, conservative). For the 'conservative' strategy, less burst spikes are labeled as background spikes in step 1, increasing the maximal true positive rate for step 2. However, the false positive rate is also higher. The final score d'_{step2} is the maximum of the objective function for step 2 (α is always 1). We investigated how the final score depends on all combinations of signal-to-noise and degree of conservatism (α, **Figure 5.6C**). For low signal-to-noise (<4) it is better to be 'greedy', whereas for high signal-to-noise (>4) it is better to be 'conservative'. Hence, in recordings with few background spikes, giving more weight to preservation of burst spikes is more important than removing background spikes in step 1. However, for recordings with many background spikes, equal weight for preservation of burst spikes and removing background spikes is optimal. The optimal cut-off threshold for step 1 is lower for the 'greedy' strategy than for the 'conservative' strategy (**Figure 5.6D**). And for step 2, the optimal cut-off threshold is slightly higher for the 'greedy' strategy compared to the 'conservative' strategy (**Figure 5.6E**).

From the optimal thresholds $\theta_{1,optimal}$ and $\theta_{2,optimal}$ determined in the simulations, the optimal ratios for $\frac{\theta_1}{\theta_2}$ can be constructed. **Figure 5.6F** shows how the

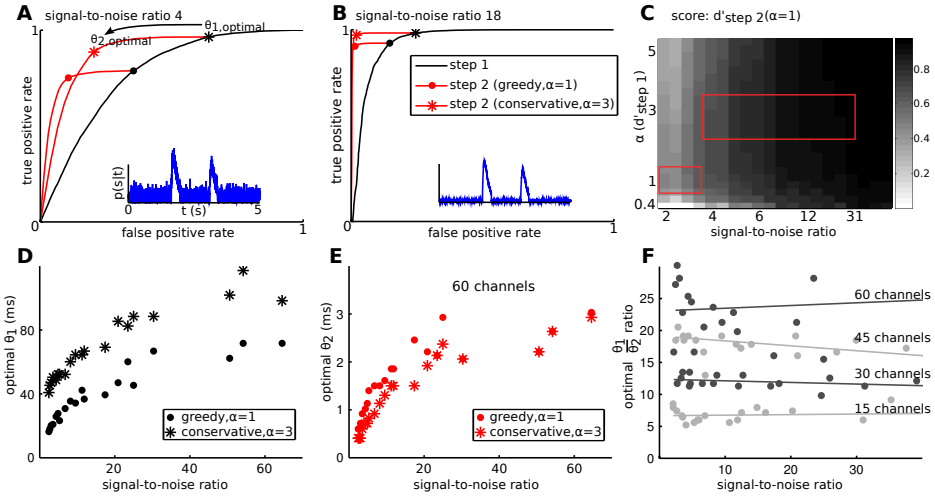

Figure 5.6: The objective function for the 2-step method. Optimal classification was obtained by a 'conservative' step followed by a 'greedy' step for medium and low background activity and two 'greedy' steps for high background activity. ***A*** *and* ***B****: ROC curves with the true positive rate (correctly labeled burst spikes as burst spikes) and false positive rate (background spikes labeled incorrectly as burst spikes) for step 1 (black line) and step 2 (red line) of the 2-step method. The 'greedy' and 'conservative' strategy resulted in a different* $\theta_{2,optimal}$*, and this depended on the signal-to-noise ratio. The spike probability (blue line) indicates the signal-to-noise level.* ***C****: The maximum of the objective function (*d'_{step2}*) depends on the choice of* α *(y-axis), and this in turn depends on the signal-to-noise ratio (x-axis). For low and medium signal-to-noise, it is optimal to use the 'greedy' strategy (small red box). For higher signal-to-noise, it is optimal to use the 'conservative' strategy (large red box).* ***D****: The optimal cut-off threshold for step 1 in the 'greedy' strategy and the 'conservative' strategy depends on the signal-to-noise ratio.* ***E****: The optimal cut-off threshold for step 2 in the 'greedy' strategy and the 'conservative' strategy for 60 channels depends on the signal-to-noise ratio.* ***F****: The ratio* $\frac{\theta_1}{\theta_2}$ *depends on the number of recording channels, but is independent of the signal-to-noise ratio.*

optimal ratio scales with the the number of recording channels and is independent of signal-to-noise ratio.

The iterative method is used to find the optimal cut-off threshold to separate burst and background spikes (flowchart in **Figure 5.5A**). The iterative method starts with the largest cut-off threshold (i.e. θ_1=1 second, θ_2=40 millisecond), and spikes with ISI_{pre} and ISI_{post} larger than the cut-off threshold are labeled background spikes and removed from the distribution. The cut-off thresholds

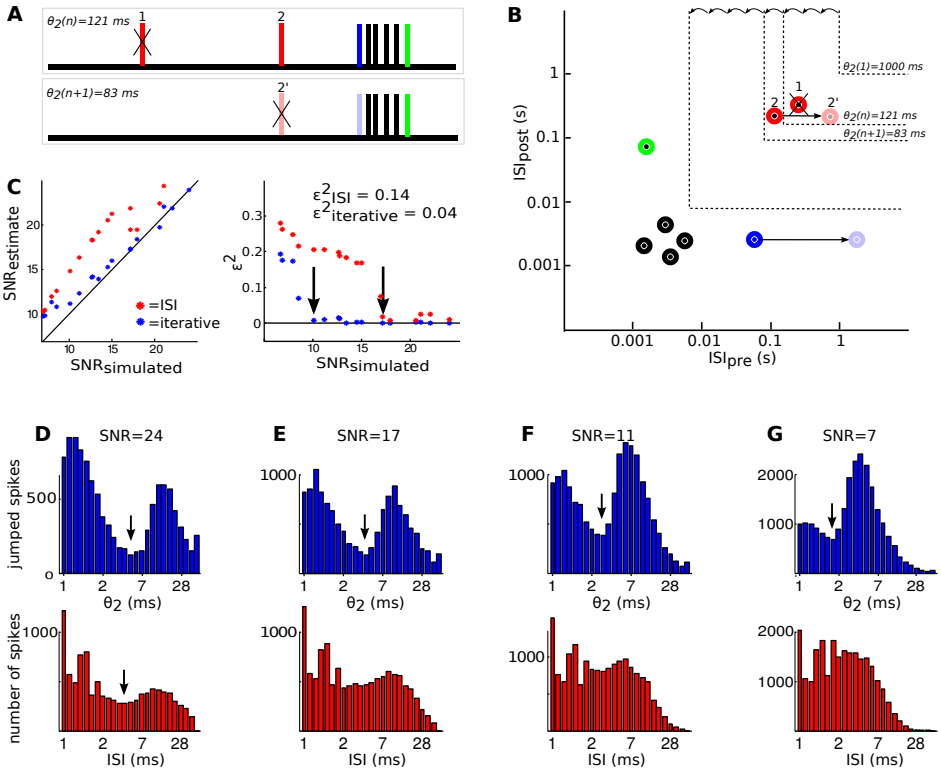

Figure 5.7: Optimal cut-off thresholds for the iterative method. The iterative method lowers the cut-off thresholds θ_1 and θ_2 stepwise. ***A****: For each step, the spikes with ISI_{pre} and ISI_{post} exceeding the cut-off are removed from the distribution.* ***B****: By removing a spike from the distribution, the ISI_{pre} and ISI_{post} of their neighbouring spikes changes. The spikes that jump into the top-right (background) quadrant are referred to as 'jumped' spikes.* ***C****: The optimal cut-off threshold $\theta_{2,optimal}$ is determined from the interspike interval distribution (red dots) or from the 'jumped' spike distribution of the iterative method (blue dots). The left panel shows the error calculated as the renormalized difference (**Equation 5.9**) between the estimated and simulated signal-to-noise ratio.* ***D-G****: Distribution of 'jumped' spikes for each step of the iterative method (blue bars) and the interspike interval histogram (red bars). The local minima represents the optimal cut-off threshold to separate burst from background spikes. The iterative optimal threshold is similar to the interspike interval optimal threshold for high signal-to-noise (**D**) and is better for medium and low signal-to-noise (**E-G**).*

are lowered in logarithmic steps (**Figure 5.7A** and **B**). By removing a spike, the ISI_{pre} and ISI_{post} of the spikes just before and after the removed spikes

change. When a background spike is removed, neighbouring background spikes are likely to 'jump' to the top-right quadrant (the quadrant with ISI_{pre} and ISI_{post} larger than θ_2). The optimal cut-off threshold for step 2 is determined from the local minimum in the distribution of 'jumped' spikes. Alternatively, the optimal thresholds can be determined from the interspike interval distribution. Using the iterative method, the estimation of the optimal cut-off threshold θ_2 is improved 70% compared to an interspike interval based method (**Figure 5.7C**). The distribution of the 'jumped' spikes and the interspike interval distribution depend on the signal-to-noise ratio (**Figure 5.7D-G**). For high signal-to-noise (**Figure 5.7D**), the optimal cut-off threshold θ_2 is easily determined for both the iterative method and the interspike interval distribution. For low signal-to-noise ratio (**Figure 5.7E-G**), the optimal cut-off thresholds can still be determined in the iterative method, but not for the interspike interval method to quantify this difference in performance (**Figure 5.7C, right panel**). We calculate the error between the simulated and estimated signal-to-noise ratio (Equation 5.9) as:

$$\epsilon^2 = \frac{1}{N}\sum_{i}^{N}\left(\frac{\tilde{x}_i}{x_i} - 1\right)^2 \tag{5.12}$$

Where N is the number of simulated datasets, x_i the simulated signal-to-noise for simulated dataset i and $\tilde{x}_i$ the estimated signal-to-noise for dataset i.

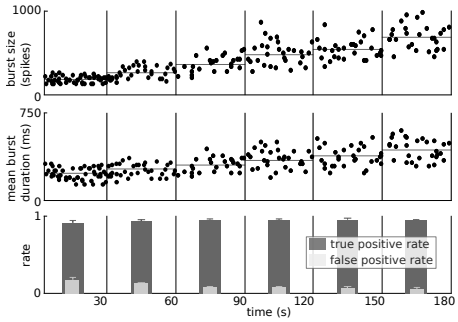

Figure 5.8: The 2-step method is robust for non-stationary network activity. The network parameters are changed across short time windows (30 seconds). Nevertheless, the burst and background spikes are separated with high true positive rates (burst spikes labeled correctly as burst spikes) and low false positive rates (background spikes labeled incorrectly as burst spikes) for non-stationary data. Each black dot represents a simulated dataset; the dots are plotted spread out across the 30 s interval to reduce visual clutter (25 datasets for each 30 second window).

The 2-step method is also appropriate to study the effects of pharmacological manipulations or in diseases, which cause non-stationary network dynamics (**Figure 5.8**). To illustrate this, we changed the model network parameters every

30 seconds. Despite the non-stationarity, the burst and background spikes are separated with high true positive rates (correctly labeled burst spikes as burst spikes) and low false positive rates (incorrectly labeled background spikes as burst spikes).

We tested the 2-step and iterative pre-processing methods on real data (example shown in **Figure 5.9**). The return map of real recordings (**Figure 5.9A**) shows background spikes (red) in the top-right corner. A cut-off threshold separated the background spikes and core (black), first (green) and last (blue) spikes of bursts (**Figure 5.9B**). In example cases, bursts were counted by an experienced observer (**Figure 5.9C**). The example recordings contain low, medium and high levels of background spiking. We also performed statistics on a large set of real recordings (n=71, data not shown), and both the 2-step method ($p<0.001$) and the iterative method ($p<0.001$) showed significant improvement in the reliability of burst detection (Section 5.3.10). The iterative method provided a modest, but not significant improvement of the burst detection reliability on real data relative to the two-step method.

The performance of the 2-step pre-processing method was also tested on simulated data (**Figure 5.10**), using the three burst detection methods (Section 5.3.8). A test for normality showed that the fraction of simulated bursts recovered from the analysis had normal statistics for each of the 2 x 3 conditions (Shapiro-Wilk test, $p<0.05$). We then applied for each group (i.e. ISI, burstlet and spike density method) a paired t-test to assess the differences between the burst detection without and with the 2-step pre-processing method. We found that the burst detection applied after our pre-processing produced results closer to the actual number of bursts. Moreover, there is a statistically significant difference between the results obtained for burst detection with and without our 2-step pre-processing method (paired t-test, $p<0.05$). This result is consistent for all the three burst detection procedures.

5.5 Discussion

The importance of synchronized network activity is still debated within the neuroscience community [22, 25]. To further understand the role of bursting in neuronal network maturation, formation and signal processing, it is important to develop reliable methods to discriminate 'bursting' from 'non-bursting' events [3, 16].

In the past, interspike interval return map analysis has been used on intracellular recordings from neurons that generate bursts with few background spikes, such as central pattern generators, like the pyloric circuit of lobster stomatogastric nervous system. The resulting return map clearly separates into four quadrants with the initial, middle and end spikes of the burst [32]. Clustering techniques were also used to analyse these single cell spike trains based on first order and higher order ISI return maps [33, 34], which is a promising method to classify electrophysiological behaviour [35].

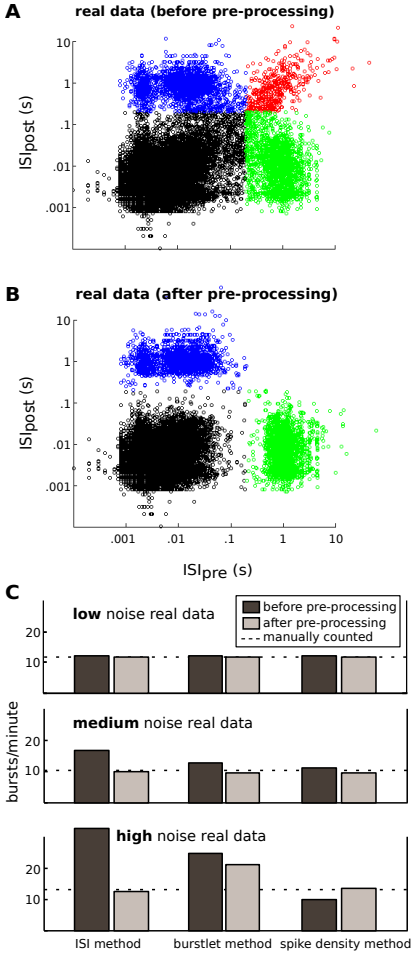

*Figure 5.9: Examples of burst detection before and after 2-step method on real data. The return map of real data before (**A**) and after (**B**) the 2-step method. The return map shows the core burst spikes (black), the first spikes of bursts (green), the last spikes of bursts (blue) and background spikes (red). **C**: Example real recordings, grouped into low, medium and high noise data by an experienced observer. The bursts are manually counted (dotted line) and their number is compared to those obtained from the three burst detection methods before and after the 2-step method.*

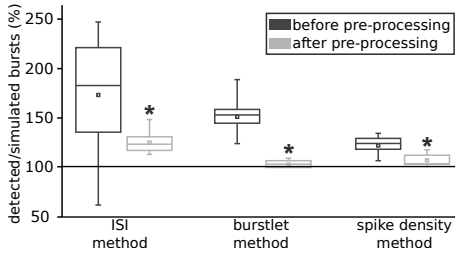

Figure 5.10: Burst detection before and after the pre-processing method on simulated data. Three burst detection methods are performed on simulated data without and with the 2-step pre-processing method. After the 2-step method, the performance of the three burst detection methods are significantly ($p<0.05$) increased.

Here we use the higher order features of the return map and present two methodological alternatives of our pre-processing method, the 2-step method and the iterative method, to separate the burst from background spikes in multi-channel activity. These methodological alternatives differ in the cut-off threshold selection, the key parameter to separate burst and background spikes. In the 2-step method, heuristics are used to select the cut-off thresholds. Using a stochastic model to simulate burst and background spikes, we determined the optimal strategies for the 2-step method. We show that with high background noise, the 'greedy' strategy is optimal. In the 'greedy' strategy, the true positive spikes (burst spikes) and true negative spikes (background spikes) are equally important. With low background noise, a more 'conservative' strategy is optimal. In the 'conservative' strategy, preserving true positive spikes is more important than identifying true negative spikes. Typical values for 60 channel MEA recordings for step 1 are 25-100 milliseconds and typical step 2 values range from 1 to 10 milliseconds. The ratio for step 1 and step 2 cut-off thresholds scales with the number of recording channels, but not with the signal-to-noise ratio. The 2-step method can be improved by repetition of step 1 and step 2. We suggest to use only the number of active recording channels, determined by a firing rate threshold, for determining the cut-off ratio $\frac{\theta_1}{\theta_2}$ (**Figure 5.6**). The iterative method is a data-driven method to determine the optimal cut-off thresholds. We show that the optimal cut-off thresholds found with the iterative method are 70% improved compared to estimating the optimal threshold from an interspike interval-based method.

The performance of the iterative method outperforms the 2-step method slightly in the large dataset of real recordings. The advantage of the iterative method compared to the 2-step method is that the cut-off threshold can be determined for each recording independently. Other researchers may find it more appropriate to use a fixed cut-off threshold in the 2-step method to analyze all recordings with the same parameter settings. The 2-step method is also the pref-

ered method for real-time data analysis because the adaptive threshold of the iterative method is more difficult to determine.

To test the pre-processing method, we simulated bursts using a stochastic model based on parameters from a large experimental dataset [14]. Spiking neural networks are increasingly complex and biological plausible [36–39]. Burst detection methods must be sensitive to typical firing rate profiles. The double-exponential shape was implemented to reflect the firing rate profile in experimental recordings. Nonstationarity and background noise are easily manipulated in a stochastic model. We recommend this model to qualitatively test existing and new burst detection methods. The pre-processing methods proposed here only include the relation with directly neighbouring spikes, but can be extended by including higher order relations between spikes. Higher order relations could possibly further improve separation of burst from background spikes by including spatiotemporal relations or relations typically found at the start or end of bursts. The proposed pre-processing methods are not constrained to neuronal culture network activity, but can also be applied to other in vitro and in vivo systems to improve burst detection reliability.

Multichannel neuronal recordings generate complex and often noisy data. A robust burst detection pipeline is important to study the effect of pharmacological manipulation, genetic modification as in animal models for neurological diseases, and network maturation on network activity patterns. Currently there is increasing interest in culturing human cell material, such as human embryonic or induced pluripotent stem cell derived neurons (for review see [40, 41]), which are thought to provide important future tools for developmental and drug screening studies, as well as for regenerative medicine. During network formation and maturation such cultures have been shown to establish a rich and variable spectrum of single action potential firing and bursting patterns [42, 43]. The pre-processing method introduced here is a first step in describing robust methods sensitive to the dynamical changes in network activity that occur in cultured networks upon pharmacological or genetic manipulation.

References

[1] SJ Eglen, J Demas, and ROL Wong. "Mapping by Waves: Patterned Spontaneous Activity Regulates Retinotopic Map Refinement". In: *Neuron* 40.6 (2003), pp. 1053–1055.

[2] AG Blankenship and MB Feller. "Mechanisms underlying spontaneous patterned activity in developing neural circuits". In: *Nat Rev Neurosci* 11.1 (2010), pp. 18–29.

[3] EJ MacLaren, P Charlesworth, MP Coba, and SGN Grant. "Knockdown of mental disorder susceptibility genes disrupts neuronal network physiology in vitro". In: *Molecular and Cellular Neuroscience* 47.2 (2011), pp. 93–99.

[4] JE Lisman. "Bursts as a unit of neural information: making unreliable synapses reliable". In: *Trends in Neurosciences* 20.1 (1997), pp. 38–43.

[5] A Vidybida. "Testing of information condensation in a model reverberating spiking neural network". In: *International Journal of Neural Systems* 21.03 (2011), pp. 187–198.

[6] SM Sherman. "Tonic and burst firing: dual modes of thalamocortical relay". In: *Trends in Neurosciences* 24.2 (2001), pp. 122–126.

[7] DC Cooper, S Chung, and N Spruston. "Output-Mode Transitions Are Controlled by Prolonged Inactivation of Sodium Channels in Pyramidal Neurons of Subiculum". In: *PLoS Biol* 3.6 (2005), e175.

[8] CT Li, M Poo, and Y Dan. "Burst Spiking of a Single Cortical Neuron Modifies Global Brain State". In: *Science* 324.5927 (2009), pp. 643–646.

[9] J Larson and G Lynch. "Induction of synaptic potentiation in hippocampus by patterned stimulation involves two events". In: *Science* 232.4753 (1986), pp. 985–988.

[10] DM Diamond, TV Dunwiddie, and GM Rose. "Characteristics of Hippocampal Primed Burst Potentiation in vitro and in the Awake Rat". In: *Journal of Neuroscience* 8.11 (1988), pp. 4079–4088.

[11] J Yang et al. "Thalamic Network Oscillations Synchronize Ontogenetic Columns in the Newborn Rat Barrel Cortex". In: *Cerebral Cortex* 23.6 (2013), pp. 1299–1316.

[12] CL Torborg, KA Hansen, and MB Feller. "High frequency, synchronized bursting drives eye-specific segregation of retinogeniculate projections". In: *Nat Neurosci* 8.1 (2005), pp. 72–78.

[13] R Khazipov and HJ Luhmann. "Early patterns of electrical activity in the developing cerebral cortex of humans and rodents". In: *Trends in Neurosciences* 29.7 (2006), pp. 414–418.

[14] D Wagenaar, J Pine, and S Potter. "An extremely rich repertoire of bursting patterns during the development of cortical cultures". In: *BMC Neuroscience* 7.1 (2006), p. 11.

[15] M Chiappalone et al. "Opposite Changes in Glutamatergic and GABAergic Transmission Underlie the Diffuse Hyperexcitability of Synapsin IDeficient Cortical Networks". In: *Cerebral Cortex* 19.6 (2009), pp. 1422–1439.

[16] MA Clifford, JK Kanwal, R Dzakpasu, and MJ Donoghue. "EphA4 expression promotes network activity and spine maturation in cortical neuronal cultures". In: *Neural Development* 6.21 (2011), pp. 1–13.

[17] M Frega et al. "Cortical cultures coupled to Micro-Electrode Arrays: A novel approach to perform in vitro excitotoxicity testing". In: *Neurotoxicology and Teratology* 34.1 (2012), pp. 116–127.

[18] M Chiappalone, A Vato, L Berdondini, M Koudelka-hep, and S Martinoia. "Network dynamics and synchronous activity in cultured cortical neurons". In: *International Journal of Neural Systems* 17.02 (2007), pp. 87–103.

[19] L Turnbull, E Dian, and G Gross. "The string method of burst identification in neuronal spike trains". In: *Journal of Neuroscience Methods* 145.1-2 (2005), pp. 23–35.

[20] M Chiappalone et al. "Burst detection algorithms for the analysis of spatio-temporal patterns in cortical networks of neurons". In: *Neurocomputation* 65-66 (2005), pp. 653–662.

[21] V Pasquale, S Martinoia, and M Chiappalone. "A self-adapting approach for the detection of bursts and network bursts in neuronal cultures". In: *Journal of Computational Neuroscience* 29 (2010), pp. 213–229.

[22] FE Kapucu et al. "Burst analysis tool for developing neuronal networks exhibiting highly varying action potential dynamics". In: *Frontiers in Computational Neuroscience* 6.38 (2012).

[23] D Wagenaar, TB DeMarse, and SM Potter. "MeaBench: A toolset for multi-electrode data acquisition and on-line analysis". In: *Proceedings of the 2nd International IEEE EMBS* (2005), pp. 518–521.

[24] CR Legendy and M Salcman. "Bursts and recurrences of bursts in the spike trains of spontaneously active striate cortex neurons". In: *Journal of Neurophysiology* 53.4 (1985), pp. 926–939.

[25] D Ko, CJ Wilson, CJ Lobb, and C Paladini. "Detection of bursts and pauses in spike trains". In: *Journal of Neuroscience Methods* 211.1 (2012), pp. 145–158.

[26] JC Bezdek. *Pattern Recognition with Fuzzy Objective Function Algorithms*. Norwell, MA, USA: Kluwer Academic Publishers, 1981. ISBN: 0306406713.

[27] JV Toups, J Fellous, PJ Thomas, TJ Sejnowski, and PH Tiesinga. "Finding the Event Structure of Neuronal Spike Trains". In: *Neural Computation* 23.9 (2011), pp. 2169–2208.

[28] ZI Botev, JF Grotowski, and DP Kroese. "Kernel density estimation via diffusion". In: *Annals of Statistics* 38.5 (2010), pp. 2916–2957.

[29] A Maccione et al. "A novel algorithm for precise identification of spikes in extracellularly recorded neuronal signals". In: *Journal of Neuroscience Methods* 177.1 (2009), pp. 241–249.

[30] RQ Quiroga, Z Nadasdy, and Y Ben-Shaul. "Unsupervised Spike Detection and Sorting with Wavelets and Superparamagnetic Clustering". In: *Neural Computation* 16.8 (2004), pp. 1661–1687.

[31] J van Pelt, PS Wolters, MA Corner, WLC Rutten, and GJA Ramakers. "Long-term characterization of firing dynamics of spontaneous bursts in cultured neural networks". In: *Biomedical Engineering, IEEE Transactions on* 51.11 (2004), pp. 2051–2062.

[32] A Szücs, RD Pinto, MI Rabinovich, HDI Abarbanel, and AI Selverston. "Synaptic modulation of the interspike interval signatures of bursting pyloric neurons". In: *Journal of Neurophysiology* 89 (2003), pp. 1363–1377.

[33] JP Segundo, G Sugihara, P Dixon, M Stiber, and LF Bersier. "The spike trains of inhibited pacemaker neurons seen through the magnifying glass of nonlinear analyses". In: *Neuroscience* 87.4 (1998), pp. 741–766.

[34] R Dodla and CJ Wilson. "Quantification of Clustering in Joint Interspike Interval Scattergrams of Spike Trains". In: *Biophysical Journal* 98.11 (2010), pp. 2535–2543.

[35] RJ Martis et al. "Application of higher order cumulant features for cardiac health diagnosis using ECG signals". In: *International Journal of Neural Systems* 23.04 (2013), p. 1350014.

[36] H Adeli and S Ghosh-Dastidar. "Spiking Neural Networks". In: *International Journal of Neural Systems* 19.04 (2009), pp. 295–308.

[37] N Kasabov, S Schliebs, S Matsuda, and A Mohemmed. "SPAN: Spike Pattern Association Neuron for learning spatio-temporal spike patterns". In: *International Journal of Neural Systems* 22.04 (2012), p. 1250012.

[38] A Oliver, V Canals, A Morro, and JL Roselló. "Hardware implementation of stochastic spiking neural networks". In: *International Journal of Neural Systems* 22.04 (2012), p. 1250014.

[39] H Nishimura, T Yamanishi, and J Liu. "Modeling fluctuations in default-mode brain network using spiking neural network". In: *International Journal of Neural Systems* 22.04 (2012), p. 1250016.

[40] MWGDM de Groot, RHS Westerink, and MML Dingemans. "Don't Judge A Neuron Only by Its Cover: Neuronal Function in In Vitro Developmental Neurotoxicity Testing". In: *Toxicological Sciences* 132.1 (2013), pp. 1–7.

[41] WS Clay, FP Matthew, and PD Yvonne. "Human induced pluripotent stem cells and their use in drug discovery for toxicity testing". In: *Toxicology Letters* 219.1 (2013), pp. 49–58.

[42] B Zimmer et al. "Coordinated waves of gene expression during neuronal differentiation of embryonic stem cells as basis for novel approaches to developmental neurotoxicity testing". In: *Cell Death & Differentiation* 18.3 (2010), pp. 383–395.

[43] TJ Heikkila et al. "Human embryonic stem cell-derived neuronal cells form spontaneously active neuronal networks in vitro". In: *Experimental Neurology* 218.1 (2009), pp. 109–116.

Chapter 6

Euchromatin histone methyltransferase-1 regulates cortical neuronal network development

This chapter is submitted for publication:

M.B. Martens, J. Classen, M. Frega, L. Epping, M. Benevento, H. van Bokhoven, P.H.E. Tiesinga*, D. Schubert* and N.N. Kasri* (2016). *Euchromatin histone methyltransferase-1 regulates cortical neuronal network development. Submitted* to Scientific Reports

6.1 Abstract

Heterozygous mutations or deletions in the human euchromatin histone methyltransferase 1 (*EHMT1*) gene cause Kleefstra syndrome, a neurodevelopmental disorder that is characterized by impaired memory, autistic-like features and severe intellectual disability (ID). Neurodevelopmental disorders including ID and autism may be related to deficits in activity-dependent wiring of brain circuits during development. Although Kleefstra syndrome has been associated with dendritic and synaptic defects in mice and Drosophila, little is known about the role of EHMT1 in the development of cortical neuronal networks. Here we used Multi-Electrode Arrays and intracellular recordings to investigate the impact of EHMT1 deficiency at the network and single-cell level. We show that EHMT1 deficiency impaired network activity during the transition from uncorrelated background action potential activity to synchronized network bursting. The rate of spontaneous bursting and excitatory synaptic currents were transiently reduced, whereas miniature excitatory postsynaptic currents were not affected. This delayed early network formation in EHMT1-deficient networks ultimately resulted in more irregular bursting patterns later in development. These data demonstrate that EHMT1 is critical for normal development of action potential activity in neural circuits. The experimentally observed developmental impairments could result in a temporal misalignment between different activity-dependent developmental processes, which could contribute to the pathophysiology of Kleefstra syndrome.

6.2 Introduction

Intellectual disability (ID) affects 2-3% of the population and is characterized by an intelligence quotient (IQ) below 70 and an impairment of normal adaptive behavior that presents itself before the age of 18 [1–3]. ID disorders are phenotypically heterogeneous and have been associated with a large number of genes [1]. ID has since long been proposed to be a disease of the synapse, with the underlying assumption that synaptic malfunction can severely affect network connectivity. This assumption is supported by the observation that ID genes converge on common signaling cascades that impinge on synaptic function. Examples include pathways involved in synaptic plasticity, Rho- and Ras- GTPase signalling and, more recently, epigenetic regulation [4, 5]. In accordance with the correlation between epigenetic dysregulation and ID, evidence is accumulating that epigenetic actions regulate synaptic function and memory [5, 6].

Kleefstra syndrome (KS) is a neurodevelopmental disorder caused by the haploinsufficiency of the human euchromatin histone methyltransferase 1 (EHMT1) gene [7, 8]. KS is characterized by ID, general developmental delay, childhood hypotonia, craniofacial abnormalities and autistic-like behavioral problems. In addition, *EHMT1* has also been associated with ASD [9] and schizophrenia [10]. EHMT1 (GLP) together with its paralog EHMT2 (G9a) form a chromatin re-

modeling complex that catalyzes the dimethylation of histone H3 at lysine 9 (H3K9me2), a post-translational modification associated with repression of gene transcription [11]. H3K9me2 is an epigenetic mark that is dynamically regulated and has been associated with cognition in mouse and Drosophila [12–16]. Consequently, genetic and pharmacological manipulations of *EHMT1* and *EHMT2 in vivo* in mice, and manipulations of the sole homolog of *EHMT1* and *EHMT2*, *EHMT*, in Drosophila, have shown deficits in learning and memory [12–16].

At the cellular level, neurons in the CA1 area of the hippocampus of *Ehmt1*$^{+/-}$ mice showed reduced dendritic branching and spine density [12, 17], phenotypes that were also observed in Drosophila lacking EHMT and that could be rescued by reintroduction of EHMT in adult flies. In addition, *Ehmt1*$^{+/-}$ mice showed increased paired-pulse facilitation at the CA3-CA1 synapse, indicative for a presynaptic deficit associated with a reduced release probability [12]. Intracellular recordings further revealed that miniature excitatory postsynaptic currents (mEPSC) frequencies, but not their amplitudes, were significantly reduced in *Ehmt1*$^{+/-}$ CA1 pyramidal neurons. Although these data point toward a synaptic deficit, it is yet unclear what the impact is of EHMT1 deficiency during critical periods of early postnatal development at the level of cortical network activity. Increasing evidence suggest that there are sensitive time periods during development in which a neuronal network is susceptible for disturbances caused by gene loss-of-function or environmental factors [18–20]. Developmental impairments could result in a temporal misalignment between different activity-dependent developmental processes leading to neuronal network miswiring.

Here, we used Multi-Electrode Arrays (MEAs) and intracellular recordings to measure network and single cell activity during neuronal network development in cortical cultures. Cultured neurons grown on MEAs typically self-assemble into functionally connected networks that exhibit isolated spontaneous action potentials as well as periodical synchronized bursts of action potentials [21]. MEAs are ideally suited to investigate *in vitro* spontaneous activity during development [22]. Recently, monitoring the properties of spontaneous action potential activity of self-organizing *in vitro* neuronal networks over time was shown to be a valuable tool for investigating the role of specific genes in neuronal network formation [23–25]. However, until now, few studies have measured the impact of loss of ID-associated genes during neuronal development [25]. We utilized RNA interference to reduce EHMT1 expression in cortical neurons grown in culture [25]. Using MEA and intracellular recordings, we found that EHMT1 deficiency impaired spontaneous network activity and lowered firing rates during early development, whereas basal, action potential-independent excitatory synaptic transmission was unaffected. The development towards a network state of synchronized bursting activity in EHMT1-deficient neuronal networks was delayed by several days compared to control networks. Furthermore, we found that later in development EHMT1 deficiency led to network activity with increased irregularity in the timing of the bursts. These data thus indicate that EHMT1 is required for proper cortical neuronal development.

6.3 Material and Methods

6.3.1 Cell culture

All animal procedures were approved by the Animal Care Committee, Radboud University Nijmegen Medical Centre, The Netherlands, (RU-DEC-2011-021, protocol number: 77073). The day before the plating, glass cover slips (Ø 14 mm, Menzel GmbH, Braunschweig, Germany) treated with 65% nitric acid (Sigma-Aldrich, St. Louis, MO, USA, 84380) and MEAs were coated with 0.0125% Polyethylenimine (PEI, Sigma-Aldrich, St. Louis, MO, USA, P3143) overnight. After a triple wash to remove residual PEI, a seeding medium containing Neurobasal medium (1x, Gibco Fisher Scientific, Waltham, MA, USA, 21103-049), 10% Fetal Bovine Serum (FBS, Sigma-Aldrich, St. Louis, MO, USA, F7524), 2% Supplement B27 (B27, Gibco Fisher Scientific, Waltham, MA, USA, 17504-044) and 1% Penicillin/Streptomycin (Pen/Strep, Sigma-Aldrich, St. Louis, MO, USA, P4333) was added to the MEAs and cover slips. Cortices were dissected from Wistar rat pups on embryonic day 18 (E18). The cortices were dispersed in Hanks' Balanced Salt Solution (HBSS) without Mg or Ca (Gibco Fisher Scientific, Waltham, MA, USA, 14185-045), containing 0.3 M Hepes (pH 7.3, Sigma-Aldrich, St. Louis, MO, USA, H4034) and adjusted to a pH of 7.3 with NaOH. The tissue was digested with 0.25% Trypsine (Gibco Fisher Scientific, Waltham, MA, USA, 15090-049) for 15 min at 37 °C and then mechanically dissociated using fire polished glass Pasteur pipettes. The cell suspension was filtered with a 70 m cell strainer (Falcon Fisher Scientific, Waltham, MA, USA, 352350) to remove larger pieces. The cells were plated on cover slips with a cell density of 50,000 and 75.000 cells/cover slip for sEPSC and mEPSC measurements respectively, and 350,000 cells/chip for MEA recordings. Four hours after plating half of the medium was replaced by culturing medium containing Neurobasal Medium with 2% B27, 1% Pen/Strep and 1% GlutaMAX (Gibco Fisher Scientific, Waltham, MA, USA, 35050-038). At 24 hours after plating, the cells were infected with a virus expressing both GFP and a short hairpin RNA (shRNA) that interferes with the mRNA that codes for EHMT1 (Ehmt1-sh) which effectively reduced EHMT1 expression levels by approximately 55% (**Supplementary Figure 6.5A-B**), which was compared to expression in WT cultures or the effect of transfecting with scrambled (control) shRNA. Finally, twice a week half of the medium was refreshed. The cells were incubated in a humidified atmosphere of 95% O_2 and 5% CO_2 at 37 °C.

6.3.2 Multi-Electrode Arrays

We recorded the electrophysiological activity of cortical neuronal networks at days *in vitro* (DIV) 10, 13, 15 and 17 for at least 20 minutes by means of Micro-Electrode Arrays (MEAs). MEAs consisted of 60 titanium nitride planar electrodes (model 4QMEA1000, Multi Channel Systems, Reutlingen, Germany)

that were embedded in a glass substrate and insulated by a thin layer of silicon nitride. Recordings were performed using the USB-MEA60-Inv-BC-System (Multi Channel Systems, Reutlingen, Germany). After 1200x amplification, signals were recorded at a sampling frequency of 10 kHz. Data acquisition was done by MCRack software (Multi Channel Systems, Reutlingen, Germany). We used a perforated tube through a small water reservoir to deliver a humidified atmosphere of 95% O_2 and 5% CO_2 into a small perspex chamber that was placed on the recording head-stage to mimic incubator conditions. While the culture was in the recording chamber, the temperature was kept at 37 °C using a ground element temperature controller (TC02, Multi Channel Systems, Reutlingen, Germany). Cultures were kept sterile using a MEA interface ring (Culture Chamber Interface Ring, Multi Channel Systems, Reutlingen, Germany) that was sealed with a sheet of fluorinated ethylene-propylene (ALA Scientific Instruments, Farmingdale, NY, USA) to allow gas exchange [26]. Transport of the cultures from the incubator to the recording setup can lead to transients in activity [27], therefore the first 5 minutes of the recordings were not used in the analysis. Data were obtained from 9 different batches of cells, yielding 25 control networks and 19 EHMT1-deficient networks, whose electrophysiological activity of was recorded during development.

6.3.3 Intracellular recordings

Recordings were performed in oxygenated (95% O_2 and 5% CO_2) Artificial Cerebrospinal Fluid (ACSF) containing (in mM): 124 NaCl, 1.25 NaH_2PO_4, 3 KCl, 26 $NaHCO_2$, 11 Glucose, $CaCl_2$, 1 $MgCl_2$, adjusted to pH of 7.4 with NaOH, at 30 °C. The cover slips containing the primary cortical cultures were transferred to a submerged fixed-stage recording chamber in an upright microscope (BX51WI, Olympus, Hamburg, Germany). The positioning of the cover slip and the cells were assessed with infrared enhanced quarter-field illumination. Recording of suitable cells was performed using a SEC-05L amplifier (npi-electronics, Tamm, Germany). Borosilicate glass patch pipettes (electrode resistance 5-6 MΩ) were filled with (in mM): 115 $CsMeSo_3$, 20 CsCl, 10 HEPES, 2.5 $MgCl_2$, 4 Na_2ATP, 0.4 NaGTP, 10 Na-Posphocreatine, 0.6 EGTA adjusted to a pH of 7.4 with CsOH and to approx. 304 mOsmol using Milli-Q water. The signal was low-pass filtered at 3 kHz and 2 kHz for the spontaneous action potential-evoked excitatory postsynaptic currents (sEPSC) and miniature excitatory postsynaptic currents (mEPSC) respectively, and digitized at 20 kHz using a Micro1401-3 interface (Cambridge Electronic Design Limited, Cambridge, England). Data were recorded and stored using PC-based software (Signal for Windows, Cambridge Electronic Design Limited, Cambridge, England). Electrophysiological experiments included: (1) characterization of the intrinsic properties under current-clamp conditions by injecting hyperpolarizing current pulses (25 pA, gain of 1 and a duty cycle of 1/4); (2) voltage-clamp recordings of mEPSC (1 M tetrodotoxin (Tocris, Bristol, UK) and 1 M picrotoxin (Tocris, Bristol, UK), gain of 1, duty cycle of 1/4); (3) voltage-

clamp recordings of sEPSC (gain of 1, duty cycle of 1/8). Data were recorded, stored and analyzed with Signal (Cambridge Electronic Design, Cambridge, UK) and event detection was performed with MiniAnalysis (Synaptosoft Inc, Decatur, GA, USA). For all the experiments, only the recordings with a low level of noise (<2 standard deviation of the mean noise) were taken into account. For each cell a maximum of 300 events were detected. For the traces that contained bursts, the bursts were counted by visual inspection, where bursts were defined as five or more consecutive events occurring so close together that the baseline was not reached between events, clearly caused by input from synchronized firing of a population of neurons. sEPSC data were obtained from a total of 151 cells (control cells and EHMT1-deficient cells) during DIV 10, 13, 15 and 17 and mEPSC data were obtained from a total of 116 cells (control cells and EHMT1-deficient cells) during DIV 10, 13 and 15. Numbers per DIV and per condition are given in the figure legends.

6.3.4 MEA data analysis

Data were processed and analyzed using an automated, scripted procedure developed in MATLAB (The Mathworks, Natick, MA, USA).

Pre-processing

Data was high-pass filtered (300 Hz, 6th order Butterworth) to remove the slow components while retaining the action potential activity. For offset correction, the median of the absolute value of the signal (M(|signal|)) was subtracted for each recording to center the signal around zero. We use the median of the signal because it is less sensitive to large outliers in the data caused by action potentials than the mean of the signal.

Channel selection

We required activity on 20 or more electrodes for the culture to be included in the analysis. The channel selection was performed following three criteria: (1) electrodes were discarded when the absolute value of the median of the noise exceeded 3.5 μV, which happened for 1.3% of recorded electrodes (**Supplementary Figure 6.6A**); (2) firing rates that exceeded 8 Hz were discarded, which occurred on 0.7% of the recorded electrodes (**Supplementary Figure 6.6B**); and (3) electrodes were excluded from the analysis when the activity was less than 0.1 Hz on all of the longitudinal days on which recordings took place (DIV 10, 13, 15 and 17). The rejection rate of electrodes was not significantly different between conditions ($p > 0.05$, Mann-Whitney test). Recordings were performed longitudinally (each culture was recorded over multiple days); if on one of the recording days an electrode was rejected, this electrode was excluded from the analysis of all DIVs for that culture.

Spike detection

Spike detection was performed as previously described in [21], using a peak-to-peak detection threshold (θ_{ap}) [28], calculated as:

$$\theta_{ap} = f \cdot \mathrm{M}(|signal|) \cdot 1.5 \tag{6.1}$$

With f being the gain factor (f = 8) and M(|signal|) the median of the absolute value of the signal.

Separating burst and background action potentials

Burst and background action potentials were separated using a 2-step procedure [21] (Chapter 5). Briefly, a return map for the pre- and post interspike intervals was calculated for each action potential. In step 1, action potentials for the individual MEA electrodes were labeled as background action potentials if the pre- and post interspike interval exceeded a threshold (θ_1 = 100 ms). In step 2, action potentials from all electrodes were combined into a single action potential train. If the pre- and post interspike intervals exceeded a second threshold (θ_2 = 5 ms), action potentials were also labeled as background action potentials. This procedure effectively selects isolated background action potentials and reduces the false-positive rate for burst detection [21].

Burst detection

Bursts were detected following the pre-processing step of separating burst and background action potentials [21]. For burst detection, only the burst action potentials were used in the spike density method [21]. A burst was detected when the spike density trace crossed a predefined threshold of 10 Hz (about 0.5 spikes per channel in a 100 ms window) from below for 60 active channels. The action potentials were convolved with a Gaussian function:

$$G(t) = A \cdot e^{\frac{-(t-\tau)^2}{2\sigma^2}} \tag{6.2}$$

Where τ is the time of the convolved spike, A is the amplitude, which was set to 1 and σ is the width of the Gaussian which was set to 50 ms.

Burst duration, size and interburst interval

The burst duration is taken as the time between crossing 10 Hz from below until the activity again drops below 10 Hz. The burst size is defined as the area under

the spike density trace for the burst duration, divided by the surface area of the Gaussian with which each spike was convolved (Equation 6.2), while the interburst interval is the time between a burst end and the onset of the next burst. Cumulative probabilities for the burst size, interburst interval and burst duration were obtained using logarithmically spaced bin sizes (normalization factor is shown in **Supplementary Figure 6.7A**). These distributions reflect the relative shape of the distribution while correcting for differences in burst frequency.

Spike time irregularity

We tested two measures of spike irregularity: (1) the coefficient of variation (CV) of the interspike intervals:

$$CV_{ISI} = \frac{\sigma_{ISI}}{\mu_{ISI}} \tag{6.3}$$

With σ_{ISI} being the standard deviation and μ_{ISI} the mean of the interspike intervals on an active electrode. And (2), the Fano Factor (FF), a measure of spike number variability:

$$FF = \frac{\sigma_N^2}{\mu_N} \tag{6.4}$$

With σ_N being the standard deviation and μ_N the mean of the number of action potentials on an active electrode for a time-segment of 5 seconds. A sliding window applied at intervals of one second was used to calculate the number of action potentials for each segment. The CV_{ISI} and FF were averaged over the active electrodes and calculated separately for each DIV and culture.

Burst irregularity

We tested two measures of burst irregularity, (1) the coefficient of variation (CV) of the interburst intervals:

$$CV_{IBI} = \frac{\sigma_{IBI}}{\mu_{IBI}} \tag{6.5}$$

With σ_{IBI} being the standard deviation and $\mu_I BI$ being the mean of the interburst intervals. And (2),

$$IR = \frac{1}{N-1}\sum_{i=1}^{N} log\left(\frac{IBI_i}{IBI_{i-1}}\right) \tag{6.6}$$

With i being the index of each interburst interval (IBI) and N being the number of IBIs [29]. The CV_{IBI} and IR measures were calculated separately for each DIV and culture.

Autocovariance

The autocovariance represents the probability for a given action potential to occur at a particular time lag relative to another action potential, and thus describes how action potentials are correlated in time. The autocovariance was calculated as:

$$C_{xx}(\tau) = \frac{1}{T-|\tau|}E\{(x(n+\tau)-\mu_x)\cdot(x(n)-\mu_x)\} \tag{6.7}$$

Where $C_{xx}(\tau)$ is the autocovariance for action potentials on electrode x at time lag τ (where $0 < |\tau| < 2$ seconds). The expectation E is taken across samples n and with μ_x being the mean firing rate of that electrode. The autocovariance was normalized by the duration of the recording (T), which was adjusted by the absolute time lag $|\tau|$. As we used a high sampling rate (10 kHz) yielding a noisy autocovariance, it was smoothed across τ with a 5 ms moving average. To perform statistics, we calculated the autocovariance half-width, which is the width at which the autocovariance is equal to half its maximal value. The peak of the autocovariance was normalized for each recording separately (normalization factors are shown in **Supplementary Figure 6.7B**).

6.3.5 Statistical tests

Data are expressed as mean ± standard error of the mean (SEM). Statistical analysis was performed using MATLAB (R2012a, The Mathworks, Natick, MA, USA). The data submitted to statistical analysis was often (59%) non-normal, as indicated by skewness [30] (we tested for normality using the Jarque-Bera test, implemented as jbtest in MATLAB). Hence, we used the Mann-Whitney test, implemented as ranksum in MATLAB [31]. We tested whether the means of the set of statistics calculated from the MEA and intracellular recordings differed across conditions for any given DIV. These p-values were aggregated for each DIV value; significant values were then corrected for multiple comparisons using the false discovery rate (FDR) method, incorporating potential dependencies between p-values [32, 33]. To calculate the FDR we used the mafdr function in MATLAB

using the polynomial selection method for the FDR parameter lambda. FDR was set to not increase significance level, which would have occurred at DIV 13 due to the strong significance found in many parameters.

6.4 Results

6.4.1 Network activity during development

In the first set of experiments we investigated how EHMT1 deficiency in neurons affected the development of neuronal population activity. We monitored spontaneously generated action potential activity in dissociated cortical neuronal wild-type (WT, control) cultures on MEAs and in cultures in which EHMT1 expression was downregulated by approximately 50% through RNA interference. To this end we infected cortical neurons with a lentivirus expressing a shRNA against *EHMT1* at 1 day *in vitro* (DIV) and recorded extracellular action potential activity in individual cultures over time at DIV 10, 13, 15 and 17 (**Figure 6.1A**) from 60 electrodes in the MEAs (**Figure 6.1B**). The pattern of action potential activity of the neuronal networks consisted of background (spatially and temporally isolated) action potentials and synchronous, network-wide bursts of action potentials (**Figure 6.1C**). Within 10 days of plating spontaneous activity could be reliably recorded (**Figure 6.1**) in control cultures on MEAs. As development progressed, we found that the firing rate and frequency of bursting increased, reaching stationary values at DIV 15. Action potential activity at DIV 10 has been reported to be mostly uncorrelated, and a transition to the typical state of repetitive synchronized firing occurs after two weeks *in vitro* for normal cortical neuronal cultures [22, 34, 35]. We recorded a reduction of 18% in the action potential firing rate for the EHMT1-deficient networks compared to the control networks during the early developmental stage represented by DIV 13 ($p=0.037$, **Figure 6.1D**). Interestingly, at DIV 15 and 17 EHMT1-deficient networks reached firing rates that were comparable to the control networks, suggesting that loss of EHMT1 early in development leads to delayed network formation. In terms of burst generation, we found that the rate of synchronized bursting at DIV 13 was severely (40%) reduced ($p=0.003$), while the burst rate was comparable to the control networks at DIV 15 and 17 (**Figure 6.1E**). There was no significant difference in the number of active electrodes between conditions (42 ± 6 active electrodes for control and 39 ± 10 active electrodes for EHMT1-deficient networks, $p < 0.05$ (two-tailed t-test)).

Next, we investigated whether during development control and EHMT1-deficient networks changed the ratio between action potentials belonging to background activity and action potentials belonging to bursts [21] (Chapter 5). At DIV 10 the majority (64% for control and 71% for EHMT1-deficient networks) of action potentials were background action potentials, while at DIV 13 and later the majority (78% for control and 65% for EHMT1-deficient networks) of action potentials belonged to bursts (**Figure 6.1F**). This typical profile was present

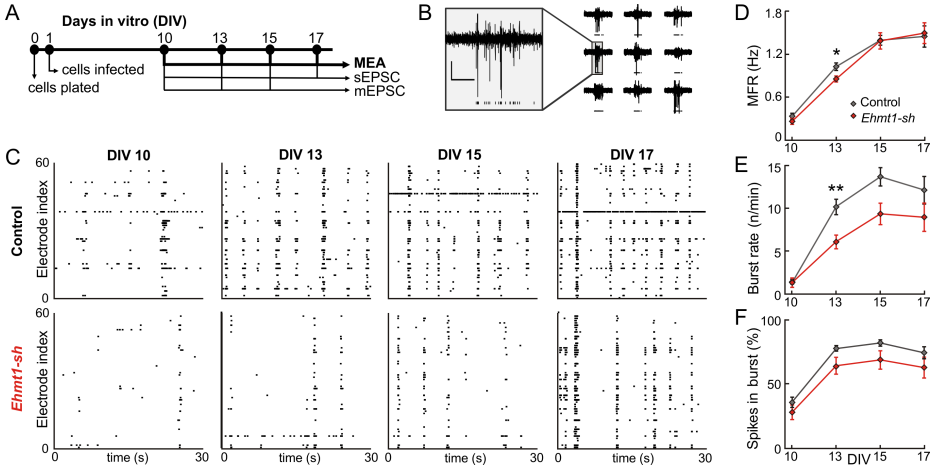

Figure 6.1: EHMT1 deficiency delays the emergence of periodic, synchronized burst activity. ***A****: Time course of experiments. Dissociated cortical neurons were plated on MEAs at embryonic day 18. After 24 hours, for the condition referred to as Ehmt1-sh, EHMT1 expression was down regulated through RNA interference. Electrophysiological recordings were performed at specific time points during development (DIV 10, 13, 15 and 17).* ***B****: Example MEA traces of extracellular action potentials on 9 adjacent electrodes. Detected action potentials are denoted by a black tick below each trace. Scale bar is 20 μV (vertical) and 100 ms (horizontal).* ***C****: Raster plots of action potential activity across 60 MEA electrodes for, from left to right DIV 10, 13, 15 and 17 respectively, and (top) WT cultures and (bottom) EHMT1-deficient cultures. Each detected action potential is indicated as a black tick.* ***D****: The mean firing rate (MFR) is the average action potential frequency that is detected on the active electrodes.* ***E****: A burst was defined as synchronous network activity for which the spike density crossed a predefined threshold (10 Hz). We plot the number of bursts per minute for different DIVs.* ***F****: We show the action potentials that fall within bursts as a percentage of the total number of detected action potentials. Data are means ± SEM. Statistics were based on n = 24 (DIV 10), 25 (DIV 13), 25 (DIV 15) and 24 (DIV 17) recordings for control and n = 19 (DIV 10), 19 (DIV 13), 19 (DIV 15) and 18 (DIV 17) for Ehmt1-sh; * denotes $p < 0.05$, ** denotes $p < 0.01$ (Mann-Whitney test, with p-values corrected for multiple comparisons using the false discovery rate method).*

for both conditions, and the ratio of burst to background action potentials was comparable throughout development (**Figure 6.1F**).

Consistent with the reduced burst rate at DIV 13 in EHMT1-deficient networks, the interburst intervals (IBIs) were significantly longer (39%) at DIV 13 (p=0.005, **Figure 6.2A**). Although at DIV 13 fewer bursts occurred for the EHMT1-deficient condition, these burst lasted longer (24%, p=0.001, **Figure 6.2A-B**). The mean burst size (number of action potentials per burst), however, was not different (**Figure 6.2A**).

Taken together, at DIV 13 the overall firing rate was reduced and fewer bursts occurred in the EHMT1-deficient networks. Furthermore, when a burst occurred, the propagation of action potential activity through the network was prolonged. The deficiencies were transient since the values of these statistics were not significantly different from control networks at DIV 15 and 17.

6.4.2 Reduced action potential coherency during early development

The dynamics of synchronized network bursting depend on the degree of functional synaptic connectivity, which is influenced by the properties of both the pre- and postsynaptic components [25, 36, 37] as well as the graph-theoretical structure of the neuronal connectivity [38, 39]. During culture development, synaptic transmission changes from action potential-independent vesicle release to predominantly action potential-dependent release [40]. Action potential propagation is fast for networks that have vesicle release that is locked to the presynaptic action potential at short latency. We assessed the time-scale of the action potential covariance to quantify to what extent action potentials occurred within a short time window of other action potentials. At DIV 13, EHMT1 deficiency caused an increase (40%) in the action potential autocovariance halfwidth compared to control networks (p=0.001, **Figure 6.2C**). The difference in autocovariance between conditions was not significant at later developmental stages (**Figure 6.2C**). In correspondence to the longer burst duration, these results show that EHMT1 deficiency led to a reduction in the action potential coherency during early development.

6.4.3 Increased irregularity in burst timing later in development

Cultured neurons develop to a typical state of periodic, synchronized bursting [34, 41]. To investigate whether EHMT1 deficiency had an effect on more complex network activity, we measured the irregularity of the interspike and interburst intervals. The coefficient of variation of the interspike intervals (CV_{ISI}) is a measure of spike irregularity. We did not find significant changes in the CV_{ISI}, indicating no difference in irregularity in the spike timing during development (**Figure 6.2D**). However, the CV_{ISI} considers all spikes over time and does not

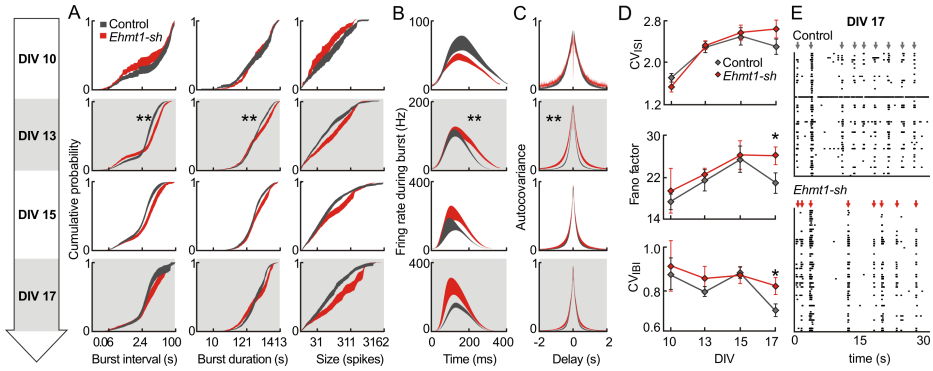

Figure 6.2: Characterization of burst dynamics. ***A****: From left to right, the normalized cumulative distribution of interburst intervals, burst duration and burst size. The burst size is defined as the number of action potentials per burst. Bin sizes were logarithmically spaced and the means of these statistics were tested for significant differences.* ***B****: To obtain the average burst profiles, each bursts was aligned to its detected onset. The spike densities were normalized to 60 electrodes and averaged across cultures for each DIV separately. A significant difference in burst duration is indicated by **.* ***C****: The normalized autocovariance of action potentials was calculated per electrode and averaged over the active electrodes for each recording. Significant difference in autocovariance halfwidth is indicated by **.* ***D****: Measures of spike and burst irregularity: coefficient of variation for the interspike intervals (CV_{ISI}), Fano Factor (FF) of the spike count and the coefficient of variation for the interburst intervals (CV_{IBI}).* ***E****: Example data displaying the increased burst irregularity for EHMT1-deficient networks at DIV 17. Electrode index is on the y-axis, each black denotes an action potential and red arrows indicate a detected burst. Data are means ± SEM. Statistics were based on $n = 24$ (DIV 10), 25 (DIV 13), 25 (DIV 15) and 24 (DIV 17) recordings for control and $n = 19$ (DIV 10), 19 (DIV 13), 19 (DIV 15) and 18 (DIV 17) for Ehmt1-sh; * denotes $p < 0.05$, ** denotes $p < 0.01$ (Mann-Whitney test, with p-values corrected for multiple comparisons using the false discovery rate method).*

take the occurrence of burst events into account. Therefore, we calculated the Fano Factor (FF) of the spike trains, which is a measure for spike number variability. We calculated the FF, averaged over the individual channels, as follows: the mean burst rate in these networks was 11.2 bursts/min, such that on average about 1 burst is expected every 5 seconds. Bursts contain many spikes in a short interval compared to a window of the same length containing action potentials during background activity. At DIV 17 the burst rate was the same for both conditions, thus we expect for irregularly spaced bursts more five second long time intervals with either no or multiple bursts. Using this time window we found that at DIV 17 the FF was higher (20%) for EHMT1-deficient networks compared to the control networks (p=0.04, **Figure 6.2D**). Therefore, we hypothesized that the increased FF was caused by an increased irregularity in the burst timing. Indeed, the EHMT1-deficient networks also had more irregular interburst intervals, as indicated by an increased value for the coefficient of variation of the interburst intervals (CV_{IBI}), (p=0.049, **Figure 6.2D**), and a 20% increase in the value of the rate-independent metric for burst irregularity (Equation 6.6, [29]), (p=0.027, example raster plot of the increased irregularity is shown in **Figure 6.2E**). Together these results show that EHMT1 deficiency resulted in an increased burst irregularity at DIV 17.

6.4.4 Reduced action potential-dependent inputs during early development

Our MEA results imply that EHMT1-deficient networks show a delayed onset of action potential and burst activity. Next, we investigated whether this delay was reflected in the general amount of spontaneously generated network activity driving the individual neurons. Using whole-cell voltage-clamp recordings at a holding potential of -60 mV we measured spontaneous excitatory postsynaptic current (sEPSC) inputs and we observed bursts which, due to the synchronized action potential input, supplied currents that saturated the amplifier (**Figure 6.3A**). The network burst rate so inferred was reduced (41%) in the EHMT1-deficient networks at DIV 13 (p=0.022, **Figure 6.3B**), which is consistent with the MEA population recordings reported in the preceding section.

The sEPSC were measured during the interburst intervals and we found that the amplitude of the synaptic inputs for EHMT1-deficient networks was not different from the control networks at any of the measured time points (**Figure 6.3C**). In contrast, the frequency of excitatory synaptic inputs was reduced (40%) at DIV 13 (p=0.004, **Figure 6.3D**). Together these data show that, besides a significant reduction in burst occurrences, EHMT1-deficient networks had a reduced frequency of synaptic inputs between bursts at DIV 13. Again this reduction in frequency was transient since no statistically significant difference in frequency was observed at DIV 15 and 17.

Finally, we compared the extent and efficiency of synaptic connections between cells of the EHMT1-deficient and the control network. To this end we

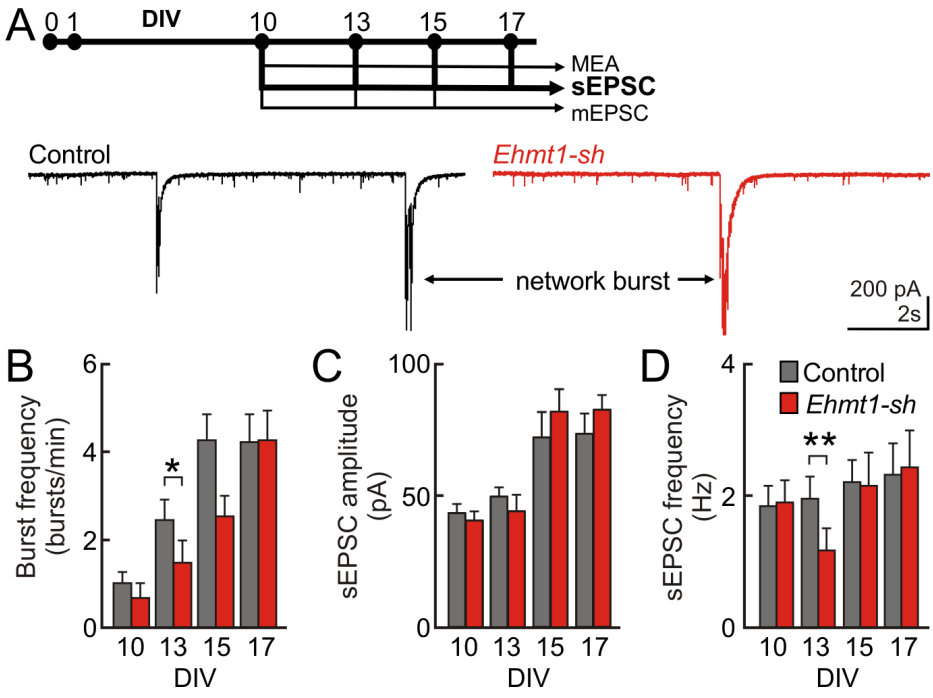

Figure 6.3: The frequency of excitatory synaptic inputs in EHMT1-deficient neuronal networks is reduced during the interburst intervals at DIV 13. ***A****: Whole-cell voltage-clamp recordings were performed in standard ACSF. Representative example traces at DIV 13 show the spontaneous excitatory synaptic inputs during the interburst intervals as well as synchronized input currents during a network bursts. Network bursts were determined by visual inspection. Network burst rate (****B****), sEPCS amplitude (****C****) and sEPSC frequency (****D****). Data are means ± SEM. Statistics were based on n = 17 (DIV 10), 20 (DIV 13), 20 (DIV 15) and 19 (DIV 17) recordings for control and n = 17 (DIV 10), 21 (DIV 13), 18 (DIV 15) and 19 (DIV 17) for Ehmt1-sh; * denotes $p < 0.05$, ** denotes $p < 0.01$ (Mann-Whitney test, with p-values corrected for multiple comparisons using the false discovery rate method).*

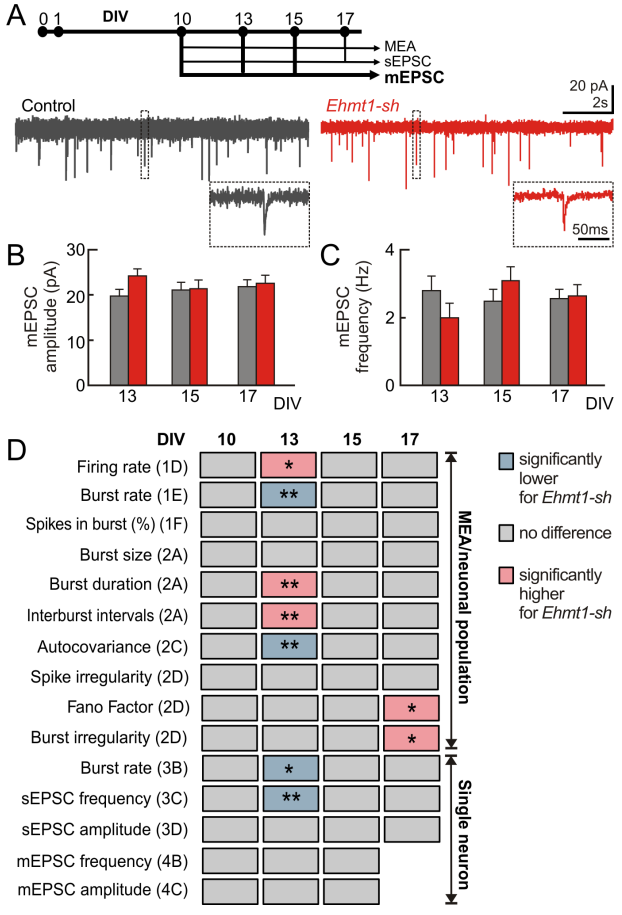

Figure 6.4: EHMT1-deficient neuronal networks show no differences in basal excitatory synaptic transmission during development. ***A****: mEPSC were recorded for DIV 10, 13 and 15 in the presence of tetrodotoxin to block action potentials and picrotoxin to block inhibitory synaptic inputs. Example traces of a whole-cell voltage-clamp recordings show mEPSCs.* ***B****: The mEPSC amplitude and (****C****): mEPSC frequency plotted as function of DIV. Data are means ± SEM. Statistics were based on n = 18 (DIV 10), 20 (DIV 13) and 20 (DIV 15) recordings for control and n = 17 (DIV 10), 20 (DIV 13) and 21 (DIV 15) for Ehmt1-sh; * denotes $p < 0.05$, ** denotes $p < 0.01$ (Mann-Whitney test, with p-values corrected for multiple comparisons using the false discovery rate method).* ***D****: Summary of the statistics derived from electrophysiological recordings of action potential activity at the network level (MEA), action potential-dependent excitatory input at the single cell level (sEPSC) and excitatory basal synaptic transmission at the single cell level (mEPSC). The labels between parentheses refer to figure panels in this Chapter, on which the test results are based. Together these data give a fingerprint of the developmental effect of EHMT1 deficiency.*

measured miniature excitatory postsynaptic currents (mEPSC) using whole-cell voltage-clamp recordings in the presence of tetrodotoxin and picrotoxin at DIV 10, 13 and 15 (**Figure 6.4A**). Remarkably, EHMT1 deficiency did not significantly change the frequency (**Figure 6.4B**) or the amplitude of mEPSC (**Figure 6.4C**) at all developmental time points tested.

Taken together, our single-cell data also indicate that EHMT1 deficiency led to a transient reduction in overall firing and burst rates, while there was no effect on action potential-independent excitatory synaptic transmission rates and excitatory synaptic strength during early development.

6.5 Discussion

In this study we used extracellular and intracellular recordings in developing cortical networks to investigate the time course of the effects of the loss of EHMT1. We demonstrated that the emergence of spontaneous network activity was delayed in cortical neurons deficient in EHMT1 compared to control conditions. This phenotype was also observed at the single neuron level in terms of a transient reduction in the frequency of spontaneous excitatory input during development, which had recovered by the end of the recording period. Finally, we showed that the transient delay in spontaneous network activity in EHMT1-deficient networks resulted in an increased burst irregularity later in development, whereas our control networks showed periodic and rhythmic bursting, which is typical for cultured neurons [22, 41].

In order to relate the mechanism by which EHMT1 produced delayed network activity maturation, we need to understand how bursts are generated and dissect out which factors affect burst rate and irregularity. To obtain bursts, there needs to be spontaneous activity and it needs to be able to recruit more and more network neurons. We (submitted) and others [42] have analyzed the stability of the spontaneous activity state. A network burst emerges stochastically: cells are spontaneously, but independently and irregularly active and the generation of an action potential depends on whether synaptic inputs, synaptic noise and neuromodulatory tone depolarize the cell sufficiently to exceed the voltage threshold [43]. When enough cells fire in coincidence, excitation to the other cells can generate a run-away process (burst) in which most cells are activated, often multiple times. Pacemaker cells are intrinsically active, regularly firing neurons [44], that were shown to best model the generation of network bursts in neuronal cultures [45]. Synaptic dynamics are furthermore important for burst behaviour, where bursts terminate when the synaptic vesicle pool are depleted [45, 46]. This determines the duration of the burst and how long the recovery takes.

We found an increased irregularity in the timing at which bursts occurred for the EHMT1-deficient networks relative to control networks at DIV 17. The irregularity of bursts is related to two factors. First, to the stochastic mechanism by which bursts are initiated, i.e. less coincidences in EHMT1-deficient networks

or less regulatory pacemakers. Second, irregularity depends on the topological pattern of neuronal wiring, i.e. less efficient propagation through the network and less effective recruitment of other neurons [38, 39, 45]. At DIV 17 we found a comparable firing rate and burst rate between conditions. Furthermore, the regularity the spike timing was not different between conditions as indicated by the coefficient of variation of the ISIs, suggesting that there was no difference between the number of pacemaker cells, which would otherwise strongly increase the spike regularity. Together, these results suggest that the increased irregularity can be related to differences in network topology. Previously we found in the hippocampus of adult *Ehmt1*$^{+/-}$ mice a reduction in the dendritic arborization and reduced spine density [12], suggesting a difference in network topology.

At the early developmental stage we observed a reduced burst rate and prolonged burst duration; this could be related to a reduction in action potential-dependent vesicle release in the EHMT1-deficient cultures during early development. We previously showed a decrease in release probability at the CA3-CA1 synapse in *Ehmt1*$^{+/-}$ mice [12]. Likewise, in our current study in cortical neurons we found a decrease in action potential-dependent input, which could thus underlie the deficits in spontaneous network activity. The impaired action-potential dependent synaptic transmission occurred during the transition from uncorrelated spiking to network-wide burst spiking, which coincided with the time point at which hippocampal neuronal cultures switch from the mode of release from exclusively spontaneous early on in development to predominantly evoked in mature neurons [40]. We computationally showed that this transition can initiate a period of rapid rewiring in brain circuits [47]. Impairments in action potential activity and synaptic transmission could thus result in miswiring of the circuitry.

Neuronal activity plays an important role in refinement of synaptic connections (for reviews see [48, 49]) and activity-dependent forms of synaptic plasticity, in particular Hebbian plasticity, guide cortical refinement and are required for the functional maturation of cortical circuits [50]. The developmental profile of neuronal activity is thus important for adequate circuit wiring. Indeed, altered wiring during early development has been proposed to underlie several phenotypes associated with neurodevelopmental disorders, including ID and autism [51–53].

Recent data suggest the existence of developmental phenotypic checkpoints that, if not met, prevent further development [18]. Misregulation during these time-windows causes cellular and network disturbances that later give rise to behavioral symptoms [18]. Given that sequentially activated gene expression programs underlie the genomic programs of synapse function [35], it seems logical that appropriate timing of epigenetic regulation during development is important for synaptic, neuronal and thereby network functioning. It is of interest to note that EHMT1 has recently been found to be important for activity-dependent remodeling of synapses and circuitry, during learning and memory as well as in the context of addiction [14, 54, 55]. Our observation that the delay in network development leads to increased network irregularity later in development thus suggests that EHMT1 could provide a developmental mechanism that enables a

rapid, efficient and reversible way to regulate gene expression during early brain maturation and to meet maturation of neuronal activity level.

EHMT1 is part of an emerging landscape of epigenetic regulators of neuronal function [1, 56]. It interacts with multiple genes that encode other epigenetic factors, and mutations in these genes can also lead to the ID phenotype that resembles the Kleefstra phenotype. In a cohort of patients with a Kleefstra syndrome-like phenotype (KSS) without mutations in *EHMT1*, we recently identified de novo mutations in four other genes, *MLL3*, *SMARCB1*, *NR1I3* and *MBD5* [8]. The corresponding proteins are directly or indirectly involved in epigenetic regulation of gene expression. How disruption of KSS genes give rise to the common clinical cognitive feature is unknown. The molecular functions of these genes are distinct, e.g. histone modification (*EHMT1*, *MLL3*), ATPase-mediated chromatin remodeling (*SMARCB1*) and nuclear receptor (*NR1I3*). Having established an electric signature for EHMT1 deficiency in cortical network development (**Figure 6.4D**) it will be interesting to investigate whether similar network deficits are created by other KSS genes. The disorganization of neuronal networks may be a simple and reliable indicator to test the KSS genes as well as the many other identified ID genes. It will be of particular interest to see whether phenotypically related IDs could be translated to specific deficiencies in neuronal networks.

In conclusion, we showed that deficiency of epigenetic factor EHMT1 impaired action potential activity during the transition from uncorrelated background spiking activity to synchronized network bursting. During this developmental stage both synchronized network bursting as well as a reduction in action potential-dependent excitatory input to the neurons was reduced. The impairment in neuronal activity early in development could relate to inappropriate wiring and irregular behavior later in development. These results support the notion that early developmental deficits could lead to irreversible changes [18, 57]. Abnormalities in firing rate and synchrony during early development and the critical period of brain wiring have been related to neuropsychiatric disorders [58]. The identification of synaptic and cellular deficits that contribute to abnormal network activity will be essential for the understanding, and ultimately treatment, of Kleefstra syndrome.

Author contributions

MM, JC and LE collected the electrophysiological data and MB generated the shRNA tools and expression data; MM and JC analyzed the data; MM and DS prepared the figures; MM, PT, DS and NNK conceptualized the study; MM, MF, HvB, PT, DS and NNK wrote the manuscript. We want to thank Martijn Selten for insightful discussions.

Acknowledgements

This research is supported by grants from the Hypatia fellowship award of the Radboudumc (to N.N.K.); the FP7-Marie Curie International Reintegration Grant (to N.N.K. grant number 277091); the Jerome Lejeune Foundation (to N.N.K); the Netherlands Organization for Scientific Research (NWO open ALW ALW2PJ/13082 to HvB/NNK); NWO grant number 62001113 (to MM).

6.6 Supplementary Figures

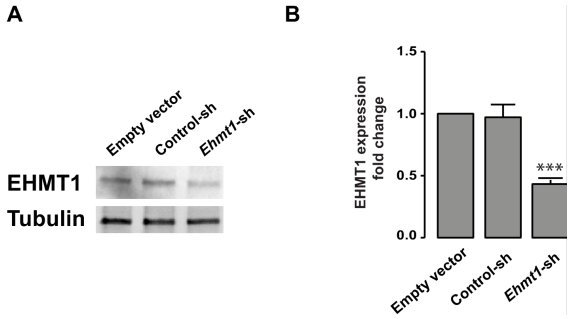

Figure 6.5: Validation of EHMT1 knockdown. ***A****: Primary cortical neurons were transduced with an empty vector, control-shRNA or Ehmt1-sh expressing lentivirus at DIV1. Protein extracts were prepared at DIV14 and were probed by immunoblotting with antibodies against EHMT1 and Tubulin.* ***B****: Quantification of the immunoblot signals of (A). Data are represented as mean ± SEM, N=3, *** indicates p<0.001 (t-test).*

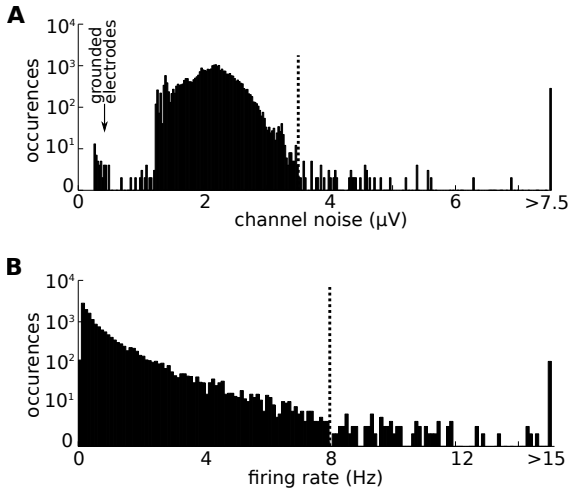

Figure 6.6: Channel noise and firing rate. ***A****: Semi-logarithmic plot of channel noise on the MEA electrodes. High noise can be caused by damage of the electrodes or bad contact to the recording device such that signal transmission is noisy. Electrodes were discarded when the absolute value of the median of the noise exceeded 3.5 µV (denoted by dotted line), which happened for 1.3% of recorded electrodes. The number of channels with noise that was discarded was not significantly different between conditions.* ***B****: Semi-logarithmic plot of the firing rates. Occasionally, very high firing rates were detected, potentially from artifacts. Firing rates that exceeded 8 Hz (denoted by dotted line) were discarded, which occurred on 0.7% of the recorded electrodes. The number of channels with high firing rates that were discarded was not significantly different between conditions.*

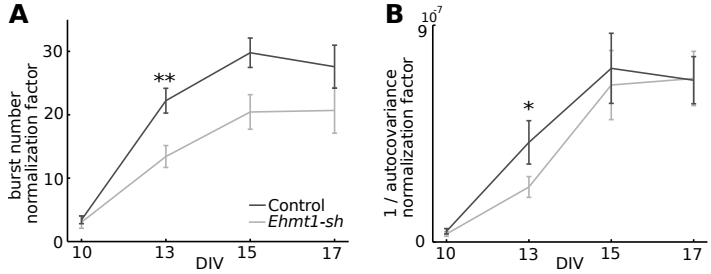

Figure 6.7: Normalization factors. ***A****: The cumulative probabilities (****Figure 6.1A****) were normalized such that the relative shape of the distribution can be compared.* ***B****: Normalization factors for the peak of the autocovariance distributions. Data are means ± SEM. Statistics were based on n = 24 (DIV 10), 25 (DIV 13), 25 (DIV 15) and 24 (DIV 17) recordings for control and n = 19 (DIV 10), 19 (DIV 13), 19 (DIV 15) and 18 (DIV 17) for Ehmt1-sh; * denotes p < 0.05, ** denotes p < 0.01 (Mann-Whitney test, with p-values corrected for multiple comparisons using the false discovery rate method).*

References

[1] H van Bokhoven. "Genetic and Epigenetic Networks in Intellectual Disabilities". In: *Annual Review of Genetics* 45.1 (2011), pp. 81–104.

[2] J Chelly, M Khelfaoui, F Francis, B Cherif, and T Bienvenu. "Genetics and pathophysiology of mental retardation". In: *Eur J Hum Genet* 14.6 (2006), pp. 701–713.

[3] K Tatton-Brown et al. "Mutations in the DNA methyltransferase gene DNMT3A cause an overgrowth syndrome with intellectual disability". In: *Nature Genetics* 46.4 (2014), pp. 385–388.

[4] W Ba, J van der Raadt, and NN Kasri. "Rho GTPase signaling at the synapse: Implications for intellectual disability". In: *Experimental Cell Research* 319.15 (2013). Special Issue: Small GTPases, pp. 2368–2374.

[5] T Kleefstra, A Schenck, JM Kramer, and H van Bokhoven. "The genetics of cognitive epigenetics". In: *Neuropharmacology* 80 (2014), pp. 83–94.

[6] S De Rubeis et al. "Synaptic, transcriptional and chromatin genes disrupted in autism". In: *Nature* 515.7526 (2014), pp. 209–215.

[7] T Kleefstra et al. "Loss-of-Function Mutations in Euchromatin Histone Methyl Transferase 1 (EHMT1) Cause the 9q34 Subtelomeric Deletion Syndrome". In: *The American Journal of Human Genetics* 79.2 (2006), pp. 370–377.

[8] T Kleefstra et al. "Disruption of an EHMT1-Associated Chromatin-Modification Module Causes Intellectual Disability". In: *The American Journal of Human Genetics* 91.1 (2012), pp. 73–82.

[9] ME Talkowski et al. “Sequencing Chromosomal Abnormalities Reveals Neurodevelopmental Loci that Confer Risk across Diagnostic Boundaries”. In: *Cell* 149.3 (2012), pp. 525–537.

[10] G Kirov et al. “De novo CNV analysis implicates specific abnormalities of postsynaptic signalling complexes in the pathogenesis of schizophrenia”. In: *Mol Psychiatry* 17.2 (2012), pp. 142–153.

[11] M Tachibana et al. “Histone methyltransferases G9a and GLP form heteromeric complexes and are both crucial for methylation of euchromatin at H3-K9”. In: *Genes & Development* 19.7 (2005), pp. 815–826.

[12] MCM Balemans et al. “Hippocampal dysfunction in the Euchromatin histone methyltransferase 1 heterozygous knockout mouse model for Kleefstra syndrome”. In: *Human Molecular Genetics* 22.5 (2013), pp. 852–866.

[13] M Benevento, M van de Molengraft, R van Westen, H van Bokhoven, and NN Kasri. “The role of chromatin repressive marks in cognition and disease: A focus on the repressive complex GLP/G9a”. In: *Neurobiology of Learning and Memory* 124 (2015), pp. 88–96.

[14] S Gupta-Agarwal et al. “G9a/GLP Histone Lysine Dimethyltransferase Complex Activity in the Hippocampus and the Entorhinal Cortex Is Required for Gene Activation and Silencing during Memory Consolidation”. In: *The Journal of Neuroscience* 32.16 (2012), pp. 5440–5453.

[15] JM Kramer et al. “Epigenetic Regulation of Learning and Memory by Drosophila EHMT/G9a”. In: *PLoS Biology* 9.1 (2011), e1000569.

[16] A Schaefer et al. “Control of Cognition and Adaptive Behavior by the GLP/G9a Epigenetic Suppressor Complex”. In: *Neuron* 64.5 (2009), pp. 678–691.

[17] MCM Balemans et al. “Reduced exploration, increased anxiety, and altered social behavior: Autistic-like features of euchromatin histone methyltransferase 1 heterozygous knockout mice”. In: *Behavioural Brain Research* 208.1 (2010), pp. 47–55.

[18] Y Ben-Ari and NC Spitzer. “Phenotypic checkpoints regulate neuronal development”. In: *Trends in Neurosciences* 33.11 (2010), pp. 485–492.

[19] T Kroon, M Sierksma, and RM Meredith. “Investigating mechanisms underlying neurodevelopmental phenotypes of autistic and intellectual disability disorders: a perspective”. In: *Frontiers in Systems Neuroscience* 7.75 (2013).

[20] JJ LeBlanc and M Fagiolini. “Autism: A Critical Period Disorder?” In: *Neural Plasticity* 921680 (2011).

[21] MB Martens, M Chiappalone, D Schubert, and PH Tiesinga. “Separating burst from background spikes in multichannel neuronal recordings using return map analysis”. In: *Int J Neural Syst* 4.24 (2014), p. 1450012.

[22] M Chiappalone, M Bove, A Vato, M Tedesco, and S Martinoia. “Dissociated cortical networks show spontaneously correlated activity patterns during in vitro development”. In: *Brain Research* 1093.1 (2006), pp. 41–53.

[23] M Chiappalone et al. “Opposite Changes in Glutamatergic and GABAergic Transmission Underlie the Diffuse Hyperexcitability of Synapsin IDeficient Cortical Networks”. In: *Cerebral Cortex* 19.6 (2009), pp. 1422–1439.

[24] MA Clifford, JK Kanwal, R Dzakpasu, and MJ Donoghue. “EphA4 expression promotes network activity and spine maturation in cortical neuronal cultures”. In: *Neural Development* 6.21 (2011), pp. 1–13.

[25] EJ MacLaren, P Charlesworth, MP Coba, and SGN Grant. “Knockdown of mental disorder susceptibility genes disrupts neuronal network physiology in vitro”. In: *Molecular and Cellular Neuroscience* 47.2 (2011), pp. 93–99.

[26] SM Potter and TB DeMarse. “A new approach to neural cell culture for long-term studies”. In: *Journal of Neuroscience Methods* 110.1-2 (2001), pp. 17–24.

[27] D Wagenaar, J Pine, and S Potter. “An extremely rich repertoire of bursting patterns during the development of cortical cultures”. In: *BMC Neuroscience* 7.1 (2006), p. 11.

[28] A Maccione et al. “A novel algorithm for precise identification of spikes in extracellularly recorded neuronal signals”. In: *Journal of Neuroscience Methods* 177.1 (2009), pp. 241–249.

[29] RM Davies, GL Gerstein, and SN Baker. “Measurement of Time-Dependent Changes in the Irregularity of Neural Spiking”. In: *Journal of Neurophysiology* 96.2 (2006), pp. 906–918.

[30] CM Jarque and AK Bera. “Efficient tests for normality, homoscedasticity and serial independence of regression residuals”. In: *Economics Letters* 6.3 (1980), pp. 255–259.

[31] HB Mann and DR Whitney. “On a Test of Whether one of Two Random Variables is Stochastically Larger than the Other”. In: *Ann. Math. Statist.* 18.1 (1947), pp. 50–60.

[32] Y Benjamini and Y Hochberg. “Controlling the False Discovery Rate: A Practical and Powerful Approach to Multiple Testing”. In: *Journal of the Royal Statistical Society. Series B (Methodological)* 57.1 (1995), pp. 289–300.

[33] P Charlesworth, E Cotterill, A Morton, S Grant, and S Eglen. “Quantitative differences in developmental profiles of spontaneous activity in cortical and hippocampal cultures”. In: *Neural Development* 10.1 (2015), p. 1.

[34] J van Pelt, PS Wolters, MA Corner, WLC Rutten, and GJA Ramakers. “Long-term characterization of firing dynamics of spontaneous bursts in cultured neural networks”. In: *Biomedical Engineering, IEEE Transactions on* 51.11 (2004), pp. 2051–2062.

[35] LM Valor, P Charlesworth, L Humphreys, CNG Anderson, and Seth GN Grant. “Network activity-independent coordinated gene expression program for synapse assembly”. In: *Proceedings of the National Academy of Sciences* 104.11 (2007), pp. 4658–4663.

[36] FJL Arnold et al. “Microelectrode array recordings of cultured hippocampal networks reveal a simple model for transcription and protein synthesis-

dependent plasticity". In: *The Journal of Physiology* 564.1 (2005), pp. 3–19.

[37] P Verstraelen et al. "Pharmacological Characterization of Cultivated Neuronal Networks: Relevance to Synaptogenesis and Synaptic Connectivity". In: *Cellular and Molecular Neurobiology* 34.5 (2014), pp. 757–776.

[38] D Guo and C Li. "Self-Sustained Irregular Activity in 2-D Small-World Networks of Excitatory and Inhibitory Neurons". In: *Neural Networks, IEEE Transactions on* 21.6 (2010), pp. 895–905.

[39] K Kitano and T Fukai. "Variability v.s. synchronicity of neuronal activity in local cortical network models with different wiring topologies". In: *Journal of Computational Neuroscience* 23.2 (2007), pp. 237–250.

[40] LC Andreae, NB Fredj, and J Burrone. "Independent Vesicle Pools Underlie Different Modes of Release during Neuronal Development". In: *Journal of Neuroscience* 32.5 (2012), pp. 1867–1874.

[41] M Chiappalone, A Vato, L Berdondini, M Koudelka-hep, and S Martinoia. "Network dynamics and synchronous activity in cultured cortical neurons". In: *International Journal of Neural Systems* 17.02 (2007), pp. 87–103.

[42] PE Latham, BJ Richmond, PG Nelson, and S Nirenberg. "Intrinsic Dynamics in Neuronal Networks. I. Theory". In: *Journal of Neurophysiology* 83.2 (2000), pp. 808–827.

[43] A Destexhe, M Rudolph, JM Fellous, and TJ Sejnowski. "Fluctuating synaptic conductances recreate in vivo-like activity in neocortical neurons". In: *Neuroscience* 107.1 (2001), pp. 13–24.

[44] S Illes et al. "Intrinsically Active and Pacemaker Neurons in Pluripotent Stem Cell-Derived Neuronal Populations". In: *Stem Cell Reports* 2.3 (2014), pp. 323–336.

[45] TA Gritsun, J Le Feber, J Stegenga, and WLC Rutten. "Network bursts in cortical cultures are best simulated using pacemaker neurons and adaptive synapses". In: *Biological Cybernetics* 102.4 (2010), pp. 293–310.

[46] M Tsodyks, A Uziel, and H Markram. "Synchrony Generation in Recurrent Networks with Frequency-Dependent Synapses". In: *The Journal of Neuroscience* 20.RC50 (2000), pp. 1–5.

[47] MB Martens, T Celikel, and PHE Tiesinga. "A developmental switch for Hebbian plasticity". In: *PLoS Computational Biology* 11.7 (2015), e1004386.

[48] LC Andreae and J Burrone. "The role of neuronal activity and transmitter release on synapse formation". In: *Current Opinion in Neurobiology* 27 (2014), pp. 47–52.

[49] GW Davis. "Homeostatic Signaling and the Stabilization of Neural Function". In: *Neuron* 80.3 (2013), pp. 718–728.

[50] H Ko et al. "The emergence of functional microcircuits in visual cortex". In: *Nature* 496.7443 (2013), pp. 96–100.

[51] Dh Geschwind and P Levitt. "Autism spectrum disorders: developmental disconnection syndromes". In: *Current Opinion in Neurobiology* 17.1 (2007), pp. 103–111.

[52] JLR Rubenstein and MM Merzenich. “Model of autism: increased ratio of excitation/inhibition in key neural systems”. In: *Genes, Brain and Behavior* 2.5 (2003), pp. 255–267.

[53] G Testa-Silva et al. “Hyperconnectivity and Slow Synapses during Early Development of Medial Prefrontal Cortex in a Mouse Model for Mental Retardation and Autism”. In: *Cerebral Cortex* 22.6 (2012), pp. 1333–1342.

[54] S Gupta et al. “Histone Methylation Regulates Memory Formation”. In: *The Journal of Neuroscience* 30.10 (2010), pp. 3589–3599.

[55] I Maze et al. “Essential Role of the Histone Methyltransferase G9a in Cocaine-Induced Plasticity”. In: *Science* 327.5962 (2010), pp. 213–216.

[56] C Mozzetta et al. “The Histone H3 Lysine 9 Methyltransferases G9a and GLP Regulate Polycomb Repressive Complex 2-Mediated Gene Silencing”. In: *Molecular Cell* 53.2 (2014), pp. 277–289.

[57] DH Bhatt, S Zhang, and W Gan. “Dendritic Spine Dynamics”. In: *Annual Review of Physiology* 71.1 (2009), pp. 261–282.

[58] JT Goncalves, JE Anstey, P Golshani, and C Portera-Cailliau. “Circuit level defects in the developing neocortex of Fragile X mice”. In: *Nat Neurosci* 16.7 (2013), pp. 903–909.

Chapter 7

Spiking activity in connected small neuronal networks

M.B. Martens

7.1 Abstract

Brain circuits perform local computations and communicate to other networks through long-range axonal connections, the effects of which have been difficult to study using the culture preparation. Here, to study action potential activity in multiple interacting small neuronal networks, we applied the flexible polymer polydimethylsilxane (PDMS) to provide topographical guidance for neuronal network growth. We grew small *in vitro* neuronal networks that connected to other small networks through microtunnels. We used Multi-Electrode Arrays (MEAs) to record the extracellular activity and observed spontaneous and evoked action potential activity in the small neuronal networks, and found firing and burst rates that were comparable to the large neuronal networks studied previously. The spontaneous and evoked activity propagated between the neuronal networks that were directly connected by microtunnels, but did not propagate to an isolated control network that was not connected by microtunnels. We discuss potential applications of PDMS microstructures on MEAs to investigate neuronal plasticity, communication and processing that were previously challenging to study in large and unstructured neuronal networks.

7.2 Introduction

Seminal work by Mountcastle described modular organisation of the cat cortex, in which neurons with similar receptive field properties are organized in cortical columns with a diameter of several hundred micrometers [1, 2]. Similarly, Hubel and Wiesel defined the hypercolumn, a cortical column that contains a complete set of receptive field properties, which was estimated to be 0.5 to 1 mm wide [3]. The functional role of such segregation into independent canonical microcircuits is not clear, but it has led to several hypotheses regarding their computational roles and data transmission capabilities (for review, see [4]).

Communication between microcircuits occurs through long-range projections or through lateral connections, particularly in the upper layers of the cortex [5]. Currently, investigating the communication and plasticity between cortical regions occurs in *in vivo* and in acute *in vitro* brain preparations [6]. Experimental techniques to record long-term neuronal activity are challenging *in vivo* and rapid detoriation of the brain *ex vivo* makes chronic recording difficult [7, 8]. Alternatively, dissociated cell cultures can be readily monitored during development [9–11]. In recent years, interest has grown in the use of the flexible polymer polydimethylsiloxane (PDMS) on Multi-Electrode Arrays (for review see [12]).

Recently, methods were developed to obtain directionality in the axonal outgrowth. Directionality could be achieved in two-compartmental models, by plating neurons in one compartment 7 days after the neurons in the other compartment were plated [12]. This approach is not suitable for developmental studies, in particular when using multiple compartments because the differences in cul-

ture age grows linearly with the number of connected compartments. Another approach to obtain directionality with cultures plated on the same day is to use nanowire structures to guide the axonal outgrowth direction [13]. The production process of nanowires is costly and requires highly specialized equipment and expertise. In another approach the directionality was obtained by producing PDMS microtunnels that had a small channel width (1-4 μm) at one tunnel entrance such that it was difficult for axons to enter the microtunnels, while the other tunnel entrance was wider (8-15 μm), which were previously shown to be large enough for axons to grow into [14]. To produce such PDMS microstructures, two layers of photoresist were used [14].

In this study we showcase a method that applies topographical guidance to obtain small neuronal microcircuits that are 1 mm wide. The circuits were interconnected laterally by axonal projections through PDMS microtunnels. We present pilot results of spontaneous and electrically evoked neuronal activity that propagates between the microcircuits.

7.3 Materials and Methods

We describe the fabrication and assembly process of the PDMS+MEA setup and the protocol to load the cells into the device.

7.3.1 PDMS fabrication

To obtain the topographically confined microstructures we used polydimethylsilxane (PDMS). PDMS is widely used for biomedical applications because of its properties of biocompatibility, transparency and permeability to gases [15]. PDMS has previously been succesfully applied to grow patterned cultures [16, 17]. First, a 10 μm layer of negative photoresist SU-8 was spin-coated on a silicon wafer. A mask, designed in AutoCAD (Autodesk, CA, USA), was overlaid on the SU-8 master. SU-8 is an epoxy-based negative photoresist: parts that are exposed to light will cross-link, whereas the other parts can be removed in a washing step. Then, PDMS pre-polymer and curing agent were mixed at a ratio of 10 to 1, poured on the SU-8 master and cured overnight in an oven at 65 °C. PDMS slabs were peeled off the silicon wafer and the microstructures were separated using a surgical knife. Around each microstructure a 0.5 cm margin was spared for easy handling. The culturing compartments were then opened using a custom made puncher. This protocol enabled cost efficient and reliable production of PDMS microstructures.

7.3.2 PDMS+MEA assembly and cell loading

The PDMS microstructures were cleaned by gently brushing, using a soft brush and ethanol, immediately followed by removal of debris using pressurized nitro-

gen. For storage, the microtunnels were placed on a glass coverslip with the channels facing down. After this treatment, the PDMS surface became hydrophobic over hours; we therefore applied 20 seconds of O_2 plasma cleaning of the microtunnels 1 hour before placing the PDMS structure on the MEA. We placed the PDMS with microtunnels facing down on a 40 μL droplet of filtered, sterile water that was pipetted onto the electrode area of the MEA. With the aid of a tweezer we positioned the PDMS such that the MEA electrodes were within the 4 compartments. After the desired position was achieved, careful suction was applied to remove the water, forming the seal between the PDMS and MEA. Seed medium (see Section 7.3.3) was pipetted into the compartments, while using a microscope to confirm that the channels filled with medium. A 40 μL droplet of seed medium was pipetted onto the PDMS structure to avoid evaporation of the small quantity of seed medium in the microtunnels. The assembled PDMS+MEA device was placed in the incubator. When the cells were ready for plating (see Section 7.3.3), the seed medium was removed from the PDMS+MEA device using gentle suction. With a small pipette tip, 2 μL of dissociated cells (concentration 1 million cells/mL) was equally distributed over the 4 compartments, such that each compartment contained 500 cells on average. Additionally, 0.75 mL seed medium was added around the PDMS structure. Around the PDMS microstructure 300.000 neurons were added for trophic support to the culture medium. The PDMS+MEA device was placed in the incubator, and after 10 minutes we placed 40 μL seed medium on top of the PDMS to avoid evaporation. The cells were then incubated for another 50 minutes to further attach to the MEA, after which we added 0.75 mL of growth medium. The final volume of the medium was 1.5 mL, which was sufficient to submerge the PMDS. The medium was shared between the support neurons and the isolated network of neurons.

7.3.3 Culture preparation

All animal procedures were approved by the Animal Care Committee, Radboud University Nijmegen Medical Centre, The Netherlands, (RU-DEC-2011-021, protocol number: 77073). MEAs were coated with 0.0125% Polyethylenimine (PEI, Sigma-Aldrich, St. Louis, MO, USA, P3143) overnight. After a triple wash to remove residual PEI, a seeding medium containing Neurobasal medium (1x, Gibco Fisher Scientific, Waltham, MA, USA, 21103-049), 10% Fetal Bovine Serum (FBS, Sigma-Aldrich, St. Louis, MO, USA, F7524), 2% Supplement B27 (B27, Gibco Fisher Scientific, Waltham, MA, USA, 17504-044) and 1% Penicillin/Streptomycin (Pen/Strep, Sigma-Aldrich, St. Louis, MO, USA, P4333) was added to the MEAs and cover slips. Cortices were dissected from Wistar rat pups on embryonic day 18 (E18). The cortices were dispersed in Hanks' Balanced Salt Solution without Mg or Ca (Gibco Fisher Scientific, Waltham, MA, USA, 14185-045), containing 0.3 M Hepes (pH 7.3, Sigma-Aldrich, St. Louis, MO, USA, H4034) and adjusted to a pH of 7.3 with NaOH. The tissue was digested with 0.25% Trypsine (Gibco Fisher Scientific, Waltham, MA, USA, 15090-049) for 15

min at 37 °C and then mechanically dissociated using fire polished glass Pasteur pipettes. The cell suspension was filtered with a 70 m cell strainer (Falcon Fisher Scientific, Waltham, MA, USA, 352350) to remove larger pieces. At 24 hours after plating, the cells were infected with a virus expressing both ChannelRhodopsin-2 and a fluorescent tag. Finally, twice a week half of the medium was refreshed. The cells were incubated in a humidified atmosphere of 95% O_2 and 5% CO_2 at 37 °C.

7.3.4 Data analysis

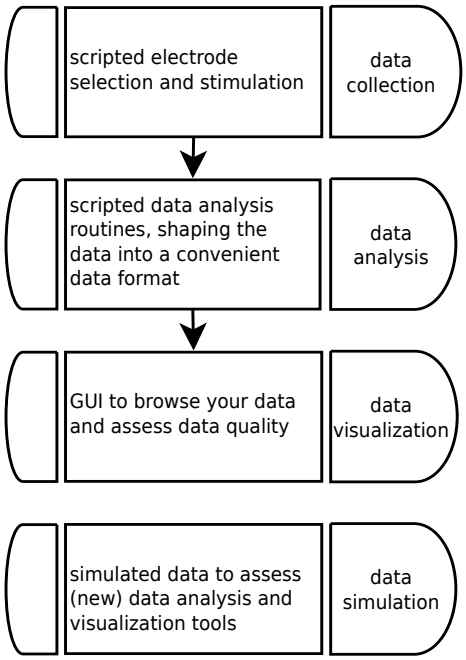

Figure 7.1: Organization of stimulation and analysis protocol. We used four independent modules that share the same data structure. The first module allows scripted control over the experiment, i.e. the timing, type and location of applied stimulation. The second module enables a data analysis pipeline. The analysed data can be easily browsed using the third module, a Graphical User Interface (GUI). The last module generates data that is similar to real data, but with a known ground truth. This data is stored in the same data format as the other three modules and therefore allows for the assessment of (new) data analysis routines.

Multi-Electrode Array recordings require multiple (pre)processing steps and detection routines. We developed a custom MATLAB (The Mathworks, Natick,

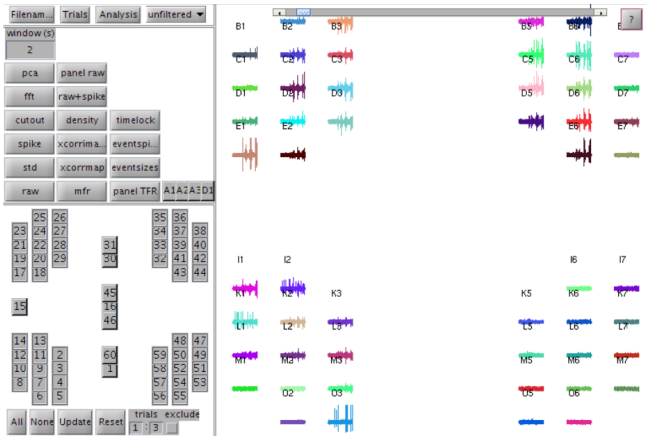

Figure 7.2: The graphical user interface (GUI) of our custom toolbox was used to visually explore the data. The control panel on the left-hand side can be used to select electrodes (bottom), analysis routines (middle) and analysis parameters (top). The data is visualized in the plotting panel on the right-hand side. The example traces show burst activity in three connected compartments, while the isolated compartment is not bursting (lower right corner).

MA, USA) toolbox, following the philosophy of the Fieldtrip toolbox [18], to facilitate the MEA data analysis pipeline. This toolbox consists of four independent modules (**Figure 7.1**). The first module allows MATLAB scripted electrode selection and stimulation. The second module contains scripted data processing functions (**Supplementary Figure 7.8**). Unprocessed and processed data can be browsed using the GUI of the third module (**Figure 7.2**). The last module contains functions for the generation of simulated data with a known ground truth. These data are stored in the same format that is used by the first three modules. The toolbox uses SI units (i.e. seconds, volts) and can deal with all available Multi Channel Systems MEA configurations.

The data analysis routines in the toolbox include spike detection algorithms, burst detection methods, cross- and autocorrelation functions, power spectrum analysis and principal component analysis. Data visualization included spike raster and spike density plots, time-frequency representation of the data and post-stimulus visualizations.

7.3.5 Statistics

Data were expressed as mean ± standard error of the mean. Statistical analysis was performed using MATLAB (R2012a, The Mathworks, Natick, MA, USA). The data submitted to statistical analysis was often non-normal, as indicated by

skewness [19](we tested for normality using the Jarque-Bera test, implemented as jbtest in MATLAB). Hence, we used the Mann-Whitney test, implemented as the ranksum test in MATLAB [20]. We tested whether the means of the set of statistics differed across conditions at any given DIV. These p-values were aggregated for each DIV value; significant values were then corrected for multiple comparisons using the false discovery rate (FDR) method, incorporating potential dependencies between p-values [21, 22]. To calculate the FDR we used the mafdr function in MATLAB using the polynomial selection method for the FDR parameter lambda.

7.4 Results

In this section we present the results and describe potential pitfalls of using PDMS microstructures to guide neurite outgrowth on multi electrode arrays (MEAs). We show examples of spontaneous and stimulus-induced neuronal activity in small neuronal networks that are connected by microtunnels.

7.4.1 Topographical guidance of neurite outgrowth using PDMS microstructures

We could reliably produce PDMS microstructures (**Figure 7.3A**). Access for the pipette was needed to be able to inject neurons into the compartments. Compartmental PDMS structures areas can be made accessible by using a single puncher. However, to apply four consecutive precisely placed punches proved to be cumbersome: many microstructures were destroyed by misaligned punches. We therefore created a custom puncher (**Figure 7.3A**). The custom puncher made it possible to align the microstructures under a light microscope, and we were able to open the four compartments consistently with a single punch (**Figure 7.3B**).

We wanted to test whether we could obtain microstructures with the appropriately width (1-4 μm as mentioned in the introduction) using a single layer of SU-8 negative photoresist. However, the microtunnels with a width that was smaller than 6 μm were prone to break (**Figure 7.3C**). In our setup we could only obtain high quality microtunnels with a width of 8 μm, so the channels were bidirectional. Using this setup we were able to confine neurite outgrowth to the PDMS microstructures (**Figure 7.3D**).

However, neurite outgrowth outside the predefined PDMS microstructures could occur when the microstructures were not sealed properly onto the MEA. Debris on the MEA could lift the microstructures high enough for the neurons to grow neurites under the PDMS or could in some cases cause the PDMS to detach in its entirety. Plasma cleaning was thus necessary to remove the debris. However, when plasma cleaning was applied the PDMS was often irreversibly bound to the MEA, resulting in the loss of the MEA. Inappropriate sealing could lead to network activity on all electrodes, including the electrodes in the isolated

control compartment. Using a testing setup of PDMS microstructures and glass coverslips, we tried several methods to avoid the irreversible binding of PDMS to the MEA: different ratios of curing agent (5:1 or 20:1), various durations of curing the PDMS in the oven (overnight or 3 days), and different cleaning methods (plasma cleaning of 5 sec or 40 seconds). However, we were not able to determine the causative factor for the irreversible binding between MEA and substrate. One potential cause is the Polyethylenimine (PEI), which could bind the PDMS to the MEA surface. The number of irreversible bindings was reduced, but not eliminated, when we applied the PEI coating after the PDMS was positioned on the glass coverslip or MEA.

To demonstrate the use of the patterning technique, we performed a pilot study on neuronal outgrowth, where we compared neurons from wild-type to *FoxP2*$^{+/-}$ mice. FoxP2 deficiency was previously related to impaired axonal outgrowth [23]. Using the PDMS microstructures on glass coverslips we found that wild-type neurons were able to develop long-range axonal projections that connect the different compartments, whereas neurons from *FoxP2* mutant mice were unable to form the long axonal projections (**Figure 7.3E**). With this example application, we demonstrated the use of PDMS on glass coverslips as a potentially affordable experimental setup to study neurite outgrowth.

7.4.2 Small neuronal networks show activity that is similar to large neuronal networks

Large neuronal networks show spontaneous synchronized burst activity, which may be altered by genetic or pharmacological manipulations ([24] and Chapter 6). Here we show spontaneous, synchronized activity in the small connected neuronal networks (**Figure 7.4**). We studied isolated small networks consisting of approximately 500 neurons (1Q) as well as three small networks of 500 neurons that were connected by long-range axonal projections (3Q). The isolated compartment showed typical synchronized bursting behaviour. The bursting of the neurons in this compartment was disconnected from the bursting of the neurons in the connected compartments. Interestingly, the neurons connected by long-range axonal projections showed burst activity, in which all three networks were bursting synchronously.

We compared the burst statistics for several (N = 2-3) MEA recordings for small neuronal networks (1Q and 3Q) to those (N = 24-25) of large neuronal networks consisting of 350.000 neurons (chip-wide) during the developmental period DIV 10, 13, 15 and 17 and found that the cumulative distributions of the burst sizes (number of spikes per burst), burst duration and interburst interval were similar for these conditions (**Figure 7.5A**). The mean firing rate for the small networks was higher early in development, which was previously found in a similar experimental setting [17]. However, after correction for multiple comparisons these findings were not statistical significant (**Figure 7.5B**). Furthermore the burst rate and burst irregularity had similar developmental profile across the dif-

ferent network sizes (**Figure 7.5C**). Although the number of repetitions should be increased to better characterize the network development of the small neuronal networks, we here demonstrated that the networks appeared healthy and showed firing and bursting statistics that are similar to large neuronal networks.

7.4.3 Stimulation evokes activity that propagates through connected small neuronal networks

Using MEA electrodes we evoked neuronal spiking activity in the isolated small neuronal network (**Figure 7.6A**) as well as in the three connected small neuronal networks (**Figure 7.6B-D**). The neuronal spiking activity from the stimulated small neuronal network propagated to the other networks which were connected by long-range axonal projections through the microtunnels. With these example results we demonstrated that the PDMS microstructures can be used to confine neuronal outgrowth of small neuronal populations on MEA. The small neuronal networks were spontaneously active with firing and burst rates similar to large neuronal networks. With electrical stimulation applied using the MEA we were able to evoke activity in one small network, and activity propagated to the networks that were connected by PDMS microtunnels.

7.5 Discussion

In this study, we demonstrated the use of PDMS microstructures to obtain small spiking neuronal networks on Multi-Electrode Arrays (MEAs). The networks showed spontaneous and stimulus induced neuronal activity that propagated to other neuronal networks that were connected by long-range axonal projections through microtunnels. We showed that the developmental activity patterns of small neuronal networks are comparable to large neuronal networks. The microstructures were designed to have an internal control compartment that was not connected to the other compartments. Inappropriate sealing between PDMS and MEA could lead to activity on all electrodes, showing the importance of an internal control compartment. To obtain appropriate sealing between PDMS and MEA, rigorous cleaning procedures were needed. However, we often encountered irreversible bonding of the PDMS to the MEA. Several causes of the irreversible bonding were explored, but we were unable to resolve this issue. Due to the high cost of the MEAs we did not attempt to increase to larger sample sizes and used the pilot recordings to demonstrate the capabilities of the experimental setup.

Previously, neuronal networks of different sizes that were recorded on several different MEA designs were shown to self-organize to a typical network bursting state [25, 26]. The typical bursting state shows large variability between burst profiles [26]. Neuronal networks that were obtained from the same batch of neurons showed a lower variability in burst profiles, and burst profile variability is lowest for bursts recorded within the same culture across days [26]. In this study,

we obtained only a small number of recording samples (N = 2-3). Using a larger sample size, it would be interesting to investigate whether variability between burst profiles is lower for the small neurons networks, and to what degree the burst profiles of a small network relate to the burst profiles of connected networks.

Investigators using large neuronal networks on MEAs have encountered difficulties in the application of plasticity protocols to obtain functional changes in spiking activity [27], although a few protocols could succesfully induce plasticity [28–30]. Plasticity protocols often involve pairing of two electrodes to strengthen the synaptic connections between these two points, thereby changing the network response. Strengthening of polysynaptic paths in networks consisting of 10-20 neurons has been shown experimentally [31]. However, strengthening polysynaptic paths in large neuronal networks on MEAs is more complex: an action potential induced in the neuron(s) around one electrode will propagate throughout the network and, for example for a random walk through a 2D square lattice, the number of steps (n) needed to travel an average distance d scales approximately as d^2 [32]. This quadratic increase in number of steps contributes to the difficulty to appropriately pair action potential activity between two points in the network, such that plasticity protocols could be applied. Therefore, our approach to use PDMS microstructures to guide long-range axonal projections to create specific network structures could be better suited to investigate the storage of spatially distributed and polysynaptic patterns (**Figure 7.7A**). Furthermore, multiple connected networks cultured on the same MEA provide additional internal controls and could use the potentially lower variability in burst profiles that are found in neurons that are cultured on the same MEA. We suggest that the experimental setup demonstrated here could be used for the detection of more subtle plasticity induced network changes compared to large neuronal networks on MEA.

Neuronal oscillations are found throughout the brain and suggested to play an important role neuronal processing and stimulus selection [33]. The experimental setup demonstrated here provides the opportunity to study the role of neuronal oscillations in stimulus processing in connected neuronal networks. We showed that stimulation of the small neuronal network in the middle compartment induced activity that propagated to the outer compartments. Optical stimulation in the outer compartment can then be applied at different phases to the stimulation in the middle compartment (**Figure 7.7B** and **Supplementary Figure 7.9**). Using this setup, the role of phase and frequency in neuronal processing could be investigated.

MEAs have recently been applied to investigate the effect of genetic manipulation (Chapter 6, [34–36]) and of the brain region from which the cells were obtained [37] on the action potential activity behaviour. The experimental setup proposed here could be applied to, for example, cortical-thalamic-striatal cocultures to investigate the role of cell type on neuronal processing and behaviour (**Figure 7.7C**).

Typically, computational studies of spiking neural networks use network sizes

of several hundred neurons (Chapter 2-4). Here we demonstrated *in vitro* small neuronal networks that were approximately 500 neurons in size. We showed that these networks behave comparable to large neuronal networks in terms of firing and burst rate. Therefore, the experimental setup demonstrated here could be used to test computational predictions of network parameters that depend on a certain network structure or size.

We conclude that the protocol to obtain a reversible, but appropriate sealing between the PDMS microstructures and MEA requires further development. We demonstrated the use of multiple PDMS compartments on MEA in terms of spontaneous and evoked activity in cortical neurons. The experimental approach discussed here provides novel applications to neuronal plasticity, communication and processing that were previously challenging to study in large and unstructured neuronal networks.

Acknowledgements and author contribution

MM and VC designed the lithography masks; VC produced the masters in the clean room; MM and SM designed and produced the custom puncher; MM, LE and VC produced and tested the PDMS microstructures in the lab of WH; PD and SV collected FoxP2 data; MM, DS, NNK and PT collected and analyzed MEA data; MM and PT wrote the manuscript. This research was funded by NWO (MM, grant number 62001113).

MM is Marijn Martens, VC is Venkat Chokkalingam, LE is Lisa Epping, SM is Stijn Martens, PD is Paolo Devanna, SV is Sonja Vernes, WH is Wilhelm Huck, NNK is Nael Nadif Kasri, DS is Dirk Schubert, PT is Paul Tiesinga.

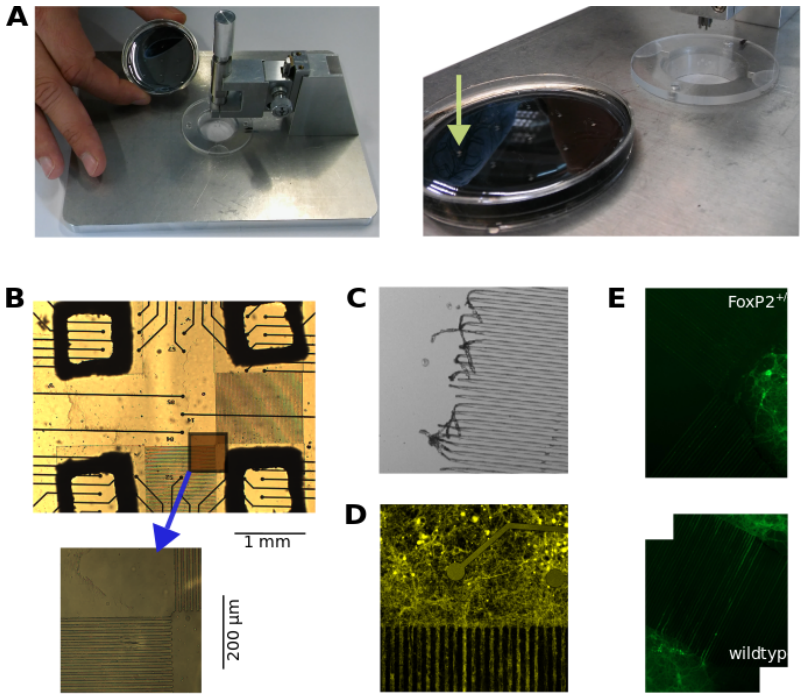

Figure 7.3: Topographical guidance of neurite outgrowth using PDMS microstructures on Multi-Electrode Arrays (MEAs). ***A****: Cured PDMS slabs that contain nine microstructures (one microstructure is indicated by the yellow arrow). We used a custom puncher to simultaneously punch four appropriately sized and spaced holes through the PDMS slabs. Alignment under a light microscope was used to ensure accurate punching of the microstructures.* ***B****: Topview of a PDMS microstructure with four compartments after punching. The microstructure is positioned on the MEA using a light microscope. Each compartment had a surface area of 1.44 mm^2. The inset shows the microtunnels, with dimensions as follows: 8 µm wide, 10 µm high and 1 mm long. The microtunnels are large enough for neurite outgrowth, but not large enough for somas to enter. Three compartments are connected by the microtunnels, while the isolated compartment serves as the control.* ***C****: Support columns of the mold required a minimal width of 8 µm in our setup. Support columns that were smaller would often lead to damage of the molds in the production process.* ***D****: We plated neurons in the PDMS microstructures and infected the cells with a virus containing the construct for ChannelRhodopsin-2 and a yellow fluorescent tag. If the PDMS and MEA had bonded correctly, the somas would remain restricted to the compartments and the neurite outgrowth was properly restricted by the PDMS microstructure.* ***E****: Example application of PDMS microstructures. Neurons from* FoxP2$^{+/-}$ *embryonic mice were unable to extend neurite outgrowth throughout the microtunnels (top), whereas wild-type neurons were able to connect to neighbouring populations (bottom).*

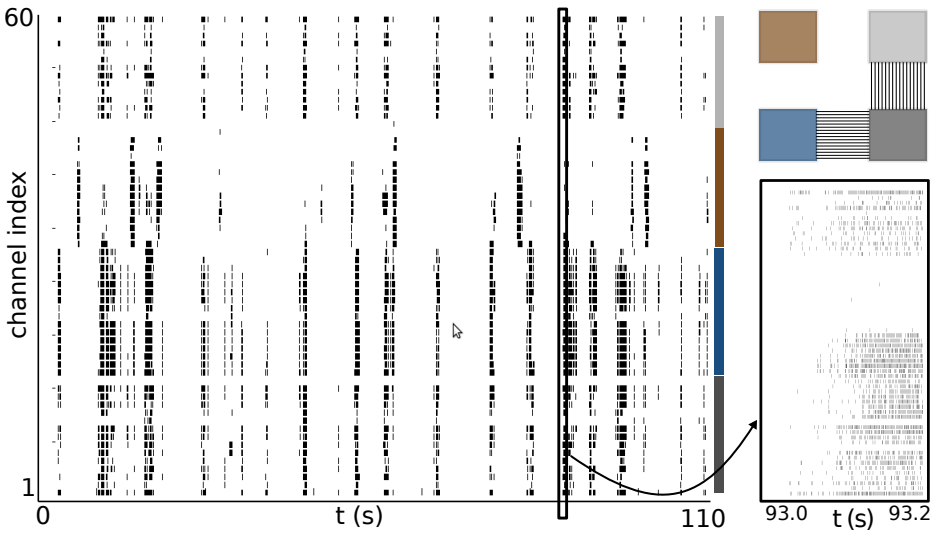

Figure 7.4: Spontaneous activity in small connected neuronal networks. The rasterplot shows each spike as a black bar, with the 60 MEA electrodes ordered on the vertical axis. The electrodes are sorted by location, electrodes in the same compartment are grouped together; the four colors denote the electrodes that belong to the same compartment in the PDMS+MEA setup. The electrodes denoted by the brown color belong to the isolated compartment; the neuronal network in this compartment shows synchronized bursting activity. The compartments that are connected by the microtunnels show synchronized activity across the three small neuronal networks. The inset on the right shows the individual spikes during one burst that occurred for the connected networks.

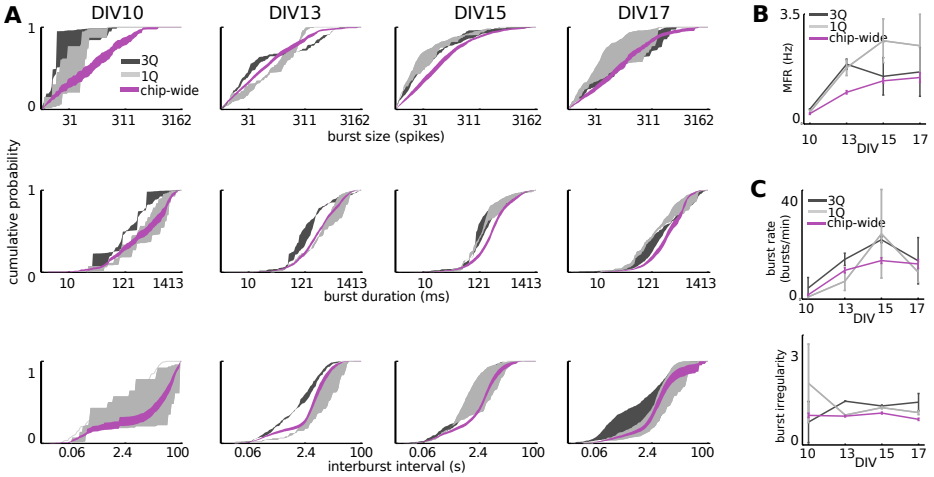

Figure 7.5: Pilot data of small neuronal networks show similar spike and burst activity compared to large neuronal networks. ***A****: The cumulative distributions of the burst size (number of spikes per burst, top), burst duration (middle) and interburst interval (bottom) were not significantly different between conditions after correcting for multiple testing. Conditions were the isolated compartment (1Q, approximately 500 neurons), the connected compartments (3Q, approximately 1500 neurons) and the large neuronal networks consisting of 350.000 neurons (chip-wide) for the four developmental timepoints DIV 10-17.* ***B****: The mean firing rate increases during development for the three different types of network structure. The apparent earlier increase in mean firing rate is not significant after correcting for multiple comparisons.* ***C****: The burst rate and burst irregularity were similar between conditions during development. N = 2 for DIV 10,13 and 15, and N = 3 for DIV 17 for the small neuronal networks (1Q, 500 neurons, and 3Q, 1500 neurons), and N = 24-25 for the large neuronal networks (chip-wide, 350,000 neurons).*

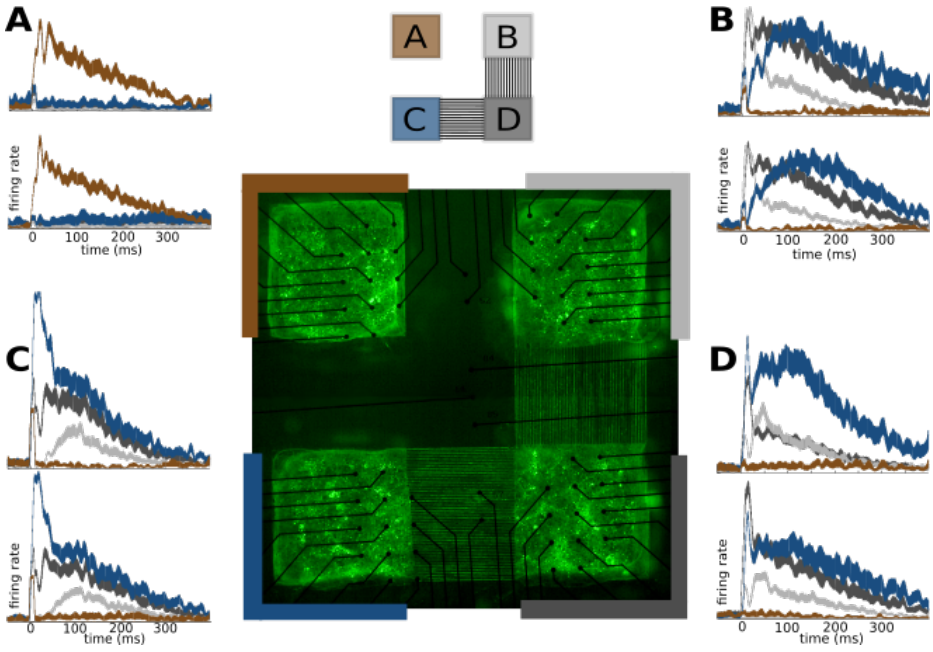

Figure 7.6: Evoked activity in a small neuronal network propagates to connected networks by long-range axonal connections. ***A****: Neuronal activity is evoked by electrical stimulation in the isolated compartment (denoted by brown color), while the other compartments remain silent (color code as indicated in the central inset). Each detected spike is convolved with a Gaussian to obtain the post-stimulus spike density trace. Top graph shows the post-stimulus spike density shows the activity of 40 stimulations (mean activity ± S.E.M.). The lower graph shows the post-stimulus spike density 1 hour later, the responses are similar over time.* ***B-D****: Letter indicates the stimulated compartment. Stimulation evokes activity in the small neuronal networks that was in the stimulated compartment as well as in the small networks that were connected through long-range axonal projections through the microtunnels.*

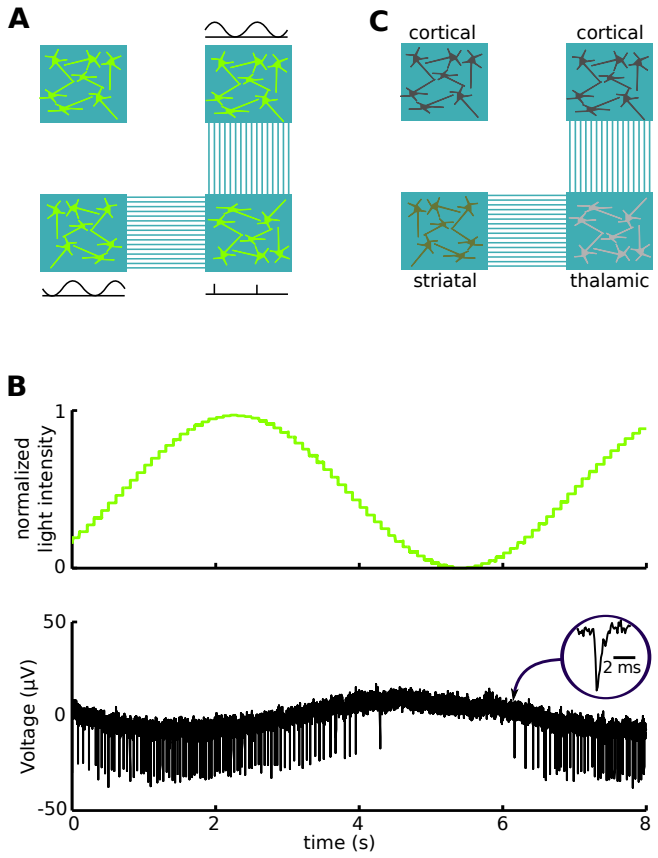

Figure 7.7: Potential applications of PDMS microstructures on MEAs. ***A****: Schematic of PDMS microstructures containing neurons that express ChannelRhodopsin-2. Electrical or optical stimulation protocols could be applied in individual compartments, thereby activating the neurons using specific sequences. Example applications include novel plasticity protocols and studies on the role of the oscillations in communication between neuronal networks.* ***B****: Example of neuronal activity recorded by a MEA electrode while the neurons are stimulated using an optical oscillatory stimulation. The neuronal spiking activity is entrained by the optical stimulation.* ***C****: Cells are added separately for each compartment of the PDMS microstructure. Therefore, neurons from different neuronal populations can be added to the different compartments, allowing for the study of neuronal communication between different cell types.*

7.6 Supplementary Figures

```
addpath(genpath('/home/marijn/meatoolbox/'))
filenames4Q % load filenames
conditions = [1 2]; % select conditions
sessions{1} = 1:length(Q4{1}); % select files
sessions{2} = 1:length(Q4{2}); % select files

for con = conditions
   for ses = sessions{con}
      clear data
      cfg.savefilename = [Q4{con}{ses}.dir 'analyzed/basal.mat'];
      fn             = dir([Q4{con}{ses}.dir '*.mcd']);
      data           = [];
      cfgini         = [];
      cfgini.trial   = 0;
      cfgini.channels = 1:60;
      for trl = [Q4{con}{ses}.basal]
         nsdata             = sonar_mcd2matlab([Q4{con}{ses}.dir fn(trl).name]);
         cfgini.trial       = cfgini.trial+1;
         cfg                = cfgini;

         cfg.layout         = '4QMEA1000';
         data               = sonar_matlab2sonar(cfg,data,nsdata);
         clear nsdata
         cfg.filtertype     = 'highpass';
         cfg.filterdesign   = 'butterworth';
         cfg.filterfreq     = 300;
         data               = sonar_filter(cfg,data);

         cfg.baselinetype   = 'median';
         data               = sonar_baseline(cfg,data);

         cfg.sigmafactor    = 8;
         cfg.peaklifetime   = 0.0015;
         data               = sonar_spikedetectpeakpeak(cfg,data);

         cfg.xcorrdelay     = -.005;
         cfg.xcorrwindow    = -.010;
         data               = sonar_xcorr(cfg,data);
         cfg.acorrtau       = 2;
         data               = sonar_acorr(cfg,data);
      end
      data.info.div   = Q4{con}{ses}.div;
      data.info.cultid = Q4{con}{ses}.cultid;
      data.info.sisters= Q4{con}{ses}.sisters;
      cfg.savefilename = [Q4{con}{ses}.dir 'analyzed/basal.mat'];
      sonar_save(cfg,data)
   end
end
```

Figure 7.8: Example script to pre-process MEA data using the custom MATLAB toolbox shown in Figure 7.1. A configuration file (cfg) and a data structure (data) are used in several pre-processing and data analysis routines.

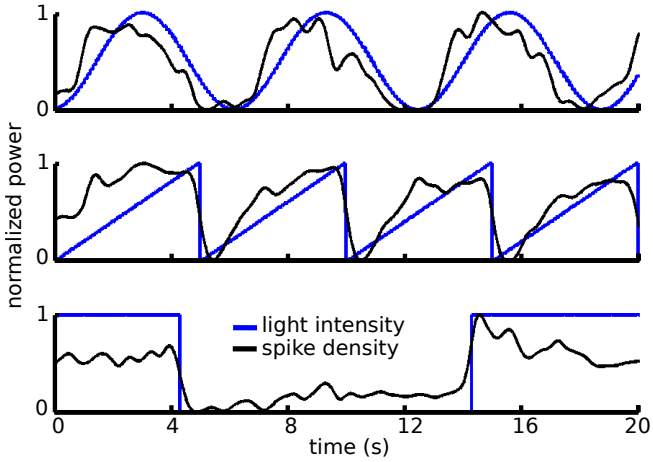

Figure 7.9: Patterened optical stimulation induces spike activity in neurons that were infected with ChannelRhodopsin-2. The normalized spike density (black traces) follows the LED light intensity (blue traces). The wavelength of the light emitted by the LED was 470 nm. For visualization, the spike density and LED light intensity were normalized to one.

References

[1] VB Mountcastle. "Modality and topographic properties of single neurons of cat′s somatic sensory cortex". In: *Journal of Neurophysiology* 20.4 (1957), pp. 408–434.

[2] VB Mountcastle. "The columnar organization of the neocortex". In: *Brain* 120.4 (1997), pp. 701–722.

[3] DH Hubel and TN Wiesel. "Sequence regularity and geometry of orientation columns in the monkey striate cortex". In: *The Journal of Comparative Neurology* 158.3 (1974), pp. 267–293.

[4] AM Bastos et al. "Canonical microcircuits for predictive coding". In: *Neuron* 76.4 (2013), pp. 695–711.

[5] WH Bosking, Y Zhang, B Schofield, and D Fitzpatrick. "Orientation Selectivity and the Arrangement of Horizontal Connections in Tree Shrew Striate Cortex". In: *The Journal of Neuroscience* 17.6 (1997), pp. 2112–2127.

[6] T Celikel, VA Szostak, and DE Feldman. "Modulation of spike timing by sensory deprivation during induction of cortical map plasticity". In: *Nat Neurosci* 7.5 (2004), pp. 534–541.

[7] Y Buskila et al. "Extending the viability of acute brain slices". In: *Scientific Reports* 4 (2014), p. 5309.

[8] M Brecht et al. “Novel Approaches to Monitor and Manipulate Single Neurons In Vivo”. In: *The Journal of Neuroscience* 24.42 (2004), pp. 9223–9227.

[9] CM Hales, JD Rolston, and SM Potter. “How to Culture, Record and Stimulate Neuronal Networks on Micro-electrode Arrays (MEAs)”. In: *Journal of Visualized Experiments* 39.1940-087X (2010).

[10] M Chiappalone, A Vato, L Berdondini, M Koudelka-hep, and S Martinoia. “Network dynamics and synchronous activity in cultured cortical neurons”. In: *International Journal of Neural Systems* 17.02 (2007), pp. 87–103.

[11] J van Pelt, PS Wolters, MA Corner, WLC Rutten, and GJA Ramakers. “Long-term characterization of firing dynamics of spontaneous bursts in cultured neural networks”. In: *Biomedical Engineering, IEEE Transactions on* 51.11 (2004), pp. 2051–2062.

[12] L Pan et al. “An In Vitro Method to Manipulate the Direction and Functional Strength Between Neural Populations”. In: *Frontiers in Neural Circuits* 9.32 (2015).

[13] W Hallstrom et al. “Rectifying and Sorting of Regenerating Axons by Free-Standing Nanowire Patterns: A Highway for Nerve Fibers”. In: *Langmuir* 25.8 (2009), pp. 4343–4346.

[14] J Peyrin et al. “Axon diodes for the reconstruction of oriented neuronal networks in microfluidic chambers”. In: *Lab Chip* 11.21 (2011), pp. 3663–3673.

[15] A Mata, AJ Fleischman, and S Roy. “Characterization of Polydimethylsiloxane (PDMS) Properties for Biomedical Micro/Nanosystems”. In: *Biomedical Microdevices* 7.4 (2005), pp. 281–293.

[16] AM Taylor, DC Dieterich, HT Ito, SA Kim, and EM Schuman. “Microfluidic local perfusion chambers for the visualization and manipulation of synapses”. In: *Neuron* 66.1 (2010), pp. 57–68.

[17] M Bisio, A Bosca, V Pasquale, L Berdondini, and M Chiappalone. “Emergence of Bursting Activity in Connected Neuronal Sub-Populations”. In: *PLoS ONE* 9.9 (2014), e107400.

[18] R Oostenveld, P Fries, E Maris, and J Schoffelen. “FieldTrip: Open Source Software for Advanced Analysis of MEG, EEG, and Invasive Electrophysiological Data”. In: *Computational Intelligence and Neuroscience* 9 (2011), p. 156869.

[19] CM Jarque and AK Bera. “Efficient tests for normality, homoscedasticity and serial independence of regression residuals”. In: *Economics Letters* 6.3 (1980), pp. 255–259.

[20] HB Mann and DR Whitney. “On a Test of Whether one of Two Random Variables is Stochastically Larger than the Other”. In: *Ann. Math. Statist.* 18.1 (1947), pp. 50–60.

[21] Y Benjamini and Y Hochberg. “Controlling the False Discovery Rate: A Practical and Powerful Approach to Multiple Testing”. In: *Journal of the*

Royal Statistical Society. Series B (Methodological) 57.1 (1995), pp. 289–300.

[22] P Charlesworth, E Cotterill, A Morton, S Grant, and S Eglen. "Quantitative differences in developmental profiles of spontaneous activity in cortical and hippocampal cultures". In: *Neural Development* 10.1 (2015), p. 1.

[23] SC Vernes et al. "Foxp2 Regulates Gene Networks Implicated in Neurite Outgrowth in the Developing Brain". In: *PLoS Genet* 7.7 (2011), e1002145.

[24] MB Martens, M Chiappalone, D Schubert, and PH Tiesinga. "Separating burst from background spikes in multichannel neuronal recordings using return map analysis". In: *Int J Neural Syst* 4.24 (2014), p. 1450012.

[25] R Segev et al. "Long Term Behavior of Lithographically Prepared *In Vitro* Neuronal Networks". In: *Phys. Rev. Lett.* 88.11 (2002), p. 118102.

[26] D Wagenaar, J Pine, and S Potter. "An extremely rich repertoire of bursting patterns during the development of cortical cultures". In: *BMC Neuroscience* 7.1 (2006), p. 11.

[27] DA Wagenaar, J Pine, and SM Potter. "Searching for plasticity in dissociated cortical cultures on multi-electrode arrays". In: *Journal of Negative Results in Biomedicine* 6.1477-5751 (2006), p. 16.

[28] M Chiappalone, P Massobrio, and S Martinoia. "Network plasticity in cortical assemblies". In: *European Journal of Neuroscience* 28.1 (2008), pp. 221–237.

[29] J le Feber, T Witteveen, TM van Veenendaal, and J Dijkstra. "Repeated stimulation of cultured networks of rat cortical neurons induces parallel memory traces". In: *Learning & Memory* 22.12 (2015), pp. 594–603.

[30] P Massobrio, J Tessadori, M Chiappalone, and M Ghirardi. "In Vitro Studies of Neuronal Networks and Synaptic Plasticity in Invertebrates and in Mammals Using Multielectrode Arrays". In: *Neural Plasticity* 1.1 (2015), p. 196195.

[31] G Bi and M Poo. "Distributed synaptic modification in neural networks induced by patterned stimulation". In: *Nature* 401.6755 (1999), pp. 792–796.

[32] WH McCrea and FJW Whipple. "Random Paths in Two and Three Dimensions". In: *Proc. Roy. Soc. Edinburgh* 60 (1940), pp. 281–298.

[33] P Fries. "Neuronal Gamma-Band Synchronization as a Fundamental Process in Cortical Computation". In: *Annual Review of Neuroscience* 32.1 (2009), pp. 209–224.

[34] M Chiappalone et al. "Opposite Changes in Glutamatergic and GABAergic Transmission Underlie the Diffuse Hyperexcitability of Synapsin IDeficient Cortical Networks". In: *Cerebral Cortex* 19.6 (2009), pp. 1422–1439.

[35] MA Clifford, JK Kanwal, R Dzakpasu, and MJ Donoghue. "EphA4 expression promotes network activity and spine maturation in cortical neuronal cultures". In: *Neural Development* 6.21 (2011), pp. 1–13.

[36] EJ MacLaren, P Charlesworth, MP Coba, and SGN Grant. “Knockdown of mental disorder susceptibility genes disrupts neuronal network physiology in vitro”. In: *Molecular and Cellular Neuroscience* 47.2 (2011), pp. 93–99.

[37] TT Kanagasabapathi et al. “Functional connectivity and dynamics of cortical-thalamic networks co-cultured in a dual compartment device”. In: *Journal of Neural Engineering* 9.3 (2012), p. 036010.

Chapter 8

General discussion and conclusions

Brain circuits play an important role in the processing of, selection from and response to the constant stream of information about our environment. The external input is translated into action potential activity, the language of the brain. Action potential activity is involved in brain circuit rewiring during development (for review, see [1, 2]). Activity-dependent forms of synaptic plasticity, in particular plasticity induced by the relative timing of action potentials between connected neurons, so-called spike timing-dependent plasticity (STDP), which is a form of Hebbian plasticity, guide the formation of functional brain circuits [3]. In this thesis, we studied action potential activity and brain circuit rewiring during development, both *in silico* and *in vitro*. I start by discussing the implications of the computational part of the thesis, that is the developmental programs that underlie how brain circuits mature, specifically in terms of Hebbian plasticity (Section 8.1) and discuss the functional properties of mature circuits, sensitivity and stability, both in terms of network structure and the properties of short-term plasticity (Section 8.2). I then follow up by discussing our experimental study on the maturation of neuronal networks (Section 8.3). I end by considering how the combined experimental and computational methodology used in the thesis is useful to address neurodevelopmental disorders, and how this translates into future work (Section 8.4).

8.1 Developmental switch in Hebbian plasticity

Sensory information rewires sensory maps in the visual, somatosensory and auditory cortex during critical periods in development [4], which includes irreversible changes in the connectivity [5]. The onset of Hebbian plasticity can open a critical period [6], but how, where and when Hebbian plasticity develops is currently not clear [7]. We showed that a developmental transition in neurotransmitter release mode enables maturation of spike-timing dependent plasticity, and could thus be used to switch on Hebbian plasticity (Chapter 2). As such, this computa-

tional model mechanistically links the neurotransmitter release mode to Hebbian plasticity and learning in brain circuits during development.

The neurotransmitter release mode depends on the protein composition at the axonal terminal (for reviews see [8, 9]). We re-analyzed the human transcriptome [10] for developmental mRNA expression profiles of the relevant calcium-sensitive proteins and found that these profiles were consistent with our prediction that a switch in release mode occurs during development (Chapter 2). Furthermore, we computationally showed that the balance between the various release modes can control the rate of Hebbian plasticity (Chapter 2). The axonal terminal protein composition determines the balance between the release modes. Appropriate adjustment of this composition could thus function to regulate the rate of Hebbian plasticity. Furthermore, the composition may be regulated per individual cell or even within a cell at the level of individual axonal terminals, thereby allowing precise regulation of the rate of Hebbian plasticity. We hypothesize that pertinent transcriptional programs can regulate the onset and rate of Hebbian plasticity during development. This hypothesis is in line with recent views that the anatomy and function of the brain is mainly determined by prenatal transcriptional programs [10–12]. Understanding these programs is an essential aspect of translational research with a focus on neurodevelopmental disorders.

8.2 Sensitivity and stability in brain circuits

Even after maturation (preceding section), brain circuits in sensory areas have to learn, and be sensitive to, external input. For example, rodents can be trained to use their whiskers to detect an object that predicts a reward and respond with licking to obtain this reward [13]. The neural responses in barrel cortex to whisker stimulation are hypothesized to play an important role in performing sensory tasks [14]. It is possible to train rats to report a small number of externally induced spikes from single neurons in the sensory cortex [15, 16]. However, the barrel cortex also shows spontaneous action potential activity that is unrelated to external input [17–19]. Therefore, for brain circuits there is a trade-off between stability against noise and sensitivity to external input.

We studied whether particular wiring schemes in brain circuits can simultaneously improve stability and sensitivity. We found that networks with anti-correlations in the number of afferent (in-degree) and efferent (out-degree) synaptic connections could perform stimulus detection while remaining in a stable network state for higher levels of noise compared to positively correlated in- and out-degree networks (Chapter 3). We conclude that stimulus detection could be enhanced by anti-correlation in the degree distribution.

For standard growth models the number of pre- and postsynaptic connections for each neuron is unconstrained because each synapse is generated independently (for overview see Chapter 1). Networks that form according to these growth models have no correlation in the degree distribution. We showed that synaptic

selection by Hebbian plasticity can reshape networks with no correlation in the degree distribution into networks with anti-correlations in the degree distribution (Chapter 3). Currently, correlations in the degree distribution have not been directly quantified experimentally due to various technical limitations [20]. We suggest that by quantifying the expression of proteins typically found in the pre- and postsynaptic compartments of single neurons, the number of pre- and postsynaptic contacts can be estimated. Hence, expression data could be used to study (developmental changes in) correlations in the degree distribution.

Recently, Doron and coworkers showed that the discharge pattern of evoked spikes in single neuron stimulation affected detection probability: injections of irregular spike trains were able to evoke behavioural responses, whereas regular spike trains were not able to influence behaviour [15]. Rats are also more sensitive to irregular patterns in whisker deflection compared to regular deflections [21]. These experiments suggest that brain networks are more sensitive to the irregular spike trains induced by external stimuli, while simultaneously providing stability against more regular incoming action potential activity from noise.

We studied the role of spike train irregularity and found that in spiking neural networks and binary networks, the stimulation of a single neuron with an irregular spike train resulted in a higher probability to induce a network-wide burst of action potentials compared to regular spike trains (Chapter 4). The detection rate of irregular spike trains depended on the short-term plasticity (STP) profile of the presynaptic neuron. Thus, by adjusting the STP profile, the neurons could tune sensitivity to spike train irregularity [22]. Sensory stimuli under natural conditions often consist of temporally irregular sequences of events [21]. We hypothesize that neuronal networks are tuned to detect the irregular spike trains evoked by sensory stimuli.

During development, external inputs constantly modify the synaptic strength and network connectivity [23]. However, it seems likely that the plasticity that drives learning can only be meaningful in the context of otherwise stable, reproducible, and predictable baseline neural function [1]. How can we maintain a stable baseline neural function while also be sensitive to perturbations caused by external input? We have mechanistically shown, using a computational model, that the trade-off between sensitivity to external input and stability to spontaneous neuronal network activity can be optimized by organization of the network structure (Chapter 3) and the temporal structure of the spike train (Chapter 4). However, the overall level of network action potential activity is also important for brain circuit development [24], and can be regulated at several time scales (for overview see Chapter 1 and next section).

8.3 Action potential activity and brain circuit wiring

Neurons have a physiologically preferred level of action potential activity (putatively defined in terms of calcium concentration [25, 26]) such that deviations from this level can trigger homeostatic responses to restore action potential activity to their target activity level [1, 27]. Homeostatic control of neural function can be mediated by the regulation of ion channel expression, neurotransmitter receptor abundance, or modulation of presynaptic release [1, 26, 28]. The brain has developmental genetic programs, which are conserved across species [29], that determine the anatomy and function of brain circuits [10–12], including synapse assembly [30]. Misregulation in the timely activation of the appropriate developmental sequences could thus lead to cellular and network disturbances, ultimately leading to observable behavioral symptoms [31].

Gene expression can be regulated by epigenetic factors, which are particularly important for cellular programming during early development [32, 33]. Epigenetic factors can regulate the amount of mRNA (and thereby protein) expression without changing the DNA sequence, for example through DNA methylation or histone modifications such as methylation, acetylation and phosphorylation [34, 35]. Euchromatin histone methyltransferase-1 (EHMT1) is an epigenetic regulator involved in the modification of the chromatin structure by mono- and dimethylation of lysine 9 on histone H3 [36–38], thereby regulating developmental and neuronal genes [39]. Heterozygous mutations or deletions in *EHMT1* cause Kleefstra syndrome, a neurodevelopmental disorder that is characterized by impaired memory, autistic-like features and severe intellectual disability (ID) [40, 41]. We were interested in the effect of EHMT1 deficiency on the emergence of structured network activity during development. We used Multi-Electrode Arrays (MEAs) and intracellular recordings to study the action potential activity in cultures of developing cortical neurons. Cortical neurons in culture show typical synchronized network activity, often referred to as bursts [42, 43]. We first developed a pre-processing method to improve the analysis of action potential activity on MEAs (Chapter 5). For the EHMT1-deficient cortical cultures we found a reduction in the burst rate and firing rate during early development (Chapter 6). Later in development these rates were restored to their wild-type values. However, the burst patterns at this later stage were more irregular for the EHMT1-deficient neurons (Chapter 6). The transient reduction in action potential activity during early development thus resulted in impaired network activity later in development.

Action potential activity is a read-out of brain circuit functioning. Appropriate levels of action potential activity during development are necessary for learning and wiring in functional brain circuits. Indeed, hyperactive neuronal activity during the critical learning period has been suggested to explain the phenotype of Fragile X syndrome (FXS) [44]. The FXS mouse model presents an interesting example for how genetic factors affect the development of structured

network activity. In wild type mice (*in vivo*), cortical activity changes during early development from synchronized activity, characterized by network bursts, to desynchronized activity [45]. In Fragile X mice this transition is delayed [44], yielding higher correlation coefficients between calcium transients in L2/3 neurons imaged *in vivo*. In addition, the mean firing rate during up and down states is increased. A definite mechanistic explanation has not yet conclusively been determined, but three explanations are consistent with other experimental data. First, defects in the maturation of dendritic spines in the second postnatal week, could lead to hyperconnectivity [46]. Second, less efficient inhibition could be due to decreased excitatory drive to inhibitory neurons [47, 48]. Third, defects related to membrane excitability could cause the differences in firing rate [47]. The key question is how the genetic effect can lead to the observed network changes. The experimental observations in the Fragile X mice relate network synchrony to a difference in firing rate, just as we reported for the EHMT1 deficienct neuronal cultures in Chapter 6, for which we observed a reduction in firing rate and synchrony (bursting and autocovariance) during early development. It stands to reason that one should consider and carefully evaluate the same potential causes for the EHMT1 induced delay in maturation in future experimental work utilizing the slice preparation or *in vivo* measurements.

Previous experiments in *Ehmt1*$^{+/-}$ mice showed a decrease in release probability at the CA3-CA1 synapse [49]. Likewise, in EHMT1-deficient cortical neurons, we found a decrease in action potential-dependent synaptic input (Chapter 6). The impaired action-potential dependent synaptic transmission was temporally aligned to the transition from uncorrelated spiking to network-wide burst spiking, which also coincided with the time point at which hippocampal neuronal cultures switch their mode of release from exclusively spontaneous to predominantly evoked [50]. As we showed in Chapter 2, the transition from action potential-independent neurotransmitter release to action potential-dependent release initiates a period of rapid circuit rewiring. Impairments in action potential activity and synaptic transmission at this stage of development could thus lead to miswiring of the circuitry, thereby emphasizing the importance of timely regulation of gene expression and action potential activity during development. Indeed, mistiming in developmental processes [31] and altered wiring during early development has been proposed to underlie several phenotypes associated with neurodevelopmental disorders, including ID and autism [46, 51, 52]. The next step is to adapt the neural network models from Chapter 2 and 3 by including the appropriate homeostatic mechanisms and the EHMT1 induced deficiencies. This approach critically needs experimental data on which cell type (inhibitory versus excitation), and which proteins are most strongly effected by the deficiency. This data can only be obtain by combining whole transcriptome techniques to determine which protein expression is affected (i.e. RNA-seq), intracellular recordings to determine effects on unitary synaptic transmission (whole-cell patch clamp, as reported in this thesis for excitatory transmission), intrinsic cell excitability and extracellular recordings to determine the changes in activity patterns (MEA, as

reported in this thesis).

The observations that action potential activity and brain circuit rewiring are important for normal brain development are supported by other recent genetic studies on MEA, in which abnormal action potential activity was linked to psychiatric disorders, such as bipolar disorder and schizophrenia [53]. Our findings in EHMT1-deficient neurons (Chapter 6) thus align with the expanding evidence that impaired action potential activity in developing neuronal circuits is related to neurodevelopmental and neuropsychiatric disorders and can thus function as a simple index with which to quantify the effect of loss-of-function of particular genes and to determine which genetic therapies might be effective.

8.4 Future directions

Monogenic forms of neurodevelopmental disorders such as ID and autism can be caused by a single mutation in more than 450 different genes [54]. For example, FXS, discussed in the section above and the most common monogenetic cause of ID and autism spectrum disorders, is associated with mutations in the FMR1 gene [55, 56]. The normal function of FMR1 includes the translational regulation of multiple mRNAs (which contain the code for proteins) [57]. Loss-of-function of FMR1 is involved in multiple cellular impairments, including altered synaptic plasticity [58]. Furthermore, loss-of-function of single epigenetic and transcription factors, including EHMT1 (Chapter 6) and FOXP2 (Figure 7.3), has been implicated in neurodevelopmental disorders [40, 41, 59].

Given that for none of the known monogenetic causes of neurodevelopmental disorders any treatment is available, it is likely that it will take much more time and may require the implementation of novel research strategies to unravel the etiology of epigenetically determined and/or polygenic brain disorders (in which genetic variants affecting multiple genes are required to cause the disorder) e.g. ID and polygenic forms of autism [54, 60–62].

I expect that monitoring action potential activity during critical periods of brain development will be important to understand neurodevelopmental disorders. Technologies have enabled the longitudinal monitoring of neuronal cultures during development, and large-scale initiatives heavily invest in technologies to record brain activity *in vivo* [63]. We developed PDMS microstructures that can be placed on MEAs to record action potential activity in small connected neuronal networks, with the aim of studying learning and communication (Chapter 7). The structured networks that we obtained could allow for experiments that are currently difficult to perform in large neuronal networks on MEAs. Experiments on large, unstructured networks have encountered difficulties in the application of plasticity protocols to obtain functional changes in spiking activity [64], although a few protocols did succesfully induce plasticity [65–67]. The four quadrant approach piloted in Chapter 7 will help to improve application of plasticity protocols, because the cells can be spatially targeted.

I speculate that computational neuroscience has an important role in the construction of platforms to integrate and analyse the large quantities of data that are generated by these new technologies [68]. Computational neuroscience can formalize factors that affect brain circuit function, including learning (Chapter 2) and sensitivity and stability (Chapter 3 and 4). The goal of these developments should be to understand *when* and *where* neuronal dysfunction occurs, and integrate knowledge to better understand *why* it occurs, and ultimately bring these results together to understand *how* neuronal network activity could be restored.

To understand misregulation in action potential activity, a detailed description of the factors that contribute to neuronal circuit functioning is important. We observed several advantages to studying development of action potential activity in neuronal cell cultures compared to chronic *in vivo* recordings, including (1) rapid, low-cost genetic and/or pharmacological manipulation, (2) access to tools for longitudinal monitoring and (3) carefully controlled external input during development. For studying genes that code for epigenetic or transcription factors, it is important to realise that when multiple cellular functions are disrupted simultaneously during disease, the impairment may not be additive, but multiplicative in terms of adaptation to sudden changes in action potential activity (Figure 8.1). Recordings from, and computational modelling of, cultured neurons are valuable to understand and predict (misregulation) in brain circuits. Brain circuits are highly adaptive, exemplified by studies that have shown that deleting a gene coding for a particular ion channel invokes compensatory changes in the expression of other ion channels [1, 28, 69–71]. I expect that for therapeutic intervention in neurodevelopmental disorders it may therefore not be necessary to compensate for all cellular dysfunctions and that restoring key molecular deficits at the appropriate time may be sufficient to ameliorate symptoms.

Traditionally, scientific research has been a hypothesis-driven investigation of an observation (Figure 8.2A). For example, a group of patients displays a similar disease phenotype X (an observation), which is potentially caused by a genetic defect (a hypothesis). One can then test this hypothesis by comparing the genomes between the patients and a control group (the experiment). The outcome of this study, for example a particular hit for a gene causing disease X, is a new observation.

We suggest and have also applied (Chapters 2 and 3) an approach in which computational modeling is used to generate novel hypotheses, which are then translated into molecular targets (Figure 8.2B). For example, computational models could assist in the exploration of brain dynamics to generate a hypothesis about a specific cellular dysfunction. The cellular dysfunction should be translated into molecular targets, such that specific experiments aimed at modulating these targets can be designed and, eventually, the outcome of these experiments can even be predicted using the ever increasing amount of publicly available data.

The amount of protein that is expressed varies among cell types, developmental stages and brain regions [10–12]. Furthermore, on average each person carries approximately 250 to 300 loss-of-function variants in annotated genes and

50 to 100 variants previously implicated in inherited disorders [72]. Therapeutic intervention for neurodevelopmental disorders may thus require detailed understanding of brain circuit development, with annotated roles for a wide range of proteins, which are ideally combined into a computational model of the (developing) brain. The ultimate goal is to be able to use the computational model to derive medication that is tailored to the individual patient (Figure 8.2C). Pioneers using a similar approach have successfully modeled *Mycoplasma genitalium*, a pathogen found in humans, accounting for all annotated gene functions found in these bacteria [73]. Up-scaling to the human brain will benefit from the recently started large-scale initiative involving analysis and data sharing infrastructure [68] as well as currently available public data bases [12, 74]. New high-throughput technological developments [75] to gather the necessary data at affordable cost (i.e. genetic and expression profiling) will allow the extensive characterization of neurons [76] and accelerate the contribution of computational neuroscience to the generation of novel hypotheses and eventually to the development and application of personalized medicine for neurodevelopmental disorders.

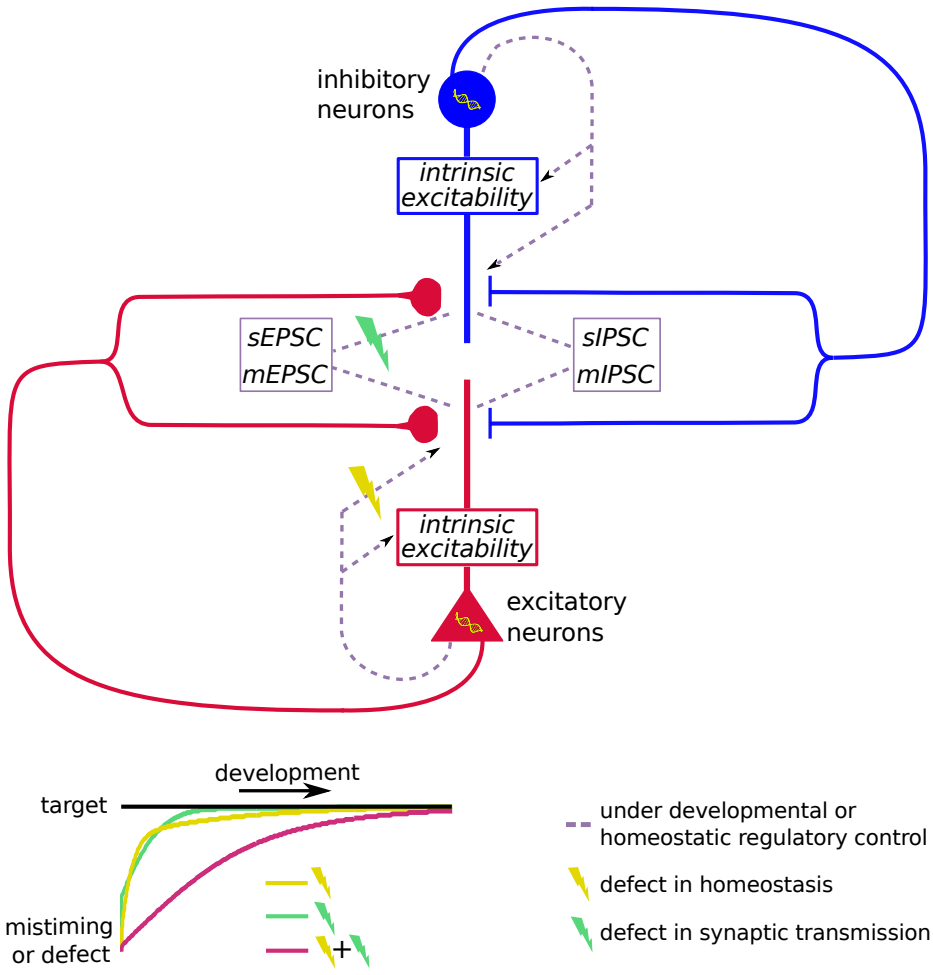

Figure 8.1: Action potential activity is regulated at multiple levels in recurrent brain circuits. Inhibition (depicted in blue) and synaptic communication (subdivided in spontaneous vesicle exocytosis (SVE) and evoked vesicle exocytosis (EVE)) provide immediate control of action potential activity, on a timescale of milliseconds to seconds, whereas homeostatic plasticity (purple striped lines) provide network stability over longer time scales of hours to days. Defects (denoted by a lightning symbol) in a synaptic or cellular process could lead to abnormal action potential activity in neuronal networks. Simultaneous defects in multiple processes could either cancel (not shown) or cause a multiplicative (red trace) impairment in reaching the target action potential activity level [77].

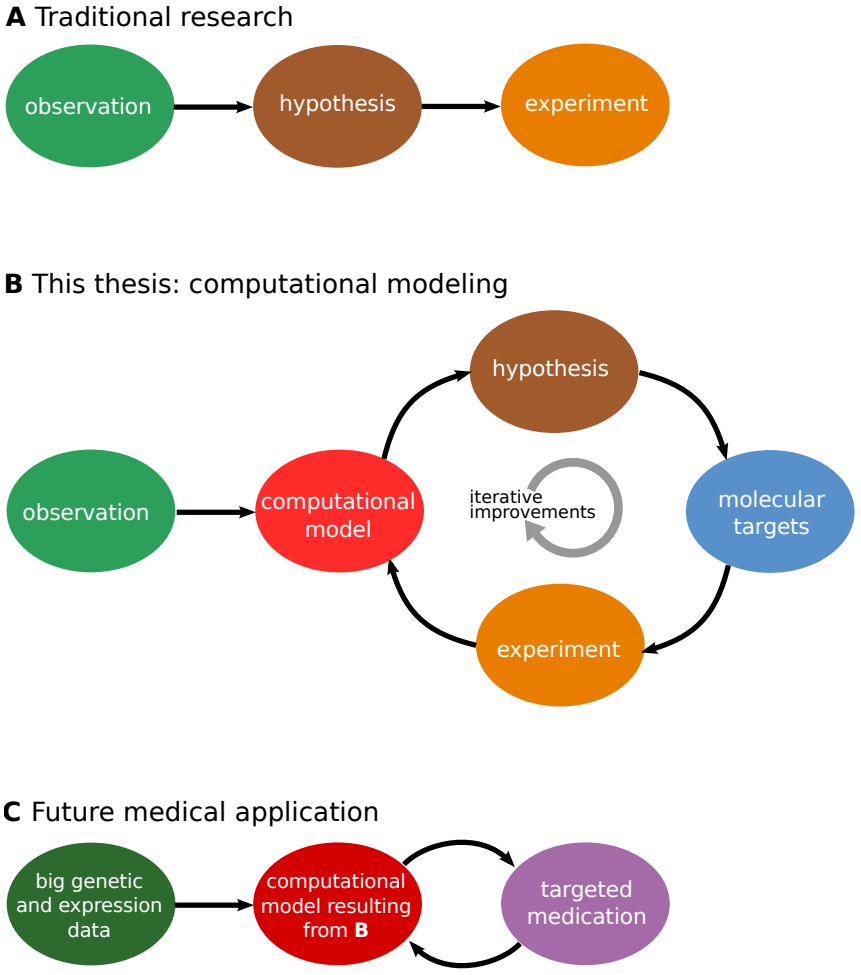

Figure 8.2: Computational modeling and neuroscience research. ***A****: Traditionally, observations have been the inspiration for hypothesis-driven experiments.* ***B****: Observations can also be studied through computational models. Computational models can provide for more targeted novel hypothesis generation because they can make the link between small-scale molecular effects and large-scale brain dynamics and behaviour. Importantly, as demonstrated in this thesis, the computational hypotheses and predictions should be translated into molecular targets. Experiments* in vitro *and* in vivo *using these molecular targets can accept (or reject) the hypotheses and thereby iteratively improve the computational model.* ***C****: The ultimate goal is to apply the computational model (from* ***B****) to predict targeted medication from "big" genetic and expression data, potentially for individual patients.*

References

[1] GW Davis. "Homeostatic Signaling and the Stabilization of Neural Function". In: *Neuron* 80.3 (2013), pp. 718–728.

[2] LC Andreae and J Burrone. "The role of neuronal activity and transmitter release on synapse formation". In: *Current Opinion in Neurobiology* 27 (2014), pp. 47–52.

[3] D Ko, CJ Wilson, CJ Lobb, and C Paladini. "Detection of bursts and pauses in spike trains". In: *Journal of Neuroscience Methods* 211.1 (2012), pp. 145–158.

[4] RS Erzurumlu and P Gaspar. "Development and critical period plasticity of the barrel cortex". In: *European Journal of Neuroscience* 35.10 (2012), pp. 1540–1553.

[5] DH Bhatt, S Zhang, and W Gan. "Dendritic Spine Dynamics". In: *Annual Review of Physiology* 71.1 (2009), pp. 261–282.

[6] T Toyoizumi et al. "A Theory of the Transition to Critical Period Plasticity: Inhibition Selectively Suppresses Spontaneous Activity". In: *Neuron* 80.1 (2013), pp. 51–63.

[7] P Caroni, F Donato, and D Muller. "Structural plasticity upon learning: regulation and functions". In: *Nat Rev Neurosci* 13.7 (2012), pp. 478–490.

[8] R Jahn and D Fasshauer. "Molecular machines governing exocytosis of synaptic vesicles". In: *Nature* 490.7419 (2012), pp. 201–207.

[9] PS Kaeser and WG Regehr. "Molecular Mechanisms for Synchronous, Asynchronous, and Spontaneous Neurotransmitter Release". In: *Annual Review of Physiology* 76.1 (2014), pp. 333–363.

[10] MJ Hawrylycz et al. "An anatomically comprehensive atlas of the adult human brain transcriptome". In: *Nature* 489.7416 (2012), pp. 391–399.

[11] JA Miller et al. "Transcriptional landscape of the prenatal human". In: *Nature* 508.7495 (2014), pp. 199–206.

[12] Hyo J Kang et al. "Spatio-temporal transcriptome of the human brain". In: *Nature* 478.7370 (2011), pp. 483–489.

[13] D Huber et al. "Multiple dynamic representations in the motor cortex during sensorimotor learning". In: *Nature* 484.7395 (2012), pp. 473–478.

[14] CCH Petersen and S Crochet. "Synaptic Computation and Sensory Processing in Neocortical Layer 2/3". In: *Neuron* 78.1 (2013), pp. 28–48.

[15] G Doron, M von Heimendahl, P Schlattmann, AR Houweling, and M Brecht. "Spiking Irregularity and Frequency Modulate the Behavioral Report of Single-Neuron Stimulation". In: *Neuron* 81.3 (2014), pp. 653–663.

[16] AR Houweling and M Brecht. "Behavioural report of single neuron stimulation in somatosensory cortex". In: *Nature* 451.7174 (2008), pp. 65–68.

[17] AL Barth and JFA Poulet. "Experimental evidence for sparse firing in the neocortex". In: *Trends in Neurosciences* 35.6 (2012), pp. 345–355.

[18] DS Greenberg, AR Houweling, and JND Kerr. “Population imaging of ongoing neuronal activity in the visual cortex of awake rats”. In: *Nat Neurosci* 11.7 (2008), pp. 749–751.

[19] CPJ de Kock and B Sakmann. “Spiking in primary somatosensory cortex during natural whisking in awake head-restrained rats is cell-type specific”. In: *Proceedings of the National Academy of Sciences* 106.38 (2009), pp. 16446–16450.

[20] JC Vasquez, AR Houweling, and PHE Tiesinga. “Simultaneous stability and sensitivity in model cortical networks is achieved through anti-correlations between the in- and out-degree of connectivity”. In: *Frontiers in Computational Neuroscience* 7.156 (2013).

[21] A Lak, E Arabzadeh, and ME Diamond. “Enhanced Response of Neurons in Rat Somatosensory Cortex to Stimuli Containing Temporal Noise”. In: *Cerebral Cortex* 18.5 (2008), pp. 1085–1093.

[22] H Markram, Y Wang, and M Tsodyks. “Differential signaling via the same axon of neocortical pyramidal neurons”. In: *Proceedings of the National Academy of Sciences* 95.9 (1998), pp. 5323–5328.

[23] A Maffei and A Fontanini. “Network homeostasis: a matter of coordination”. In: *Current Opinion in Neurobiology* 19.2 (2009), pp. 168–173.

[24] GG Turrigiano and SB Nelson. “Homeostatic plasticity in the developing nervous system”. In: *Nat Rev Neurosci* 5.2 (2004), pp. 97–107.

[25] E Marder and J Goaillard. “Variability, compensation and homeostasis in neuron and network function”. In: *Nat Rev Neurosci* 7.7 (2006), pp. 563–574.

[26] T OLeary, AH Williams, A Franci, and E Marder. “Cell Types, Network Homeostasis, and Pathological Compensation from a Biologically Plausible Ion Channel Expression Model”. In: *Neuron* 82.4 (2014), pp. 809–821.

[27] G Turrigiano. “Too Many Cooks? Intrinsic and Synaptic Homeostatic Mechanisms in Cortical Circuit Refinement”. In: *Annual Review of Neuroscience* 34.1 (2011), pp. 89–103.

[28] S Bergquist, DK Dickman, and GW Davis. “A Hierarchy of Cell Intrinsic and Target-Derived Homeostatic Signaling”. In: *Neuron* 66.2 (2010), pp. 220–234.

[29] AD Workman, CJ Charvet, B Clancy, RB Darlington, and BL Finlay. “Modeling Transformations of Neurodevelopmental Sequences across Mammalian Species”. In: *The Journal of Neuroscience* 33.17 (2013), pp. 7368–7383.

[30] LM Valor, P Charlesworth, L Humphreys, CNG Anderson, and Seth GN Grant. “Network activity-independent coordinated gene expression program for synapse assembly”. In: *Proceedings of the National Academy of Sciences* 104.11 (2007), pp. 4658–4663.

[31] Y Ben-Ari and NC Spitzer. “Phenotypic checkpoints regulate neuronal development”. In: *Trends in Neurosciences* 33.11 (2010), pp. 485–492.

[32] M Fagiolini, CL Jensen, and FA Champagne. "Epigenetic influences on brain development and plasticity". In: *Current Opinion in Neurobiology* 19.2 (2009). Development, pp. 207–212.

[33] I Cantone and AG Fisher. "Epigenetic programming and reprogramming during development". In: *Nat Struct Mol Biol* 20.3 (2013), pp. 282–289.

[34] TL Bale. "Epigenetic and transgenerational reprogramming of brain development". In: *Nat Rev Neurosci* 16.6 (2015), pp. 332–344.

[35] M Benevento, M van de Molengraft, R van Westen, H van Bokhoven, and NN Kasri. "The role of chromatin repressive marks in cognition and disease: A focus on the repressive complex GLP/G9a". In: *Neurobiology of Learning and Memory* 124 (2015), pp. 88–96.

[36] M Tachibana et al. "Histone methyltransferases G9a and GLP form heteromeric complexes and are both crucial for methylation of euchromatin at H3-K9". In: *Genes & Development* 19.7 (2005), pp. 815–826.

[37] H He and N Lehming. "Global effects of histone modifications". In: *Briefings in Functional Genomics & Proteomics* 2.3 (2003), pp. 234–243.

[38] JC Rice et al. "Histone Methyltransferases Direct Different Degrees of Methylation to Define Distinct Chromatin Domains". In: *Molecular Cell* 12.6 (2003), pp. 1591–1598.

[39] C Mozzetta et al. "The Histone H3 Lysine 9 Methyltransferases G9a and GLP Regulate Polycomb Repressive Complex 2-Mediated Gene Silencing". In: *Molecular Cell* 53.2 (2014), pp. 277–289.

[40] T Kleefstra et al. "Loss-of-Function Mutations in Euchromatin Histone Methyl Transferase 1 (EHMT1) Cause the 9q34 Subtelomeric Deletion Syndrome". In: *The American Journal of Human Genetics* 79.2 (2006), pp. 370–377.

[41] T Kleefstra et al. "Disruption of an EHMT1-Associated Chromatin-Modification Module Causes Intellectual Disability". In: *The American Journal of Human Genetics* 91.1 (2012), pp. 73–82.

[42] M Chiappalone, M Bove, A Vato, M Tedesco, and S Martinoia. "Dissociated cortical networks show spontaneously correlated activity patterns during in vitro development". In: *Brain Research* 1093.1 (2006), pp. 41–53.

[43] M Chiappalone, A Vato, L Berdondini, M Koudelka-hep, and S Martinoia. "Network dynamics and synchronous activity in cultured cortical neurons". In: *International Journal of Neural Systems* 17.02 (2007), pp. 87–103.

[44] JT Goncalves, JE Anstey, P Golshani, and C Portera-Cailliau. "Circuit level defects in the developing neocortex of Fragile X mice". In: *Nat Neurosci* 16.7 (2013), pp. 903–909.

[45] P Golshani et al. "Internally Mediated Developmental Desynchronization of Neocortical Network Activity". In: *The Journal of Neuroscience* 29.35 (2009), pp. 10890–10899.

[46] G Testa-Silva et al. "Hyperconnectivity and Slow Synapses during Early Development of Medial Prefrontal Cortex in a Mouse Model for Mental Retardation and Autism". In: *Cerebral Cortex* 22.6 (2012), pp. 1333–1342.

[47] JR Gibson, AF Bartley, SA Hays, and KM Huber. "Imbalance of Neocortical Excitation and Inhibition and Altered UP States Reflect Network Hyperexcitability in the Mouse Model of Fragile X Syndrome". In: *Journal of Neurophysiology* 100.5 (2008), pp. 2615–2626.

[48] SM Paluszkiewicz, Martin BS, and Huntsman MM. "Fragile X Syndrome: The GABAergic System and Circuit Dysfunction". In: *Developmental Neuroscience* 33.5 (2011), pp. 349–364.

[49] MCM Balemans et al. "Hippocampal dysfunction in the Euchromatin histone methyltransferase 1 heterozygous knockout mouse model for Kleefstra syndrome". In: *Human Molecular Genetics* 22.5 (2013), pp. 852–866.

[50] LC Andreae, NB Fredj, and J Burrone. "Independent Vesicle Pools Underlie Different Modes of Release during Neuronal Development". In: *Journal of Neuroscience* 32.5 (2012), pp. 1867–1874.

[51] Dh Geschwind and P Levitt. "Autism spectrum disorders: developmental disconnection syndromes". In: *Current Opinion in Neurobiology* 17.1 (2007), pp. 103–111.

[52] JLR Rubenstein and MM Merzenich. "Model of autism: increased ratio of excitation/inhibition in key neural systems". In: *Genes, Brain and Behavior* 2.5 (2003), pp. 255–267.

[53] EJ MacLaren, P Charlesworth, MP Coba, and SGN Grant. "Knockdown of mental disorder susceptibility genes disrupts neuronal network physiology in vitro". In: *Molecular and Cellular Neuroscience* 47.2 (2011), pp. 93–99.

[54] H van Bokhoven. "Genetic and Epigenetic Networks in Intellectual Disabilities". In: *Annual Review of Genetics* 45.1 (2011), pp. 81–104.

[55] EJ Kremer et al. "Mapping of DNA instability at the fragile X to a trinucleotide repeat sequence p(CCG)n". In: *Science* 252.5013 (1991), pp. 1711–1714.

[56] S Zeidler, RK Hukema, and R Willemsen. "The quest for targeted therapy in fragile X syndrome". In: *Expert Opinion on Therapeutic Targets* 19.10 (2015), pp. 1277–1281.

[57] C Bagni and BA Oostra. "Fragile X syndrome: From protein function to therapy". In: *American J of Medical Genetics Part A* 161.11 (2013), pp. 2809–2821.

[58] KM Huber, SM Gallagher, ST Warren, and MF Bear. "Altered synaptic plasticity in a mouse model of fragile X mental retardation". In: *Proceedings of the National Academy of Sciences* 99.11 (2002), pp. 7746–7750.

[59] SC Vernes et al. "Foxp2 Regulates Gene Networks Implicated in Neurite Outgrowth in the Developing Brain". In: *PLoS Genet* 7.7 (2011), e1002145.

[60] H van Bokhoven and JM Kramer. "Disruption of the epigenetic code: An emerging mechanism in mental retardation". In: *Neurobiology of Disease* 39.1 (2010), pp. 3–12.

[61] T Kleefstra, A Schenck, JM Kramer, and H van Bokhoven. "The genetics of cognitive epigenetics". In: *Neuropharmacology* 80 (2014), pp. 83–94.

[62] G Poelmans, B Franke, DL Pauls, JC Glennon, and JK Buitelaar. "AKAPs integrate genetic findings for autism spectrum disorders". In: *Translational Psychiatry* 3.6 (2013), e270.

[63] H Shen. "Neurotechnology: BRAIN storm". In: *Nature* 503 (2013), pp. 26–28.

[64] DA Wagenaar, J Pine, and SM Potter. "Searching for plasticity in dissociated cortical cultures on multi-electrode arrays". In: *Journal of Negative Results in Biomedicine* 6.1477-5751 (2006), p. 16.

[65] M Chiappalone, P Massobrio, and S Martinoia. "Network plasticity in cortical assemblies". In: *European Journal of Neuroscience* 28.1 (2008), pp. 221–237.

[66] J le Feber, T Witteveen, TM van Veenendaal, and J Dijkstra. "Repeated stimulation of cultured networks of rat cortical neurons induces parallel memory traces". In: *Learning & Memory* 22.12 (2015), pp. 594–603.

[67] P Massobrio, J Tessadori, M Chiappalone, and M Ghirardi. "In Vitro Studies of Neuronal Networks and Synaptic Plasticity in Invertebrates and in Mammals Using Multielectrode Arrays". In: *Neural Plasticity* 1.1 (2015), p. 196195.

[68] A Abbott. "Brain-simulation and graphene projects win billion-euro competition". In: *Nature* (2013).

[69] A Van Wart and G Matthews. "Impaired Firing and Cell-Specific Compensation in Neurons Lacking Nav1.6 Sodium Channels". In: *The Journal of Neuroscience* 26.27 (2006), pp. 7172–7180.

[70] JN MacLean, Y Zhang, BR Johnson, and RM Harris-Warrick. "Activity-Independent Homeostasis in Rhythmically Active Neurons". In: *Neuron* 37.1 (2003), pp. 109–120.

[71] AM Swensen and BP Bean. "Robustness of Burst Firing in Dissociated Purkinje Neurons with Acute or Long-Term Reductions in Sodium Conductance". In: *The Journal of Neuroscience* 25.14 (2005), pp. 3509–3520.

[72] The 1000 Genomes Project Consortium. "A map of human genome variation from population-scale sequencing". In: *Nature* 467.7319 (2010), pp. 1061–1073.

[73] JR Karr et al. "A Whole-Cell Computational Model Predicts Phenotype from Genotype". In: *Cell* 150.2 (2012), pp. 389–401.

[74] *Allen Brain Atlas [Internet]*. `http://www.brain-map.org`. 2015.

[75] ML Metzker. "Sequencing technologies [mdash] the next generation". In: *Nat Rev Genetics* 11.1 (2010), pp. 31–46.

[76] A Zeisel et al. "Cell types in the mouse cortex and hippocampus revealed by single-cell RNA-seq". In: *Science* 347.6226 (2015), pp. 1138–1142.

[77] MB Ramocki and HY Zoghbi. "Failure of neuronal homeostasis results in common neuropsychiatric phenotypes". In: *Nature* 455.7215 (2008), pp. 912–918.

Summary

We can learn from and adapt to our environment, an astonishing feat that is made possible because of circuits in our brain that are plastic. We observe our environment using sensory organs which translate information into electrical pulses called action potentials, the language of the brain. Action potentials play an important role in the rewiring (shaping) of brain circuits, particularly during development. Abnormal action potential activity and incorrect brain circuit rewiring are thought to underlie a number of neurodevelopmental disorders. In this thesis we used *in silico* (computer) and *in vitro* (cell culture) techniques to understand the role of action potential activity in the emergence of brain circuits.

In **Chapter 1**, we introduced concepts regarding the development of brain circuits and discussed cellular mechanisms that regulate the level of action potential activity. We then explained the use of the Multi-Electrode Array (MEA) technique, which we applied to perform many of our experiments.

In **Chapter 2**, we computationally studied the onset of an important form of learning, so-called Hebbian plasticity. Neurons are connected by synapses: contact points that can release neurotransmitters to chemically transmit information from one neuron to another. Neurotransmitters can be released via various mechanisms (modes), which differ in their timing of release relative to an action potential. We showed that a developmental transition in neurotransmitter release mode can initiate Hebbian plasticity. The balance between the various release modes determined the rate at which Hebbian plasticity occurred. These findings thus showed a novel mechanism by which Hebbian plasticity in brain circuits can be regulated.

In **Chapter 3**, we computationally investigated the stability and sensitivity of brain circuits. Stability of brain circuits is important to avoid action potential responses caused by irrelevant electrical fluctuations, also called 'noise'. At the same time, the brain circuits need to be sensitive to similarly-sized electrical inputs from our sensory organs. Optimizing stability and sensitivity simultaneously is difficult. Each neuron in a brain circuit has a number of incoming connections from other neurons (in-degree) and a number of outgoing connections to other neurons (out-degree). We showed that brain circuits in which neurons have a high

out-degree and also a low in-degree (or *vice versa*), displayed increased stability to high levels of noise, while remaining sensitive to external action potential input in comparison to other network structures. Thus, the brain may use this wiring strategy to improve both the stability and sensitivity in brain circuits.

In **Chapter 4**, we computationally studied brain circuit sensitivity to single neuron stimulation. Here, we found that the temporal ordering of the action potentials had an effect on stimulus detectability. Sensory stimuli often consist of action potential trains that have high irregularity in action potential sequences. Hence, brain circuits may use irregularity in action potential trains to their advantage when detecting natural stimuli in a noisy environment.

Chapter 5 described a methodological study to detect action potential bursts, which indicate a synchronous activation of neuronal networks, and furthermore allows to filter out noisy background action potentials. We tested this method on data that we collected using MEAs. MEAs consist of electrodes embedded in a glass substrate on which neuronal cell cultures are grown. The electrodes record action potentials of nearby neurons. We found that the detection of a burst of action potentials was difficult when existing detection methods were used. Therefore, we developed a pre-processing method to increase the reliability of burst detection and verified our method using culture recordings as well as simulated data.

In **Chapter 6**, we experimentally studied the role of the gene that encodes the epigenetic regulator Euchromatin Histone Methyltransferase 1 (EHMT1) in neurodevelopment. In humans, a loss-of-function mutation in this gene causes Kleefstra syndrome, an intellectual disability disorder. Using MEA and intracellular recordings from neuronal cell cultures, we observed that EHMT1 deficiency led to a reduction in the action potential and burst rates early in development, which later in development resulted in disorganized network activity. These developmental impairments may contribute to the pathophysiology of Kleefstra syndrome.

In **Chapter 7**, we developed a method to grow, on MEAs, small neuronal networks in polymer compartments that are connected to each other. This new technique allows investigations on neuronal plasticity, communication and processing that were previously challenging when performed in large neuronal networks cultured on MEAs without compartments.

In **Chapter 8**, we discussed our findings in a broader context and provided an outlook on future developments in the field of computational neuroscience, with a focus on clinical relevance.

Taken together, our computational results and cell culture recordings provide insights into the emergence of brain circuits during development, and as such contribute to our understanding of the etiology of neurodevelopmental disorders.

Samenvatting

We nemen onze omgeving waar en kunnen ons eraan aanpassen, een verbazingwekkende prestatie die mogelijk gemaakt wordt door de plasticiteit (vormbaarheid) van netwerken van zenuwcellen in onze hersenen. De verworven informatie wordt door onze zintuigen omgezet naar elektrische pulsen, zogenaamde actiepotentialen, de taal van het brein. Actiepotentialen hebben een belangrijke rol bij de vorming van onze hersennetwerken, met name tijdens de vroege ontwikkelingsfase. Men denkt dat abnormale activiteit van actiepotentialen en afwijkende vorming van hersennetwerken verantwoordelijk zijn voor het ontstaan van hersenontwikkelingsstoornissen. In dit proefschrift gebruikten wij *in silico* (computer) en *in vitro* (celkweek) technieken om inzicht te krijgen in de rol van actiepotentialen bij de vorming van hersennetwerken.

In **Hoofdstuk 1** introduceerden we concepten betreffende de ontwikkeling van hersennetwerken en bespraken we cellulaire mechanismen die het niveau van actiepotentiaalactiviteit regelen. Ook werd uitleg gegeven over de Multi-Electrode Array (MEA) techniek die we voor veel van onze experimenten gebruikt hebben.

In **Hoofdstuk 2** bestudeerden we het aanschakelen van zogenaamd Hebbiaans leren, een belangrijke vorm van synaptische plasticiteit die betrokken is bij leren. Zenuwcellen zijn met elkaar verbonden via synapsen: de contactpunten die chemische boodschappers (neurotransmitters) af kunnen geven om informatie over te dragen van de ene zenuwcel naar een andere zenuwcel. Neurotransmitters kunnen op verschillende manieren (modes) worden afgegeven. Deze modes verschillen doordat de actiepotentiaal direct kan leiden tot neurotransmitter-afgifte of dat de actiepotentiaal kan leiden tot neurotransmitter-afgifte op een later tijdstip. De balans tussen deze modes bepaalde de snelheid waarmee Hebbiaans leren plaatsvond. Deze bevinding liet dus een nieuw mechanisme zien waarmee Hebbiaans leren gereguleerd kan worden in hersennetwerken.

In **Hoofdstuk 3** gebruikten we computersimulaties om de stabiliteit en gevoeligheid van hersennetwerken te bestuderen. Stabiliteit is belangrijk om te voorkomen dat irrelevante elektrische fluctuaties, ook wel ruis genoemd, leiden tot een te grote hoeveelheid actiepotentiaalactiviteit. Tegelijkertijd is het belangrijk dat hersennetwerken gevoelig blijven voor elektrische signalen vanuit onze zintuigen die in

orde van grootte vergelijkbaar zijn met de ruis. Het gelijktijdig optimaliseren van stabiliteit en gevoeligheid is moeilijk. Elke zenuwcel in een netwerk heeft een aantal inkomende contactpunten vanuit andere zenuwcellen (de in-degree) en een aantal uitgaande contactpunten naar andere zenuwcellen (de out-degree). Wij lieten zien dat hersennetwerken waarin zich cellen bevinden met een hoge out-degree en ook een lage in-degree hebben (of *vice versa*), stabieler waren bij hoge hoeveelheden ruis, terwijl ze toch gevoelig bleven voor externe input van actiepotentialen. De hersenen kunnen deze strategie dus gebruiken om zowel de stabiliteit als de gevoeligheid van hersennetwerken te verbeteren.

In **Hoofdstuk 4** bestudeerden we met computersimulaties de gevoeligheid van hersennetwerken ten aanzien van stimulatie in één enkele zenuwcel. Wij vonden hierbij dat de regelmaat in de tijdsintervallen waarmee actiepotentialen het netwerk ingestuurd werden, bepalend was voor de gevoeligheid van het netwerk. Zintuigen sturen relatief veel onregelmatige signalen naar hersennetwerken, wat dus een manier kan zijn om signalen uit de omgeving beter te kunnen detecteren.

Hoofdstuk 5 beschreef een methodologische studie om 'bursts' van actiepotentialen te detecteren. Bursts geven aan dat zenuwcellen tegelijk geactiveerd zijn. Bovendien kan deze methode gebruikt worden om ruis uit de data te filteren. We testten deze methode op MEA data. MEAs zijn elektrodes die verwerkt zijn in een glazen plaat waarop de zenuwcellen gekweekt worden en waarmee (bursts van) actiepotentialen gemeten kunnen worden. Bestaande methodes voor het detecteren van bursts waren ontoereikend voor ons onderzoek. Met de hier ontwikkelde methode konden we de betrouwbaarheid van de burst-detectie verbeteren.

In **Hoofdstuk 6** bestudeerden we met behulp van elektrofysiologische metingen, zoals MEA, de rol van een gen dat codeert voor de epigenetische regulator Euchromatine Histon Methyltransferase 1 (EHMT1) tijdens de vroege ontwikkeling. Bij mensen veroorzaakt een 'loss-of-function' mutatie in dit gen het Kleefstra-syndroom, een stoornis van het intellect. We vonden dat een tekort aan EHMT1 in kweekjes van zenuwcellen leidde tot een verminderde actiepotentiaalactiviteit tijdens de vroege ontwikkeling, waarbij dit later in de ontwikkeling leidde tot een grotere wanorde in de activiteit van de kweekjes. Dit waargenomen ontwikkelingsprofiel kan bijdragen aan de pathofysiologie van het Kleefstra-syndroom.

In **Hoofdstuk 7** lieten we zien hoe kleine hersennetwerken, die groeien op een MEA, met elkaar verbonden kunnen worden via microtunnels. Deze techniek biedt nieuwe mogelijkheden om plasticiteit en communicatie te bestuderen; zulke onderzoeken zijn moeilijk uit te voeren met grote hersennetwerken.

In **Hoofdstuk 8** plaatsten we onze bevindingen in een bredere context en gaven we een overzicht van ontwikkelingen die we voorzien binnen de neurowetenschappen, waarbij we vooral aandacht schonken aan de klinische relevantie.

Samenvattend geven de resultaten verkregen uit onze computermodellen en celkweek-metingen meer inzicht in de vorming van hersennetwerken tijdens de ontwikkeling, en als zodanig dragen ze bij aan het begrip van het ontstaan van hersenontwikkelingsstoornissen.

Dankwoord

Graag wil ik beginnen met mijn dank uit te spreken voor de steun, inzichten en inspiratie die ik in de afgelopen jaren van iedereen heb mogen ontvangen en welke de basis zijn geweest voor dit proefschrift. Ik heb hierdoor niet alleen de mogelijkheid gekregen om het vakgebied te leren kennen, maar ook mijzelf.

Paul, allereerst wil ik jou bedanken voor de ontwikkeling die ik onder jouw begeleiding heb kunnen doormaken. Ik kreeg de vrijheid om te ontdekken en met een vraag kon ik meteen bij je terecht. Je antwoorden waren precies en duidelijk, en je wist me altijd uit te dagen tot meer. Onze discussies waren zeer leerzaam voor mij, en ik waardeer dat je hierbij openstond voor andere visies (hoe bedoel je, 'eigenwijs'?). Ik hoop dat we nog lange tijd ideeën uit kunnen wisselen en nieuwe bevindingen doen binnen de Neuroinformatica.

Data-analyse is natuurlijk het meest interessant op data die je zelf verzameld hebt. Dirk en Nael, het e-phys duo, ik wil jullie bedanken voor het mogelijk maken van de data-verzameling. Dirk, je enthousiasme voor wetenschap was altijd aanstekelijk, en je vrolijkheid zeer welkom op de lange experimentele dagen. Nael, bedankt voor de experimentele technieken en inzichten die je mij geleerd hebt, en voor een kijk in de medische wereld.

Ook wil ik graag de Radboud Universiteit, het Donders Instituut en de Nederlandse Organisatie van Wetenschappelijk Onderzoek (NWO) bedanken voor de (financiële) ondersteuning van mijn onderzoek en de mogelijkheden die mij geboden zijn.

Research is not done in isolation, and I am incredibly happy about the many inspirational, encouraging and enthusiastic colleagues I was privileged to meet. John van Opstal, your words of wisdom were always accompanied by a beautiful speech on how every aspect of life could be improved. You truly have been a scientific and personal inspiration to me for many years, thank you. Tansu Celikel, your broad views on science and career have been very helpful to me.

Our encounters were highly instructive and I hope they will lead to many more. Michela Chiappalone, thank you for the friendly and educational hosting in your lab in Genova, I have learned from and enjoyed those months a lot! Sonja Vernes, Venkat Chokkalingam, Wilhelm Huck, Raoul Memmesheimer and Arthur Houweling, thank you for the open collaborations and many interesting discussions.

Doing research at two departments means you meet many colleagues and, consequently, have lots of birthday cakes! Charl, Marije, Rembrandt, Tara, Max, Laurens, Martijn, Vivien, Stephanie, Marco, Monica, Moritz, Jori, Jon-Ruben, Astrid and Inge, and all Donders colleagues whom I had the pleasure to meet and work with during my PhD, I want to thank all of you. It was great to encounter the various research interests and aspirations everyone has. As Bilbo Baggings expressed, as a compliment, in the book *The Lord of the Rings* (by J.R.R. Tolkien): "I don't know half of you half as well as I should like; and I like less than half of you half as well as you deserve".

Graag wil ik de studenten bedanken die meegewerkt hebben aan dit onderzoek. Teun, Lisa, Eline, Michel en Jessica, bedankt voor de frisse blik en uitdagende houding, maar vooral voor het harde werk en doorzettingsvermogen, waarvan de resultaten te zien zijn in dit boekje.

Veel dank aan mijn vrienden en de families Martens en Kersten voor de interesse in mijn persoonlijke ontwikkeling gedurende deze tijd en vooral voor alle leuke momenten samen. Peter and Rebecca, for all the guidance in life, and the many bro-moments along the way. Rein, Ard, Bart en Roy, samen opgegroeid en (een beetje) volwassen geworden, ik hoop dat we dit nog lang kunnen volhouden. Joep en Minke, Pim en Vera, Arno en José, Frans, Roel en Lotte, Lisa en Sven, en alle studievrienden, dank voor het gelach, de leuke bier- en bordspelavonden, falafel zonder jullie smaakt toch minder. Sport is voor mij belangrijk geweest voor het tot stand komen van dit boekje; ik wil daarom de *Aeoli, Hydrofielers* en *United-Rebels* bedanken voor de leuke activiteiten afgelopen jaren.

Beste huisgenoten, bedankt voor het meeleven met mijn PhD. Rein, al jaren laat jij *thuis als thuis* voelen. Lieke, bedankt voor alle leuke en nieuwe momenten samen, en ook voor de steun tijdens mijn PhD-tijd.

Geert, de afrondfase van mijn PhD-tijd betekende ook de opstart van een nieuwe uitdaging. Ik ben dankbaar voor de vrijheid, betrokkenheid en het vertrouwen gedurende deze tijd.

Ine, we just met, but you make things look very bright.

Anneke en Gerard, voor alle steun tijdens mijn PhD-tijd, bedankt. Anneke, je altijd aanwezige interesse in mijn bezigheden was een grote motivatie bij het maken van dit proefschrift, bedankt hiervoor. Ook bedankt voor het laten zien dat er andere dingen zijn dan papierwerk, waardoor ik vele leuke ervaringen rijker ben geworden. Gerard, we houden allebei stug vol dat je niet eigenwijs bent, zolang het maar klopt wat je zegt. Je bent een grote inspiratie voor mijn dagelijkse zoektochten naar nieuwe bevindingen, bedankt voor alle aandacht die je hieraan geeft. Dankzij de door jullie aangeboden belevenissen en uitdagende prikkels tijdens de 'emergence' van mijn 'brain circuits' kijk ik terug op een zeer leuke ontwikkelingsperiode.

De auteur

Curriculum vitae

Marijn Martens (1986) behaalde in 2004 zijn gymnasiumdiploma met de profielen Natuur & Techniek en Natuur & Gezondheid. In 2008 rondde hij de Bachelor Scheikunde aan de Radboud Universiteit in Nijmegen af; hiervan werd als onderdeel een studiejaar doorgebracht aan de Western Washington University in de Verenigde Staten. De Master Cognitive Neuroscience aan het Donders Graduate School for Cognitive Neuroscience rondde hij *cum laude* af in 2010. Hij was in 2008 mede-oprichter van βetahunter, een online platform om banen in de natuurwetenschappen te koppelen aan bèta-wetenschappers; βetahunter werd in 2010 verkocht. Marijn verkreeg in 2010 een TOPTalent NWO beurs en voerde daarmee zijn promotie-onderzoek uit binnen de afdeling Neuroinformatica van het Donders Institute for Brain, Cognition and Behaviour. Als onderdeel hiervan werd in 2011 een 4-maands werkbezoek afgelegd bij het Istituto Italiano di Tecnologia in Genua, Italië. In 2015 verwierf hij een tweejarige Europese Samenwerkings-Innovatie subsidie (EFRO OP-Oost programma) voor de start-ups DrugTargetID en orikami, waardoor hij momenteel werkt als projectleider om een app te maken waarmee MS-specialisten een persoonlijke diagnose, prognose en uiteindelijk behandeling kunnen bieden op basis van het individuele patiëntenprofiel (DiaPro MS-app).

Curriculum vitae

Marijn Martens (1986) obtained in 2004 his gymnasium diploma with the profiles Nature & Technology and Nature & Health. In 2008 he obtained a Bachelor in Chemistry at Radboud University Nijmegen; this included a year of study at Western Washington University in the USA. He obtained *cum laude* a Master in Cognitive Neuroscience at the Donders Graduate School for Cognitive Neuroscience in 2010. He was in 2008 co-founder of βetahunter, an online platform to connect science jobs to β-scientists; βetahunter was sold in 2010. Marijn was awarded in 2010 the TOPTalent NWO grant and used this grant for his PhD-research at the Department of Neuroinformatics at the Donders Institute for Brain, Cognition and Behaviour. In 2011, as part of his PhD, he had a 4-months working visit at the Istituto Italiano di Tecnologia in Genova, Italy. In 2015 he obtained a two-year European Collaboration Innovation subsidy (EFRO OP-Oost program) for the start-ups Drug Target ID and orikami, where he currently works as project leader to create an app in order to support MS specialists with personal diagnosis, prognosis and eventually treatment using a profile of the individual patient (DiaPro MS-app).

Publicatielijst

1. **M.B. Martens**, R.F. Van der Willegen, A.J. Van Opstal (2010). *Head-unrestrained gaze shifts of macaque monkeys to audiovisual targets*, Proc of the Cognitive Neuroscience Master of the Radboud University; 6(1):24-52.
2. P. Bremen, R.F. Van der Willigen, M.M. Van Wanrooij, D.F. Schaling, **M.B. Martens**, T.J. Van Grootel, A.J. van Opstal (2010). *Applying double-magnetic induction to measure head-unrestrained gaze shifts: calibration and validation in monkey*, Biological Cybernetics; 103(6):415-32.
3. **M.B. Martens**, M. Chiappalone, D. Schubert, P.H.E. Tiesinga (2014). *Separating burst from background spikes in multichannel neuronal recordings using return map analysis*, International Journal of Neural Systems; 24(4):1450012.
4. **M.B. Martens**, T. Celikel, P.H.E. Tiesinga (2015). *A developmental switch for Hebbian plasticity*, PLoS Computational Biology; 11(07):e1004386.
5. **M.B. Martens**, J. Classen, M. Frega, L. Epping, M. Benevento, H. van Bokhoven, P.H.E. Tiesinga, D. Schubert, and N.N. Kasri (2016). *Euchromatin histone methyltransferase 1 regulates cortical neuronal network development. Submitted* to Scientific Reports.
6. **M.B. Martens**, A.R. Houweling, P.H.E. Tiesinga (2016). *Anti-correlations in the degree distribution increase stimulus detection performance in noisy spiking neural networks. Under review* at Journal of Computational Neuroscience.
7. T. van Gils, P.H.E. Tiesinga, **M.B. Martens** (2016). *Stimulus detection probability is increased by spike train irregularity.* In preparation for publication.
8. C.J.H.M. Klemann, G.J.M. Martens, M. Sharma, **M.B. Martens**, O. Isacson, T. Gasser, J.E. Visser, G. Poelmans (2016). *Lipid and lipoprotein signalling is key in Parkinsonś disease. Submitted* to Nature Medicine.

Donders Graduate School for Cognitive Neuroscience

For a successful research institute, it is vital to train the next generation of young scientists. To achieve this goal, the Donders Institute for Brain, Cognition and Behaviour established the Donders Graduate School for Cognitive Neuroscience (DGCN), which was officially recognised as a national graduate school in 2009. The Graduate School covers training at both Master's and PhD level and provides an excellent educational context fully aligned with the research programme of the Donders Institute.

The school successfully attracts highly talented national and international students in biology, physics, psycholinguistics, psychology, behavioral science, medicine and related disciplines. Selective admission and assessment centers guarantee the enrolment of the best and most motivated students.

The DGCN tracks the career of PhD graduates carefully. More than 50% of PhD alumni show a continuation in academia with postdoc positions at top institutes worldwide, e.g. Stanford University, University of Oxford, University of Cambridge, UCL London, MPI Leipzig, Hanyang University in South Korea, NTNU Norway, University of Illinois, North Western University, Northeastern University in Boston, ETH Zürich, University of Vienna etc.. Positions outside academia spread among the following sectors: specialists in a medical environment, mainly in genetics, geriatrics, psychiatry and neurology. Specialists in a psychological environment, e.g. as specialist in neuropsychology, psychological diagnostics or therapy. Positions in higher education as coordinators or lecturers. A smaller percentage enters business as research consultants, analysts or head of research and development. Fewer graduates stay in a research environment as lab coordinators, technical support or policy advisors. Upcoming possibilities are positions in the IT sector and management position in pharmaceutical industry. In general, the PhDs graduates almost invariably continue with high-quality positions that play an important role in our knowledge economy.

For more information on the DGCN as well as past and upcoming defenses please visit:
`www.ru.nl/donders/graduate-school/donders-graduate/`